Universidade de Aveiro Departamento de Ambiente e Ordenamento
2008

Ana Margarida Lobo Lourenço da Costa

Modelação de microscala da exposição a poluentes atmosféricos em áreas urbanas

Microscale modelling of exposure to atmospheric pollutants in urban areas

Tese apresentada à Universidade de Aveiro para cumprimento dos requisitos necessários à obtenção do grau de Doutor em Ciências Aplicadas ao Ambiente, realizada sob a orientação científica do Doutor Carlos Borrego, Professor Catedrático do Departamento de Ambiente e Ordenamento da Universidade de Aveiro.

Apoio financeiro da Fundação para a Ciência e Tecnologia (FCT) e do Fundo Social Europeu (FSE) no âmbito do III Quadro Comunitário de Apoio pela Bolsa de Doutoramento Refª SFRH/BD/11097/2002.

Apoio financeiro da Fundação Calouste Gulbenkian (FCG) no âmbito do Projecto SaudAR e da Comissão Europeia no âmbito do Projecto AIR4EU (FP6-2002-SSP-1).

o júri

presidente

Doutor Henrique Manuel Morais Diz
Professor Catedrático da Universidade de Aveiro

Doutor Peter Builtjes
Professor Catedrático da Freie Universitat Berlin

Doutor Carlos Alberto Diogo Soares Borrego
Professor Catedrático da Universidade de Aveiro (Orientador)

Doutora Ana Isabel Couto Neto da Silva Miranda
Professora Associada da Universidade de Aveiro

Doutora Teresa Filomena Vieira Nunes
Professora Associada da Universidade de Aveiro

Doutor Nelson Augusto Cruz de Azevedo Barros
Professor Associado da Faculdade de Ciência e Tecnologia da Universidade Fernando Pessoa

Doutora Myriam Alexandra dos Santos Batalha Dias Nunes Lopes
Professora Auxiliar Convidada da Universidade de Aveiro

agradecimentos

Escrever estas palavras de agradecimento marcam um momento muito especial na minha vida.... estou finalmente a terminar a minha Tese de Doutoramento!
E mais do que cinco anos em seis capítulos, esta Tese representa todo um percurso que fiz no grupo de investigação GEMAC durante os últimos oito anos, e que se traduziu, sem dúvida, num crescimento profissional e pessoal.

Os meus primeiros agradecimentos são dirigidos ao meu orientador, e amigo, Prof. Doutor Carlos Borrego, pelos vastos conhecimentos que me transmitiu, pelas imprescindíveis críticas e sugestões no decorrer do trabalho e pelas palavras de encorajamento nos momentos mais difíceis.

À Prof. Doutora Ana Isabel Miranda deixo uma palavra muito especial de agradecimento pela revisão cuidada da Tese e pelas mensagens de ânimo que me ajudaram a acreditar que era possível chegar ao fim.

Agradeço igualmente a todos os gemaquianos que ao longo destes anos foram como uma grande família, capaz de partilhar problemas, alegrias e mais do que tudo, a amizade. Guardo com grande estima as discussões científicas que fui tendo ao longo do trabalho, os incentivos constantes e o apoio recebido na revisão final do documento. Deixo aqui um obrigado muito especial, e sem nenhuma ordem em particular, à Anabela, à Joana V., à Cristina, ao Jorge, ao Pedro S., à Oxana, ao Richard, à Helena e ao Pedro C.

Não podia deixar de agradecer às pessoas mais importantes da minha vida. À minha família, marido, pais, irmão, sogros, tios, pelo apoio incondicional que sempre me deram.

Especialmente quero agradecer aos meus queridos pais pela confiança que me incutiram ao longo dos meus anos de vida, pelo sentido de responsabilidade e pela mensagem constante de coragem para ultrapassar os problemas da vida.

As minhas últimas palavras de agradecimento estão revestidas de uma importância especial e são dirigidas ao meu querido marido e amigo Paulo, que me apoiou incansavelmente em todos os momentos, suportou os meus períodos de necessário isolamento e, que com muito amor e carinho me encorajou a completar esta importante etapa nas nossas vidas.

palavras-chave

Microscala, modelação numérica, qualidade do ar exterior e interior, taxa de ventilação, exposição humana.

resumo

A poluição atmosférica é considerada um dos maiores problemas ambientais, afectando em particular a saúde das populações urbanas. Esta problemática tem um impacto directo no ambiente exterior, mas assume especial relevância nos espaços interiores, onde a população dispende a maior percentagem do seu tempo. Para a avaliação dos impactos da poluição atmosférica na saúde das populações é necessário proceder à estimativa da exposição humana aos poluentes atmosféricos nos ambientes exterior e interior.

Os principais objectivos deste trabalho centram-se no desenvolvimento de um modelo de exposição tridimensional de microscala (MEXPO) para a estimativa da exposição individual de curto termo aos poluentes PM_{10} e NO_2, e na sua aplicação à área urbana de Viseu, com dados de duas campanhas experimentais, com o intuito de avaliar a exposição de crianças com problemas respiratórios aos referidos poluentes. O modelo de exposição tem capacidade para estimar os campos tridimensionais de vento e de concentração no ar ambiente, considerando a influência dos edifícios existentes na área urbana. O modelo simula, igualmente, as taxas de ventilação natural e as concentrações de poluentes no interior dos edifícios.

O modelo de exposição inclui um modelo *Computational Fluid Dynamic* (CFD) de qualidade do ar para a estimativa dos campos exteriores de vento e de concentração de poluentes. O referido modelo CFD foi previamente validado de acordo com uma metodologia específica para modelos de microscala, e que inclui a utilização de critérios de validação desenvolvidos para o estudo da dispersão de poluentes em áreas urbanas.

A aplicação do modelo de exposição à área urbana de Viseu para os dois períodos experimentais permitiu estimar quais as crianças mais expostas a concentrações de PM_{10} e NO_2. Estes resultados estão directamente relacionados com o tempo dispendido pelas crianças no interior das suas residências e pelos valores de concentração determinados para esses espaços interiores. As crianças mais expostas terão uma maior probabilidade de desenvolver problemas respiratórios.

A metodologia desenvolvida poderá ser usada como uma primeira abordagem para a estimativa da exposição individual a poluentes, substituindo a utilização de técnicas de medição directa intrusivas e dispendiosas.

O modelo de exposição desenvolvido poderá ter ainda um papel relevante na aplicação a cenários futuros de alterações climáticas com influência no clima urbano, permitindo conhecer as concentrações futuras de poluentes no espaço urbano exterior e interior, e, consequentemente, estimar a futura exposição humana a poluentes atmosféricos.

keywords

Microscale, numerical modelling, outdoor and indoor air quality, air exchange rate, human exposure.

abstract

Air pollution is a major environmental health problem focusing on the ambient air quality in cities but also on the air quality of indoor environments, where people spend most of their time. In order to evaluate the real impacts of urban air pollution in the population health is necessary to undergo a complete assessment of human exposure to atmospheric pollutants that includes both outdoor and indoor exposure assessments.

The main goals of this study are the development of a three-dimensional (3D) Microscale EXPOsure model (MEXPO) to estimate the short-term individual exposure to PM_{10} and NO_2 and its application to the Viseu urban area, using experimental data from two field campaigns, in order to assess the exposure to the referred pollutants on children with known respiratory problems. To perfom this goal the exposure model is able to estimate the outdoor flow and pollutant concentrations, considering the influence of the urban built-up area, as well to assess the air exchange rates as result of natural ventilation mechanisms. The indoor pollutant concentrations on the defined microenvironments are also estimated by the model. With the purpose of estimating the outdoor pollutant dispersion, the exposure model MEXPO includes a Computational Fluid Dynamic model (CFD) model that has the advantage to fully characterize the flow and the transport of the urban air pollution on a 3D basis. The CFD model was successfully evaluated according to a established procedure, using specific model acceptance criteria that were defined in agreement with the intended model purpose, which is the study of meteorology and pollutant dispersion in urban areas.

The application of MEXPO to the Viseu urban area allowed determining the most exposed children to PM_{10} and NO_2 concentrations during both campaigns. These children are therefore more sensitive to develop respiratory problems such as asthma.

The developed methodology may be seen as a valid approach to assess the individual human exposure to atmospheric pollutants in urban areas, replacing direct measurement techniques that are considered invasive and expensive. The developed exposure model has also an important role in the application to future climate change scenarios with direct consequences in the urban climate, allowing to determine the future human exposure to atmospheric pollutants and, consequently, also the future outdoor and indoor atmospheric pollutants concentrations in an urban area.

TABLE OF CONTENTS

LIST OF FIGURES ..... **V**

LIST OF TABLES ..... **XI**

NOMENCLATURE ..... **XIII**

LIST OF ABBREVIATIONS ..... **XV**

1. INTRODUCTION **1**

1.1. Overview 1

1.2. State of the art on microscale exposure modelling 8

1.3. Research objectives and structure of the work 13

2. AIR QUALITY MODELLING IN THE URBAN ENVIRONMENT **15**

2.1. Microscale models 15

2.2. VADIS CFD model 19

2.2.1. FLOW module 20

2.2.1.1. Turbulence modelling *22*

2.2.1.2. Discretisation method *26*

2.2.1.3. Near-wall flow treatment *27*

2.2.1.4. Initial conditions *28*

2.2.2. DISPER module 29

2.2.3. Functioning scheme 30

3. EVALUATION OF MICROSCALE CFD MODELS **33**

3.1. Philosophy of model evaluation 35

3.1.1. Scientific evaluation 37

3.1.2. Verification 38

3.1.3. Validation 39

3.1.3.1. Potential validation data sets *40*

3.1.3.2. How should the model be run and the results interpreted *40*

3.1.3.3. What variables to compare *41*

3.1.3.4. How should the variables be compared *42*

3.1.3.5. Exploratory data analysis 42
3.1.3.6. Metrics for a model validation 42
3.1.3.7. Quality acceptance criteria 44
3.2. Evaluation of VADIS CFD model 45
3.2.1. The Mock Urban Setting Test 47
3.2.2. Setting-up and running VADIS CFD model 55
3.2.2.1. Choice of target variables 55
3.2.2.2. Choice of the computational domain 55
3.2.2.3. Choice of the computational grid 56
3.2.2.4. Initial conditions 57
3.2.2.5. Running conditions 57
3.2.3. Post-processing of model outputs 57
3.2.4. Exploratory data analysis 58
3.2.5. Statistical analysis 79
3.2.6. Discussion of results 82
4. MICROSCALE EXPOSURE MODELLING 85
4.1. The microscale exposure model MEXPO 85
4.1.1. Microenvironment definition 88
4.1.2. Time-activity pattern 88
4.1.3. Outdoor pollutant concentrations 89
4.1.4. Indoor pollutant concentrations 89
4.1.4.1. Indoor emissions 90
4.1.4.2. Penetration coefficient and decay rate 92
4.1.4.3. Air exchange rate 92
4.2. Ventilation of buildings 94
4.2.1. Natural ventilation 95
4.2.2. Ventilation standards 97
5. ASSESSMENT OF INDIVIDUAL EXPOSURE TO ATMOSPHERIC POLLUTANTS 101
5.1. The SAUDAR project 101
5.2. MEXPO application 103
5.2.1. Modelling input data 105
5.2.1.1. Built-up area characterisation 105

5.2.1.2. Traffic emissions *107*
5.2.1.3. Boundary conditions *110*
5.2.1.4. 3D microenvironment definition *114*
5.2.1.5. Time-activity profiles *115*
5.2.2. Modelling results 117
5.2.2.1. Natural ventilation rate *117*
5.2.2.2. Outdoor air quality *123*
5.2.2.3. Indoor air quality *130*
5.2.2.4. Individual exposure *142*
5.2.2.5. Discussion of results *146*

6. CONCLUSIONS 149

REFERENCES 153

APPENDIX 167

APPENDIX A - Scientific Evaluation and Model Verification. 169

LIST OF FIGURES

Figure 1.1 - Urban population potentially exposed to exceedances of EU urban air quality standards for PM_{10}, NO_2, Benzene and CO - 1995 and 2010 [EEA, 2001]..... 3

Figure 1.2 - Chain of events related to the health effects of air pollution [Hertel *et al.*, 2001]..... 3

Figure 2.1 - Characteristic time scale (abscissa) and characteristic horizontal scale (ordinate) of common atmospheric phenomena (a), and of atmospheric models (b) [Moussiopoulos, 2003]. 16

Figure 2.2 - A schematic view of the flow in a street canyon (adapted from [Britter, 2003]). 17

Figure 2.3 - Schematic representation of input and output data for FLOW and DISPER modules. 20

Figure 2.4 - Flow and cartographic grids used in VADIS model. 31

Figure 2.5 - Obstacles and sources coordinates definition used in VADIS model. 32

Figure 3.1 - Phases of modelling and simulation and the role of *verification* and *validation* [Schlesinger, 1979]. Taken from Oberkampf *et al.* (2004). 36

Figure 3.2 - Ilustration of Hit rate. 44

Figure 3.3 - Photograph of the MUST array experiment. 48

Figure 3.4 - 3D perspective of the setup and identification of the VIP car location. 49

Figure 3.5 - Schematic view of the experimental setup. 50

Figure 3.6 - Model on the turn table for -45° wind direction and roughness elements, inside the WOTAN wind tunnel. 51

Figure 3.7 - Reference coordinate system for the -45º test case. 52

Figure 3.8 - Flow measurement positions for the -45º wind direction. 53

Figure 3.9 - Location of the emission source and the concentration measurement points for the -45º wind direction. 54

Figure 3.10 - Horizontal plane of flow and dimensionless concentration of passive tracer at 2 m height. 58

Figure 3.11 - Fine UV measurement positions for -45º approach flow. 59

Figure 3.12 - Contour plots of dimensionless U velocity component at fine UV positions (z=0.9 m) for: (a) 0.5 m grid model resolution and (b) wind tunnel experimental data. 60

Figure 3.13 - Contour plots of dimensionless U velocity component at fine UV positions (z=1.575 m) for: (a) 0.5 m grid model resolution and (b) wind tunnel experimental data. 61

Figure 3.14 - Contour plots of dimensionless U velocity component at fine UV positions (z=2.55 m) for: (a) 0.5 m grid model resolution and (b) wind tunnel experimental data. 61

Figure 3.15 - Contour plots of dimensionless V velocity component at fine UV positions (z=0.9 m) for: (a) 0.5 m grid model resolution and (b) wind tunnel experimental data. 62

Figure 3.16 - Contour plots of dimensionless V velocity component at fine UV positions (z=1.575 m) for: (a) 0.5 m grid model resolution and (b) wind tunnel experimental data. 63

Figure 3.17 - Contour plots of dimensionless V velocity component at fine UV positions (z=2.55 m) for: (a) 0.5 m grid model resolution and (b) wind tunnel experimental data. 63

Figure 3.18 - Horizontal profiles of dimensionless U, V and W components, and TKE, for Y=60 m, at 1.275 m height (*mod* and *WT* notations represent the numerical results and wind tunnel data, respectively). 65

Figure 3.19 - Horizontal profiles of dimensionless U, V and W components, and TKE, for Y=60 m, at 2.55 m height (*mod* and *WT* notations represent the numerical results and wind tunnel data, respectively). 66

Figure 3.20 - Horizontal profiles of dimensionless U, V and W components, and TKE, for Y=60 m, at 5.1 m height (*mod* and *WT* notations represent the numerical results and wind tunnel data, respectively). 67

Figure 3.21 - Horizontal profiles of dimensionless U, V and W components, and TKE, for Y=-45 m, at 1.275 m height (*mod* and *WT* notations represent the numerical results and wind tunnel data, respectively). 68

Figure 3.22 - Horizontal profiles of dimensionless U, V and W components, and TKE, for Y=-45 m, at 2.55 m height (*mod* and *WT* notations represent the numerical results and wind tunnel data, respectively). 69

Figure 3.23 - Horizontal profiles of dimensionless U, V and W components, and TKE, for Y=-45 m, at 5.1 m height (*mod* and *WT* notations represent the numerical results and wind tunnel data, respectively). 70

Figure 3.24 - Vertical profiles of dimensionless U, V and W components, and TKE, at location 1 (*mod* and *WT* notations represent the numerical results and wind tunnel data, respectively)..... 71

Figure 3.25 - Vertical profiles of dimensionless U, V and W components, and TKE, at location 6 (*mod* and *WT* notations represent the numerical results and wind tunnel data, respectively)..... 73

Figure 3.26 - Vertical profiles of dimensionless U, V and W components, and TKE, at location 12 (*mod* and *WT* notations represent the numerical results and wind tunnel data, respectively)..... 74

Figure 3.27 - Horizontal profiles of dimensionless concentration at 42 m, 99 m, 142 m distance from the emission source. 76

Figure 3.28 - Scatter plots of the dimensionless U and W wind components, and TKE, for all vertical profiles..... 77

Figure 3.29 - Scatter plots of the dimensionless U and V components, and TKE, for all horizontal layers. 78

Figure 3.30 - Scatter plot of the dimensionless concentration for all horizontal layers. 79

Figure 4.1 - Schematic representation of MEXPO model. 86

Figure 4.2 - Definition of the 3D microenvironment matrix. 88

Figure 4.3 - Schematic representation of the methodology for estimation of indoor concentration from outdoors in buildings (ϑ -outdoor wind speed ($m.s^{-1}$); C_{out}-outdoor pollutant concentration ($\mu g.m^{-3}$)). 90

Figure 4.4 - Natural ventilation of a building by the three dominant mechanisms [Straw, 2000]..... 95

Figure 4.5 - Pressure effect from wind. 96

Figure 4.6 - Required ventilation rates per person for dwellings and offices in standards [EC, 2003]. 98

Figure 5.1 - Location of the study area: (a) within Portugal and (b) within the urban area of Viseu. 102

Figure 5.2 - MEXPO study domain located in Viseu city centre. 104

Figure 5.3 - 3D representation of buildings of the study area. 106

Figure 5.4 - 2D horizontal perspective of building's and road's location within the study domain. 106

Figure 5.5 - Schematic representation of TREM input data. 107

Figure 5.6 - Hourly PM_{10} emissions during weekdays and weekend in the winter period. 108

Figure 5.7 - Hourly NO_x emissions during weekdays and weekend in the winter period. 109

Figure 5.8 - Hourly PM_{10} emissions during weekdays and weekend in the summer period. 109

Figure 5.9 - Hourly NO_x emissions during weekdays and weekend in the summer period. 110

Figure 5.10 - MM5/CAMx simulation domains [Borrego *et al.*, 2007b]. 111

Figure 5.11 - City map of Viseu presenting the location of the mobile air quality laboratories (red dots). 111

Figure 5.12 - Wind speed and direction results from MM5 model for the winter (a) and summer (b) periods. 113

Figure 5.13 - Hourly PM_{10} and NO_2 concentrations results from CAMx model for the winter period. 114

Figure 5.14 - Hourly PM_{10} and NO_2 concentrations results from CAMx for the summer period. 114

Figure 5.15 - Time-activity profiles of the selected children. 116

Figure 5.16 - Simulated hourly ventilation rates in children's bedrooms for the winter period. 118

Figure 5.17 - Simulated hourly ventilation rates in Marzovelos and ASAC classrooms for the winter period. 118

Figure 5.18 - Simulated hourly ventilation rates in children's bedrooms for the summer period. 119

Figure 5.19 - Simulated hourly ventilation rates in Marzovelos and ASAC classrooms for the summer period. 120

Figure 5.20 - Simulated average ventilation rates for the winter and summer campaigns. 120

Figure 5.21 - Measured ventilation rates in Marzovelos classroom during winter (a) and summer (b) campaigns. 122

Figure 5.22 - Horizontal view at 4.5 m height of flow and PM_{10} concentration fields for the 20th January 2006 at 4 p.m.. 124

Figure 5.23 - Horizontal view at 4.5 m height of flow and NO_2 concentration fields for the 20th January 2006 at 4 p.m.. 125

Figure 5.24 - Horizontal view at 4.5 m height of flow and PM_{10} concentration fields for the 20th June 2006 at 4 p.m. 125

Figure 5.25 - Horizontal view at 4.5 m height of flow and NO_2 concentration fields for the 20th June 2006 at 4 p.m.. 126

Figure 5.26 - Measured and simulated daily average PM_{10} concentrations at the Marzovelos mobile laboratory for the winter period. 127

Figure 5.27 - Measured and simulated hourly average NO_2 concentrations at the Marzovelos mobile laboratory for the winter period. 127

Figure 5.28 - Measured and simulated daily average PM_{10} concentration at the Marzovelos mobile laboratory for the summer period. 128

Figure 5.29 - Measured and simulated hourly average NO_2 concentration at the Marzovelos mobile laboratory for the summer period. 128

Figure 5.30 - Hourly PM_{10} indoor concentrations simulated for the winter period. 131

Figure 5.31 - Weekly average indoor PM_{10} concentrations for the winter period. 132

Figure 5.32 - (a) Hourly and (b) average indoor/outdoor ratio of PM_{10} concentrations simulated for the winter period. 133

Figure 5.33 - Measured and simulated daily average PM_{10} indoor concentrations in Marzovelos classroom for the winter period. 133

Figure 5.34 - Hourly NO_2 indoor concentrations simulated for the winter period. 135

Figure 5.35 - (a) Hourly and (b) average indoor/outdoor ratio of NO_2 concentrations simulated the winter period. 135

Figure 5.36 - Measured and simulated average indoor NO_2 concentrations in Marzovelos classroom and in children's bedrooms for the winter period. 136

Figure 5.37 - Hourly PM_{10} indoor concentrations simulated for the summer period. 137

Figure 5.38 - Weekly average indoor PM_{10} concentrations for the summer period. 138

Figure 5.39 - (a) Hourly and (b) average indoor/outdoor ratio of PM_{10} concentrations simulated for the summer period. 139

Figure 5.40 - Measured and simulated daily average PM_{10} indoor concentrations in Marzovelos classroom for the summer period. 139

Figure 5.41 - Hourly NO_2 indoor concentrations simulated for the summer period. 141

Figure 5.42 - (a) Hourly and (b) average indoor/outdoor ratio of NO_2 concentrations simulated for the summer period. 141

Figure 5.43 - Measured and simulated average indoor NO_2 concentrations in Marzovelos classroom and in children's bedrooms for the summer period. 142

Figure 5.44 -(a) Hourly individual exposure and (b) daily average individual exposure to PM_{10} for the winter period. 143

Figure 5.45 - Weekly average individual exposure to PM_{10} for the winter period. 143

Figure 5.46 - (a) Hourly individual exposure and (b) daily average individual exposure to NO_2 for the winter period. 144

Figure 5.47 - Weekly average individual exposure to NO_2 for the winter period. 144

Figure 5.48 - (a) Hourly individual exposure and (b) daily average individual exposure to PM_{10} for the summer period. 145

Figure 5.49 - Weekly average individual exposure to PM_{10} for the summer period. 145

Figure 5.50 - (a) Hourly individual exposure and (b) daily average individual exposure to NO_2 for the summer period. 146

Figure 5.51 - Weekly average individual exposure to NO_2 for the summer period. 146

LIST OF TABLES

Table 1.1 - Air quality standards defined by the European Union and the World Health Organisation. 4

Table 1.2 - I/O functions [Borrego *et al.*, 2006]. 12

Table 3.1 - Modelling Quality objectives established by the European Directives collected by [Borrego *et al.*, 2005]. 34

Table 3.2 - Computer runtimes for flow and dispersion modules for the three resolutions. 57

Table 3.3 - Model acceptance criteria. 79

Table 3.4 - Hit rate calculations for U, V, W and TKE for 0.5 m, 1 m and 2 m model resolutions. 80

Table 3.5 - Detailed hit rate calculations for U, V, W and TKE for 0.5 m model resolution. 81

Table 3.6 - Statistical analysis of concentration results for 0.5 m, 1 m and 2 m model resolutions. 82

Table 4.1 - Summary of parameters used in MEXPO model. 94

Table 4.2 - Portuguese standards for minimum ventilation rates. 99

Table 5.1 - Statistical analysis for 1 km modelling results for the winter and summer campaigns [Borrego *et al.*, 2007b]. 112

Table 5.2- Location height of residential, school, ASAC and transport microenvironments. 115

Table 5.3 - Statistical analysis of modelling results for PM_{10} and NO_2 concentrations in winter and summer campaigns at the mobile laboratory location. 129

Table 5.4 - Summary of MEXPO model results for the winter and summer periods. 147

Table A.1 - Basic information for the Scientific Evaluation questionnaire. 169

Table A.2 - Steps to perform Model Verification. 170

Table A.3 - VADIS model description under COST 732 Model Inventory [URL 1]. 171

NOMENCLATURE

ρ	density	[kg.m^{-3}]
P	pressure	[kg.m^{-1}.s^{-2}]
u	instantaneous velocity	[m.s^{-1}]
μ	dynamic viscosity	[kg.m^{-1}.s^{-1}]
τ_{ij}	viscous stress	[N.m^{-2}]
x_i, x_j	coordinate variable	[m]
T	temperature	[K]
λ	thermal conductivity	[W.m^{-1}.K^{-1}]
R	ideal gas constant	[J. kg^{-1}.K^{-1}]
C_p	specific heat	[J. kg^{-1}.K^{-1}]
g	gravity	[m.s^{-2}]
β	coefficient of thermal expansion	[K^{-1}]
δ_{ij}	Kronecker delta {δ_{ij}=1 if i=j; δ_{ij}=0 if i≠j}	
k	turbulent kinetic energy	[m^2.s^{-2}]
ε	rate of dissipation of turbulent kinetic energy	[m^2.s^{-3}]
$C_?$	constants; k- ε model: ?=1,2,3, μ	[-]
R_i	Richardson number	[-]
ν	kinematic viscosity	[m^2.s^{-1}]

K	Von Karman constant	[-]
C	concentration	[µg.m^{-3}]
Q_{is}	mass source flow	[µg.h^{-1}]
E_i	exposure for person i	[µg.m^{-3}.h]
a	air exchange rate	[h^{-1}]
Q_v	volume flow rate	[m^3.h^{-1}]
V	room volume	[m^3]
ϑ	wind speed	[m.s^{-1}]
E	opening effectiveness coefficient	[-]
k	decay rate	[h^{-1}]
A	window opening area	[m^2]
p	penetration coefficient	[-]

LIST OF ABBREVIATIONS

AQ-FWD	Air Quality Framework Directive
ASAC	After School Activity Centre
CFD	Computational Fluid Dynamic
EEA	European Environment Agency
EU	European Union
FID	Flame Ionization Detector
HVAC	Heating, Ventilating and Air Conditioning
LDA	Laser-Doppler-Anemometry
LES	Large Eddy Simulation
LPD	Lagrangian Particle Dispersion
MDS	Model Documentation System
MUST	Mock Urban Setting Test
PID	Photo-Ionization Detector
PM	Particle Matter
RANS	Reynolds Averaged Navier-Stokes
RSECE	Regulamento dos Sistemas Energéticos e de Climatização dos Edifícios
TKE	Turbulent Kinetic Energy
UVIC	Ultraviolet Ion Collector
WHO	World Health Organisation
WOTAN	Environmental Wind Tunnel Laboratory

1. INTRODUCTION

Clean air is considered to be a basic requirement of human health and well-being. However, air pollution continues to cause a significant threat to health worldwide [Fenger *et al.*, 1998].

1.1. Overview

In the beginning of the XXI century it is becoming undeniable the direct and indirect consequences of air pollution to the Earth's environmental equilibrium: climate change, ozone layer depletion and global warming are considered one of today's major world concerns.

Still however, the most direct impacts of air pollution are felt in cities. Over the last 50 years, the world's urban population has grown faster (~2.7 %.yr^{-1}) than the total population (~1.8 %.yr^{-1}) [Gurjar and Lelieveld, 2005]. In the particular case of Europe, one of the most urbanised world continents, today approximately 70 % of its population (560 million) is urban, while urban areas (with a population density above 100 inhabitants.km^{-2}) account for some 25 % of the European Union's (EU) territory [EEA, 2007].

Urban areas are considered major sources of air pollution. In the past, urban air pollution was considered a local problem mainly associated with domestic heating and industrial emissions, which are now controllable to a great extent. Despite significant improvements in fuel and engine technology, present day urban environments are mostly dominated by traffic emissions [Colvile *et al.*, 2001; Fenger, 1999].

The combination of traffic emissions and densely packed buildings flanking narrow streets (street canyons) that characterise most of the urban environments is responsible for complex air pollutants concentration patterns including high peaks concentrations,

common known as hot spots. This is often the case near busy traffic axis in city centres, where urban building arrangements and microclimate may contribute to the creation of poor air dispersion conditions at street level.

Streets are in fact one of the most important urban elements, where population and traffic density are relatively high, and where human exposure to hazardous pollutants is expected to frequently occur [Xiaomin *et al.*, 2006]. Recent studies support that the adverse health effects due to air pollution close to major roads are larger than those of general pollution in the urban area [Edwards *et al.*, 2001; van Wijnen and van der Zee, 1998]. In this sense, population living and working close to major transport infrastructure may be at risk due to increased levels of air pollution. Estimations refer that approximately 9 % of the EU population would live closer than 200 meters from a major road with more than 3 million vehicles per year. The same study accounts for 25 % of the EU population living closer than 500 meters from such a major road [EC, 2006b].

During the last decade a significant improvement on urban air quality in Europe has been verified as result of mitigation policies in pollutant emissions from transport. This trend is expected to continue with the continuing implementation of restrictive EU directives on traffic emissions. However, the outlook for 2010 using Auto Oil II emission scenarios [EC, 2000] shows that 70 % of the EU urban population will still be exposed to PM_{10} (fraction of suspended particle matter with aerodynamic diameter less than 10 micrometer) levels exceeding the limit values, some 20 % to NO_2 (Nitrogen dioxide) exceedances, 15 % to Benzene exceedances and approximately 5 % to CO (Carbon monoxide) (Figure 1.1). This prevision distinguishes traffic exhaust emissions from other existent sources that in case of PM_{10} are mainly related to secondary and directly emitted particles transported over long distances. The figure indicates “potential exposure” as estimates are based on the assumption of exposure for a person permanently in ambient air (i.e. not taking into account indoor exposure) [EEA, 2001].

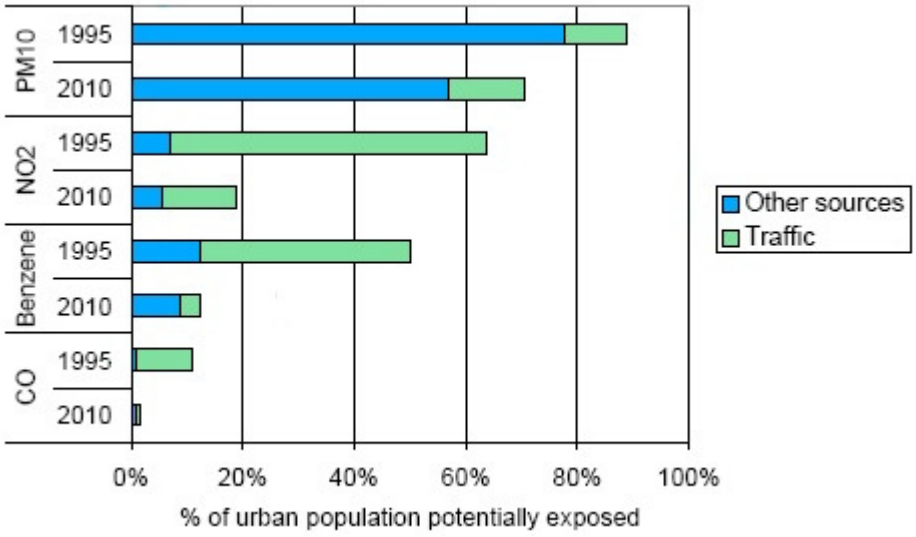

Figure 1.1 - Urban population potentially exposed to exceedances of EU urban air quality standards for PM_{10}, NO_2, Benzene and CO - 1995 and 2010 [EEA, 2001].

It is now generally recognised that many of the substances directly emitted by vehicles in the ambient air or indirectly produced through photochemical reactions represent a serious hazard for human health [Hoek *et al.*, 2000; WHO, 2001]. Particle Matter (PM) and Nitrogen Oxides (NO_x) are considered one of the most important traffic related pollutants with known acute and chronic effects on human health [Curtis *et al.*, 2006].

Health effects of air pollution is the result of a chain of events, which include release of pollution, atmospheric transport, dispersion and transformation and uptake of pollution before the health effects take place (Figure 1.2). The conditions for these events vary considerably and have to be accounted for, in order to ensure a proper assessment [Hertel *et al.*, 2001].

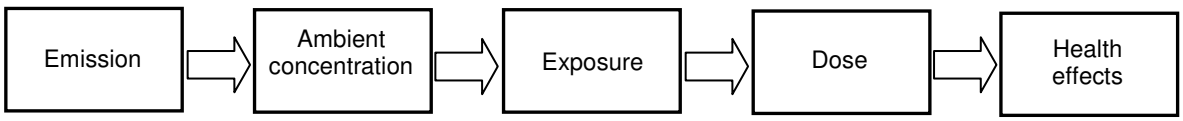

Figure 1.2 - Chain of events related to the health effects of air pollution [Hertel *et al.*, 2001].

Depending on the effects on human beings related to each substance, atmospheric pollutants are regulated with respect to different exposure times. The EU has developed an extensive body of legislation which establishes health based standards and objectives for a number of pollutants in air to be applied to all member states (Air Quality Framework Directive (AQ-FWD) - Council Directive 96/62/EC and Daughter Directives; New

Directive on Ambient Air Quality and Cleaner Air for Europe - IP/07/1895 and MEMO/07/571). The World Health Organisation (WHO) has also established its own air quality guidelines to offers guidance to governments around the world to improve air quality in their cities in order to protect people's health [WHO, 2000; WHO, 2006]. Table 1.1 summarizes the air quality standards established by both organisations.

Table 1.1 - Air quality standards defined by the European Union and the World Health Organisation.

	European Legislation	WHO
Pollutants	**Limit value**	**Air quality guidelines**
PM_{10}	50 $\mu g.m^{-3}$ (24 h) 40 $\mu g.m^{-3}$ (1 year)	50 $\mu g.m^{-3}$ (24 h) 20 $\mu g.m^{-3}$ (1 year)
$PM_{2.5}$	- 25 $\mu g.m^{-3}$ (1 year)*	25 $\mu g.m^{-3}$ (24 h) 10 $\mu g.m^{-3}$ (1 year)
NO_2	200 $\mu g.m^{-3}$ (1 h) 40 $\mu g.m^{-3}$ (1 year)	200 $\mu g.m^{-3}$ (1 h) 40 $\mu g.m^{-3}$ (1 year)
SO_2	350 $\mu g.m^{-3}$ (1 h) 125 $\mu g.m^{-3}$ (24 h) 20 $\mu g.m^{-3}$ (1 year)	500 $\mu g.m^{-3}$ (10 min) 20 $\mu g.m^{-3}$ (24 h)
Benzene	5 $\mu g.m^{-3}$ (1 year)	-
CO	10 $mg.m^{-3}$ (8 h)	100 $mg.m^{-3}$ (15 min) 60 $mg.m^{-3}$ (30 min) 30 $mg.m^{-3}$ (1 h) 10 $mg.m^{-3}$ (8 h)
O_3	240 $\mu g.m^{-3}$ (1 h) Alert threshold 180 $\mu g.m^{-3}$ (1 h) Information threshold 120 $\mu g.m^{-3}$ (8 h) Health protection	100 $\mu g.m^{-3}$ (8 h)
Pb	0.5 $\mu g.m^{-3}$ (1 year)	0.5 $\mu g.m^{-3}$ (1 year)

***** Limit value defined according to the New Directive on Ambient Air Quality and Cleaner Air for Europe (IP/07/1895 and MEMO/07/571), adopted on April 14th 2008.

Stricter air quality standards for annual means of PM_{10} and $PM_{2.5}$ are found in WHO guidelines compared to EU regulations. The daily limit value for $PM_{2.5}$ was still not included in the newest EU Directive on Ambient Air Quality being currently only established by the WHO.

More demanding thresholds are also found in WHO legislation for SO_2 and O_3 pollutants compared with EU guidelines. Limit values for NO_2, Pb and CO are equally settled by both organisations, nevertheless a more detailed temporal resolution is provided for CO by the WHO. Currently, benzene limit values are only established in the EU legislation.

However, concern focuses not only on ambient air quality in cities but also on indoor air quality in home and at workplace. In fact, the highest air pollution exposures occur in the indoor environment where people spend 80 to 90% of their time, and the percentage is still overall higher for some specific groups as children, elderly, disabled or sick people [EC, 2006a; WHO, 2001]. Some of the worst and most distressing respiratory problems triggered by air pollution are among children, since they can be particularly sensitive to environmental stresses [EEA, 2005]. Children, as sensitive human beings, can be regarded as 'biomarkers' for environmental threats, not only because they are more at risk but because they can also provide early warnings of hazards to others, as well as being effective points of intervention for the prevention of disease in their later lives [EEA, 1999].

In contrast to the elaborated and implemented EU ambient air policies, under the form of the Air Quality Framework Directives and the New Directive on Ambient Air Quality and Cleaner Air for Europe, an integrated EU policy on indoor air quality is not available. Currently, indoor air quality is fragmentally tackled in sector oriented policies through several EU Directives: construction products directive (89/106/EEC); energy performance of buildings directive (2002/91/EC); gas appliances directive (1990/396/EEC); heating appliances directive (1992/42/CEE); eco-design directive (2005/32/EC); dangerous substance directive (1976/646/EEC); general product safety directive (2001/95/EC). These EU directives include explicitly an indoor air quality aspect, or indirectly regulate indoor air quality, but none of them establishes fixed indoor air quality standards [Avgelis and Papadopoulos, 2004; EC, 2007].

Concretely, the directive on energy performance of buildings (2002/91/EC) imposes its partial transpose to each member state, providing indication for the assurance of proper indoor quality. Each member state is then responsible for establishing its own indoor air quality standards. For Portugal, and according to the correspondent national legislation (Decreto-Lei nº79/2006 de 4 de Abril, Regulamento dos Sistemas Energéticos e de Climatização dos Edifícios (RSECE)), the maximum reference indoor concentration is settle for the following pollutants: 0.15 $mg.m^{-3}$ (PM_{10}), 1800 $mg.m^{-3}$ (CO_2), 12.5 $mg.m^{-3}$ (CO), 0.2 $mg.m^{-3}$ (O_3), 0.1 $mg.m^{-3}$ (formaldehyde), and 0.6 $mg.m^{-3}$ (VOC's). These limit values followed the recommendations of the WHO. Supplementary national legislation is currently being prepared in order to establish the temporal basis of the reference indoor concentrations and the measurement methodology to be used for the assessment of indoor air quality.

The already mentioned WHO air quality guidelines are currently also applicable to indoor environments, but new specific standards on indoor air quality are expected to be published till 2009 [WHO, 2007].

Indoor air pollutants are derived from a wide range of sources, including the occupants and their activities (e.g. smoking, cooking, vacuuming), heating appliances, furnishings, building materials and penetration of contaminated air from outdoors. The number of pollutants present in the indoor environment and their diversity is immense. The main indoor air pollutants are: inorganic pollutants (Carbon monoxide, Nitrogen oxides - NO_2 and NO -, Particulate Matter, Carbon dioxide - indicator of ventilation rate); organic pollutants (volatile organic compounds, formaldehyde); and specific indoor air pollutants (environmental tobacco smoke, man-made mineral fibres, radon) [EC, 2006b; WHO, 2000].

A major source of pollutants to indoor air is in fact ambient air pollution due to traffic and urban and industrial activities, which come into the building through the ventilation system or by infiltration (building envelop permeability) [EC, 2006a; Götschi *et al.*, 2002; Hodgson *et al.*, 1992; Liao *et al.*, 2004]. In particular, and in the absence of smoking, the most important source of indoor air particles is usually outdoor air. Penetration of particles from outdoor air into indoor spaces is therefore a matter of great interest for indoor air exposure [EC, 2006a]. The same applies to other pollutants, such as NO_2, which have as major source indoors the outside air (vehicle emission) [Bostrom, 1993; EC, 2006a; Poupard *et al.*, 2005]. Local peak concentrations in residences can be also originated from specific sources, e.g. gas stoves, wood stoves, fireplaces, kerosene heaters and candles. In offices, electrostatic equipment (photocopying machines and laser prints) should be accounted as major sources of NO_2. Tobacco smoke is also a contributing source of this pollutant [EC, 2006a].

In order to evaluate the real impacts of urban air pollution in the population health is then necessary to undergo a complete assessment of human exposure to atmospheric pollutants that includes both outdoor and indoor exposure assessments. It is important to distinguish between long- and short-term exposures because of the differences in their health effects. Thus, the long-term is related to extended time periods of exposure leading to chronic health effects, whereas in the short-term, high exposure may show little effect on human beings unless extremely high concentrations are reached.

Exposure studies can be carried out with the aim of obtaining estimates of the exposure of the individual (personal exposure) or for a larger population group (population exposure), through direct or indirect methods. Direct methods are measurements made by personal portable exposure monitors or biological markers. These are, however, invasive and expensive techniques. The personal exposure monitoring devices that people carry with them must be lightweight, silent, highly autonomous and still one week is about the maximum time that any population representative sample of individuals will comply with personal exposure measurements. On the other side, biological markers are indicators of changes or events in human biological systems. For example, a metabolite of some exogenous substance found in a person's blood or urine might be considered a marker of the person's exposure to that substance in the environment.

In indirect methods, the exposure is determined by combining information about the time spent in specific locations, called microenvironments, with the pollutants concentrations at these same places. A microenvironment is defined as a three-dimensional space where the pollution concentration at some specified time is spatially uniform or has constant statistical properties [Hertel *et al.*, 2001]. The microenvironment can be the interior of a car, inside a house, inside an office or school, outdoors. A constraint for using the indirect methods is that the residence time of the person (termed the time-activity pattern) needs to be known together with the pollution concentrations in each of the microenvironments at the time when the person is present.

Data from fixed monitoring sites are frequently used as an approach to characterise outdoor concentrations in urban areas. Nevertheless, these local measurements cannot reflect the complex temporal and spatial distribution of pollutants concentrations observed in urban areas. Also, often, monitoring in streets is performed at 2.5 to 3 m height, which is above the heads of pedestrians.

Another possibility is using modelling techniques to estimate outdoor and indoor pollutants concentrations to different locations where people spend their time. In this sense, air quality models can be used as important tools for the assessment of exposure to atmospheric pollutants since they are able to provide detailed information on wind flow and pollutant transport in urban areas. Air quality models have also the major advantage of contributing to estimate past and predict future exposures, as well as exposures for large populations, that cannot be achieved by monitoring [EC, 2006a].

1.2. State of the art on microscale exposure modelling

Field measurements, laboratory-scale physical modelling and air pollution modelling techniques are the common tools used to study the wind flow and pollutants distribution in urban areas [Li *et al.*, 2006; Sabatino *et al.*, 2007]. Air pollution measurements provide quantitative information concerning pollutants concentration but are limited to specific locations where air quality stations are sited. On the other hand, wind-tunnel experiments have the capability to examine the effects of various parameters individually or in a controlled combination. For example, Park *et al.* (2004) characterized the dispersion of vehicle emissions by conducting wind tunnel tests and applying tracer gas techniques.

The need of accurate evaluation of the flow field and the pollution dispersion in an urban area without using complex experimental setups has updated the role of air pollution modelling. This technique is also the only method that quantifies the relationship between emissions and concentrations, including the consequences of future scenarios and the determination of abatement strategies [Builtjes, 2003].

There is a plethora of different air quality models specially developed for, or simply used, in local or street canyon applications (e.g. statistical, receptor, screening, box, street canyon, gaussian and computational fluid dynamics (CFD)) [Vardoulakis *et al.*, 2003]. The physical and/or mathematical principles allow distinguishing between the different models.

Recently, and with the continuous increase of hardware capabilities and the optimisation of numerical methods, CFD has become an attractive tool to predict flow and concentration fields near buildings. CFD modelling is a general term used to describe the analysis of systems involving fluid flow, heat transfer and associated phenomena (e.g. chemical reactions) by means of computer-based numerical methods. It is a powerful modelling technique spanning a wide range of industrial and more recently environmental and biomedical applications [Gosman, 1999]. Many works can be found in the literature reporting on the use of computational fluid dynamics techniques to model flow and pollutant dispersion around isolated buildings or groups of buildings [Borrego *et al.*, 2003b; Li *et al.*, 2006; Neofytou *et al.*, 2006; Sabatino *et al.*, 2007].

CFD's are the only models that allow a detailed estimation of spatial and temporal distribution of air pollutants in complex urban areas, contributing to the identification of sensitive urban areas in terms of air quality and with potential harmful effects to human health. Air quality models may then serve as useful tools for indirect estimation of human

exposure to outdoor air pollutants, providing valuable information concerning pollutants concentration in the ambient air where people meet [EC, 2006a].

Studies were recently published relating human exposure estimation in urban areas with ambient air concentrations determined with CFD modelling applications. The three-dimensional (3D) CFD model MISKAM have been successively implemented to provide better assessments of exposure to traffic related air pollutants in urban areas [Lohmeyer *et al.*, 2002]. Borrego *et al.* (2006) developed a methodology to estimate population exposure to traffic-related particulate air pollution in urban areas based on the estimation of ambient pollutant concentrations with the CFD model VADIS. Results for the Lisbon city centre showed a large number of persons exposed to PM levels exceeding the legislated limit values. Computational fluid dynamics was also used by McNabola *et al.* (2008) to investigate whether pedestrians using the boardwalk would have a lower air pollution exposure than those using the adjoining footpath along the road. The results of the study show significant reductions in pedestrian exposure to both traffic derived particulates and hydrocarbons along the boardwalk as opposed to the footpath.

Recent examples of outdoor exposure assessment using simpler air quality models are also available. The semi-empirical street canyon model OSPM was applied to 22 selected street sections in Copenhagen (Denmark) to determine the exposure to air pollution from traffic of the bus drivers and letter carriers operating along the study area during their working days [Hertel *et al.*, 1996]. Johansson *et al.* (1999) evaluated population exposure to NO_2 and particulate matter within the SHAPE study (Stockholm study on health effects of air pollution and their economic consequences) using information from a multiple-source emission and Gaussian dispersion modelling system.

In some cases, models have been developed specifically for exposure modelling based in a time-microenvironment-activity concept. This modelling approach calculates exposure as the product of the concentration in a microenvironment and the time spent in that microenvironment. Thus total exposure is the sum of the exposures in all microenvironments during the time of interest.

Exposure models can be classified as statistical, mathematical (numerical) and mathematical (numerical)-stochastic models [Kousaa *et al.*, 2002]. Statistical models are based on the historical data and capture the past statistical trend of pollutants [Goyala *et al.*, 2006] The mathematical modelling involves application of emission inventories, combined with atmospheric dispersion and population activity modelling. The stochastic

approach attempts to include a treatment of the inherent uncertainties of the model (e.g., caused by the turbulent nature of atmospheric flow) [Burke *et al.*, 2001].

Mathematical modelling utilising emission and dispersion models is also called deterministic modelling. Most recently, mathematical exposure models applied to urban areas have been presented by Jensen (1999), Kousaa *et al.* (2002) and Wu *et al.* (2005). The model presented by Jensen (1999) is based on the utilisation of traffic flow computations and the operational street pollution model (OSPM) for evaluating outdoor air pollutant concentrations in urban areas. The activity patterns of the population have been evaluated using various administrative databases and standardised time-activity profiles. The modelling system utilises a GIS in combining and processing the concentration and population activity data. The model was applied to evaluate population exposure in one specific municipality in Denmark. An advantage of this system is that the application of a street canyon dispersion model facilitates a fine-scale spatial resolution (meters or tens of meters). However, the complexity of the model computations requires a limitation in the spatial domain to be evaluated; the computations for a more extensive area, such as that of a major city, were not possible.

Kousaa *et al.* (2002) presented a mathematical model to determine the human exposure to ambient air pollution in an urban area through the combination of predicted pollutant concentrations, information on people's activities (such as the time spent at home, in the workplace and at other places of activity during the day) and location of the population. Time-microenvironment activity data for the working-age population was obtained from the EXPOLIS study (Air pollution distributions within adult urban populations in Europe). The concentrations of NO_2 were modelled over the Helsinki Metropolitan Area using both CAR-FMI and UDM-FMI models, to evaluate the dispersion of pollution originating from vehicular traffic and the dispersion from stationary sources, respectively.

An Individual Exposure Model (IEM) was developed by Wu *et al.* (2005) to retrospectively estimate the long-term average exposure of the individual children from Southern California to CO, NO_2, PM_{10}, $PM_{2.5}$, and elemental carbon of ambient origin. In the IEM model, pollutant concentrations due to both local mobile source emissions and meteorologically transported pollutants were taken into account by combining a line source dispersion model (CALINE4) with a regional air quality model (SMOG). Information from the Southern California Children's Health Study (CHS) survey was used to group each child into a specific time-activity category, for which corresponding time-activity profiles were sampled.

The information needed in such exposure studies include location of the activity, the period or time when the activity took place (e.g., time of day, phase in life), and the duration of the activity. A review of time–activity patterns in exposure assessment is given in Ackermann-Liebrich *et al.* (1995).

Nevertheless, none of the current exposure models applied to urban areas take into account the importance of 3D pollutant transport on the exposure assessment of people living in high-rise apartment buildings. Jo and Lee (2006) demonstrated the importance of this type of studies for a correct assessment of exposure by analysing the relation of measured outdoor and indoor pollutants concentrations of lower-floors and higher-floors in a building located near a major traffic road in Korea.

Once the outdoor concentration has been calculated by air quality models, the indoor pollutant concentration can be modelled based on an understanding of the ways in which indoor air becomes exchanged with outdoor air, together with the deposition or decay dynamics of the pollutants, and with indoor emission source rates characterisation. Several methodologies exist to estimate indoor air pollution concentrations from outdoor modelled concentrations. These include a variety of empirical approaches based on statistical evaluation of test data and a least-squares regression analysis; deterministic models based on a pollutant mass balance around a particular indoor air volume; or a combination of both approaches. Most of the currently available studies [Baek *et al.*, 1997; Borrego *et al.*, 2006; Chau *et al.*, 2002; Monn, 2001; Wu *et al.*, 2005] are based on experimental data, resulting from measurements of outdoor and indoor concentrations for different microenvironments in order to establish a relation between indoor and outdoor (I/O) concentrations. There are several parameters affecting the I/O ratio, such as: the penetration coefficient, the deposition rate and the air exchange rate between the indoor and the outdoor air, and that are directly dependent on the types of ventilation used (natural ventilation, mechanical ventilation or both) [Liao *et al.*, 2004]. The penetration coefficient, p, is a measure of the ability of a pollutant to penetrate the building envelope ($0 \leq p \leq 1$) [Riley *et al.*, 2002]. On the other hand, the air exchange rate is a measure at which outside air replaces indoor air in a space. As the contribution of these phenomena may be very different from one building to another, measured indoor to outdoor concentration ratios (I/O) may vary significantly [Poupard *et al.*, 2005]. Ventilation is therefore a major driver of air quality in indoor environments since it promotes the dilution of concentrations from indoor sources and, on the other hand, works as a transport mechanism for outside pollutants be brought inside [EC, 2003].

Outside air enters into the building due to infiltration through cracks and openings in the building envelope[1], via natural ventilation when windows are open, as well as via forced ventilation systems that induce air exchange, such as fans, and blowers [Milner *et al.*, 2005].

Simple I/O relations were used in Borrego *et al.* (2006) to determine PM_{10} indoor concentrations ($\mu g.m^{-3}$) in different microenvironments based on estimated outdoor concentrations and considering diurnal and nocturnal periods (Table 1.2). The day/night time is classified not as a function of sunlight but in relation to the human activity pattern. These empirical functions were extrapolated from outdoor and indoor concentration measurements and derive from different published studies [EPA, 1997; Gulliver and Briggs, 2004].

Table 1.2 - I/O functions [Borrego *et al.*, 2006].

Microenvironment	I/O function
Residence	$C_{indoor}(day) = 48 + 0.51C_{outdoor}$ $C_{indoor}(night) = 20 + 0.52C_{outdoor}$
Office	$C_{indoor}(day) = 48(1-0.14) + 0.51C_{outdoor}$ $C_{indoor}(night) = 20(1-0.14) + 0.52C_{outdoor}$
Schools	$C_{indoor} = 48(1-0.24) + 0.51C_{outdoor}$
In vehicle	$C_{car} = 13.1 + 0.83C_{outdoor}$

The previous empirical I/O relations do not explicitly account for the specific characteristics of the building, such as the ventilation rate and the penetration coefficient. This fact restrains the use of these empirical factors in other urban areas for a more precise quantification of indoor concentrations from outdoors.

Kruize *et al.* (2003) proposed a general empirical formulation to estimate indoor concentrations in case of no measured data available:

$$C_{in} = C_{out}\,p_i + S_i \qquad (1.1)$$

where C_{out} is the ambient outdoor concentration, p_i the effective penetration factor of the air pollutant in microenvironment i and S_i the contribution of indoor sources in microenvironment i.

[1] Building envelope includes everything that separates the interior of a building from the outdoor environment, including the doors, windows, walls, foundation, basement slab, ceiling, roof and insulation.

To calculate indoor concentrations due to penetration of outdoor air, a single-compartment, steady-state mass balance equation is presented in Koutrakis *et al.* (1992) and Burke *et al.* (2001):

$$C_{in} = \frac{paC_{out}}{a+k} + \frac{Q_{is}}{(a+k)V} \qquad (1.2)$$

where p is the penetration coefficient; a the air exchange rate (AER) (h^{-1}); k the decay rate (h^{-1}); Q_{is} the mass flux generated by indoor sources ($\mu g.h^{-1}$), and V is is the room or building interior volume (m^3).

In Burke *et al.* (2001) and Kruize *et al.* (2003), the air exchange rate, one of the parameters that most influence the relation between outdoor and indoor concentrations, was extrapolated from existing databases from the study area. This imply that large experimental setups were previously conducted to measure the air exchange rate for each building, information that is not often accessible for all urban areas.

Recently the outdoor airflow and pollutant dispersion, and the penetration of outdoor pollutants indoor in an isolated urban building were investigated computationally using a CFD model [Lai and Chan, 2007]. The objective was to study how outdoor pollutants penetrate indoor and relate this pattern to different building geometric configurations. This methodology, however, only allows the application to a unique building and not to a complex urban area. The high resolution mesh and consequent computational effort necessary for a full characterisation of flow around the building openings restrain the possibility of extending this study to a larger group of buildings.

Numerical ventilation modelling can be a valuable tool to help determine air exchange rates when measurements are not available. In the current state of knowledge no work was still conducted on integrating numerical ventilation modelling in mathematical exposure models. The same applies in the integration of building resolving models, like CFD models, leaving an important development area for the assessment of exposure, which will be addressed in this work.

1.3. Research objectives and structure of the work

This work intends to contribute to the study of human exposure to atmospheric pollutants in urban built-up areas. In this sense, the main goals of this study are the development of a three-dimensional (3D) Microscale EXPOsure model (MEXPO) to estimate the short-term

individual exposure to atmospheric pollutants and its application to a specific urban area in order to assess the exposure to air pollutants of children with known respiratory problems.

In MEXPO model, the flow and outdoor pollutants concentrations fields around buildings are determined through a microscale CFD model. The theoretical bases of this type of models are described in Chapter 2, as well as, its functioning scheme.

For microscale air quality models be used with confidence in exposure studies, they need to be properly tested and evaluated. Chapter 3 presents an evaluation protocol for microscale models. The results of its application through a validation exercise are also described in the same chapter.

MEXPO model is described in detail in Chapter 4. Special attention is given to the characterisation of outdoor pollutants transport processes to indoors in order to assess indoor concentrations. Ventilation modelling appears as an important tool to predict the air exchange rates in wind-induced natural ventilated spaces.

Chapter 5 describes the experimental field campaigns conducted during summer and winter periods in a selected urban area, that allowed the characterization of air quality in different microenvironments and the determination of the time-activity pattern of children present in the study area. In the same chapter is presented the application of the MEXPO model to the study area in order to estimate the short-term individual exposure to air pollutants of children. Indoor and outdoor concentrations, and ventilation rates, estimated with MEXPO model are compared with site measurements.

Chapter 6 presents the conclusions of the work and indicates possible tasks to be developed in the future.

2. AIR QUALITY MODELLING IN THE URBAN ENVIRONMENT

The impact of air pollution on urban environments became an important research issue in Bitan (1992), Georgii (1969) and Oke (1988), leading to numerous modelling studies related to the influence of buildings and other urban structures on pollutant accumulation/dissipation patterns. Nowadays, the fundamentals of the physical and chemical processes occurring during air pollutant transport in the urban atmosphere are understood to a large extent. In particular, modelling of such processes has recently experienced a remarkable growth with the rapid increase of computer capabilities.

2.1. Microscale models

Air quality models can be classified with respect to the scale of the phenomena they are developed to simulate. In fact, scale separation has proven to be a quite successful approach for atmospheric modelling, because different approximations and parameterisations can be applied for the different phenomena occurring in the different scales (Figure 2.1 a). Specific-scale models should be capable of simulating in detail phenomena occurring in that scale [Moussiopoulos, 2003].

For the urban area, in particular, it is possible to distinguish the local scale models, which include street canyon models, and the urban scale models (Figure 2.1 b). The former are resolving buildings and other obstructions in the urban canopy, the latter describe them by means of suitable parameterisations, i.e. mathematical formulae linking characteristic properties of the urban canopy to other key model variables. The phenomena at the local and urban scales have a horizontal extension of several meters to 500 km and a characteristic time scale of several minutes to several days.

Both *local scale model* and *microscale model* designations are commonly used to classify the same scale phenomena in urban applications adjusted to domain sizes of the order of several tens of metres to a few quilometres (street canyons, city quarters). The different classification lies on the intersection of the engineers and the meteorologists perspectives of cities. In order to keep a coherent approach, the *microscale model* designation was adopted along this work.

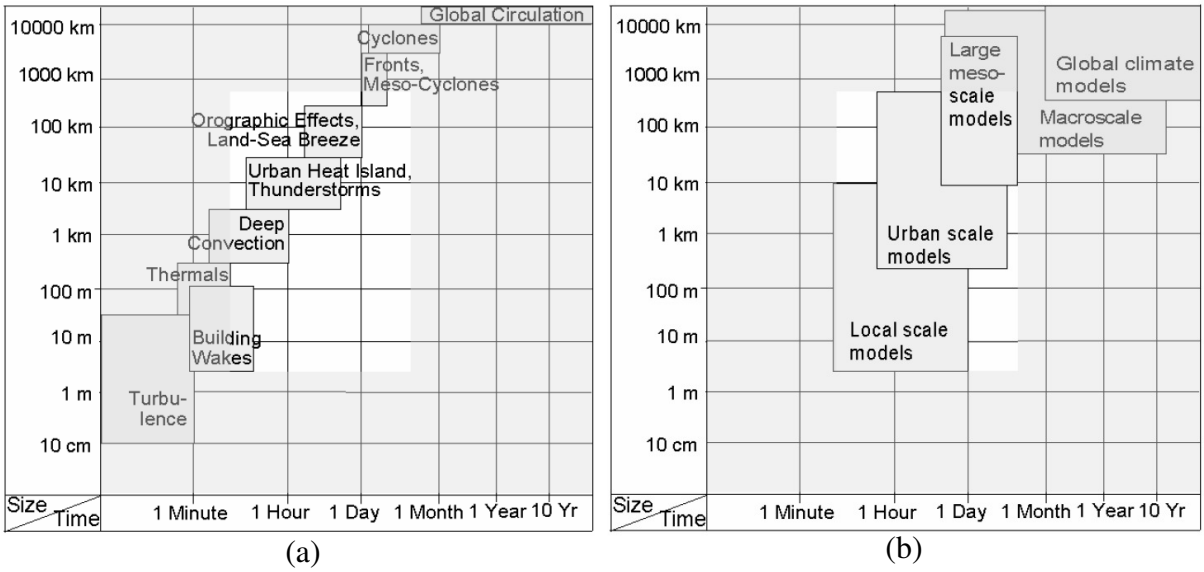

Figure 2.1 - Characteristic time scale (abscissa) and characteristic horizontal scale (ordinate) of common atmospheric phenomena (a), and of atmospheric models (b) [Moussiopoulos, 2003].

Within microscale domains, the street scale is of particular interest for urban air quality as it is the smallest scale that encompasses one of the main pollutant sources, the vehicles and an important receptor, the public, and thus is likely to be the scale that determines the extreme values of pollutant concentration.

The term street canyon ideally refers to a relatively narrow street with buildings lined up continuously along both sides [Nicholson, 1975]. However, the same term has been used to refer to larger streets, also called avenue canyons. In the real world, a broader definition of the term has been applied, including urban streets that are not necessarily continuously flanked by buildings on both sides, allowing thus for some openings on the walls of the canyon.

A street canyon constitutes the basic geometric unit of urban areas. This unit is also bounded by the ground surface at the bottom and the roof level at the top. It has a distinct

climate where microscale meteorological processes dominate [Oke, 1988] and the air ventilation and pollutant removal are mainly through the roof level.

The most important features of street-canyon micro-climate are the wind-induced flow patterns, such as air recirculation. These unique micro-scale meteorological processes not only affect the local air quality but also the comfort of the city inhabitants [Bottema, 1993].

The wind flow pattern inside street canyons depends on their geometry, in particular, the building-height-to-street-width aspect ration (H/W, where H is the building height and W is the street width) (Figure 2.2). The flow on this scale has been characterised as a recirculating eddy within the street canyon driven by the wind flow at the top with a shear layer separating the above-canyon flow from that is within [Hosker, 1985]. When the street canyon is relatively deep the primary vortex will not extend to the ground and there may be a weak contra-rotating vortex near the ground. The primary vortex may not extend completely across the street if the street canyon is relatively shallow. There are variations on this flow due to wind directions not normal to the street axis, different street canyon geometries from the simple idealised one, and the mean flow and turbulence generated by vehicles within the street canyon [Pavageau *et al.*, 2001].

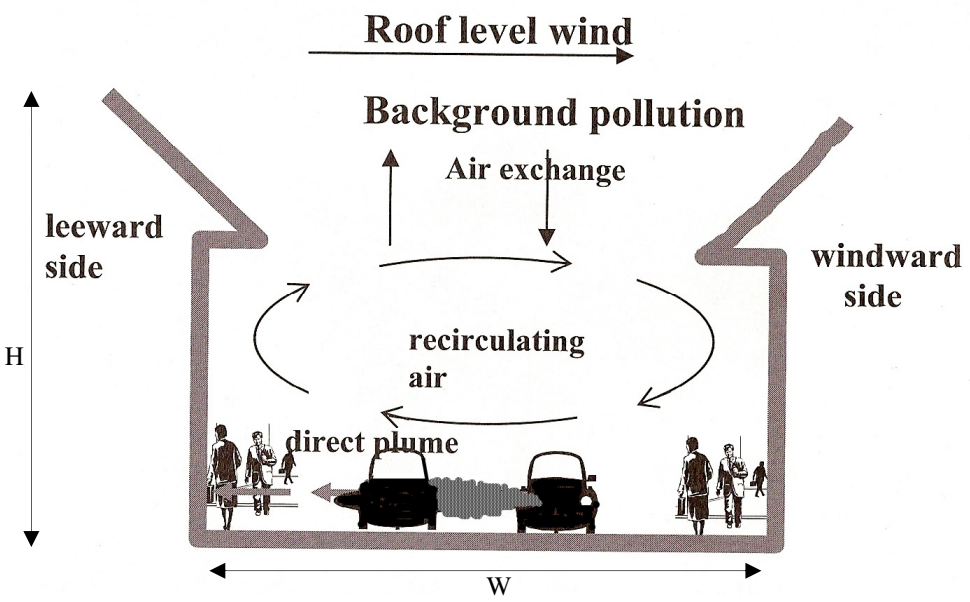

Figure 2.2 - A schematic view of the flow in a street canyon (adapted from [Britter, 2003]).

Pollutant emissions from vehicles will dilute as they exit the vehicle exhaust initially through a jet-like mixing process, followed by the turbulence in the vehicle wake, then by

the turbulence in the street canyon as a whole. The recirculating eddy will advect the pollutants released near the ground level towards the lee wall and away from the downwind wall. Thus higher concentrations are anticipated and observed on the lee wall.

The average level of pollutant concentrations within the street canyon is a balance between the emissions within the canyon, and the exchange of pollutants between the street canyon and the flow above, and/or with other streets. The exchange is a two-way process with street-sourced material being removed and material from other sources upwind being brought into the street [Britter, 2003].

The current state of the art on street canyon pollution research over microscale domains includes the use of Computational Fluid Dynamics models. As it was mentioned in Chapter 1, CFD models emerged mainly during the last decade due to continuous increase of hardware capabilities and the optimisation of numerical methods as an accurate tool for predicting urban airflow patterns and air pollutants dispersion in urban environments [Borrego *et al.*, 2003b; Hassan and Crowther, 1998; Jicha *et al.*, 2000]. With high spatio-temporal resolutions, they can give more comprehensive information on the flow and pollutant transport phenomenon.

CFD can be divided into Reynolds averaged Navier-Stokes equation (RANS) modelling and Large Eddy Simulation (LES). RANS is a CFD method that uses turbulence models to simulate the turbulent flow. This type of model is currently the industrial standard in engineering practice. RANS can be modified to handle urban and microscale wind flow problems and are the most commonly adopted CFD models in calculating street-canyon wind flow. In LES modelling the time-dependent flow equations are solved for the mean flow and the largest eddies, whereas the effects of the small eddies are modelled. Since the largest eddies interact strongly with the mean flow and contain most of the energy, this approach results in a good model of the main effects of turbulence. Compared with RANS models, LES has the advantage of describing the large scale turbulent structures and hence, can be used in a more accurate and reliable way in the prediction of the flows over bluff bodies that involve unsteady separation and vortex shedding [Yang, 2004]. However, this technique is presently at the research stage and the calculations are too costly to merit consideration in the current computation capabilities. Although anticipated improvements in computer hardware may change this perspective in the future, this work will be focused in the RANS modelling technique.

The following subchapter describes the theoretical and functioning aspects of VADIS CFD model that was developed and has been continuously improved at the Department of Environment and Planning of the University of Aveiro. VADIS CFD model was used in this work as the main feature of the Microscale Exposure Model (MEXPO) for the determination of flow and outdoor pollutant concentrations in urban areas.

2.2. VADIS CFD model

The CFD model VADIS was developed in 1998 at the Department of Environment and Planning of the University of Aveiro as a tool to estimate flow and pollutants dispersion resulting from accidental and uncontrolled releases of chemical products to the atmosphere, under unfavourable and complex dispersion conditions (low wind speed), near a single obstacle [Martins, 1998].

Since its first version, VADIS has been in continuous development. It was adapted to the calculation of urban air pollution due to traffic road emissions in urban built-up areas by improving its capability to support multi-obstacle and multi-source description, as well as, time varying flow fields and time varying emissions. These updates allowed the evaluation of maximum short-term local concentrations of traffic related pollutants in urban geometries, specially under low wind speed conditions [Borrego *et al.*, 2003b].

A graphical interface with the purpose of a friendlier user access was developed in the scope of SUTRA (Sustainable Urban TRAnsportation) European project allowing, in a simple way, to configure the input parameters of VADIS model, and to represent graphically the input and the output data [Borrego *et al.*, 2002].

VADIS structure is based on two modules, FLOW and DISPER (Figure 2.3). The first module, FLOW, is a Reynolds Averaged Navier-Stokes (RANS) prognostic model with a standard k-ε turbulence closure that calculates the wind components, the turbulent viscosity, the pressure, the turbulent kinetic energy, the energy dissipation and the temperature 3D fields through the finite volume method. The second module, DISPER, applies the lagrangian approach to the computation of the 3D concentration field of inert pollutants using the wind field estimated by FLOW [Borrego et al., 2003b].

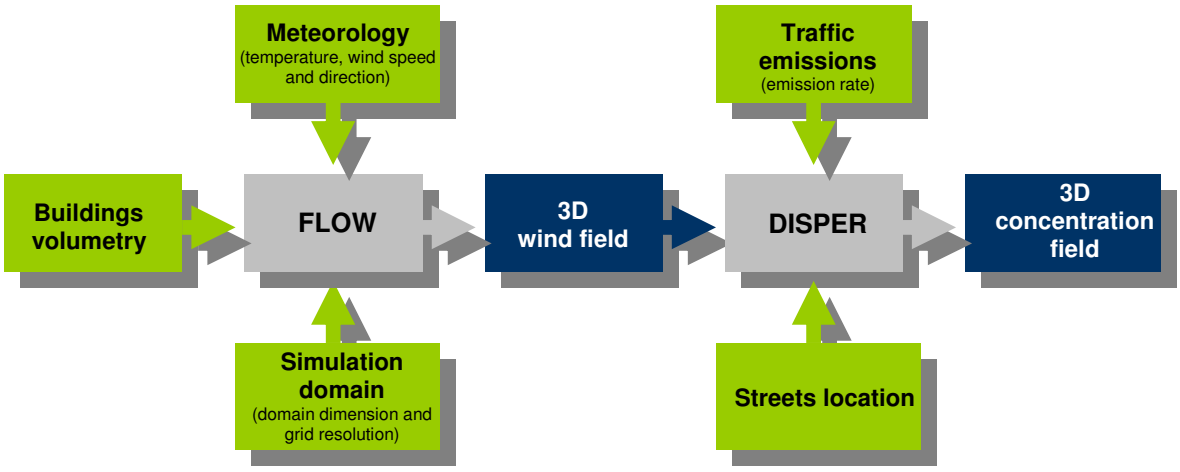

Figure 2.3 - Schematic representation of input and output data for FLOW and DISPER modules.

According to Figure 2.3, VADIS requires information that allows characterising the simulation domain, the meteorological conditions at the entrance of the domain, and the emissions for the considered period of time.

The separation of flow estimation from pollutants dispersion can be seen as a major advantage of VADIS compared with the common CFD models that resolve the advection-diffusion equation coupled with flow equations. This feature allows to obtain a flow database for a specific urban area, that is permanently available for the estimation of pollutants dispersion with a lower computer running time.

The theoretical basis of VADIS CFD model, namely of FLOW and DISPER modules, and its functioning scheme are described in the following subchapters.

2.2.1. FLOW module

The fundamental governing equations of fluid dynamics, i.e. the continuity, momentum and energy equations are included in the FLOW module. These equations are the mathematical statements of three fundamental physical principles: conservation of mass, Newton's second law and first law of thermodynamics.

The equation for the conservation of mass (also referred to as the continuity equation) is discretised by means of a mass balance for a finite control volume. Thus for a steady incompressible fluid with uniform temperature, the incoming mass flow is equal to the outgoing mass flow (Eqn.2.1).

$$\frac{\partial u_i}{\partial x_i} = 0 \qquad (2.1)$$

By applying Newton's second law of motion, the relationship between the forces on a control volume of fluid and the acceleration of the fluid gives an expression for the conservation of momentum (or Navier-Stokes equations). The Cartesian tensor notation can be used to write the Navier-Stokes equations for an incompressible Newtonian fluid, excluding in the context of boundary layer flows the term that describes the influence of the earth's rotation (Coriolis effect) (Eqn. 2.2). Also, in FLOW module the inertia term is replaced by a new one that includes the effect of buoyancy [Andrade, 1988].

$$\rho u_j \frac{\partial u_i}{\partial x_j} = -\frac{\partial P}{\partial x_i} + \mu \frac{\partial^2 u_i}{\partial x_j^2} + \rho \beta g_i (T - T_0) \quad \text{(i= 1,2,3)} \qquad (2.2)$$

The first law of thermodynamics states that the rate of change of energy of a fluid particle is equal to the rate of heat addition to the fluid particle plus the rate of work done on the particle. The energy equation (Eq. 2.3) can be written as

$$\rho C_p u_i \frac{\partial T}{\partial x_i} = \lambda \frac{\partial^2 T}{\partial x_i^2} \qquad (2.3)$$

assuming simplifications on the temporal term and on the term related to the increase of enthalpy due to viscous dissipation, and using the temperature variable instead of enthalpy.

The equation of state (Eqn. 2.4) provide the linkage amongst the energy equation, mass conservation and the momentum equations allowing the determination of velocity, temperature and pressure throughout the flow field. The ideally gas law adequaly describes the state of gases in the boundary layer (Eqn. 2.4):

$$P = \rho RT \qquad (2.4)$$

where, from Eqn.2.1 to Eqn.2.4:

ρ density [kg.m^{-3}]

P pressure [kg.m^{-1}.s^{-2}]

u instantaneous velocity [m.s^{-1}]

μ dynamic viscosity [kg.m^{-1}.s^{-1}]

τ_{ij} viscous stress [N.m^{-2}]

x_i, x_j coordinate variable [m]

T temperature [K]

λ thermal conductivity [$W.m^{-1}.K^{-1}$]

R ideal gas constant [$J.\ kg^{-1}.K^{-1}$]

C_p specific heat [$J.\ kg^{-1}.K^{-1}$]

g gravity [$m.s^{-2}$]

β Coefficient of thermal expansion [K^{-1}]

2.2.1.1. Turbulence modelling

The instantaneous Navier-Stokes equations can, at the present, only be solved for the most simple flows, i.e. laminar flows and some transitional flows (transitional in terms of laminar fluid becoming turbulent). For more complex turbulent flows that display high Reynolds number, such as those found in the vast majority of wind engineering situations, and considering the presently computer limitations, the Navier-Stokes equations need to be averaged in order to be applied. For this purpose, the instantaneous velocity, $\hat{u}$, can be assumed to comprise the sum of a mean component, u, and a turbulent component, u' as shown in equation (2.5).

$$u = \bar{u} + u' \tag{2.5}$$

In order to produce a set of time-averaged equations, equation (2.5) is substituted into equations (2.1) (2.2) and (2.3), which is then integrated over time to obtain mean flow equations. All terms of the considered equations, except the second term on the right side of equation (2.2) and the right term of equation (2.3), contain only a single fluctuating quantity. For this reason, the averaging process results in the instantaneous value being replaced by the mean of each variable in question. As a result of this process an extra term appears on the right-side of the energy and Navier-Stokes equations corresponding to the contribution of turbulence

Energy: $$-\rho \frac{\partial}{\partial x_j}(\overline{u_j' T'}) \tag{2.6}$$

Momentum: $$-\rho \frac{\partial}{\partial x_j}(\overline{u_i' u_j'}) \tag{2.7}$$

The term $-\overline{u_i' u_j'}$, representing the Reynolds stress tensor is symmetric, hence there are six independent unknown Reynolds stress components (three normal stresses and three shear stresses). In order to close the system of mean flow equations, assumptions are needed for the extra unknown terms generated by the averaging process. This procedure of solving closure problems is called turbulence modelling.

Turbulence modelling is used to achieve closure of the time-averaged governing fluid flow equations by providing a scheme for the evaluation of the Reynolds stress terms. This turbulence modelling technique, identified as the RANS approach, is used in the FLOW module.

RANS models are based on the concept of eddy viscosity. This concept assumes that an analogy exists between the action of viscous stresses and Reynolds stresses on the mean flow. Boussinesq proposed that the Reynolds stresses could be linked to mean rates of deformation, i.e.,

$$-\overline{u_i' u_j'} = \nu_t \left(\frac{\overline{\partial u_i}}{\partial x_j} + \frac{\overline{\partial u_j}}{\partial x_i} \right) - \frac{2}{3} \delta_{ij} k \qquad (2.8)$$

where $\nu_t = \mu_t / \rho$ (turbulent kinematic viscosity and turbulent dynamic viscosity, respectively) and *k* is the turbulent kinetic energy given by $k = 1/2(u_i'^2) = TKE / \rho$

In 1879 Reynolds assumed as equivalent the turbulent viscosity and the turbulent diffusivity, despite the ratio between both parameters, named the turbulent Schmidt number, is defined in literature between 0.7 and 1. The same analogy can be used to define the turbulent diffusivity of other variables. Consequently,

$$\overline{-u_i' T'} = \Gamma_T \frac{\partial T}{\partial x_j} \qquad (2.9)$$

where Γ_T is named turbulent thermal diffusivity. These diffusivities are usually related to the turbulent viscosity by contants named turbulent Prandtl number of variable X, that are represented by σ_x. The turbulent Prandtl number for temperature can be used to define $\Gamma_T = \nu_t / \sigma_T$.

Using the above mentioned approximation and considering that *u*, *P* and *T* variables are now representing average values, the Navier-Stokes equation (2.2) can be presented as

$$\rho u_j \frac{\partial u_i}{\partial x_j} = -\frac{\partial P}{\partial x_i} - \frac{\partial}{\partial x_j}\left(\mu \frac{\partial u_i}{\partial x_j}\right) - \frac{\partial}{\partial x_j}\left(\mu_t \frac{\partial u_i}{\partial x_j}\right) + \rho\beta g_i (T - T_0) \qquad (2.10)$$

Considering that the effective viscosity is $\mu_e = \mu + \mu_t$ the final form of Eqn. (2.10) is

$$\rho u_j \frac{\partial u_i}{\partial x_j} = -\frac{\partial P}{\partial x_i} - \frac{\partial}{\partial x_j}\left(\mu_e \frac{\partial u_i}{\partial x_j}\right) + \rho\beta g_i (T - T_0) \qquad (2.11)$$

By analogy the energy equation is

$$u_i \frac{\partial T}{\partial x_i} = \frac{\partial}{\partial x_i}\left(\Gamma_e \frac{\partial T}{\partial x_i}\right) \qquad (2.12)$$

where $\Gamma_e = \frac{\nu}{\sigma} + \frac{\nu_t}{\sigma_T}$.

VADIS FLOW module uses the standard k-ε turbulence model to provide values for the turbulent viscosity. The k-ε model solves the transport equations for the turbulent kinetic energy, *k*, and the rate of dissipation of turbulent kinetic energy, *ε*.

The standard k-ε model is the most commonly used and validated turbulence model in engineering applications. The popularity of this model is due to its robustness in a wide range of industrially relevant flows, relatively low computational costs and generally better numerical stability than more complex turbulence models [Versteeg and Malalasekera, 1995]. However, the weakness of this model is traduced in the over prediction of the turbulent kinetic energy in regions of flow impingement and re-attachment, leading to poor prediction of the boundary flow around leading edges and bluff bodies. Also, flow separation from surfaces under the action of adverse pressure gradients is often poorly predicted. The real flow is likely to be much closer to separation (or more separated) than the calculations suggests [Yang, 2004].

From the Navier-Stokes equations it is possible to deduce the conservation equation for the TKE [Stull, 1988],

$$u_j \frac{\partial k}{\partial x_j} = -\frac{\partial}{\partial x_j}\left(\overline{u_j' k} + \overline{u_j' \frac{p'}{\rho}}\right) - \overline{u_i' u_j'} \frac{\partial u_i}{\partial x_j} - \beta g_j \overline{u_j' T'} - \nu \overline{\frac{\partial u_i'}{\partial x_j}} \overline{\frac{\partial u_i'}{\partial x_j}} \qquad (2.13)$$

In this expression, the first term represents the advection, the second one the turbulent transport, the third the *k* production (G_k), the fourth the buoyancy (I_k) and, finally, the fifth is the dissipation (ε) term.

The turbulent transport term is simplified to a diffusion term, using the turbulent viscosity definition:

$$\frac{\partial}{\partial x_j}\left(\frac{\nu_t}{\sigma_k}\frac{\partial k}{\partial x_j}\right) \tag{2.14}$$

The production term (G_k) is converted to

$$\nu_t \frac{\partial u_i}{\partial x_j}\left(\frac{\partial u_j}{\partial x_i}+\frac{\partial u_i}{\partial x_j}\right) \tag{2.15}$$

As in turbulent transport, it can be used the definition of $\overline{u_j'T'}$ to write the term of generation/destruction of k by the buoyancy forces (I_k):

$$\beta g_j \frac{\nu_t}{\sigma_T}\frac{\partial T}{\partial x_j} \tag{2.16}$$

Finally, a transport equation will be derivate for the last term, ε. Considering that

$$\varepsilon = \nu\overline{\frac{\partial u_i'}{\partial x_j}\frac{\partial u_i'}{\partial x_j}} \tag{2.17}$$

from the RANS (Reynolds Average Navier-Stokes) equations it is possible to deduce the transport equation for ε for a stationary flow:

$$u_i \frac{\partial \varepsilon}{\partial x_i} = -\frac{\partial}{\partial x_i}\overline{\left(u_i'\varepsilon'\right)} + G_\varepsilon - E_\varepsilon \tag{2.18}$$

The first term on the right side of the equation is the diffusion term. ε' represents the turbulent component of ε, being used in the following expression

$$\overline{-u'\varepsilon'} = \frac{\nu_t}{\sigma_\varepsilon}\frac{\partial \varepsilon}{\partial x_i} \tag{2.19}$$

with σ_ε as the turbulent Prandtl number of ε.

G_ε and E_ε are, respectively, the terms of generation and viscous dissipation of ε.

$$G_\varepsilon - E_\varepsilon = -2\nu\overline{\frac{\partial u_i'}{\partial x_k}\frac{\partial u_i'}{\partial x_j}\frac{\partial u_k'}{\partial x_j}} - 2\left(\nu\overline{\frac{\partial^2 u_i'}{\partial {x_j}^2}}\right)^2 \tag{2.20}$$

The quantification of both production and dissipation terms is made through the following expression:

$$G_\varepsilon - E_\varepsilon = (C_1 \frac{G_k}{\varepsilon} - C_2) \frac{\varepsilon^2}{k} \qquad (2.21)$$

The generation term of TKE, G_k, is calculated through the equation of k. Symbols C represent standard model coefficients (C_1=1.44; C_2=1.92;C_3=1.44; C_μ=0.09; σ_T=0.9; σ_k=1and σ_ε=1.22) [Launder and Spalding, 1974]. These model constants have been derived through rigorous investigation of experimental data and have been found to provide the most suitable solutions to the equations over a wide range of turbulent flows.

Andrade (1988), based on various authors, proposed the use of the next expression to consider the effects of the fluctuation due to vertical temperature gradients:

$$G_\varepsilon - E_\varepsilon = C_1 \frac{\varepsilon}{k}(G_k + I_k)(1 + C_3 Ri) - C_2 \frac{\varepsilon^2}{k} \qquad (2.22)$$

In this expression, R_i represents the Richardson number, an adimensional number that relates the buoyancy forces with the mechanic forces in the generation of k:

$$Ri = \frac{g}{T} \frac{\partial T/\partial z}{(\partial u/\partial z)^2} \qquad (2.23)$$

This expression translates the atmospheric stability (R_i<0: instable; R_i =0: neutral; R_i >0: stable) [Stull, 1988].

The final equations' system for k and ε is

$$u_i \frac{\partial k}{\partial x_i} = \frac{\partial}{\partial x_i}\left(\frac{\nu_t}{\sigma_k}\frac{\partial k}{\partial x_i}\right) + G_k + \beta g_i \frac{\nu_t}{\sigma_t}\frac{\partial T}{\partial z} - \varepsilon \qquad (2.24)$$

$$u_i \frac{\partial \varepsilon}{\partial x_i} = \frac{\partial}{\partial x_i}\left(\frac{\nu_t}{\sigma_\varepsilon}\frac{\partial \varepsilon}{\partial x_i}\right) + C_1 \frac{\varepsilon}{k}\left\{G_k + \beta g \frac{\nu_t}{\sigma_t}\frac{\partial T}{\partial z}\right\}(1 + C_3 Ri) - C_2 \frac{\varepsilon^2}{k} \qquad (2.25)$$

with $\nu_t = C_\mu \frac{k^2}{\varepsilon}$.

2.2.1.2. Discretisation method

In terms of computational fluid dynamics, numerical methods refer to techniques that can be developed in order to solve the governing equations of fluid flow. It is not possible to

solve directly the governing set of partial differential equations (except for some very simple flows), hence a suitable method for approximating the differential equations by forming a set of algebric equations for the variables involved must be formed. This process is called discretisation.

VADIS FLOW module uses the finite volume method as discretisation technique. The numerical algorithm consists of a number of steps:

- Formal integration of the governing equations of fluid flow over all the (finite) control volumes of the solution domain;
- Discretisation involving the substitution of a variety of finite-difference-type approximations for the terms in the integrated equation representing flow processes such as convection, diffusion and sources - this converts the integral equations into a system of algebraic equations;
- Solution of the algebraic equations by an iterative method.

The finite volume method uses the integral form of the conservation equations as the starting point. The solution domain is subdivided into a finite number of continuous control volumes and the conservation equations are applied to each ones. At the centre of each control volume is a computational node at which the variable values are to be calculated. Interpolation (differencing) is used to express variable values at the control volume in terms of nodal values.

2.2.1.3. Near-wall flow treatment

In a turbulent flow, the presence of a wall causes a number of different effects. Specifically, near the walls, the turbulence Reynolds number approaches zero, and the mean shear normal gradients in the boundary layer flow variables become large. In order to resolve this problem, wall functions are applied in the near region that rely on the existence of the logarithmic region in the velocity profile.

The wall functions used by VADIS require several input parameters to evaluate the flow and turbulent kinetic energy in the grid point next to the walls and floor. Firstly, a dimensionless spatial variable z^+ must be evaluated by the following equation,

$$z^+ = \frac{z_p}{\nu} u_* \qquad (2.26)$$

where, z_p is the distance from the wall to the first grid point, ν is the viscosity and u_* is the friction velocity that can be determined by

$$u_* = \sqrt{\frac{\tau_w}{\rho}} \tag{2.27}$$

If the value of z^+ is greater than 11.63, the near wall grid point is considered to lie within the log-law region of the turbulent boundary layer. Within this region, the following wall function formulae are used:

$$u^+ = \frac{1}{K}\ln(Ez^+) \tag{2.28}$$

$$k = \frac{u_*^2}{\sqrt{C_\mu}} \tag{2.29}$$

$$\varepsilon = \frac{u_*^3}{K z_p} \tag{3.30}$$

where K is the Von Karman constant; E is a parameter that determines the roughness of the wall and floor (E=9.8 for smooth walls); and C_μ is a constant of the k-ε turbulence model. If the value of z^+ is inferior than 11.63, the near wall grid point is within the linear sub-layer and $u^+=z^+$.

2.2.1.4. Initial conditions

VADIS FLOW module uses as meteorological initial conditions the air temperature and the wind speed and direction, at the entrance of the domain, and at a specified reference height.

The variation of the mean wind speed with height above the ground, at the entrance of the domain, is determined in the model through the logarithmic law:

$$U = U_{ref}\left(\frac{z}{z_{ref}}\right)^{\alpha} \tag{2.31}$$

where U is the mean wind speed at height z; U_{ref} is the mean wind speed at reference height z_{ref}; α is the power law exponent that depends on the surface roughness and on the atmospheric stability.

The initial profiles for turbulent kinetic energy k and energy dissipation rate ε were calculated by the following relations:

$$k = aU^2 \tag{2.32}$$

$$\varepsilon = C_\mu^{3/4} \frac{k^{3/2}}{K \cdot z} \tag{2.33}$$

where a is a parameter that controls the inflow turbulence intensity and is specified as 0.003; C_μ is a numerical constant of the k-ε model (C_μ=0.09); and k the turbulent kinetic energy.

2.2.2. DISPER module

The DISPER module uses the lagrangian approach to determine the dispersion of pollutants in the study domain. While in the eulerian analysis the mass conservation equation is resolved for fixed control volumes, in the lagrangian approach the trajectories of each numerical particle that represent the pollutant are determined [Borrego, 1989].

Particle tracking methods are extremely popular for modelling the lagrangian dispersion characteristics of pollutants in a variety of fluid flow fields due to their flexibility and ease of use [Addison *et al.*, 1997; Leuzzi and Mont, 1998; Stohl *et al.*, 2005]. The Lagrangian Particle Dispersion (LPD) models based on particle tracking methods are also known as lagrangian statistical or stochastic models, Markov chain models, random walk models, random flight models, or lagrangian Monte Carlo models. In LPD approach, the turbulent transport is modelled by tracing the trajectories of a large number of particles as they are advected with the air flow, which is generated in prior by a wind field model and represented by mean flow and turbulent fluctuations. The release of particles may be either sequential (as a plume) or simultaneous (as a puff). Concentration fields are determined from the spatial distribution of particles. The LPD models are convenient tools to describe the pollutant transport phenomena especially when the time dependent wind field data are obtained.

Thus, in the lagrangian approach, in each time step, a particle displacement is calculated by the sum of a deterministic component obtained from the velocity field, the aleatory component related with the local turbulence and by the influence of the fluctuation forces. Excluding the part related to the fluctuation forces, this description could be used to

translate the Langevin stochastic differential equation [Lee and Naesslund, 1998] used in the model:

$$du = -\left(\frac{u}{T_L}\right)dt + du' \qquad (2.34)$$

with u as any of the three velocity spatial components, T_L as the lagrangian time scale and u' as an aleatory velocity component. The velocity field and the information about local turbulence is determined previously by the FLOW module.

The existence of solid walls in the simulation domain, such as ground and obstacles, creates an impaction and reflection phenomena of the numerical particles. As consequence, reflected particles are rebounded in the opposite direction of its previous displacement. For numerical simulations recreating wind tunnel experiments, lateral and top boundary conditions are considered as additional solid walls.

According to Zannetti (1990), the lagrangian approach demonstrates a unique simulation capacity, reproducing the major characteristics of the atmosphere stochastic behaviour with inferior computational costs, and without explicitly resolving the Navier-Stokes equations.

One of the lagrangian modelling advantages is the assurance of a correct mass balance, avoiding the numerical diffusion problems. In this case, the wind direction variation with time would oblige to consider an eulerian domain sufficiently large so that the building wake could develop in any direction and, in other hand, allowing that the domain frontiers, of entrance or way out, could be flexible, maintaining the correct mass balances.

2.2.3. Functioning scheme

In VADIS, two different grids are used: the wind and the cartographic grids (Figure 2.4). The information concerning obstacles and emission sources position and dimensions is defined on the cartographic grid. The wind field is calculated over a eulerian structured 3D grid, which is overlaid to the cartographic and rotates according to the wind direction. In this structured grid the number of cells that share a common vertex is uniform in the interior of the domain. The geometric domain is decomposed into subdomain blocks, within which a structured grid is generated. The grids dimensions and number of cells in each axis must be defined as a compromise between the required resolution, accuracy and the computational effort.

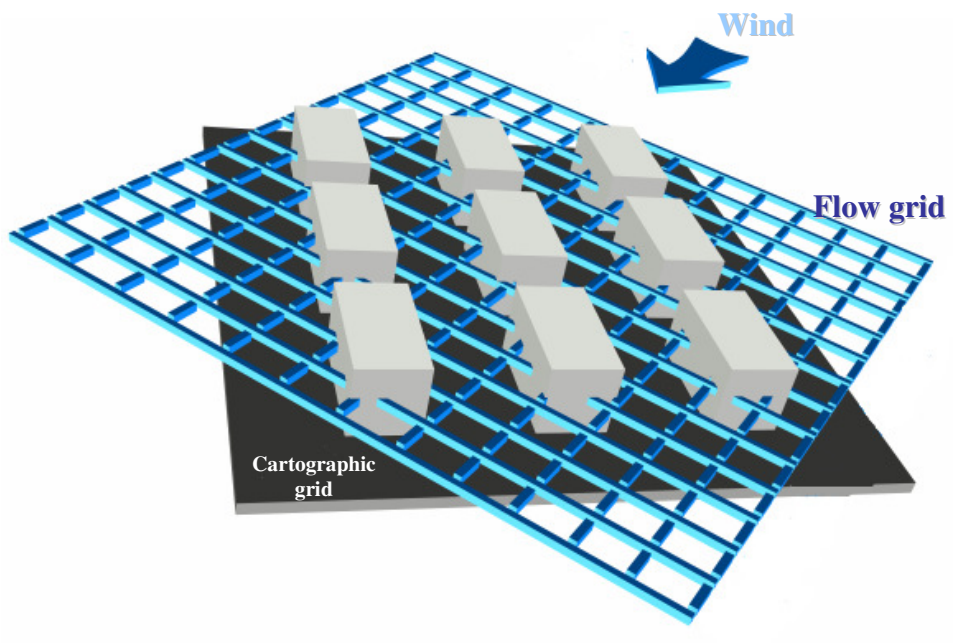

Figure 2.4 - Flow and cartographic grids used in VADIS model.

Initially, the wind field is calculated considering stationary conditions. Subsequently, the DISPER module calculates the displacement of numerical particles released over the cartographic grid, which represent the dispersion of the emitted mass of pollutant. The final result, containing the mean velocity and dispersion fields, is represented over the cartographic grid.

As VADIS uses a structured mesh, complex buildings have to be previously divided in parallelepiped sections. The relation of this approximated form with the original one depends, obviously, on the used cell resolution. The buildings can be aligned or in angle with the cartographic grid; so, for each one, the user has to define the 3D extreme coordinates of the inferior left and superior right corners, and the respective angle (between 0 and 90 degrees). The model has the capability to identify overlapping coordinates, making easier the description of more complex obstacles. Traffic emission sources are defined by the 3D extreme coordinates and emission rates, and are treated as volume source (Figure 2.5).

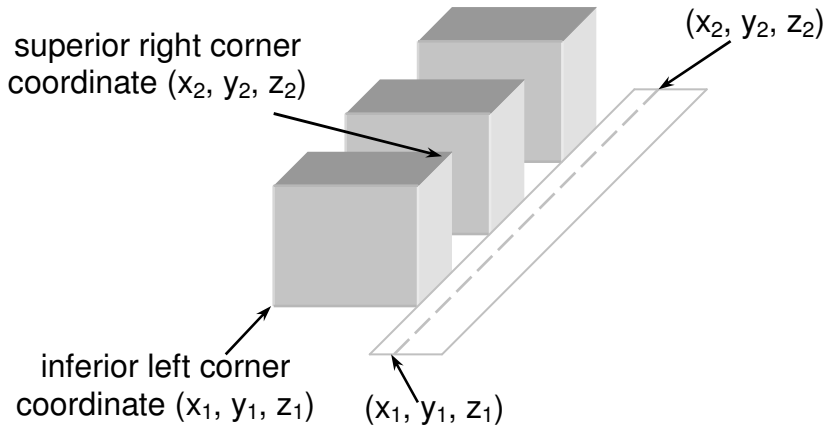

Figure 2.5 - Obstacles and sources coordinates definition used in VADIS model.

VADIS output data, represented in the cartographic grid, is constituted by the three wind velocity components, turbulent viscosity, turbulent kinetic energy, energy dissipation, pressure, temperature, and pollutant concentration in each grid cell.

3. EVALUATION OF MICROSCALE CFD MODELS

As already mentioned in the previous chapters, CFD models have the particularity to allow the detailed study of flow and dispersion in urban areas, simply by representing the geometry of every individual building in the neighbourhood. This approach has not been exploited in a systematic way, partly because in the past CFD models have been regarded as too computationally intensive to be able to run with such complicated geometry. However, with improved computer technology this is no longer the case. Within Europe the use of CFD codes for decision making is increasing both by industry and by national and local government agencies.

Nevertheless, developers of numerical models, analysts, users and decision makers face a critical question: how should confidence in modelling be objectively assessed? If the models are not of the appropriate quality (fitness-for-purpose) then it is likely that the consequent decisions will be inappropriate.

For regulatory purposes, the European Directives dictated already a first step towards the evaluation of air quality models, requiring accurate predictions of concentrations for various pollutants after comparison with air quality objectives. Specifically, the AQ-FWD and Daughter Directives establish new requirements for air quality modelling, including the definition of Modelling Quality Objectives as a measure of the acceptability of modelling results.

The measure of model quality proposed by the Directive is traduced by the estimation of the uncertainty for modelling and its comparison with the Quality Objectives defined for each quality indicator (Table 3.1).

Table 3.1 - Modelling Quality objectives established by the European Directives collected by [Borrego *et al.*, 2005].

Pollutant	Quality Indicator	Quality Objective	Directive
SO_2, NO_2, NO_x	Hourly mean	50-60%	1999/30/EC
	Daily mean	50%	
	Annual mean	30%	
PM_{10}, Pb	Annual mean	50%	
CO	8-hour mean	50%	2000/69/EC
Benzene	Annual mean	50%	
Ozone	8-hour daily maximum	50%	2002/3/EC
	1-hour average	50%	

The uncertainty for modelling and objective estimation is defined in this legislation as the maximum deviation of the measured and calculated concentration levels, over the period considered, by the limit value, without taking into account the timing of the events.

This definition was considered ambiguous and unclear in several studies conducted for the implementation of the AQ-FWD and Daughter Directives in real modelling applications [Borrego *et al.*, 2005; Flemming and Stern, 2007]. The question of timing is relevant for those hourly and daily limits, or target values, which are defined as a number of allowed exceedances of a given threshold concentration. Moreover, the model quality objectives for the allowed uncertainty are given as a relative quantity, without clear guidance on how to calculate this relative uncertainty.

Additional interpretation problems of the EU Directives may rise concerning the model uncertainty requirements, since there is no distinction on the uncertainty analysis between short- and long-term model applications. In this sense, the averaging period for modelling uncertainty estimation of PM_{10}, Pb and Benzene pollutants that is defined for one year restrictcts the uncertainty estimation process of models with feasible temporal applications of several days, such as CFD models [Borrego *et al.*, 2005].

The Modelling Quality Objectives proposed by the Directive were also questioned in this study: Does a modelling uncertainty value of 50 % indicate a good model performance or can guarantee reliable results for decision makers? This analysis suggests that work is still need to be made in the improvement of the current legislation, mainly in the development of a coherent, structured and widely accepted quality assurance procedure throughout Europe for models and their application to pollutant dispersion in cities.

In this sense, industry and local authorities supported by the current legislation can be seen as important drivers towards the development of a formalized evaluation protocol for local scale models.

3.1. Philosophy of model evaluation

Models of whatever type are only of use if their quality (fitness-for-purpose) has been quantified, documented, and communicated to potential users, ensuring that they are appropriate for a specific purpose. This process, called Model Evaluation, can enhance our confidence in the use of models developed for environmental and other problems. However, a definition of model quality is not a simple task and there is still no universal approach to it [Britter and Schatzmann, 2007b].

There is substantial experience and background in the formal evaluation of model quality for non-CFD codes, from the local to the mesoscale, particularly in the dispersion and air quality applications. These include, as example, the application to general atmospheric dispersion problems using the Model Validation Toolkit [Olesen, 1995; Olesen, 2005], mesoscale transport and dispersion models [Chang and Hanna, 2004], dense gas dispersion models [Carissimo *et al.*, 2001; Hanna *et al.*, 1993].

There is only limited evidence of formal model evaluation for CFD models used near and within the urban canopy. COST Action 615 ("Database, monitoring and modelling of urban air pollution") [Schatzmann, 2000], COST Action 715 ("Meteorology Applied to Urban Air Pollution Problems") [URL 2] and the SATURN project [Borrego *et al.*, 2003a; Moussiopoulos, 2003] initiated work in this area. The DAPPLE project in the UK [Arnold *et al.*, 2004] and VALIUM project in Germany [Schatzmann *et al.*, 2006] are recent studies directed towards model evaluation. This current deficient knowledge in the quality assurance of such models is mainly due to the lack of a generally accepted quality assurance procedure and a lack of data sets that are quality checked and generally accepted as a standard for model validation purposes.

Considering this important pitfall, COST Action 732 ("Quality Assurance and Improvement of Microscale Models") [URL 1] embraced the need to develop a coherent and structured quality assurance procedure for this type of models, which gives clear guidance to developers and users of such models as how to properly assure their quality and their proper application [Schatzmann and Britter, 2007]. It was also considered as mains goals of this COST Action to provide a systematically compiled set of appropriate

and sufficiently detailed data for model validation work in a convenient and generally accessible form and to build a consensus within the community of microscale model developers and users regarding the usefulness of the procedure [Britter and Schatzmann, 2007a].

According to the developed procedure, model evaluation is defined as the sum of processes that need to be followed for mathematical models of any type, in order to determine and quantify their performance capabilities, weaknesses and advantages in relation to the range of applications that they have been designed for, that is, their purpose.

Oberkampf *et al.* (2004) adopted a basic methodology of model evaluation from Schlesinger (1979) that was also used under COST 732. The role of model evaluation in the different phases of modelling is shown in Figure 3.1. Analysis of reality produces a *conceptual model* that comprises all the equations that are necessary to describe it, including initial and boundary conditions.

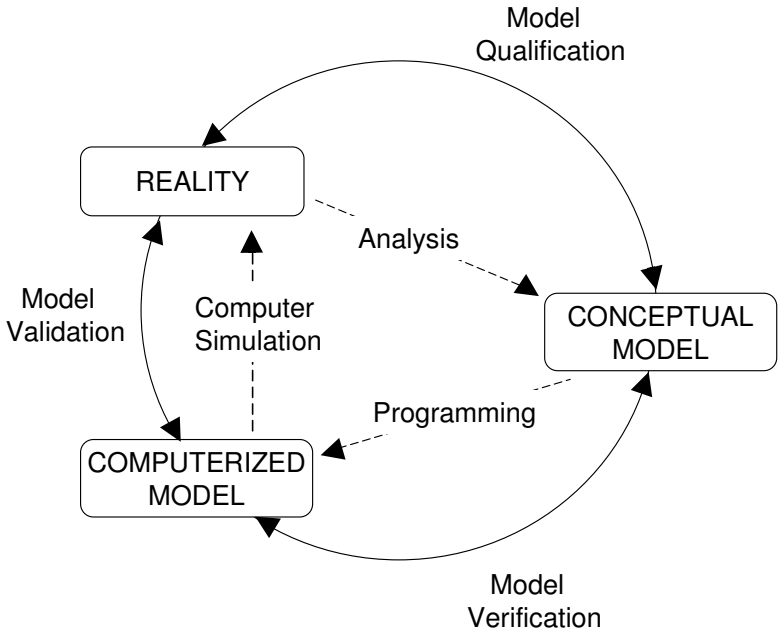

Figure 3.1 - Phases of modelling and simulation and the role of *verification* and *validation* [Schlesinger, 1979]. Taken from Oberkampf *et al.* (2004).

The appropriateness of the analysis is assessed through *qualification*, though the term *scientific evaluation* can be also used. The implementation of these equations into an operational computer program is called the *computerised model*. From Figure 3.1 it is clear that *verification* deals with the relationship between the conceptual and the computerised

model. *Validation* on the other hand deals with the relationship between the computerised model and experimental measurements.

Experience has then shown that a clear and formal protocol is still required for the evaluation of local scale models [Britter and Schatzmann, 2007a]. Under COST 732 an evaluation protocol was defined comprising three major steps: Scientific Evaluation; Model Verification; and Model Validation.

3.1.1. Scientific evaluation

A mathematical model is a set of mathematical expressions each one describing a particular process that is considered important. These equations attempt to approximate reality. In other words they represent, to a degree, simplified concepts of the reality. The underlying assumptions leading to a particular simplification have to be evaluated with respect to the range of applications, for each one separately and in connection with the whole approach. Additionally, every mathematical expression has to be defended against the state-of-the-art, taking into consideration the model type and the range of application.

Based on the above remarks it is commonly unrealistic to have a universal model for all applications. The Scientific Evaluation, the first step on model evaluation, requires then a detailed description of the model physics and chemistry and, most importantly, an assessment or judgement of the appropriateness of this scientific content for the purpose of the model.

The primary objectives of the Scientific Evaluation of a model are that:

- all important phenomena within the model's range of application are included;
- the mathematical modelling of these phenomena and the associated simplifications are well justified in terms of science and model practicality;
- the limits of model applicability are clear and explicit;
- the numerical techniques are appropriate to the intended applications.

Specifically in the area of air pollution an early attempt in Europe to give structured guidance on Scientific Evaluation was realized by the Model Evaluation Group [EC, 1994]. This Group suggested that a detailed description of the model physics and chemistry including special features, the regions of applicability and inapplicability of the model and

an assessment of the appropriateness of the scientific content should be required for a proper scientific evaluation.

In the SMEDIS Project funded by the European Union a methodology for evaluation of the dense gas dispersion models was developed [Daish *et al.*, 2000]. It was mainly based on a questionnaire to be filled by each modeller, covering all the evaluation aspects. The scientific evaluation questions refer to issues such as problems addressed by the model; the physical and chemical processes modelled; the mathematical formulation of the problem; the solution method; the output variables; and any planned scientific developments.

Additionally, the recent guideline of the VDI (the German Association of Engineers) addresses the issue of Scientific Evaluation mainly in terms of the input data, the domain and grid description, the general equation system and its simplifications, the various parameterisations that are important in micro-scale modelling, the turbulence closure, the boundary and initial conditions and the output data [VDI, 2005].

For atmospheric flows at the street or neighbourhood scale it is also worth mentioning the recommendations for the use of CFD models (RANS type) in the area of wind engineering performed under COST Action C14 ("Impact of Wind and Storm on City life and Built Environment") [Franke *et al.*, 2004]. This work addresses the problems of the basic equations, the turbulence models, the computational domain and the numerical approaches.

The Scientific Evaluation can be based on a questionnaire that systematizes all the information needed. The information obtained could then be entered in a documentation system. The approach used to develop a Scientific Evaluation questionnaire under COST 732 is described in Table A.1 of Appendix A.

3.1.2. Verification

In the context of quality assurance of CFD codes verification deals with the relationship between the *conceptual* and the *computerised* model of Figure 3.1 [Oberkampf *et al.*, 2004]. The conceptual model comprises all the equations that are necessary to describe the physical system, including initial and boundary conditions. The implementation of these equations into an operational computer program is called the computerised model or CFD code. Verification therefore is purely mathematic. On the contrary, validation deals with physics and is based on the comparison of the results of a numerical simulation with experimental measurements. Validation is therefore concerned with the question whether the conceptual models together with the computerised model are an appropriate

representation of reality while verification is concerned solely with the question whether the CFD code is an appropriate representation of the conceptual model. Or as Roache (1997) has succinctly formulated, verification is used to check whether the equations are solved right and validation is used to check whether the right equations are solved.

There are two distinct types of verification. One is code verification which is used to demonstrate that the computerised model is consistent with the CFD code as stated above, i.e. that there are no programming errors or inconsistencies in the solution algorithm [Roy, 2005]. This is normally done by the code developers. The other kind of verification is solution verification which is the estimation of the numerical error [Oberkampf *et al.*, 2004; Roache, 1997; Roy, 2005] or uncertainty [Stern *et al.*, 2001] of a specific simulation result and is to be done by the code user. Solution verification is also known as numerical error estimation [Oberkampf *et al.*, 2004].

Both kinds of verification need to quantify the discretisation error which results from the fact that a system of partial differential equations is solved with finite discretisation in space and time. The most general method for estimating the discretisation error is the Richardson extrapolation [Richardson, 1910; Richardson, 1927in Britter and Schatzmann, 2007b] which is used in code verification and solution verification.

The different steps to perform both code and solution verification are briefly described in Table A.2 of Appendix A.

3.1.3. Validation

Validation is the comparison of model predictions with experimental observations. Specifically for air pollution models this means the validation of flow (mean and turbulent velocities) and concentration predictions. A model that properly predicts the concentrations but fails with respect to the flow field would be right for the wrong reasons and must not be regarded as an applicable tool.

In order to conduct a validation it is important to decide for which purpose the model results should later be used and thus to decide the variable(s) whose prediction is the most important, e.g. is it the maximum concentration at various points in space or is the time for which the concentration is above some limit value or is it both of these. In other words the *validation objectives* have to be defined. The validation objectives will depend on the

application that is considered, so it is not possible to devise a simple and universally applicable procedure for model validation.

3.1.3.1. Potential validation data sets

A requirement of a model validation procedure will be the existence of several sets or test cases of observational data with which the simulated data can be compared. Laboratory experiments (e.g. from a small scale simulation in a wind tunnel) produce far more extensive and controlled data but may lack specific phenomena of interest such as atmospheric stability. Then, the best solution for improving data quality and the reliability of test data is a combined data set comprising laboratory and field experiments [Britter and Schatzmann, 2007a]. The field and/or laboratory data to be used for validation should undergo a preliminary analysis, such as plotting space and time patterns or testing similarity relations, so the user becomes familiar with the data and their attributes and problems.

Only a very limited set of validation data is currently available for testing and validation of 'state-of-the-art' microscale flow and dispersion models. Combined field and laboratory data are available from the MUST experiment [Biltoft, 2001], the VALIUM study [Schatzmann *et al.*, 2006], the DAPPLE project [Arnold *et al.*, 2004], the BUBBLE project [Rotach *et al.*, 2005] and the Joint Urban 2003 experiment [Allwine, 2004; Kastner-Klein *et al.*, 2004]. The data sets cover a wide range of geometrical complexity, ranging from a rather simple array of containers to the in-homogeneously structured roughness of the central business district in a modern city.

3.1.3.2. How should the model be run and the results interpreted

Franke *et al.* (2007) compiled specific guidelines based on previous initiatives (ERCOFTAC [Casey and Wintergerste, 2000], QNET-CFD [Bartzis *et al.*, 2004], VDI Guideline [VDI, 2005]) for undertaking simulations that are used to evaluate microscale models. In particular, these procedures were developed for the computation of flow in the urban and industrial environment with the statistically steady RANS equations for neutrally stratified flow fields.

The guidelines are structured according to the general steps for conducting a numerical simulation [Casey and Wintergerste, 2000; Franke *et al.*, 2004], regarding the choices on:

- target variables;
- approximate equations describing the physics of the flow;
- geometrical representation of the obstacles;
- computational domain;
- boundary conditions;
- initial conditions;
- computational grid;
- time step size;
- numerical approximations;
- iterative convergence criteria.

As this structure might indicate there is interdependence between these steps and, in general, the numerical simulations require iteration procedures between them.

The model predictions will then be based on the input data for modelling, the setting up and running of the model and any manipulation of the model outputs thought necessary. The latter refers to the necessity of post-processing model outputs to the same format as experimental data prior to the comparison of model prediction and experimental data

3.1.3.3. What variables to compare

These might be put into a hierarchy of:

- those directly relevant to the model purpose such as the concentration or the velocity (taken over a specified averaging time);
- those variables that are intermediaries in determining the variables which are directly relevant to the model purpose;
- those that are neither of the above but are a useful diagnostic of the performance of the model such as the turbulence intensity.

The question of what variables to compare is then answered by the available resources and the detail that is thought to be required.

3.1.3.4. How should the variables be compared

The answer will depend principally on the intended purpose of the model, but experimental data and model results can be compared:

- when paired in space or time, or only in space, or only in time. All three are commonly used. Paired in space and time is very important for the assessment of the turbulence model within CFD models. However the stochastic nature of atmospheric flows makes a comparison based on pairing in space and time a very severe test;
- with greater weight given to the agreement of, for example, the larger concentrations rather than the smaller, near zero ones;
- in a way that weights false positives and false negatives differently. This is a case where the consequences of over and underestimation are asymmetric;
- as a difference between the variables or as the ratio of the variables.

3.1.3.5. Exploratory data analysis

A convenient outcome of a model validation exercise is the values obtained through the application of statistical performance measures. However, such statistical measures should not stand alone as the outcome of a validation process. In parallel to the calculation of validation metrics, it is recommended to perform exploratory data analysis, where modelled and observed data are plotted in various ways. Such exploratory data analyses are well suited to highlight notable features in data and reveal shortcomings of models.

Commonly used types of plots are:

- scatter plots;
- quantile-quantile plots;
- residual analysis through residual plots (box plots and scatter plots).

3.1.3.6. Metrics for a model validation

After a paired set of experimental data and model predictions have been obtained, one or more methods of comparison must be selected and quantified. There are several standard metrics that were proposed in previous studies as basis for air quality model evaluation and

that can be used [Hanna *et al.*, 1993]. Some frequently used statistical performance measures are:

$$\text{R (Correlation Coefficient)} = \left[\frac{\sum_{i=1}^{N} (C_{oi} - \overline{C}_o)(C_{pi} - \overline{C}_p)}{\sqrt{\sigma_o}\sqrt{\sigma_p}} \right] \qquad (3.1)$$

$$\text{FAC2 = Fraction of data that satisfy } 0.5 \le \frac{C_p}{C_o} \le 2.0 \qquad (3.2)$$

$$\text{FB (Fractional Bias)} = \frac{(\overline{C_o} - \overline{C_p})}{0.5\,(\overline{C_o} + \overline{C_p})} \qquad (3.3)$$

$$\text{NMSE (Normalized Mean Square Error)} = \frac{\overline{(C_o - C_p)^2}}{\overline{C_o}\;\overline{C_p}} \qquad (3.4)$$

where C_p and C_o denotes model predictions and observations, respectively; overbar ($\overline{C}$) represents the average over the dataset; and σ_c denotes the standard deviation over the dataset. $\overline{C_o} - \overline{C_p}$ is used to define mean bias.

The Hit rate, q, is another metric that has recently been found useful for velocity models. The German VDI Guideline on prognostic mesoscale wind field models sets requirements in terms of this metric [VDI, 2005]. To evaluate the model performance, modelled and observed values of wind speed are non-dimensionalized using a reference measured wind speed which was also used to initialize the model. From the dimensionless model results P_i and dimensionless observed data O_i, a Hit rate is calculated from equation (3.5), where D is the allowed fractional deviation and W is the allowed absolute deviation.

$$q = \frac{N}{n} = \frac{1}{n}\sum_{i=1}^{n} N_i \quad with \;\; N_i = \begin{cases} 1 \;\; for \left| \frac{P_i - O_i}{O_i} \right| \le D \;\; or \;\; |P_i - O_i| \le W \\ 0 \;\; else \end{cases} \qquad (3.5)$$

Assuming an observed value O and a predicted value P, a hit is achieved if one of the following conditions is fulfilled:

- $|P_i - O_i|$ smaller than the allowed absolute deviation W;
- $\left| \frac{P_i - O_i}{O_i} \right|$ smaller than the allowed fractional deviation D.

The Hit rate can be interpreted graphically. This is illustrated in Figure 3.2.

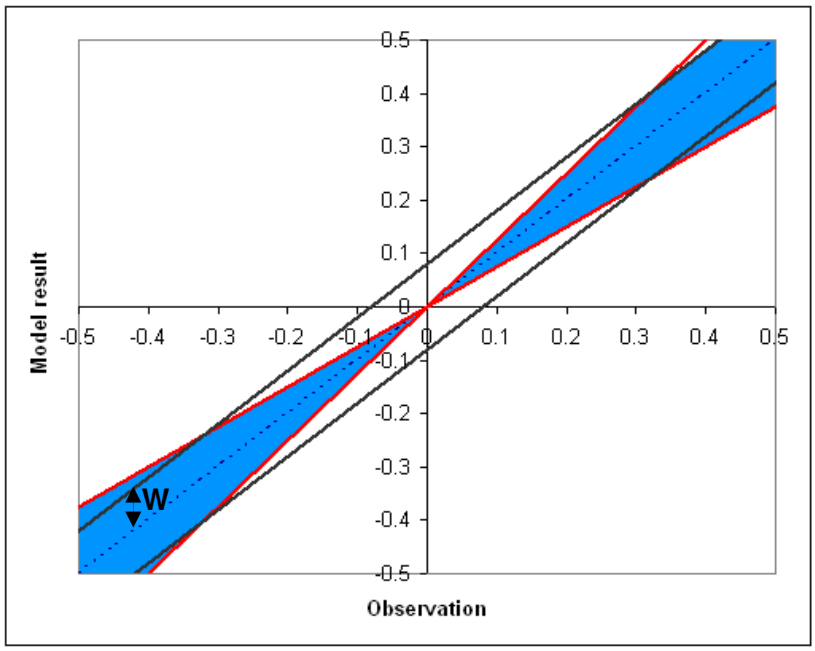

Figure 3.2 - Ilustration of Hit rate.

Two (black) lines parallel and displaced ±W in the vertical direction from the one-to-one line (dotted line) define a band of acceptance. Points that are within this band are counted as hits. Also, points within one of the two narrow sectors defined by the red lines (blue area), representing the fractional deviation, are included as hits.

3.1.3.7. Quality acceptance criteria

The validation exercise will provide qualitative and quantitative views of the model quality. However, this does not address whether or not the quality is acceptable. Quality acceptance is not possible without a clear statement of the purpose of the model and the conversion of its purpose into limit values for one, more, or all the metrics that are chosen to be relevant. This step must be performed early in any model evaluation process to "ground" the evaluation appropriately.

One useful step that can be made is to establish, with experience, values of the metrics that are typical of particular model types when applied to specific problems. In a sense, these metrics and their limit values are a quantitative statement of the "state-of-the-art" concept. As example, for comparisons with wind tunnel data, the German VDI Guideline [VDI, 2005] on windfield models requires a certain hit rate for a number of specific test cases.

For example, for wind components at specific points behind a building, the Guideline requires a hit rate of $q > 66$ % with an allowed deviation $D=0.25$.

Chang and Hanna (2004) have also summarized typical magnitudes of the above performance measures and estimates of model acceptance criteria based on extensive experience with evaluating many models with many field data sets. It was concluded that, for comparisons of maximum concentrations unpaired in space and for research-grade field experiments, "acceptable" performing models have the following typical performance measures:

- The fraction of predictions within a factor of two of observations is about 50% or greater (i.e., $FAC2 > 0.5$).
- The mean bias is within ± 30% of the mean (i.e., roughly $|FB| < 0.3$).
- The random scatter is about a factor of two to three of the mean (i.e., roughly $NMSE < 1.5$).

However, these are not firm guidelines and it is necessary to consider all performance measures in making a decision concerning model acceptance. Since most of these criteria are based on research grade field experiments, model performance would be expected to deteriorate as the quality of the inputs decreases, or as more stringent data pairing options (e.g., paired in space and time) are used.

3.2. Evaluation of VADIS CFD model

With the main purpose of enhance confidence on VADIS results, a model evaluation exercise was conducted using the previously defined protocol. All the different steps of the evaluation procedure were focused but special emphasis was given to the validation part. The overall exercise is described in this subchapter, as well as, the experimental data used for validation purposes. The participation in COST 732 allowed accessing to important and restricted information, such as the used validation data set, and also in the definition of statistical parameters and quality acceptance criteria for the chosen application.

In accordance with §3.1.1 the preferred option to conduct the Scientific Evaluation is to use a questionnaire that systematizes all the information needed. In the scope of COST 732 and in collaboration with COST Action 728 ("Enhancing mesoscale meteorological modelling capabilities for air pollution and dispersion applications") [URL 3], a Model Inventory [URL 1] was prepared to efficiently accommodate information on different

models in a common format. The information introduced in this Model Inventory concerning VADIS model is presented in Table A.3 of Appendix A.

This initiative of producing a model documentation system is not however unique. Former documentation exercises were conducted in the past in the SATURN project [Moussiopoulos, 2003] and in the European Topic Centre on Air and Climate Change (EioNet) of the European Environment Agency (EEA) [URL 4]. This last one named MDS (Model Documentation System) started in 1997 and is being continuously updated, reuniting in a large web data base several air quality models, of different scales, that are in use in Europe. For both initiatives VADIS model is fully documented.

In the second step of VADIS model evaluation, only solution verification actions were performed towards Model Verification, namely, in the reduction of the error to a negligible magnitude, by monitoring target variables as function of the iteration number, and repeating simulations on at least two more grids with systematic coarsening or refinement.

According to the German VDI Guideline on *Evaluation of prognostic microscale wind field models for flow around buildings and obstacles* [VDI, 2005] the Validation of microscale models should start with a basic test phase using wind tunnel data from a single cube experiment. In Vardoulakis *et al.* (2005) VADIS model was successfully validated against the single cube experiment CEDVAL. The model reproduced reasonably well the general flow pattern around two wall-mounted cubes of different characteristics, despite the overestimation of turbulent kinetic energy identified in the upwind impingement region. Nevertheless, the observed deviation is recognized as one of the limitations of the standard k-ε turbulence models.

Under COST 732 it was decided to undertake a model validation exercise at more complex geometries, representative of real urban areas. Based on the strict data evaluation concept of using a combination of physical modelling and field measurements, the Mock Urban Setting Test (MUST) experiment was selected as validation test. The experimental data set used for model validation purposes was not produced in the scope of this work.

The MUST test data set compiled under COST 732 used only a minor fraction of the original field and laboratory data [Britter and Schatzmann, 2007b]. The compiled test data have been homogenized, which means that a unified coordinate system, the same labels for variables and the same units were used in the field and laboratory data. However, to keep the origin of the test data clearly visible, field data and laboratory data were presented separately.

The test data set included a detailed description of the experiment; a geometry data file, with a description of the obstacles size and their individual location with respect to the reference coordinate system, as well as, the location of emission sources and measurements in the study domain; a flow file, containing the mean inflow vertical profile characteristics; a test data file compiling the flow and dispersion measurements data for both field and laboratory experiments.

Whereas the field data mainly focus on point-wise local flow and dispersion measurements, the corresponding laboratory data provide quasi-stationary flow and dispersion fields and instantaneous flow and dispersion data for well-defined boundary conditions. This important fact determined the use of the wind tunnel MUST experiment as validation test case of VADIS CFD model.

The validation work was therefore conducted through the following stages:

- use of the wind tunnel MUST experiment data;
- setting-up and running VADIS model for the MUST experiment conditions;
- post-processing model outputs to be compared with the experimental data;
- exploratory data analysis using graphical comparison between model and experimental data;
- statistical analysis;
- analysis of model results according to selected model quality acceptance criteria.

3.2.1. The Mock Urban Setting Test

The experimental setup originates from an extensive field campaign carried out on a test site of the US Army in the Great Basin Desert in 2001. The data set contains flow and dispersion data measured within an idealized urban roughness. A detailed description of the field tests can be found in Biltoft (2001) and Yee and Biltoft (2004).

A total of 120 standard size shipping containers were set up in a nearly regular array of 10 by 12 obstacles, covering an area of around 200 m by 200 m, to form an idealized roughness. In metric dimensions, the containers are 12.20 m long, 2.54 m high and 2.42 m wide.

The terrain of the field site is characterized as 'flat open terrain', an ideal horizontally homogenous roughness formed by bushes and grass land with a height of approximately

0.5 to 1 m. At a distance of about 1 km North of the test site there are sand dunes with approximately 4 to 6 m height, which were assumed to have no significant effect on the approach flow conditions at the test site. Figure 3.2 shows an overview of the MUST field experiment.

Figure 3.3 - Photograph of the MUST array experiment.

At a position near the centre of the container array, a VIP car was used, serving as collection point for sampled wind and concentration data. The size of the VIP car differs significantly from the size of the surrounding containers (6.10 m long, 3.51 m high and 2.44 m wide). Figure 3.4 shows a three-dimensional (3D) perspective of the setup array and identifies the VIP car location near the centre of the array.

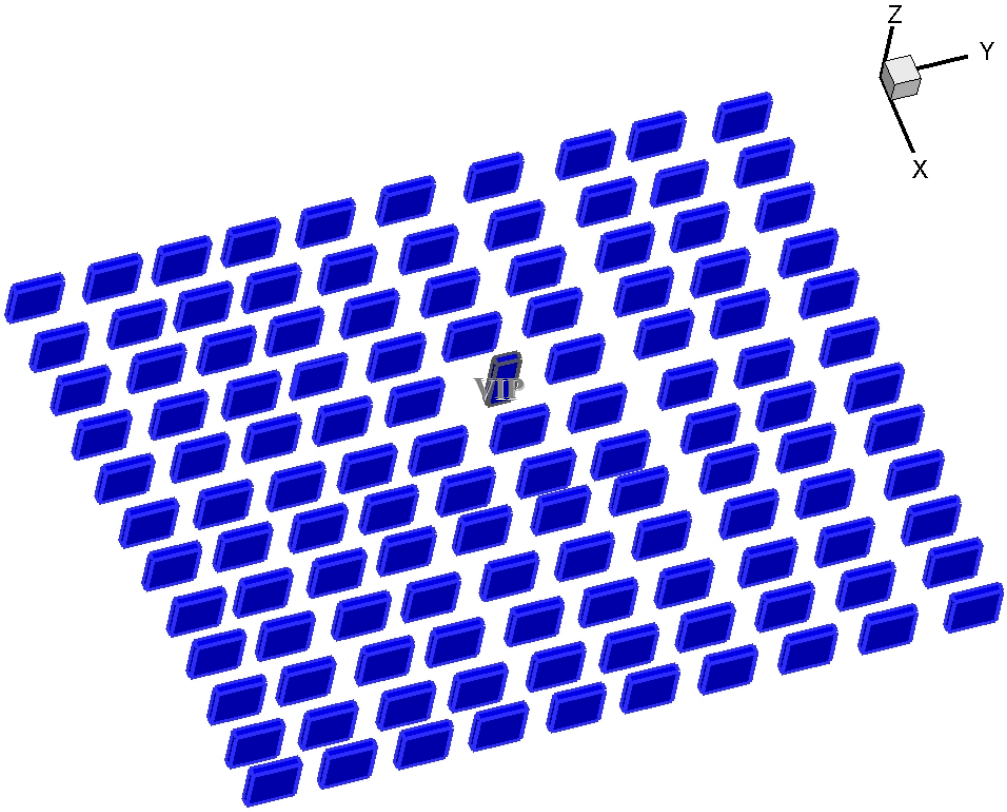

Figure 3.4 - 3D perspective of the setup and identification of the VIP car location.

The container array was not perfectly lined up because it was necessary to avoid conflicts with guy wires of measurement masts and with some survey markers. However, the exact location and orientation of each of the individual obstacles is documented with sufficient accuracy.

In Figure 3.5 the location of the emission sources, concentration detectors and measurement towers is identified using different symbols for the field setup.

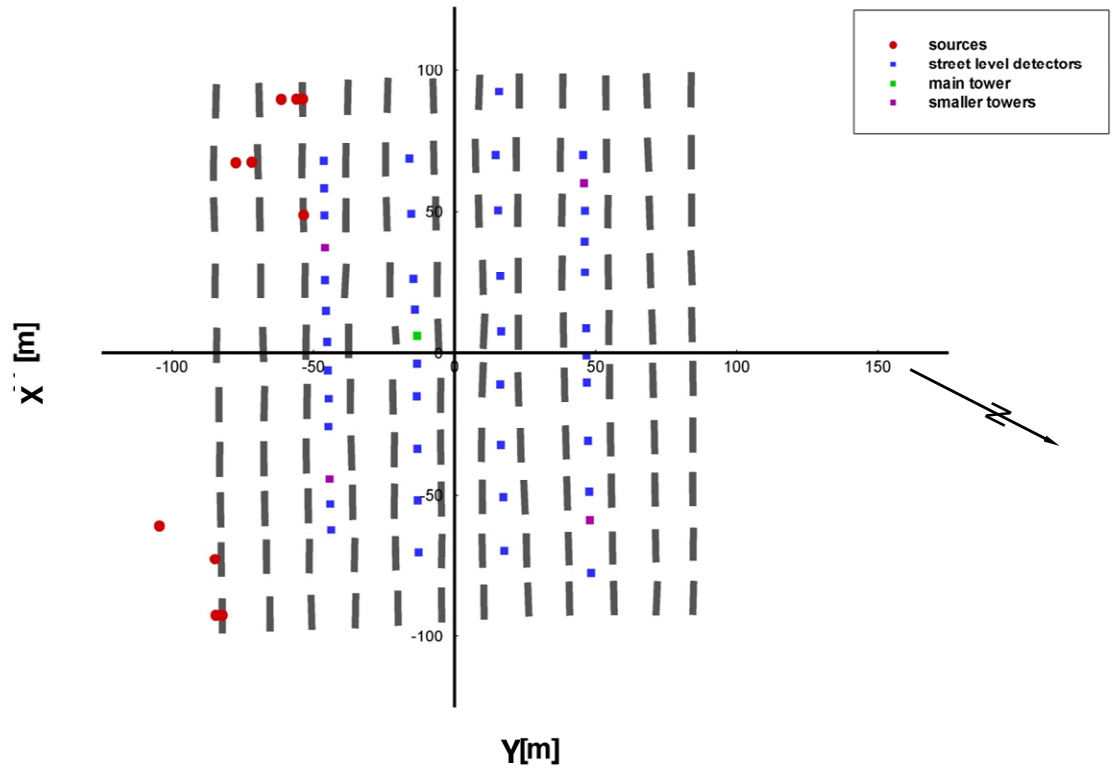

Figure 3.5 - Schematic view of the experimental setup.

For dispersion measurements fast-response photoionization detectors (PIDs) and Ultraviolet Ion Collectors (UVICs) were used, releasing propylene as tracer. Most of the dispersion measurement points were located within the streets formed by the container array. In order to capture the vertical spread of the released tracer, additional PIDs and UVICs were mounted on the measurement towers within the array.

The extensive set of instruments deployed during the field tests was completed by additional meteorological measurement devices such as a wind profiler and a SODAR for characterizing the boundary layer winds.

During the MUST field experiment, data from 68 useable trail events were collected. Release durations were chosen between 4 and 23 minutes for continuous releases with a majority of 15 minute releases. For individual puff releases, 5 s tracer discharge periods were chosen whereas the release was repeated several times during a particular field trail.

The majority of the MUST field campaigns were carried out during the late evening and night in September. From a meteorological point of view, slightly stable to very stable stratification conditions can be assumed to be present at the test site for most of the individual field trails.

The MUST field experiment was replicated in the Large Boundary Layer Wind Tunnel (WOTAN) at the Environmental Wind Tunnel Laboratory of the Hamburg University (Figure 3.6). The wind tunnel geometry was exactly scaled and even the location of the sources was precisely replicated in the model.

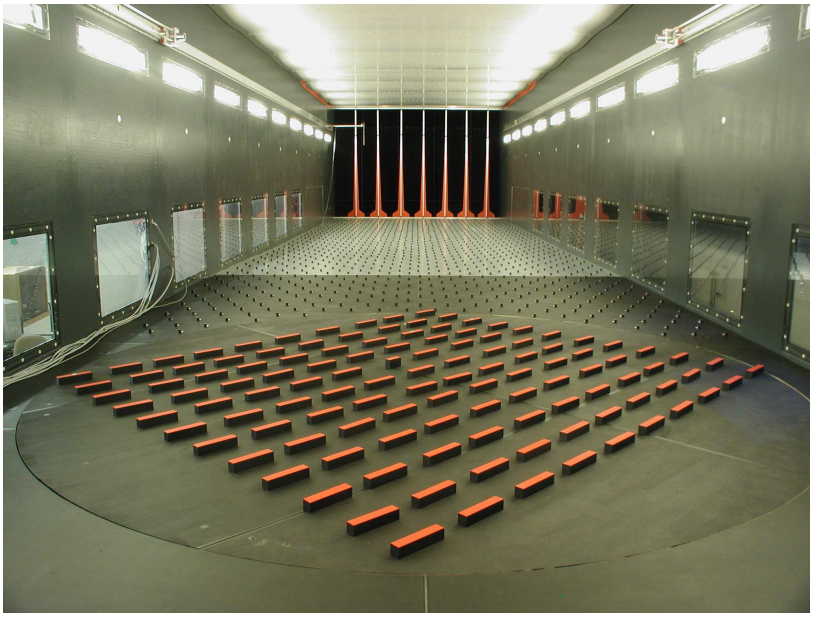

Figure 3.6 - Model on the turn table for -45° wind direction and roughness elements, inside the WOTAN wind tunnel.

Several approach flow conditions were modelled in the wind tunnel according to the available field data. From the available wind tunnel data, the -45º wind direction inflow condition was chosen, guaranteeing the existence of both wind and concentration measurement data. The wind tunnel coordinate system was subsequently converted into real scale coordinates, allowing to create the previous referred unified coordinate system. Figure 3.7 presents the reference coordinate system for the -45º test case used in this validation exercise.

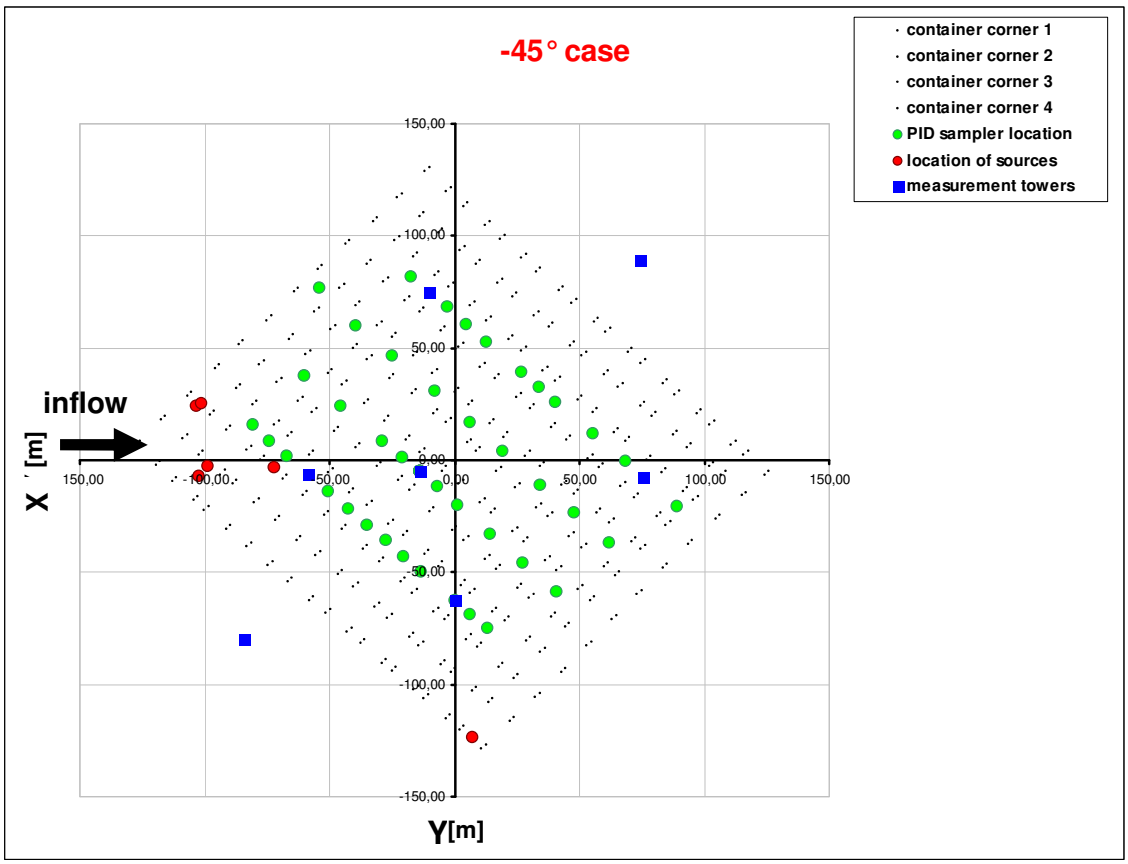

Figure 3.7 - Reference coordinate system for the -45° test case.

The non-intrusive two-components LASER-Doppler-Anemometry (LDA) technique was used to measure simultaneously flow components U and V (lateral) or U and W (vertical). For dispersion modelling, several of the source locations used during the field test were reproduced in the wind tunnel model. Due to technical reasons, the size of the source modelled in the wind tunnel had to be bigger than at full scale. Whereas the point source during field measurements was a pipe with a diameter of 0.05 m, mounted on a wire wheel or a tripod, the source(s) modelled in the wind tunnel had a corresponding diameter of 0.75 m at full scale. In the wind tunnel ethane was released as trace gas in order to simulate the dispersion of a neutrally buoyant tracer. For concentration measurements, different flame ionization detectors (FID's) were used. A slow FID system was utilized for background concentration monitoring and one or two fast FID systems were applied for time-resolved concentration fluctuation measurements.

The wind tunnel data set provided measured information on the global flow field within and above the array of obstacles at three different heights above ground. Additionally,

detailed local flow measurements were carried out for a small area between four containers located near the centre of the array.

Figure 3.8 presents the location of flow measurements for -45º wind direction. A coarse horizontal grid (marked in red) was used to measure the U and V components at three different plane heights above ground (0.5H, 1H, 2H), where H represents the container height of 2.55 m, corresponding to 1.275 m, 2.55 m and 5.1 m. A fine horizontal grid (marked in green) was also used to measure the U and V components at 0.9 m, 1.275 m, 1.575 m and 2.55 m plane heights above ground.

Positions of vertical profile measurements of U and W components are indicated in blue colour. U and W components were additionally measured at the horizontal plane 1H in the points with cyan colour. Obstacles corners are defined by the black dots.

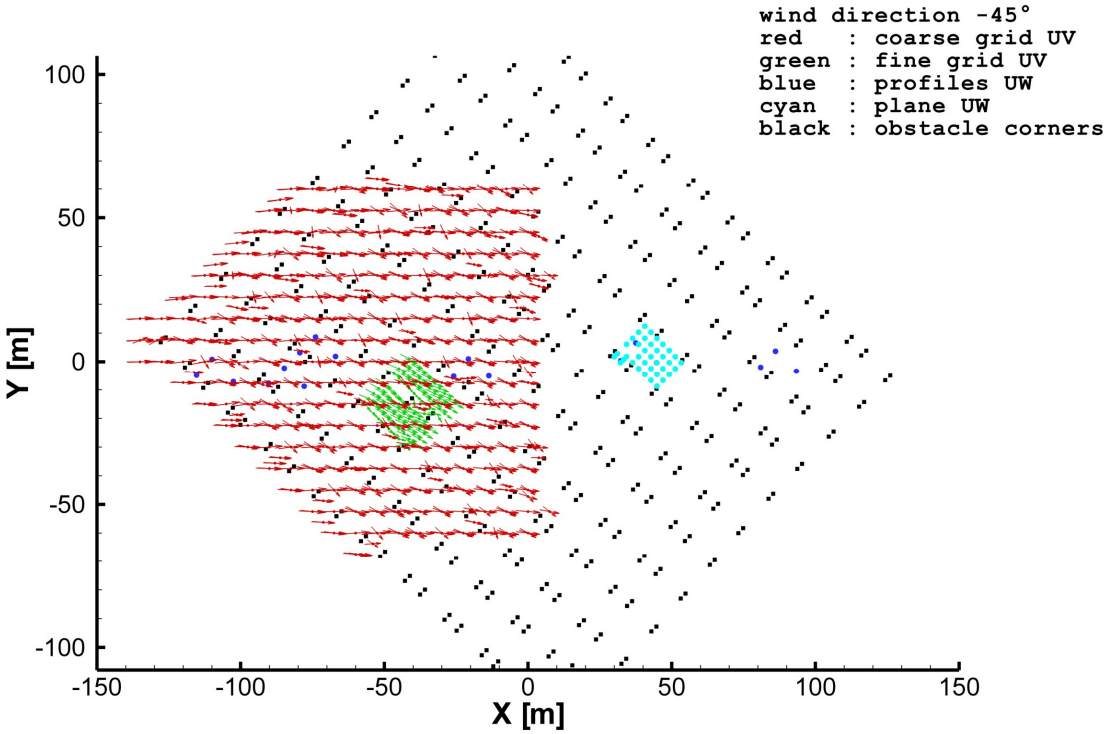

Figure 3.8 - Flow measurement positions for the -45º wind direction.

Wind tunnel results were given as dimensionless values, which enables the data to be rescaled according to the specific needs of the user/model. The results of flow measurements were non-dimensionalized using an inflow measured wind speed at a given reference height (7 $m.s^{-1}$ at 9 m height).

Results from concentration measurements in the wind tunnel provided a mean concentrations field for the -45º wind direction and for a specific source location.

Figure 3.9 presents the locations of the emission source and the concentration measurement points for the -45º.

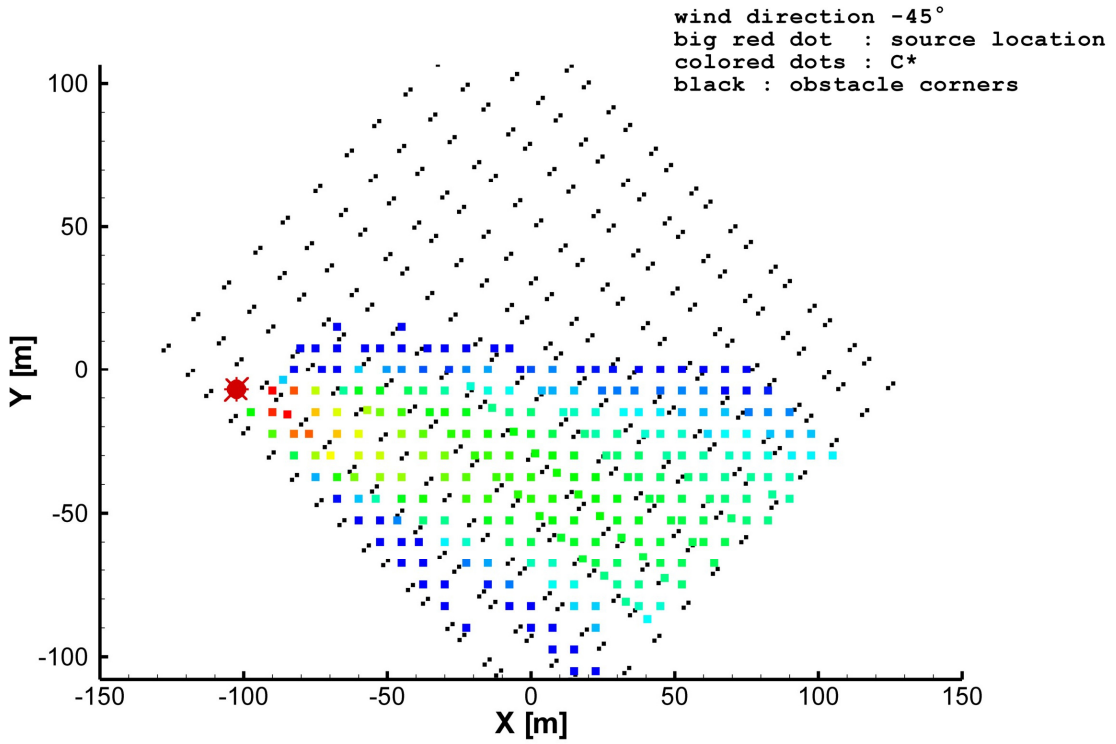

Figure 3.9 - Location of the emission source and the concentration measurement points for the -45º wind direction.

Results of dispersion measurements are given as dimensionless concentrations C^*, defined as

$$C^* = \frac{CU_{ref}H^2}{Q_{source}} \qquad (3.1)$$

where C denotes the (background-corrected) measured concentration, U_{ref} is the reference wind speed, H is the container height and Q_{source} denotes the mass source flow.

3.2.2. Setting-up and running VADIS CFD model

The simulation of flow and dispersion was performed with VADIS for the -45º test case conditions of the MUST wind tunnel experiment. The main guidelines proposed by Franke *et al.* (2004) necessary to conduct a numerical simulation with a model evaluation purpose, referred succinctly in § 3.1.3.2, were used. The following subchapters describe the different steps of the numerical simulations, mentioning also the specific guidelines.

3.2.2.1. Choice of target variables

Guideline: The first step should be the definition of the target variables. These should include the variables that are representative of the goals of the simulation and those that can be compared with the corresponding experiments [Franke *et al.*, 2007].

According to the available experimental data the target variables of this simulation are the mean velocity components, the turbulent kinetic energy (TKE) and the mean concentration.

3.2.2.2. Choice of the computational domain

Guideline: For urban areas with multiple buildings the top of the computational domain should be $5H_{max}$ away from the tallest building with height H_{max}; the lateral boundaries of the computational domain can be placed closer as $5H_{max}$ to that part of the built area. Concerning the longitudinal extension of the domain a distance of 8 H_{max} is recommended for the region in front of the built area (approach flow) and a distance of 15 H_{max} is suggested for the region behind (wake), to allow for flow development [Franke *et al.*, 2007].

Since the setup test covers an area of around 200 m by 200 m (see Figure 3.7) and following the requirements for H_{max} equal to 3.51 m, corresponding to the VIP car, a minimum simulation domain should cover 18 m for the vertical extension, 216 m for the lateral extension and a total of 260 m for the longitudinal extension of the domain.

The cartesian regular grid used in VADIS imposes that the length and the width of the domain should be similar. In this sense, a domain of 260 m (length) x 260 m (width) x 18 m (height) was defined for the numerical simulation. Convergence problems caused from a deficient development of flow in the downstream area of the study domain, determined the

use of a larger domain of 350 m (length) x 350 m (width) x 30 m (height) that guarantees the convergence of solutions.

3.2.2.3. Choice of the computational grid

Guideline: In the area of interest, at least 10 cells per cube root of the building volume should be used and 10 cells per building separation to simulate flow fields. This must be understood as the initial minimum grid resolution [Franke *et al.*, 2007].

Three different regular grid resolutions were tested for the defined domain: 2 x 2 x 2 m^3, 1 x 1 x 1 m^3 and 0.5 x 0.5 x 0.5 m^3. The designations 2 m, 1 m and 0.5 m will be used to identify the different resolutions. For the defined simulation domain these tested resolutions represent, in that order, 459 375 cells, 3 675 000 cells and 29 400 000 cells. The 0.5 m grid resolution defines 8.4 cells per cube root of the building volume and more than 10 cells per building separation, approximately acomplishing the defined guideline. The other tested grid resolutions do not accomplish the minimum requirements for model validation. In this sense, results on these model resolutions will only be shown as an example of application.

The regular grid mesh used in VADIS implies that for achieving the recommended grid resolution near the built area the total number of cells in the domain would be increasingly high. An higher grid resolution of 0.25 x 0.25 x 0.25 m^3 is in agreement with the guideline but its simulation, characterized by 235 200 000 cells, is presently limited by the existent computer capabilities.

Flow and dispersion simulations were performed in a cluster with two processors Intel XEON 2.33 GHz Dual Core and 4 GB of RAM. There is a direct relation between the runtime and the grid resolution, as it can be demonstrated by the computer runtimes of the different simulations presented for both flow and dispersion modules in Table 3.2.

Table 3.2 - Computer runtimes for flow and dispersion modules for the three resolutions.

Model	Resolution	Runtimes
Flow (Eulerian model; 200 iterations)	2 x 2 x 2 m^3	7 minutes
	1 x 1 x 1 m^3	40 minutes
	0.5 x 0.5 x 0.5 m^3	890 minutes
Dispersion (Lagrangian model)	2 x 2 x 2 m^3	17 minutes
	1 x 1 x 1 m^3	37 minutes
	0.5 x 0.5 x 0.5 m^3	391 minutes

3.2.2.4. Initial conditions

A vertical wind profile approach flow characterized by a wind speed of 7.0 $m.s^{-1}$, at 9.0 m height, with a power law exponent of 0.16 and a ground roughness length of 0.017 m was considered for the simulation. It was assumed that no background concentrations exist relatively to the ground source release of passive tracer identified in Figure 3.10**.** The tracer is emitted through a pipe with 0.75 m diameter with an emission rate of 1.34 x 10^{-5} $kg.s^{-1}$ during 60 s.

3.2.2.5. Running conditions

The FLOW module simulation was performed using 200 iterations to allow the convergence of solutions from the algebraic system of equations.

The interval to calculate the average concentrations in DISPER module was defined as 60 s, assuring that the numerical particles released from the point source would reach the output boundary.

3.2.3. Post-processing of model outputs

Flow and concentration modelling results were interpolated for the wind tunnel measurement positions with TECPLOT 360º commercial software, using the krigging method.

Modelled values of wind speed and concentration were non-dimensionalized according to the reference measured wind speed used to initialize the model (7 $m.s^{-1}$ at 9 m height) and the equation (3.1), respectively.

3.2.4. Exploratory data analysis

A qualitative analysis of VADIS model results for the -45º approach flow case is presented in this subchapter, using a graphical comparison with the wind tunnel data. More concretely, contours, vertical and horizontal plots of velocity components and turbulent kinetic energy, and profiles of dimensionless concentration are shown. The exploratory data analysis of VADIS simulations results are only presented for the 0.5 m grid resolution.

The flow and the dimensionless concentration pattern obtained with VADIS for the experiment conditions with the 0.5 m^3 grid resolution, and in a horizontal plane at 2 m above ground, is presented in Figure 3.10. The flow field is represented throught the main streamlines.

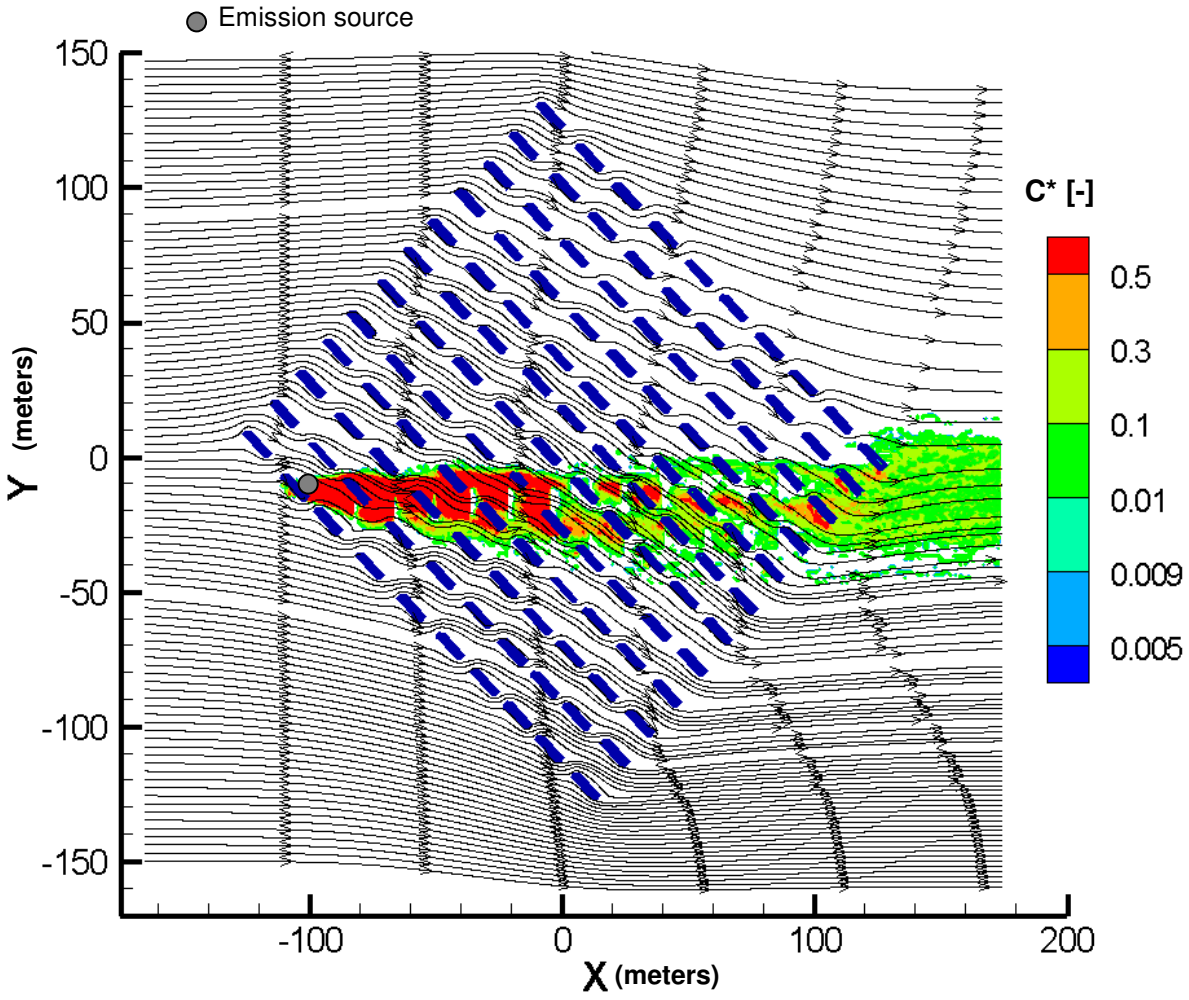

Figure 3.10 - Horizontal plane of flow and dimensionless concentration of passive tracer at 2 m height.

The analysis of Figure 3.10 shows the perturbation in the main flow caused by the presence of obstacles in the domain, producing various canyons effects within the built-up area. As

consequence, the initial inflow condition characterized by a prevailing U velocity component loose its dominance to the V component within the building area.

It is also visible the transport of the passive tracer to the positive X coordinate direction, according to the main flow represented by the streamlines. The higher dimensionless concentration value is observed in the first 100 m from the emission source, being reduced to approximately 80 % of its value in the remaining concentration field area.

Special contour plots of model results were also prepared for the fine measurement horizontal planes. Figure 3.11 presents the detailed measurement grid for the fine UV planes corresponding to the green colour representation in Figure 3.8. The fine UV planes have their designation due to the experimental measurement of both U and V components at the fine grid.

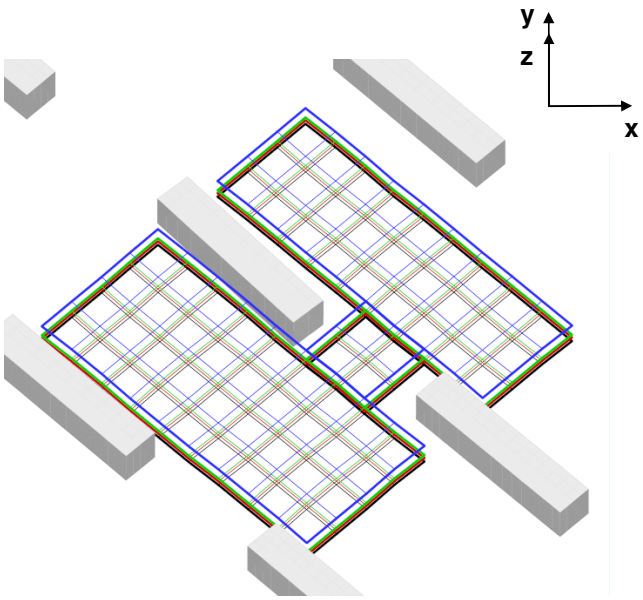

Figure 3.11 - Fine UV measurement positions for -45º approach flow.

Figures 3.12 to 3.17 present the modelling (for 0.5 m^3 grid resolution) and experimental contour plots for dimensionless U and V components at the fine measurement grid for three horizontal planes, z=0.9 m, z=1.575 m and z=2.55 m. The latter horizontal plane is slightly positioned over the building's top (building's height is 2.54 m). These representations will allow a detailed analysis of model results within the represented street canyons and at the leeward side of the central building.

The arrows presented in the modelling and experimental contour plots were created based on the values of both dimensionless U and V components.

Figure 3.12, Figure 3.13 and Figure 3.14 allow a qualitative analysis of the dimensionless U velocity component for both experimental and modelling results at the three horizontal planes: z=0.9 m, z=1.575 m and z=2.55 m.

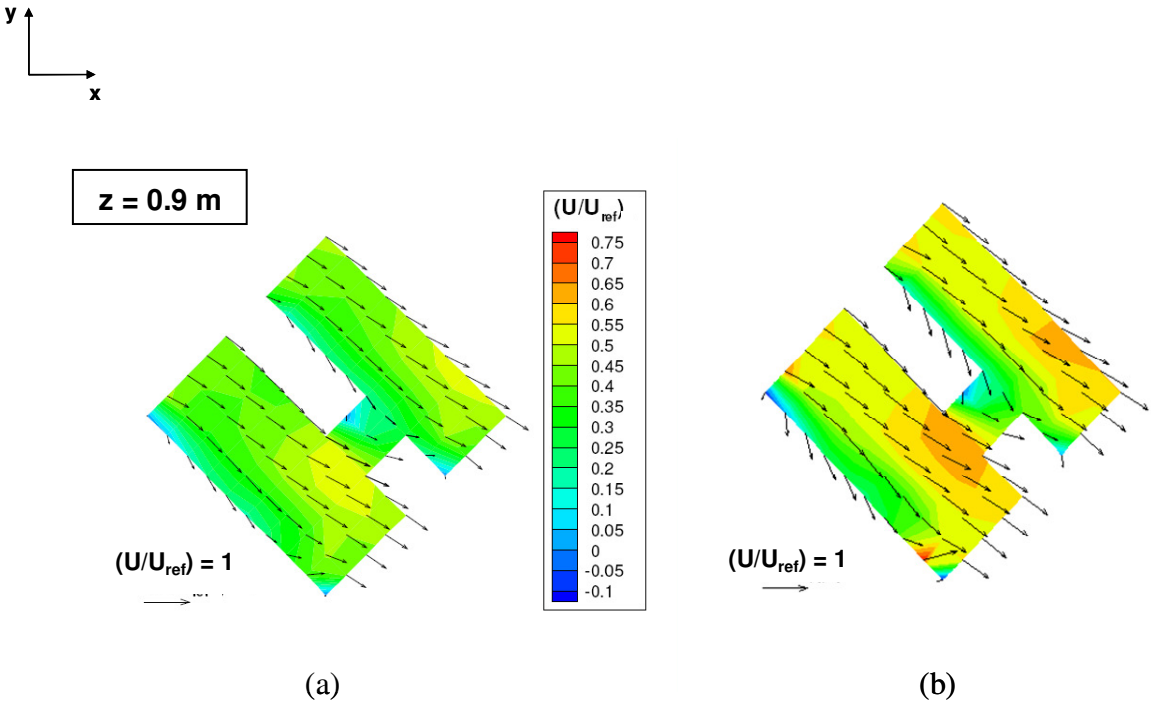

Figure 3.12 - Contour plots of dimensionless U velocity component at fine UV positions (z=0.9 m) for: (a) 0.5 m grid model resolution and (b) wind tunnel experimental data.

In Figure 3.12(b) the experimental results of dimensionless U velocity component, at 0.9 m height, show that the highest values are found at the leeward left side of the central building and, also, in the canyon located in the right side. On the other hand, the lowest values are located at the cavity zone immediately behind the central obstacle.

The modelling results (Figure 3.12(a)) present a similar spatial pattern from the experimental results, identifying the highest and lowest areas of dimensionless U velocity component. Nevertheless, a slightly model underprediction can be noticed in the entire studied domain.

The analysis of Figure 3.13(b) allows the identification of an identical spatial pattern of dimensionless U component to the one observed in Figure 3.12(b), with the highest values found at the leeward left side of the central building and in the canyon located in the right side, and the lowest values located jutst behind the building. The modelling results (Figure 3.13(a)) obtained for this horizontal plane, located at 1.575 m height, reproduce the spatial

pattern found in the experimental results despite the underprediction of the modelled values.

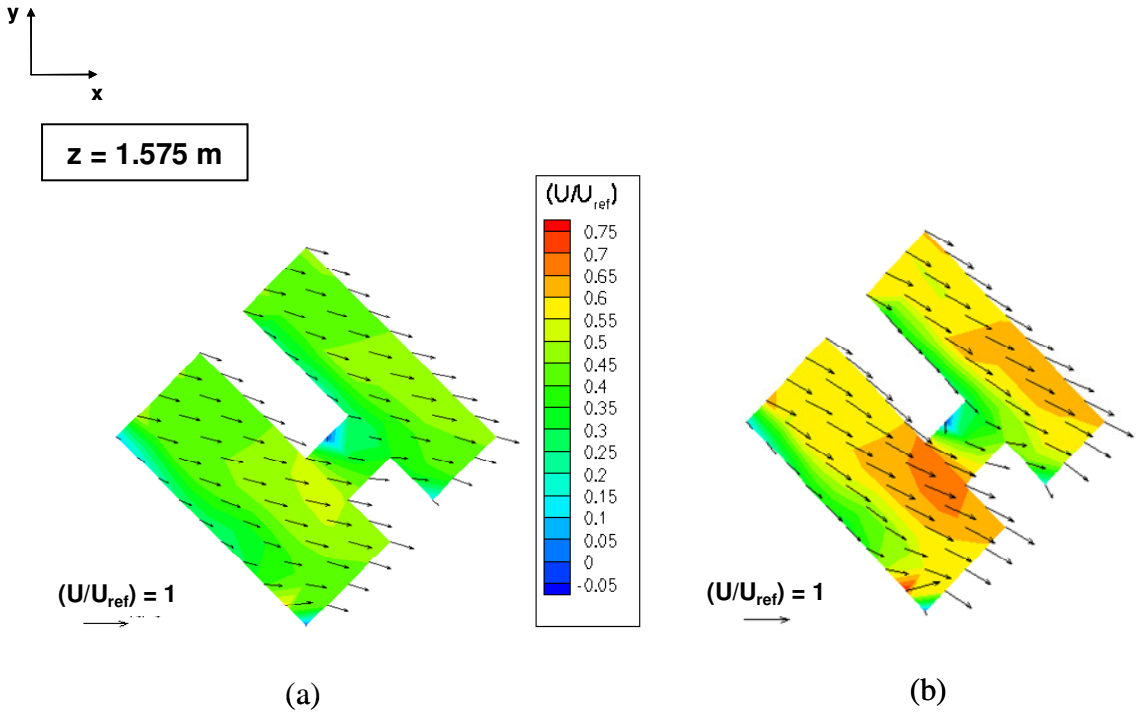

Figure 3.13 - Contour plots of dimensionless U velocity component at fine UV positions (z=1.575 m) for: (a) 0.5 m grid model resolution and (b) wind tunnel experimental data.

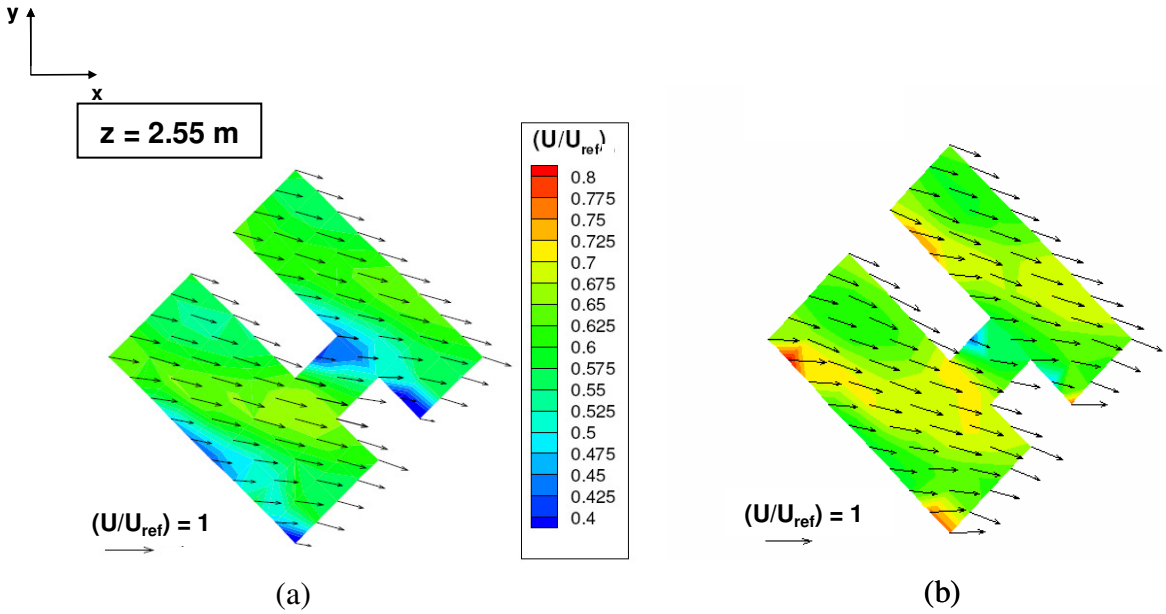

Figure 3.14 - Contour plots of dimensionless U velocity component at fine UV positions (z=2.55 m) for: (a) 0.5 m grid model resolution and (b) wind tunnel experimental data.

The experimental results of dimensionless U component, at 2.55 m height, corresponding to the top of the buildings, identify the highest velocity values near the obstacles located on the left side and the lowest values at the cavity zone immediately behind the central obstacle. Figure 3.14(a) shows that the modelling results underpredict the U velocity values over the entire domain. Moreover, VADIS model enlarges the cavity zone behind the central obstacle characyerized by the lowest U velocity values.

Figure 3.15, Figure 3.16 and Figure 3.17 presents an identical qualitative analysis of model and experimental results, at the three horizontal planes (z=0.9 m , z=1.575 m and z=2.55 m), for the dimensionless V component.

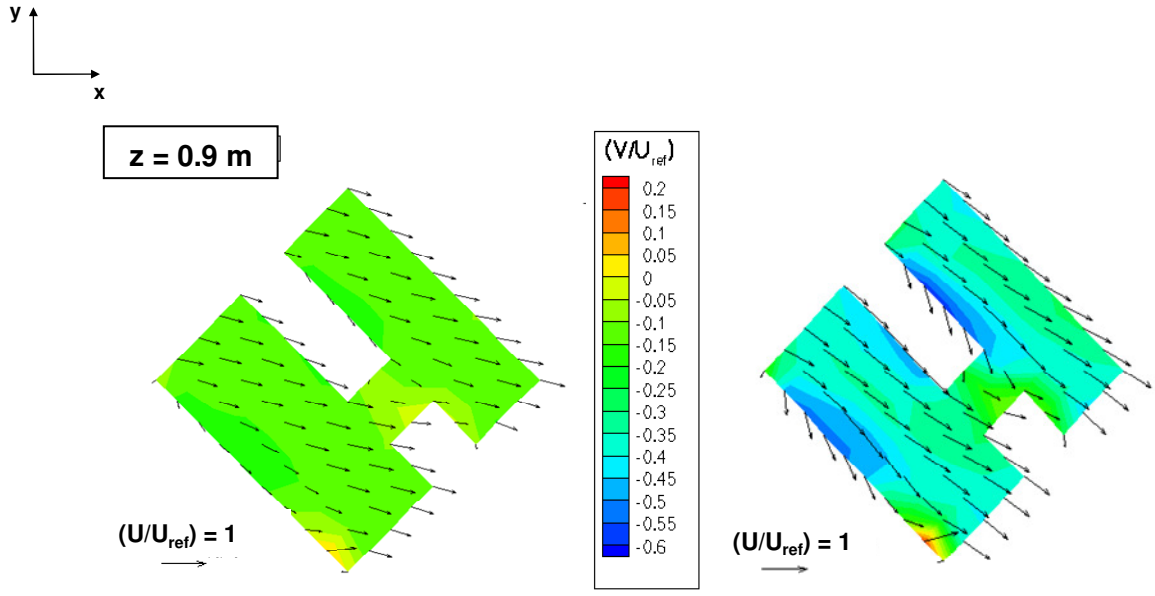

(a) (b)

Figure 3.15 - Contour plots of dimensionless V velocity component at fine UV positions (z=0.9 m) for: (a) 0.5 m grid model resolution and (b) wind tunnel experimental data.

Model results for the 0.9 m horizontal plane (Figure 3.15(a)) show an overestimation of dimensionless V component to almost the entire domain, with the exception of the leeward side of the central building and the bottom left edge of the represented domain. The spatial pattern found on those areas for the experimental representation is also encountered for the respective modelled results, despite the underestimation of their values.

At 1.575 m height, the experimental values of dimensionless V component are relatively well reproduced by the model (Figure 3.16(a) and (b)). Nevertheless, there is a slightly model overestimation at the leeward and lateral sides of the central building.

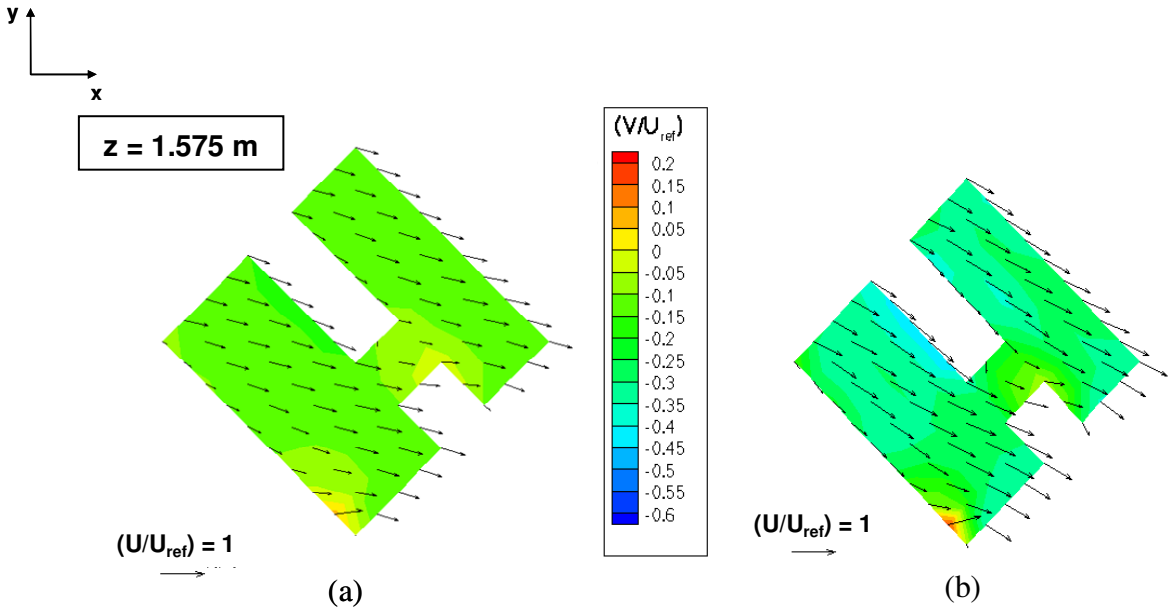

Figure 3.16 - Contour plots of dimensionless V velocity component at fine UV positions (z=1.575 m) for: (a) 0.5 m grid model resolution and (b) wind tunnel experimental data.

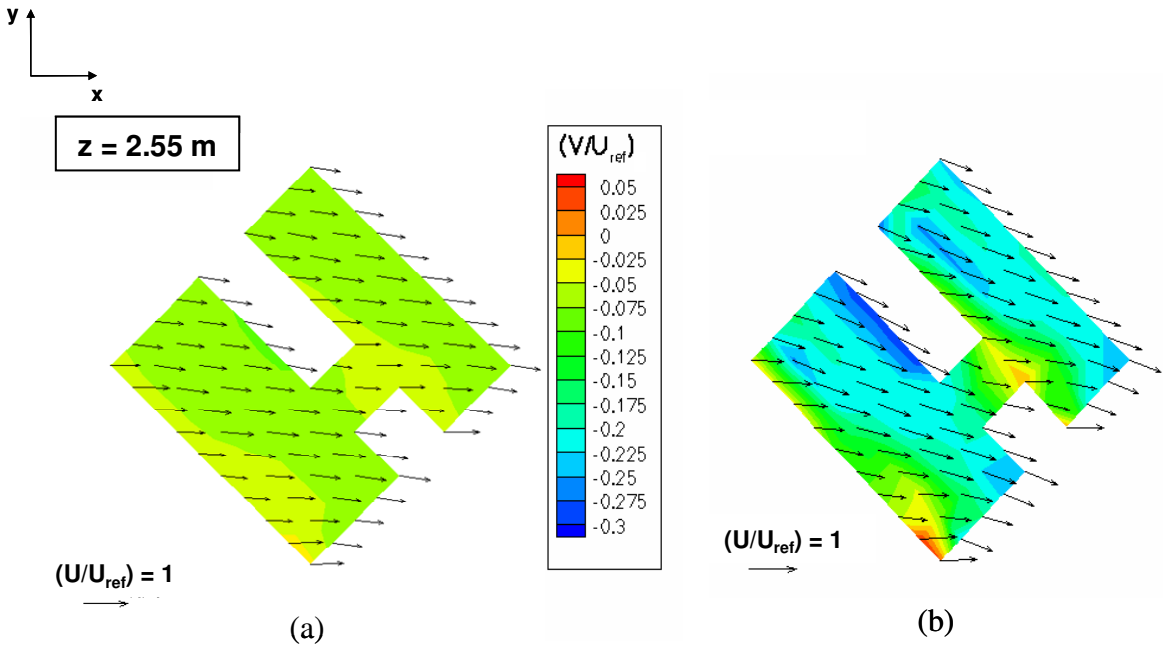

Figure 3.17 - Contour plots of dimensionless V velocity component at fine UV positions (z=2.55 m) for: (a) 0.5 m grid model resolution and (b) wind tunnel experimental data.

The model results for the 2.55 m plane present an overestimation of the V component in the lateral side of the main building and also within the two canyons. Nevertheless, it can

be noticed a comparable spatial pattern between the experimental and modelling results (Figure 3.17(a) and (b)).

Figures 3.18 to 3.23 present the modelled (0.5 m resolution) and experimental horizontal profiles of dimensionless U, V and W components, and TKE, plotted for specific locations of the study domain that are identified in the right-hand map. The *mod* and the *WT* notations represent the numerical results and wind tunnel data, respectively.

The experimental values of TKE were derived taking into account measured data for the two wind components: *U* and *V*, for the horizontal profiles (Eqn.3.2); and *U* and *W*, for the vertical profiles (Eqn. 3.3).

$$k_{o,v} = \frac{1}{2}(u^2_{RMS,o} + 2v^2_{RMS,o}) \tag{3.2}$$

$$k_{o,w} = \frac{1}{2}(u^2_{RMS,o} + 2w^2_{RMS,o}) \tag{3.3}$$

While the theoretical turbulent kinetic energy is defined as:

$$k_p = \frac{1}{2}(u^2_{RMS,p} + v^2_{RMS,p} + w^2_{RMS,p}) \tag{3.4}$$

where, the *RMS* notation is the root mean square value of wind components, representing the turbulent component of velocity; *o* and *p* stands for the observed and predicted values of variables.

This approximation should be taken into account in the comparison of the TKE modelling results with the experimental values since the assumption of the third velocity component (*W* and *V* wind components, for the horizontal and vertical profiles, respectively) in the calculation of TKE experimental values can lead to an estimation error of its values. In this sense, the analysis of the modelled and experimental TKE values will be mainly used to evaluate the evolution tendency of this variable along the selected profiles.

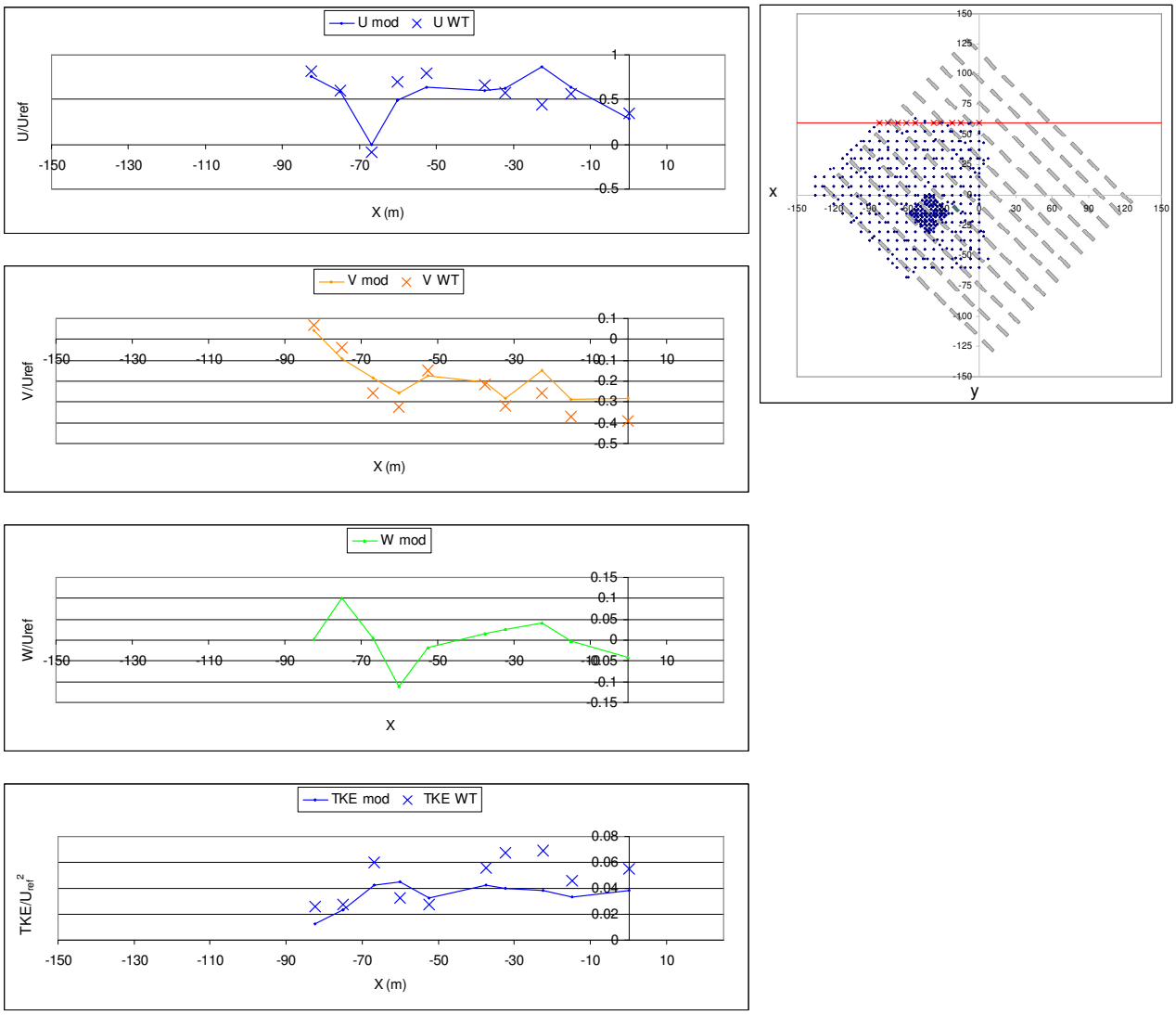

Figure 3.18 - Horizontal profiles of dimensionless U, V and W components, and TKE, for Y=60 m, at 1.275 m height (*mod* and *WT* notations represent the numerical results and wind tunnel data, respectively).

The analysis of Figure 3.18 shows that modelled U and V wind components can predict reasonably well the tendency of the experimental results with the exception of the measuring point located near the interception zone of two canyons, at X=-25 m, where it is observed an overestimation of the U component. The model behaviour for this specific point may be explained by an underprediction of the recirculating area caused by the nearest obstacles, leading to an underestimation of the main flow perturbation and consequently to an increase of the U component value.

Around the same location it is observed a larger discrepancy between the experimental and modelled TKE values, resulting in an underestimation of the modelled TKE values. The

latest can be related to an underprediction of the modelled turbulent phenomena in the area and to the experimental TKE estimation process itself, where the W component value may be overestimated by the assumption of Eqn. 3.2.

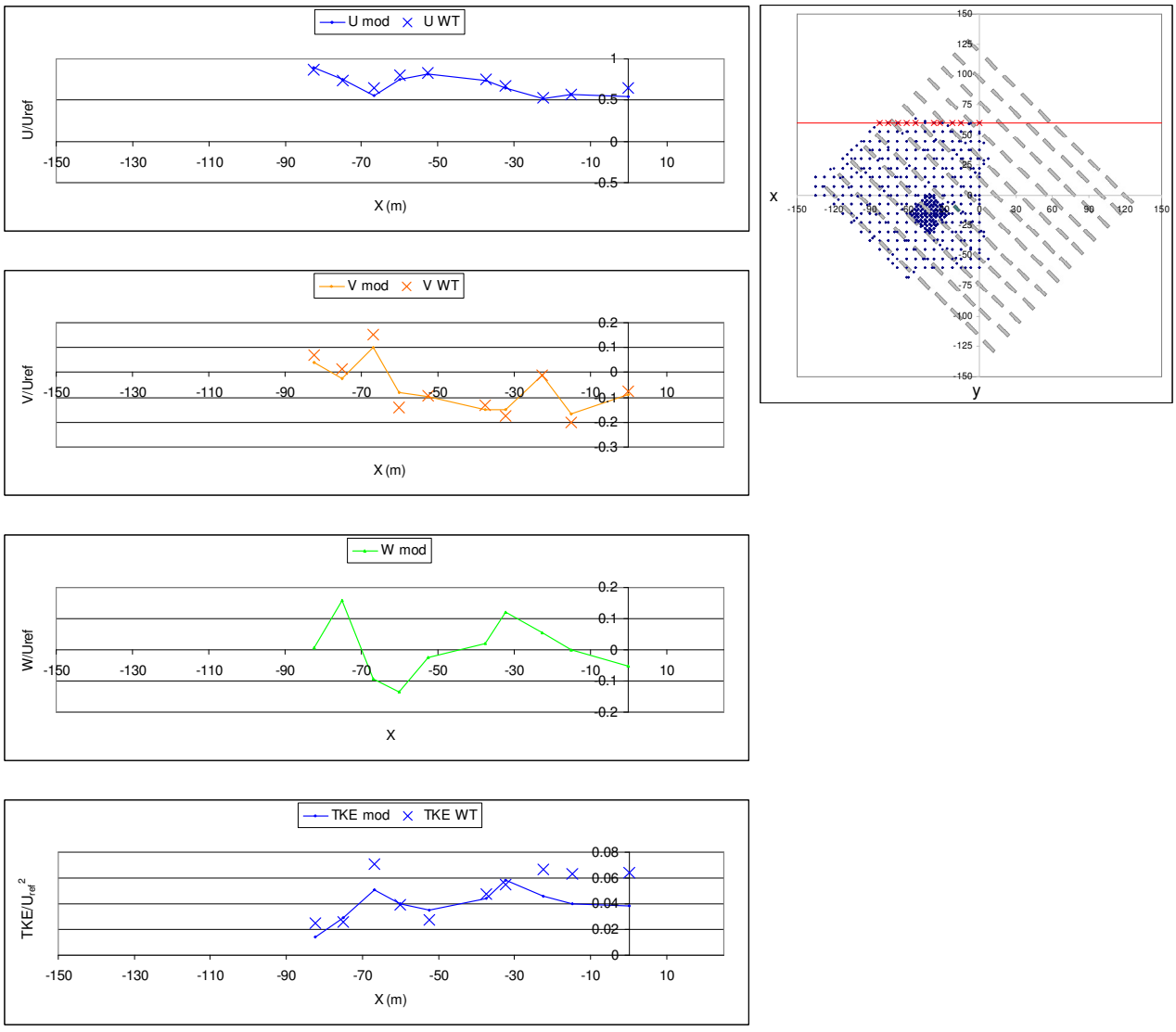

Figure 3.19 - Horizontal profiles of dimensionless U, V and W components, and TKE, for Y=60 m, at 2.55 m height (*mod* and *WT* notations represent the numerical results and wind tunnel data, respectively).

At 2.55 m height, corresponding to the top of the buildings, the modelled dimensionless U and V components present a good agreement with the corresponding experimental results (Figure 3.19). On the other side, the modelled TKE results are underestimated for the measuring positions near the Y axis. Again, the estimating process of TKE may be responsible for the observed discrepancy.

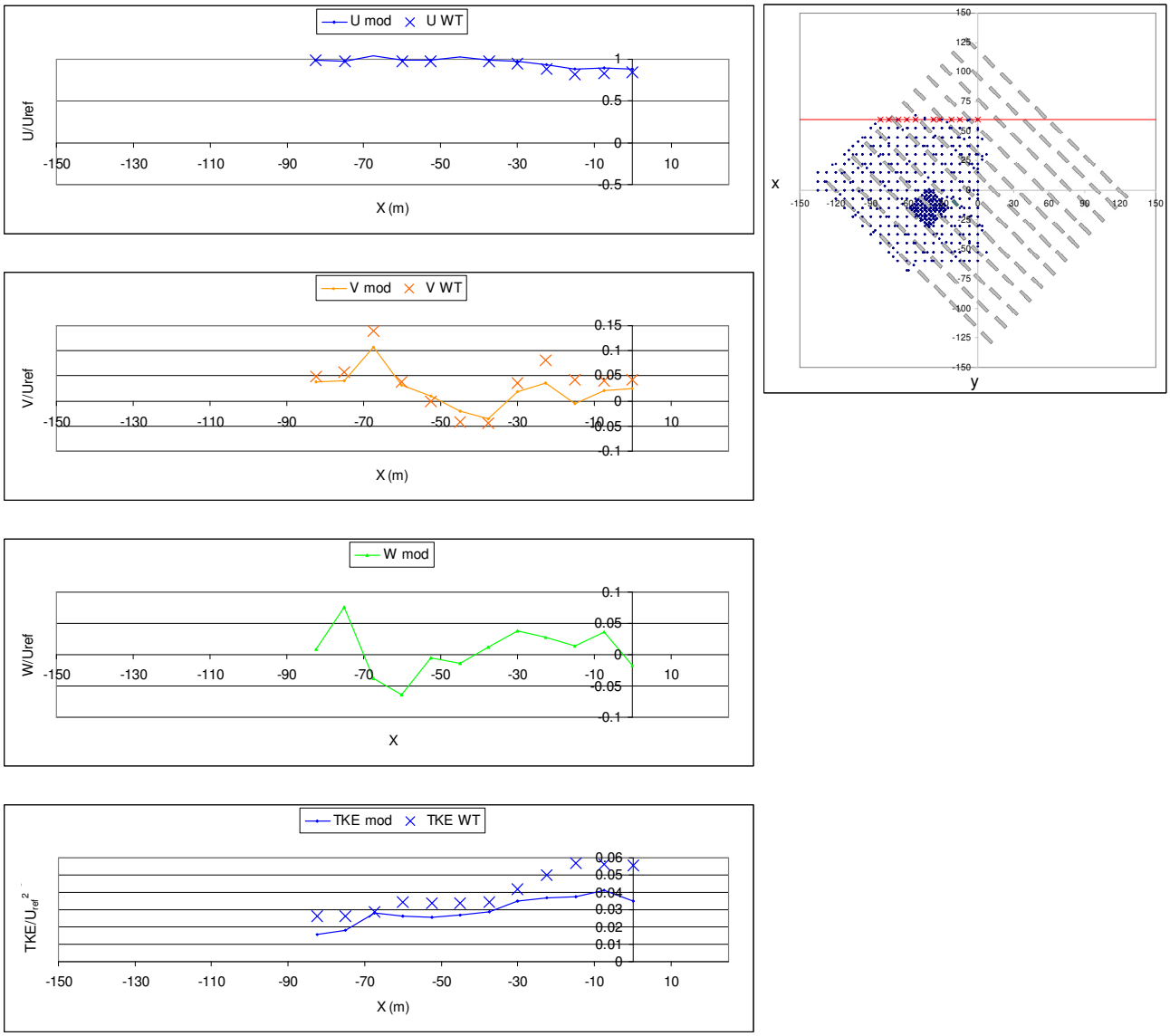

Figure 3.20 - Horizontal profiles of dimensionless U, V and W components, and TKE, for Y=60 m, at 5.1 m height (*mod* and *WT* notations represent the numerical results and wind tunnel data, respectively).

Figure 3.20 presents a good agreement between measured and estimated values of dimensionless U component and a slightly model underprediction of the V component for some measuring points near the Y axis. Nevertheless, the modelling results for the V component are able to capture the trend of the correspondent experimental values.

As it was already observed for the previous plots, there is an underestimation of the modelled TKE values that may confirm the hypothesis of a possible overprediction of the TKE experimental values due to its calculation process.

Figure 3.21, Figure 3.22, Figure 3.23 present a different horizontal profile positioned at Y=-45 m. At this location, the perturbation in the main flow is produced not only by the local obstacles but also from the turbulence generated by the obstacles located upstream.

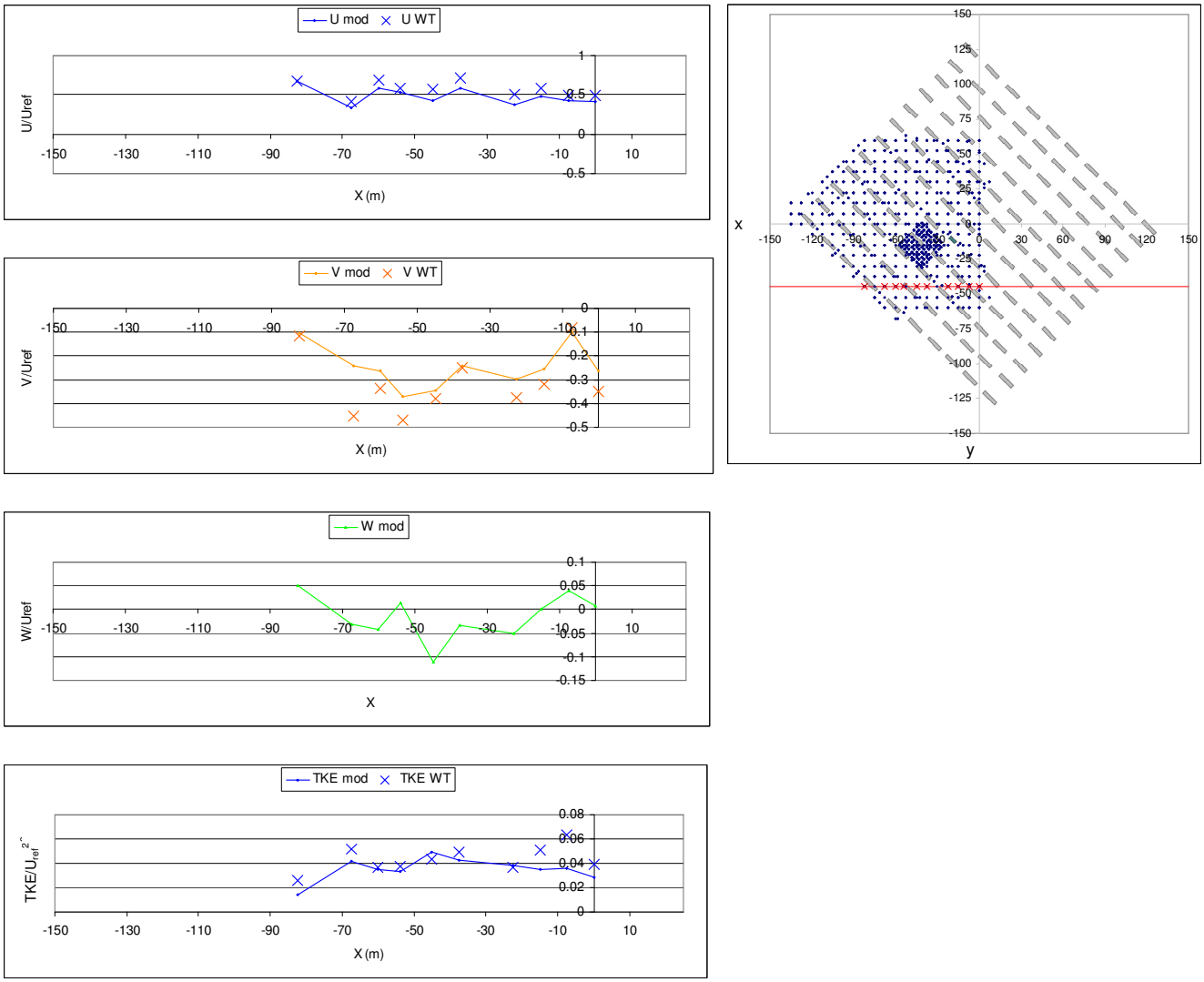

Figure 3.21 - Horizontal profiles of dimensionless U, V and W components, and TKE, for Y=-45 m, at 1.275 m height (*mod* and *WT* notations represent the numerical results and wind tunnel data, respectively).

The analysis of Figure 3.21 shows a slightly underestimation of the modelled U component in all measuring points with the exception of the outer point. Nevertheless, the modelled results for this wind component are able to simulate the tendency of the experimental data. The discrepancy found in the modelling results may be explained by a possible model overestimation of flow perturbation with upstream origin. In fact, the overestimation observed for the V component may substantiate the previous hypothesis. Once more, only the outer measuring point agrees with the experimental data. The remaining measuring

points follow the tendency of the wind tunnel data with the exception of one located at X=-68 m.

The modelled TKE values are capable of simulating the tendency of the experimental data despite an observed model underprediction at the measuring points located near the Y axis.

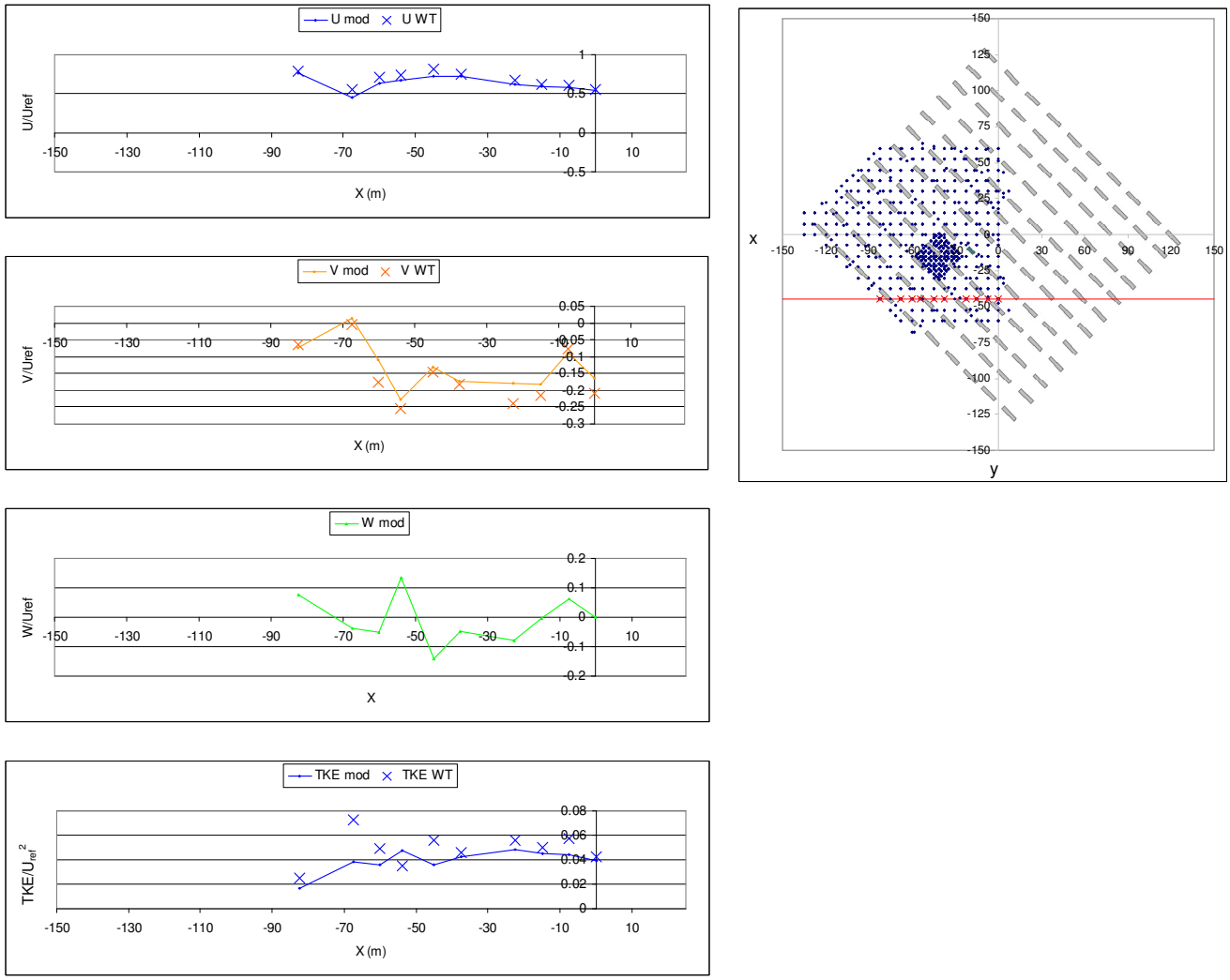

Figure 3.22 - Horizontal profiles of dimensionless U, V and W components, and TKE, for Y=-45 m, at 2.55 m height (*mod* and *WT* notations represent the numerical results and wind tunnel data, respectively).

The horizontal profile at the top of the buildings (Figure 3.22) show a better agreement of the U component with the wind tunnel data than the previous profile, despite a slightly model underprediction. It is also observed an overprediction of the modelled V component, but characterized by a capacity to predict the evolution trend of the experimental data. The modelled TKE values are generally underpredicted in all measuring points.

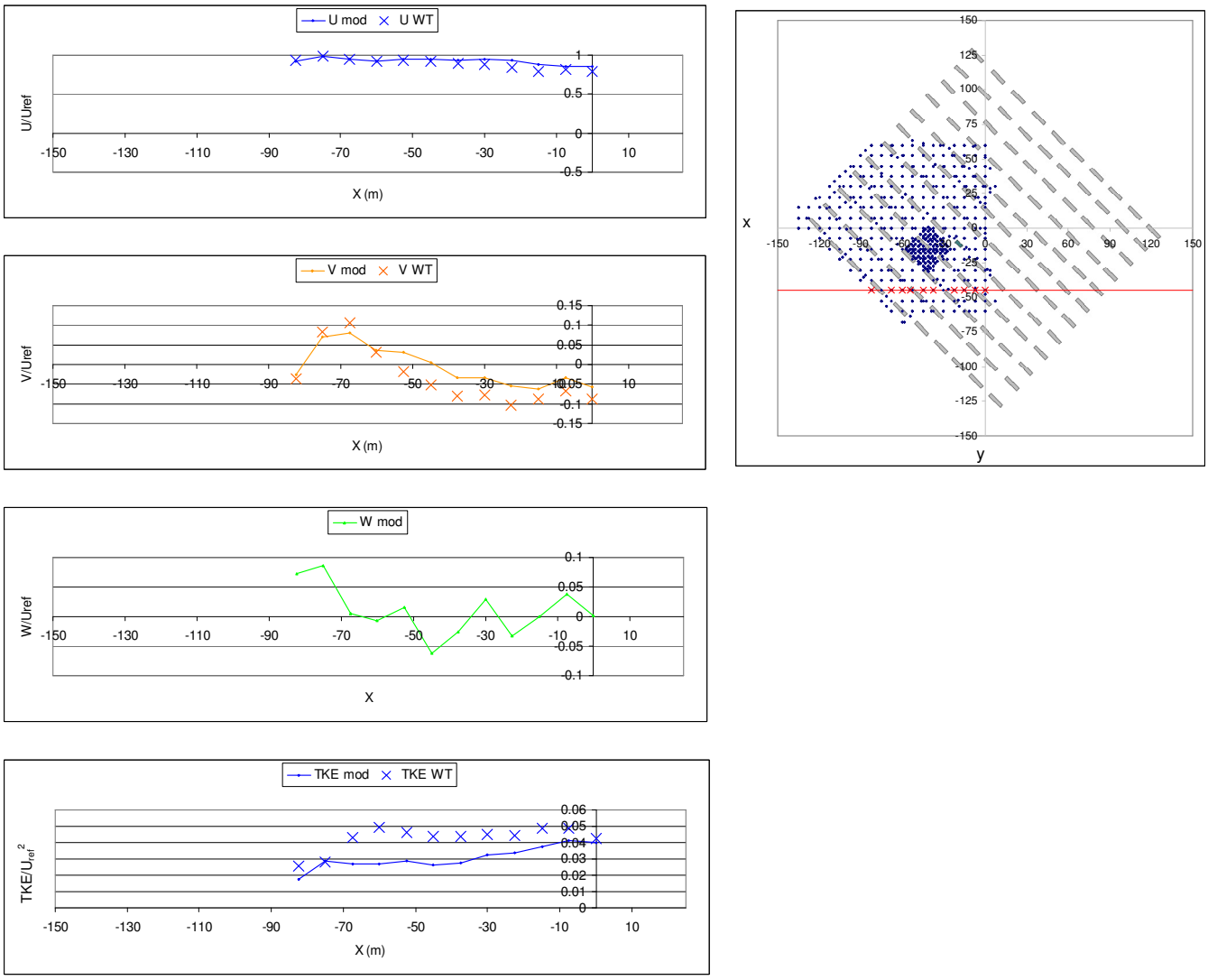

Figure 3.23 - Horizontal profiles of dimensionless U, V and W components, and TKE, for Y=-45 m, at 5.1 m height (*mod* and *WT* notations represent the numerical results and wind tunnel data, respectively).

Figure 3.23 presents the horizontal profiles at 5.1 m height, where it is possible to find a good agreement between the modelled values of U component and the wind tunnel data. There is an overestimation of the modelled V component for the majority of the measuring points but again following the tendency of the experimental data. The modelled TKE continue to underpredict the experimental values.

The vertical profiles of dimensionless U, V and W components, and TKE, are presented for the spanwise street canyon at the middle of the array, for the 0.5 m model resolution (Figure 3.24, 3.25, 3.26). The location of the different plotted profiles is shown in the attached map.

In the TKE vertical profiles the plotted variables *tkeU WT* and *tkeW WT* correspond to the contribution of the turbulent velocity wind component U and W, respectively, for the estimation of the turbulent kinetic energy.

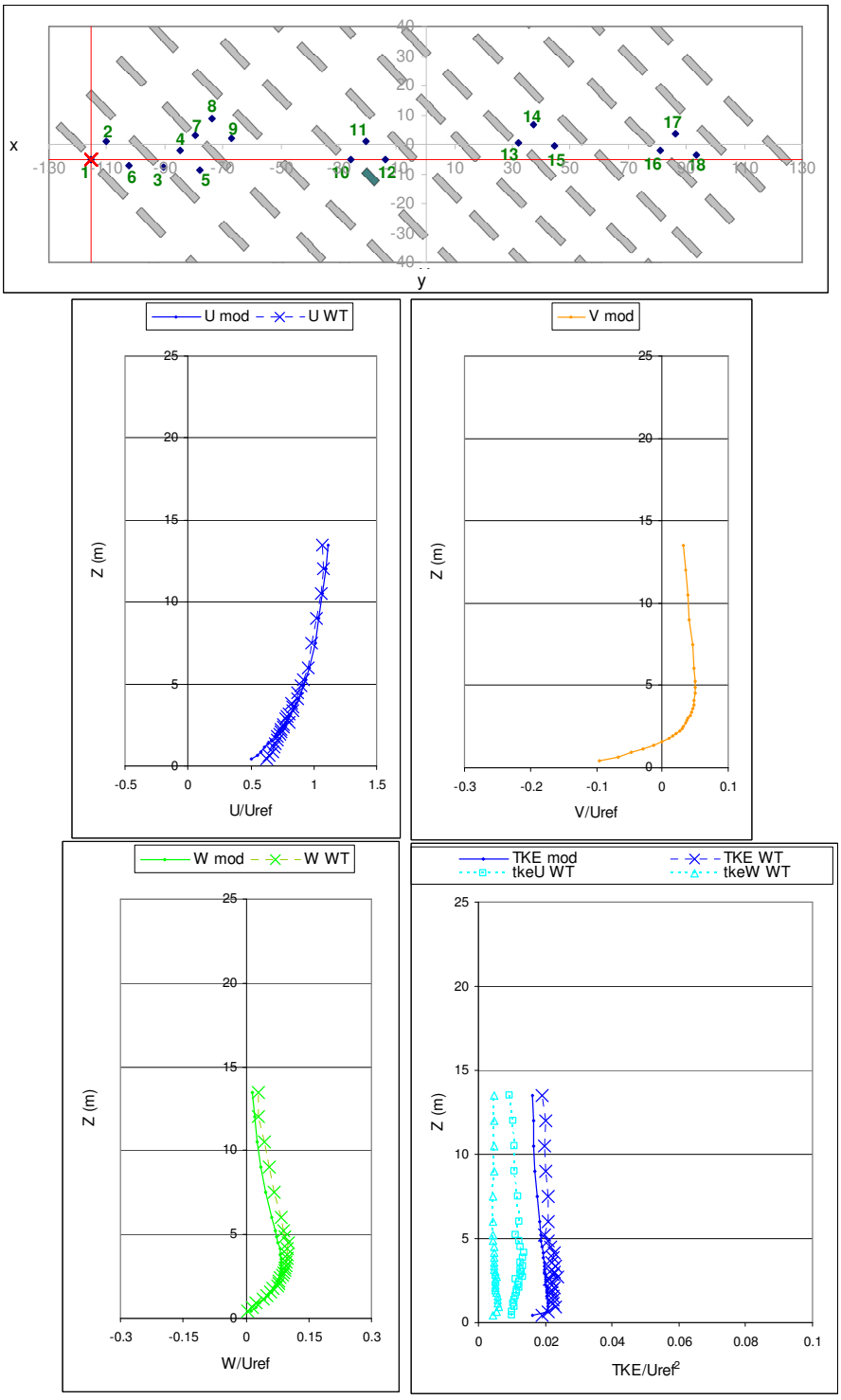

Figure 3.24 - Vertical profiles of dimensionless U, V and W components, and TKE, at location 1 (*mod* and *WT* notations represent the numerical results and wind tunnel data, respectively).

In Figure 3.24, the analysis of the vertical profile for the U wind component shows an underprediction of the modelled values till approximately 5 m height, where the influence of obstacles in the main flow is expected. The overestimation of the recirculating lenght from the upwind building, one the characteristics of the *k-ε* models, may have contributed for the underestimation of the U component. On the other side, above the 5 m height it is seen a small overprediction of the modelled results.

The W wind component profile indicates a good agreement with the experimental data till the 2.55 m height, corresponding to the top of the buildings, followed by a model underprediction. The latest indicate an underestimation of the perturbed flow with height.

The analysis of the TKE profile shows an underprediction of the modelled values that may be related with the underestimation of the modelled U and W components. It may also be observed a higher contribution of the experimental values of the U turbulent wind component to the total experimental TKE value, in comparison with the turbulent W component.

For the location 6 (Figure 3.25), the vertical profile of the modelled U wind component is underestimated till the 2.55 m height, but presented a good agreement for the remaining experimental positions. The previous mentioned handicap of the *k-ε* models related with the formation of an extended cavity zone behind the obstacles may be responsible for the decrease of the U component in this specific area.

It is observed a good model agreement for the W component despite a small model underprediction above the building's top. The modelled TKE values are underpredicted over the entire profile but with a higher discrepancy in the area between 2.50 m and 5 m above the building's height. The previous may be caused by an overestimation of the TKE experimental values due to the assumption of the V component values. Nevertheless, the modelled values present a similar evolution tendency of the experimental data.

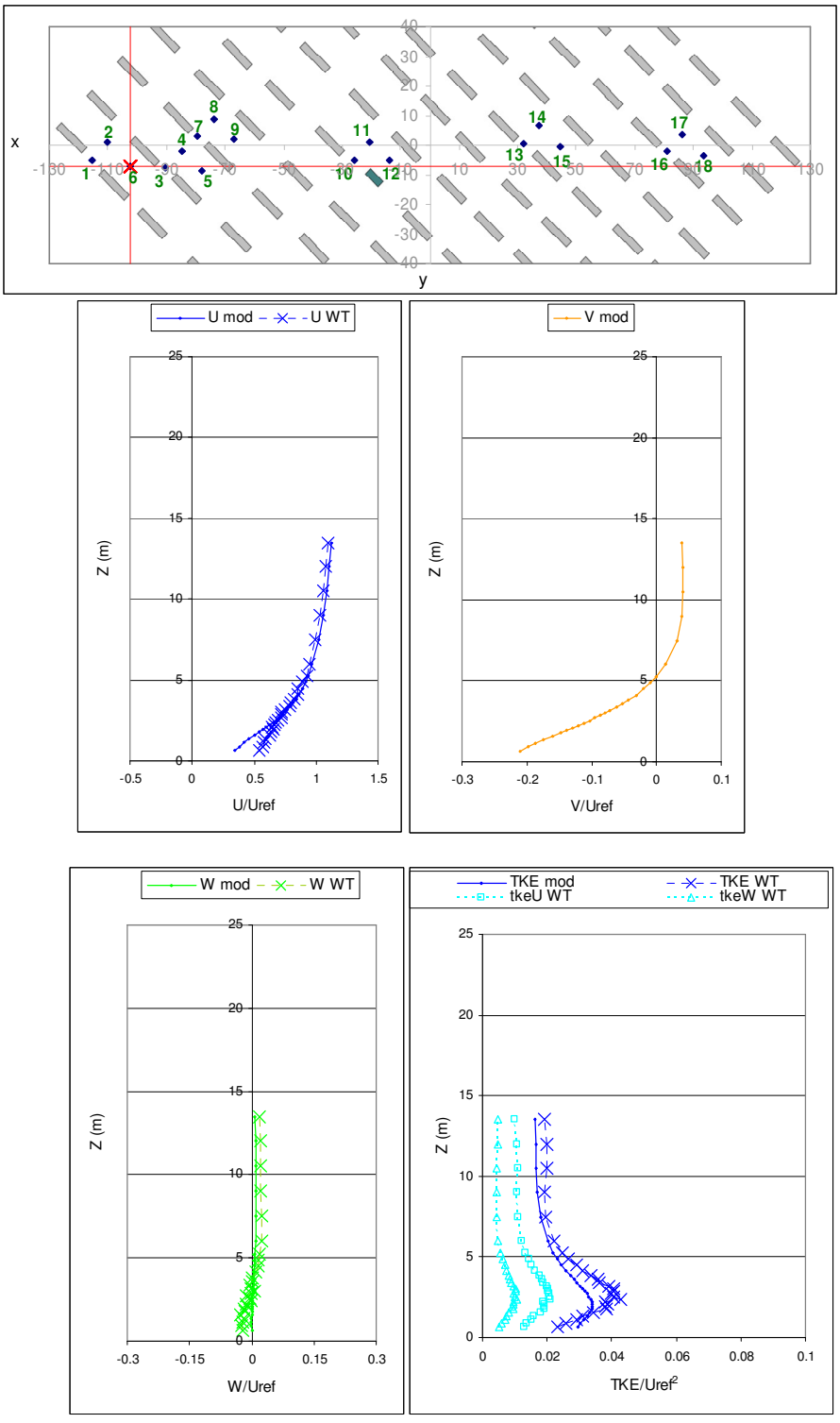

Figure 3.25 - Vertical profiles of dimensionless U, V and W components, and TKE, at location 6 (*mod* and *WT* notations represent the numerical results and wind tunnel data, respectively).

The analysis of Figure 3.26**,** presenting a vertical profile inside the domain, shows a good model prediction for the U component and an evident overprediction of the W component

till the 10 m height, indicating the non-existence of modelled vertical velocity. This may indicate an underprediction of a recirculation zone in this specific location.

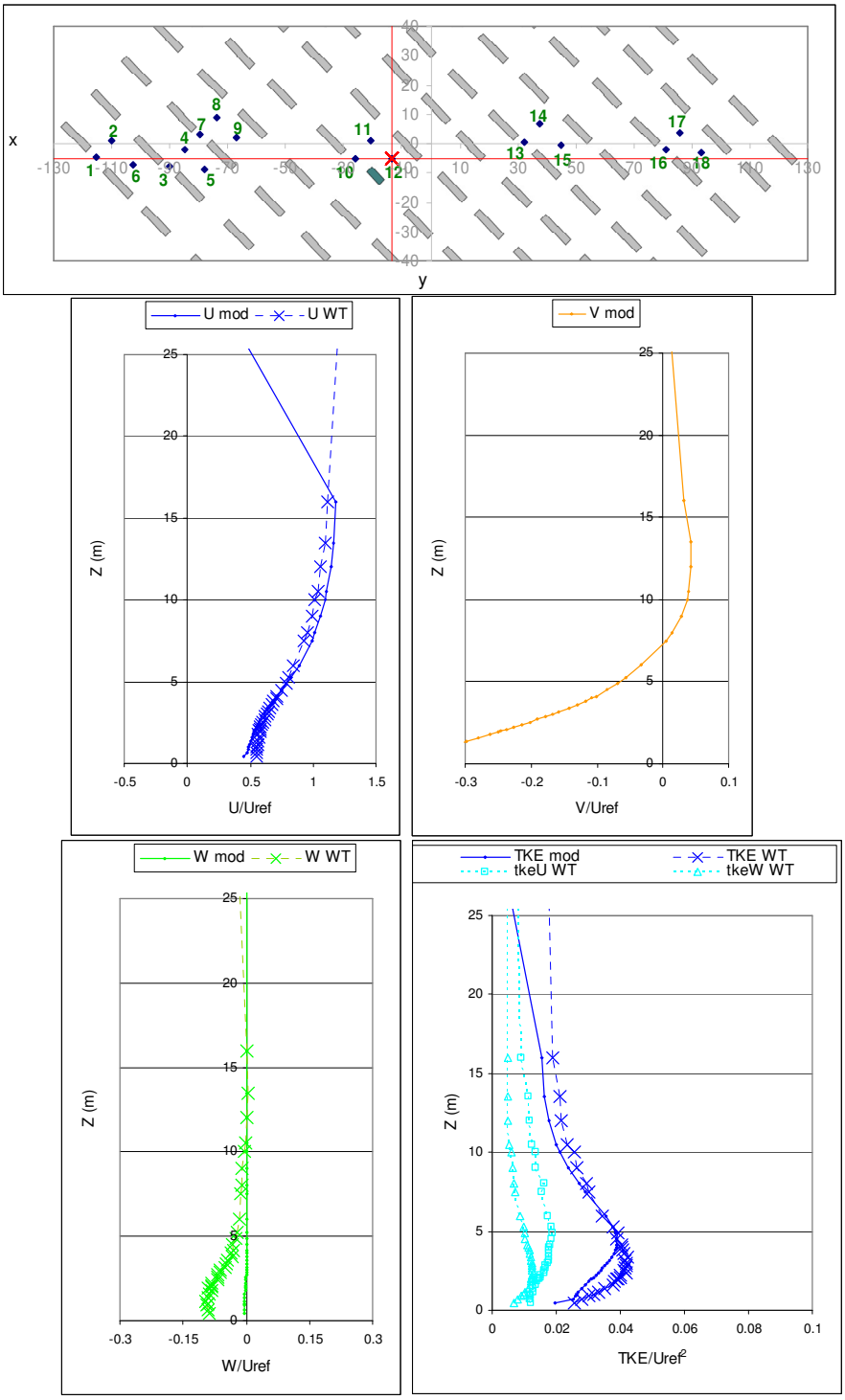

Figure 3.26 - Vertical profiles of dimensionless U, V and W components, and TKE, at location 12 (*mod* and *WT* notations represent the numerical results and wind tunnel data, respectively).

The modelled TKE profile presents a similar tendency of the experimental data despite an observed underprediction of the modelling data. Considering the model behaviour for the W component, the reasonable agreement achieved between modelled and experimental TKE data may indicate an advantage from the estimation process of experimental TKE.

In Figure 3.27**,** horizontal profiles of dimensionless concentration of passive tracer are plotted for different distances (42 m, 99 m and 142 m on the X axis) from the emission source, which is marked in the right-hand map as a red square. For this results presentation, the Cartesian axes were turned 90º on the clockwise direction.

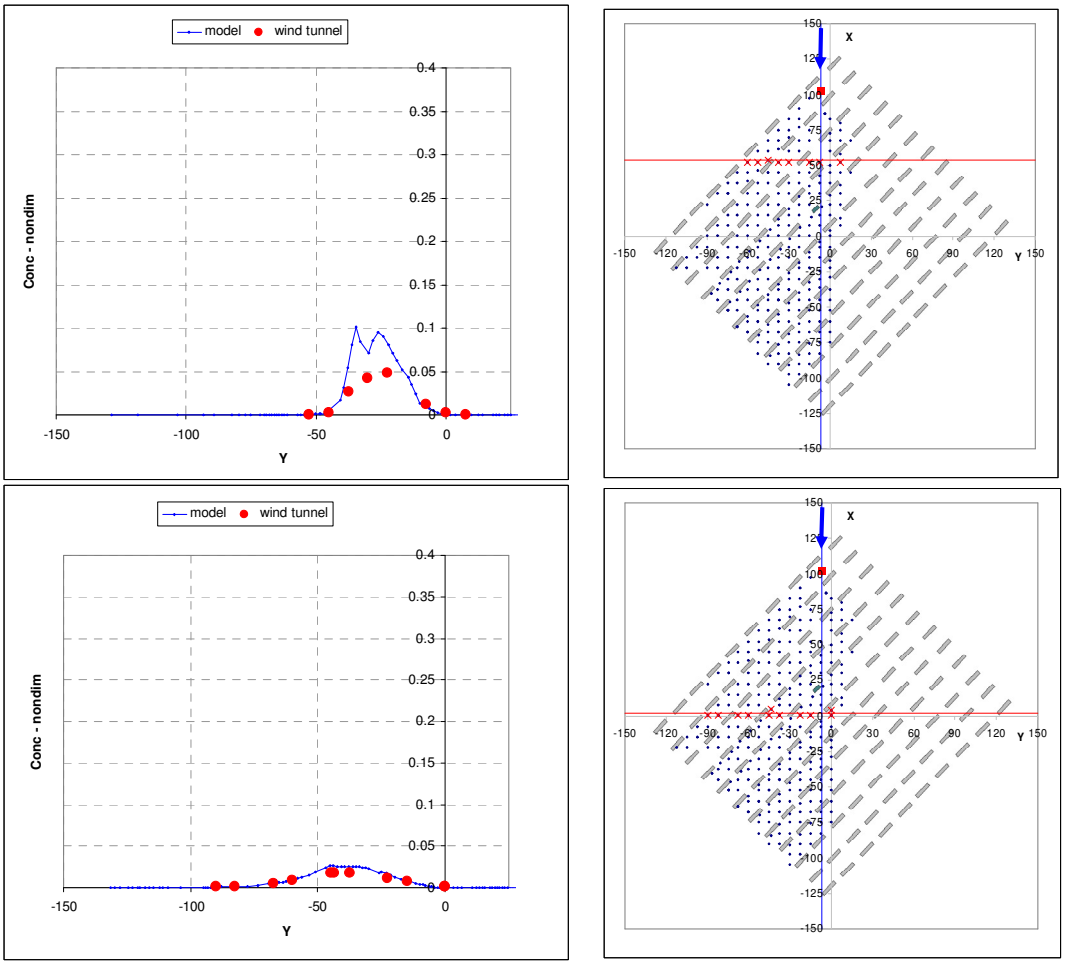

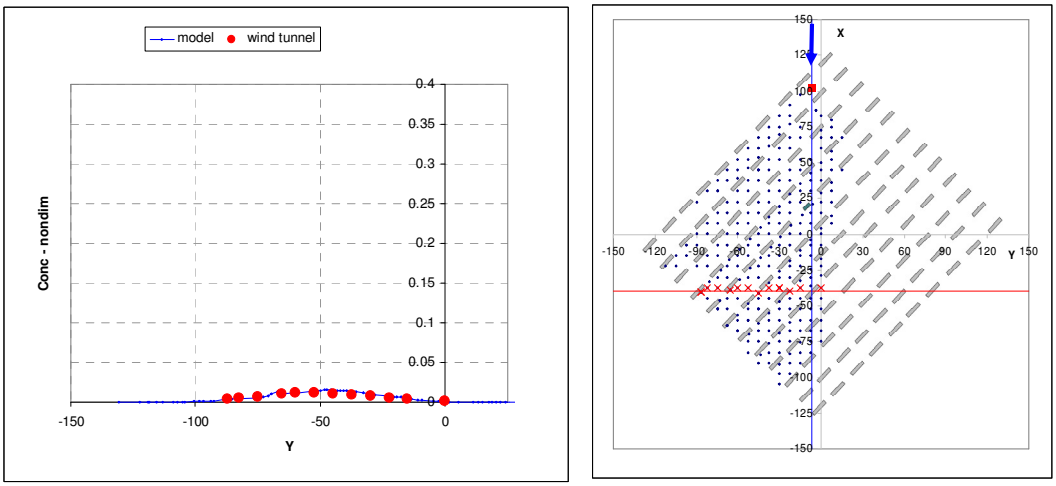

Figure 3.27 - Horizontal profiles of dimensionless concentration at 42 m, 99 m, 142 m distance from the emission source.

The analysis of Figure 3.27 indicates that there is a good agreement between modelled and experimental data for the second and third horizontal planes. At 42 m distance from the emission source, it is observed an overprediction of the modelled concentrations for the middle measuring points. This implies that the model has limitations to correctly simulate the higher concentrations near the emission source.

Figure 3.28 presents the scatter plots of the dimensionless velocity components U and W, and TKE, considering 566 modelled/measured data pairs from the sum of all vertical profiles. The location of the considered profiles is signed with circles on the attached map. The analysis of results shows a better agreement for the U component than for the W component. As it was expected, it is observed a poor correlation between the measured and modelled TKE values.

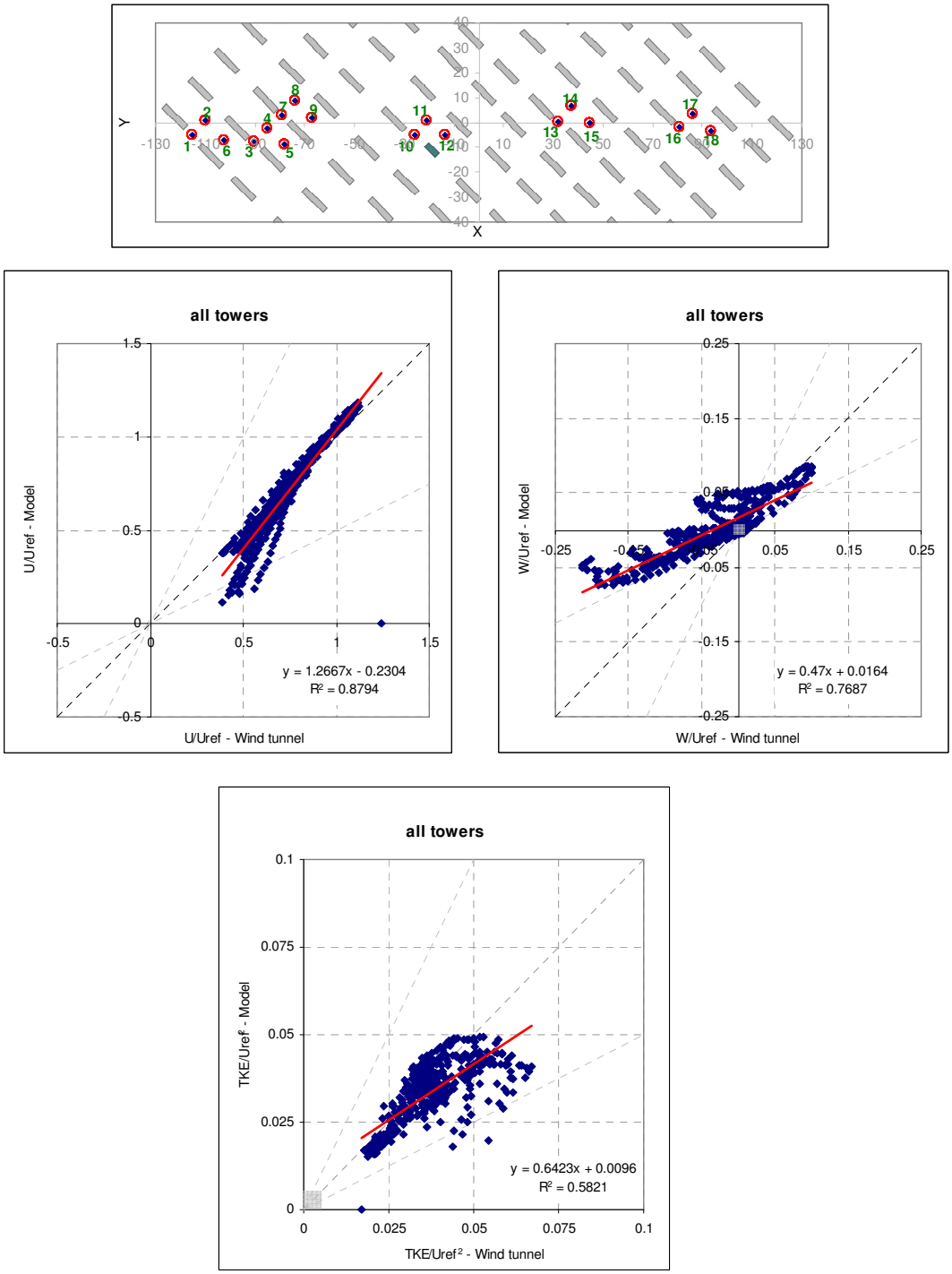

Figure 3.28 - Scatter plots of the dimensionless U and W wind components, and TKE, for all vertical profiles.

Figure 3.29 presents the scatter plots of the dimensionless velocity components U and V, and TKE, considering 732 modelled/measured data pairs from the sum of all horizontal

layers. The location of the measuring points in each horizontal layer is identified with circles in the attached map.

The analysis of results shows a good correlation between modelled and measured values of both U and V components. On the opposite side, the modelled values of TKE present a small agreement with experimental data. Nevertheless, this result should be interpreted with caution since the experimental TKE values are a result of a predictive process, as it was previously explained.

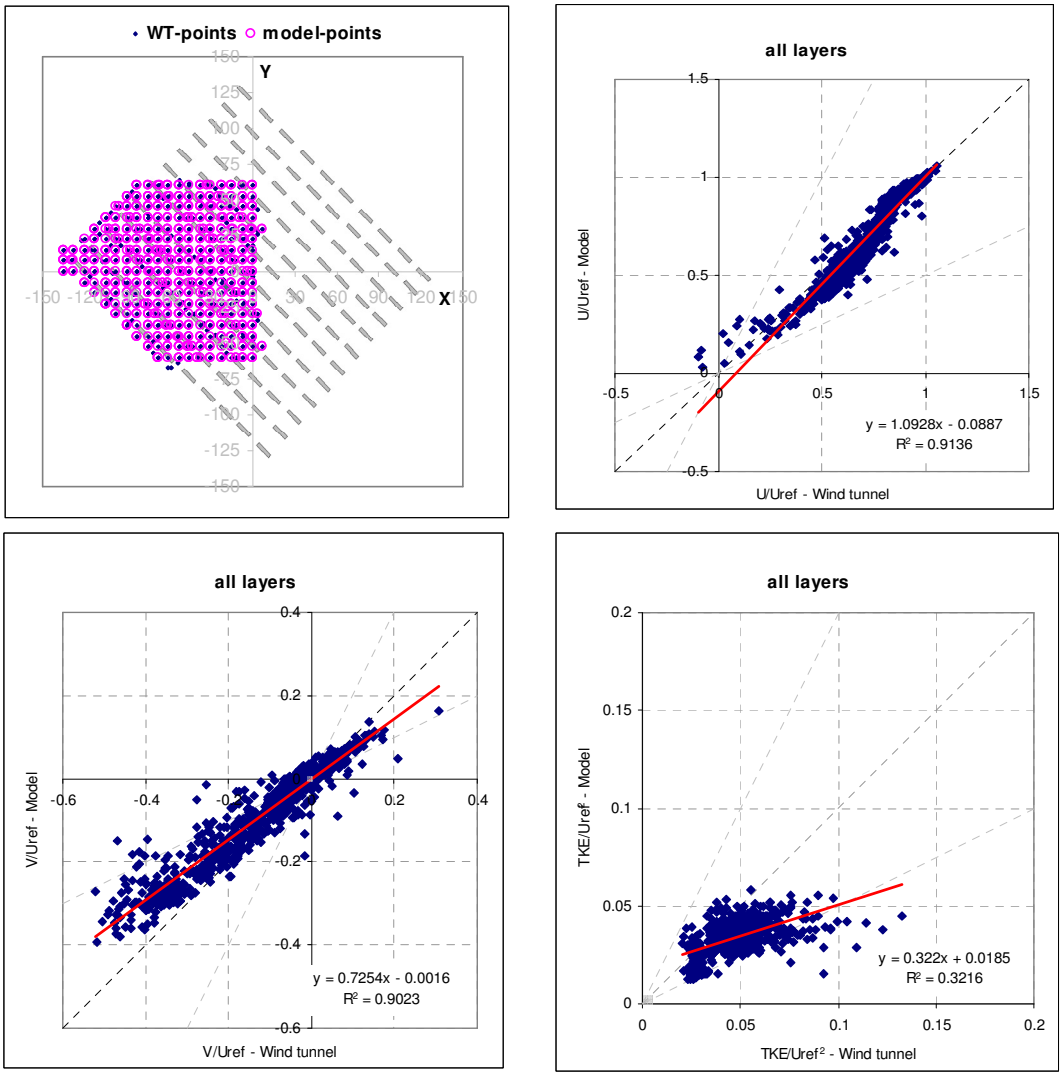

Figure 3.29 - Scatter plots of the dimensionless U and V components, and TKE, for all horizontal layers.

Figure 3.30 presents the scatter plot of the dimensionless concentration, considering 255 modelled/measured data pairs from the sum of all horizontal layers. The location of the measuring points in each horizontal layer is identified with circles in the attached map.

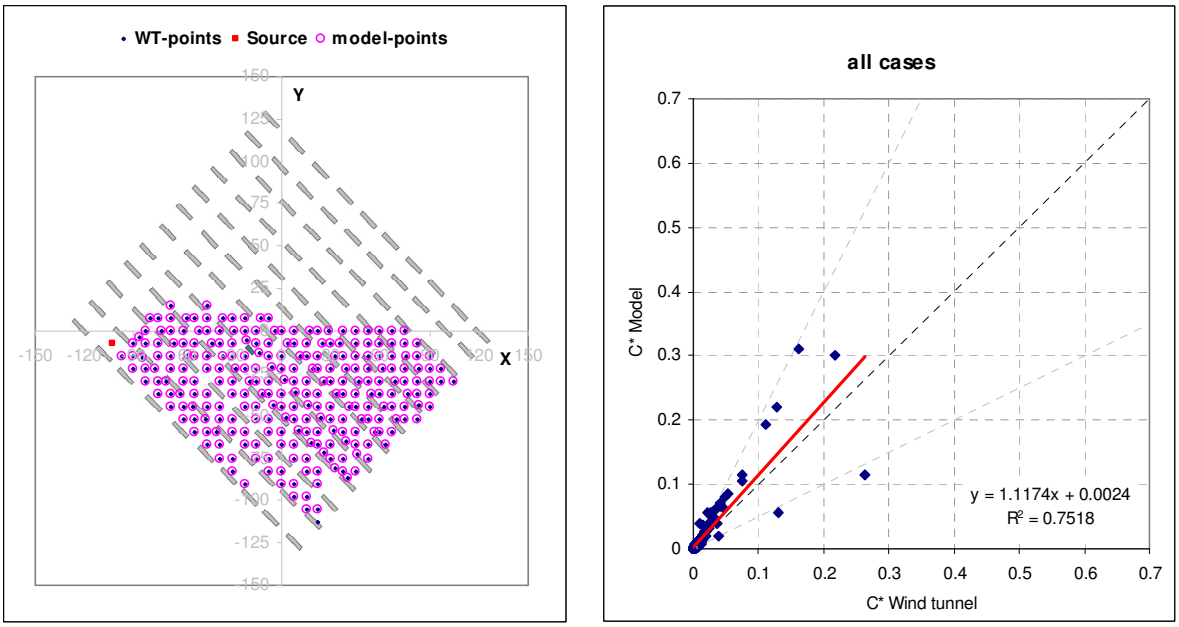

Figure 3.30 - Scatter plot of the dimensionless concentration for all horizontal layers.

The analysis of results shows an acceptable agreement between modelled and experimental concentration values.

3.2.5. Statistical analysis

VADIS results were quantitatively evaluated using a direct point-by-point comparison with wind tunnel data, focusing on the mean velocity components, the TKE and on the concentration. The statistical parameters previously presented in §3.1.3.6 were used in this evaluation.

Moreover, the model quality acceptance criteria described in §3.1.3.7 and summarized in Table 3.3 were used to conclude on the adequacy of model performance.

Table 3.3 - Model acceptance criteria.

[Olesen, 2005]	FAC2>0.5 |FB|<0.3 NMSE<4
[Chang and Hanna, 2004]	Hit rate (q) >= 0.66

The Hit rate parameter was used for the analysis of the mean wind components, the TKE, and the concentration, considering the following threshold values for the absolute (W) and relative (D) deviations: W=0.008 (U component), W=0.007 (V component), W=0.007 (W component), W=0.005 (TKE); W=0.003 (Concentration) and D=0.25 for all the analised parameters. The absolute deviation (W) threshold values used for the Hit rate estimation were decided according to the uncertainty measurement of each variable (wind components and concentration). The W threshold value for TKE was derived from the VDI Guideline [VDI, 2005].

The following statistical parameters were also used in the analysis of the concentration results: Correlation coefficient (R), FAC2, FB and NMSE.

Table 3.4 presents the hit rate calculations for U, V and W velocity components and TKE for the three modelling resolutions 0.5 m, 1 m and 2 m for the different measuring grids considered in the MUST experiment (presented in Figure 3.8) or a combination of them, namely: coarse grid; coarse grid combined with vertical profiles; fine grid; vertical profiles; fine UW plane grid; all measurement points. The statistical results on the 1 m and 2 m grid resolutions appear as an example of application, since the criteria to perform this validation exercise only allow higher model resolutions.

Table 3.4 - Hit rate calculations for U, V, W and TKE for 0.5 m, 1 m and 2 m model resolutions.

	Measurement Grids																	
	Coarse			**Coarse+Profiles**			**Fine**			**Profiles**			**Fine UW plane**			**All**		
	2 m	1m	0.5m	2 m	1m	0.5m	2 m	1m	0.5m	2 m	1m	0.5m	2 m	1m	0.5m	2 m	1m	0.5m
U	0.56	0.62	0.87	0.58	0.63	0.92	0.32	0.37	0.82	0.64	0.73	0.91	0.46	0.59	0.99	0.23	0.60	0.90
V	0.25	0.32	0.38	0.25	0.30	0.37	0.16	0.22	0.33	-	-	-	-	-	-	0.24	0.31	0.35
W	-	-	-	0.22	0.28	0.34	-	-	-	0.32	0.38	0.44	0.13	0.19	0.24	0.21	0.29	0.33
TKE	0.20	0.28	0.46	0.26	0.32	0.63	0.15	0.24	0.49	0.36	0.49	0.62	0.11	0.23	0.68	0.23	0.32	0.60

The analysis of Table 3.4 shows that the acceptance criterion for the hit rate (q>= 0.66) is only accomplished for the U component results of the 0.5 model resolution, in all measurement grids. The modelling results within the defined criterion are marked with a grey colour. In addition, the criterion is fulfilled for the TKE variable for the fine UW plane and for the highest model resolution.

The hit rate results for the V and W components are considerably below the defined criterion for the 0.5 m model resolution. It is also observed a positive result of the hit rate for the U wind component simulated, with 1 m model resolution, for the entire vertical profiles.

The aggregated results of the data used in the previous hit rate calculation do not allow studying the accuracy of the model predictions in between and above the buildings. Table 3.5 presents these detailed hit rate estimation for the 0.5 model resolution, allowing the comparison of the model performance close and far from the buildings. Accordingly, the data were aggregated below 1.5H and above 1.5H (container height H=2.54 m). Since all fine UV measurement planes are placed up to approximately the container height, their accumulated results give an impression of the performance between the buildings up to the container height.

The number of modelled/measured data pairs used in the differente hit rate estimations are signed in light grey on Table 3.5. The hit rate results within the acceptance criterion are highlighted on dark grey.

Table 3.5 - Detailed hit rate calculations for U, V, W and TKE for 0.5 m model resolution.

	z [m]	U	V	W	TKE
Coarse	1.275	0.85	0.39	-	0.39
	2.55	0.96	0.47	-	0.50
	5.1	0.99	0.22	-	0.51
Fine	0.9	0.75	0.39	-	0.33
	1.275	0.82	0.28	-	0.47
	1.575	0.83	0.31	-	0.49
	2.55	0.91	0.32	-	0.66
uw plane	2.55	0.99	-	0.24	0.68
coarse + profiles	≤ 1.5H	0.89	0.43	0.31	0.59
		890	595	295	890
all	≤ 1.5H	0.89	0.38	0.22	0.56
		1299	967	332	1299
coarse + profiles (=all)	≥ 1.5H	0.98	0.22	0.57	0.71
		454	252	202	454
coarse + profiles	all	0.92	0.37	0.34	0.63
fine uv planes	all	0.82	0.33	-	0.49
all	all	0.90	0.35	0.33	0.60

The analysis of Table 3.5 shows that all the hit rate results concerning the U component accomplish the acceptance criterion. Once more, the hit rate results for the V and W components are below this criterion. There are also good hit rate results on the TKE estimation for the fine UV plane (z=2.55 m), the fine UW plane and for all measuring points of the coarse+profile grids.

Table 3.6 presents the statistical analysis performed for the concentration results obtained for the three model resolutions, using the totality of the measuring points (260 measurements positions). The results in agreement with the acceptance criteria (Table 3.3) are signed with dark grey.

Table 3.6 - Statistical analysis of concentration results for 0.5 m, 1 m and 2 m model resolutions.

Model resolution	R	q	FAC2	FB	NMSE
0.5 m	0.751	0.679	0.969	-0.266	1.648
1 m	0.479	0.501	0.484	-0.390	3.800
2 m	0.387	0.350	0.340	-0.485	4.690

The analysis of Table 3.6 shows that the concentration results obtained for the 0.5 model resolution accomplish all the defined criteria, indicating a good model performance for this variable.

3.2.6. Discussion of results

When evaluating model performance, it is important to keep in mind the concept of fitness for purpose, meaning that the tests that the model is exposed to should reflect the purpose of the intended model application. Also, the performance of a model is not only due to the merits of the model, but also depends on the way in which it is applied. For the current exercise, the whole concept of fitness for purpose was directly related to the definition of suitable acceptance criteria for the evaluation of microscale models application to urban areas.

According to the defined acceptance criteria, the hit rate parameter was used for the evaluation of the modelled flow and concentration fields. Moreover, the FAC2, FB and NMSE statistical measures were applied to evaluate the concentration results.

The analysis of the statistical results indicates a good model performance for the U wind component and concentration, and a weak performance for the V and W wind components and TKE. However, the evaluation of the model performance concerning the flow field may be considered limited by the application of a unique parameter, the hit rate, that has also some inherent limitations such as the definition of its absolute deviation threshold. In this sense, it would be important the development of other model acceptance criteria for the evaluation of the flow field in microscale models.

Also, the results obtained for the TKE parameter must be analized with caution since the experimental TKE was derived from only two measured turbulent wind components. Its use in the current exercise allowed evaluating the evolution trend of the model results.

In the analysis of the flow model behaviour it is also important to stress the inherent limitations of the k-ε model regarding the empirical nature of their model parameters and the difficulty of wall treatment. These limitations are traduced into a recognized difficulty to correctly simulate the flow impingement and separation near obstacles, and to capture the right dimension of the recirculating vortices. These were in fact one of the possible reasons for the discrepancy found between the measured and modelled flow results within the obstacles array. The wall treatment problematic can be minimized by the increase of the grid resolution within the urban built area.

Nevertheless, the development of such detailed validation exercise allowed concluding that VADIS model is able to predict with a certain level of accuracy the flow and transport of pollutants within urban areas.

The application of the same case study for a different approach flow direction would allow a more complete validation of VADIS model for both flow and concentration variables.

4. MICROSCALE EXPOSURE MODELLING

The microscale CFD model VADIS presented in Chapter 2, and minutely evaluated in Chapter 3, was used as one of the tools to develop the Microscale EXPOsure model (MEXPO). This exposure model especially developed for urban areas will allow the estimation of the short-term individual exposure to atmospheric pollutants on a three-dimensional (3D) basis, considering information on flow and ambient pollutants concentration. A detailed description of the MEXPO model, including its methodology and working scheme is developed in subchapter 4.1.

The role of ventilation in buildings and its influence into the indoor air quality, and consequently to the indoor exposure, is addressed in subchapter 4.2. Special emphasis is given on the natural ventilation mechanisms. A review of the existent ventilation standards in Europe, including Portugal, is also presented.

4.1. The microscale exposure model MEXPO

The mathematical basis of human exposure estimation lies down on the microenvironment concept already mentioned in §1.1. This is because different microenvironments (e.g. outdoor, inside a car, inside an office, inside a school) contribute differently to the exposure estimation to atmospheric pollutants, due to both microenvironmental concentration ranges and the time fractions spent in each.

Thus, exposure is defined as the product of the concentration in a microenvironment and the time spent in that microenvironment, and the total exposure as the sum of the exposures in all microenvironments during the time of interest. The integrated exposure can be expressed as [Hertel *et al.*, 2001]:

$$E_i = \sum_j^J C_j t_{ij} \qquad [\mathrm{M.L^{-3}.T}] \qquad (4.1)$$

where, E_i is the total exposure for person i over the specified period of time; C_j is the pollutant concentration in microenvironment j; t_{ij} is the residence time of the person i in microenvironment j; and J is the total number of microenvironments.

MEXPO model uses the integrated exposure definition (Eqn.4.1) to assess individual exposure to atmospheric pollutants in urban areas, according to the structure presented in Figure 4.1.

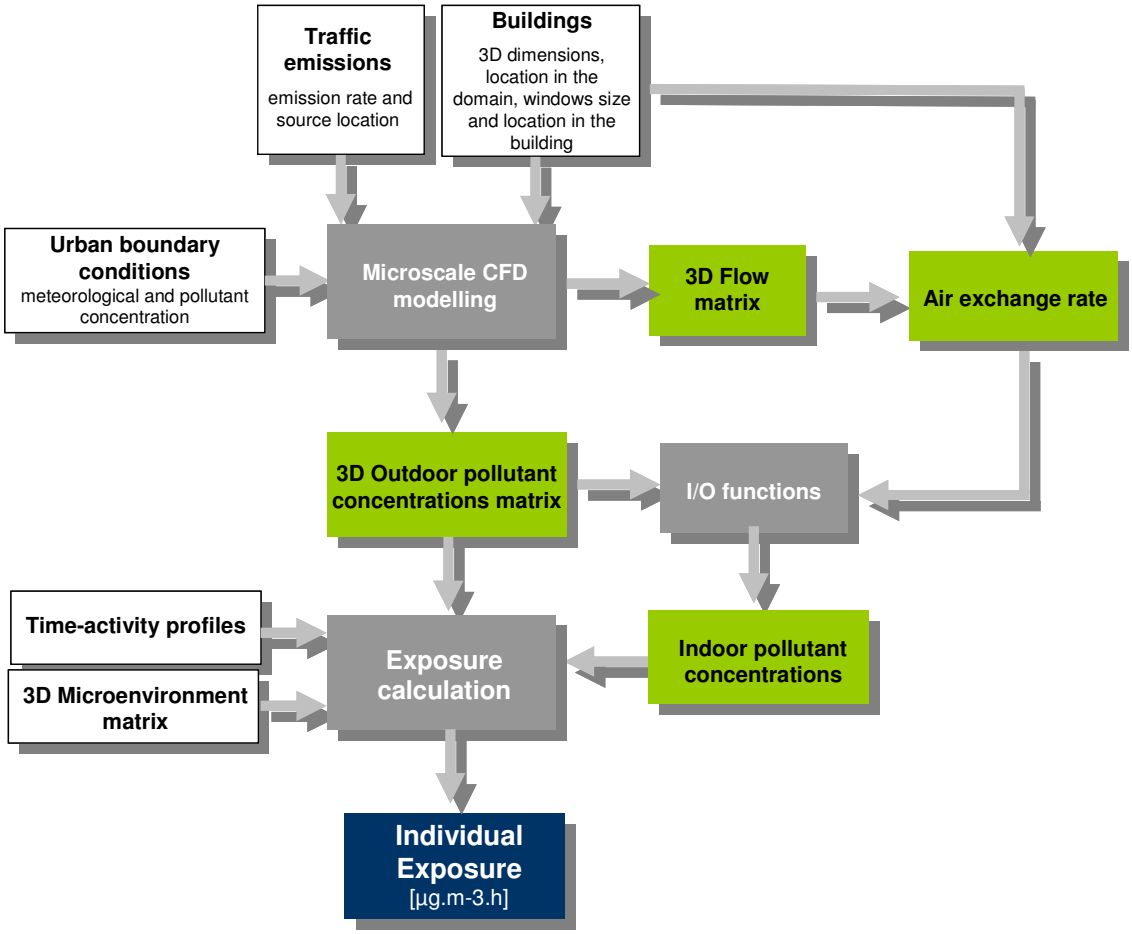

Figure 4.1 - Schematic representation of MEXPO model.

Ambient pollutant concentrations calculated by VADIS microscale model are both used, directly and indirectly, to estimate the integrated individual exposure to air pollutants through the information on the time-activity pattern of individuals on different microenvironments. Pollutants concentrations in indoor microenvironments are determined using a mass balance equation that requests information on the outdoor modelled concentrations, the indoor emission sources and the ventilation rates that characterize the

indoor space. The latest can also be predicted with MEXPO model. For this purpose, the 3D flow around buildings, estimated by the CFD microscale model, and information on windows size and location in the building are used to determine the air exchange rate for wind-induced natural ventilation conditions.

Due to its computational effort and high running times, CFD models applications have feasible simulations of one hour to several days. Therefore, this model characteristic determines that the assessment of exposure will be focused on the study of acute health effects due to short-term exposures.

In this sense, the model will be specially focused on the exposure assessment to particular pollutants with known acute effects on human health. This is the case of NO_2, where effects are believed to be related more to short term peak levels than to long term averages [EC, 1991; 2006a]. Concern about the effects of nitrogen dioxide has been focused on people with pre-existing lung disease. There have been numerous studies of people with asthma, chronic obstructive pulmonary disease, or chronic bronchitis showing that exposure to low levels of nitrogen dioxide can cause decrements in forced vital capacity and forced expiratory volume or increases in airway resistance [EC, 2005].

Particle matter was also considered in the model based on their known acute effects on human health. Health consequences from PM include acute effects such as increased daily mortality, increased hospital admission rates for exacerbation of respiratory disease, fluctuations in the prevalence of bronchodilator use and cough, and reduction in lung function [WHO, 2001].

The choice of one indicator for particulate matter also requires consideration. At present, most routine air quality monitoring systems generate data based on the measurement of PM_{10} as opposed to other particulate matter sizes. Consequently, the majority of epidemiological studies use PM_{10} as the exposure indicator [WHO, 2006]. PM_{10} represents the particle mass that enters the respiratory tract and, moreover, it includes both the coarse (particle size between 2.5 and 10 μm) and fine particles (measuring less than 2.5 μm, $PM_{2.5}$) that are considered to contribute to the health effects observed in urban environments.

Based on this fact, MEXPO model will be specially developed for the assessment of exposure to NO_2 and PM_{10} pollutants.

4.1.1. Microenvironment definition

MEXPO model defines the *outdoor*, *residential*, *school* and *transport* as main microenvironments. The 3D regular grid of the microscale model, divided into equal control volumes according to a defined model resolution, will be used to create the 3D microenvironment matrix of the study domain. This implies that each cell of the CFD model is allocated to a different microenvironment according to Figure 4.2. Traffic induced turbulence allows to consider traffic as a volume source. In this sense, the control volume cells near the ground where roads are located will be assumed as transport microenvironment.

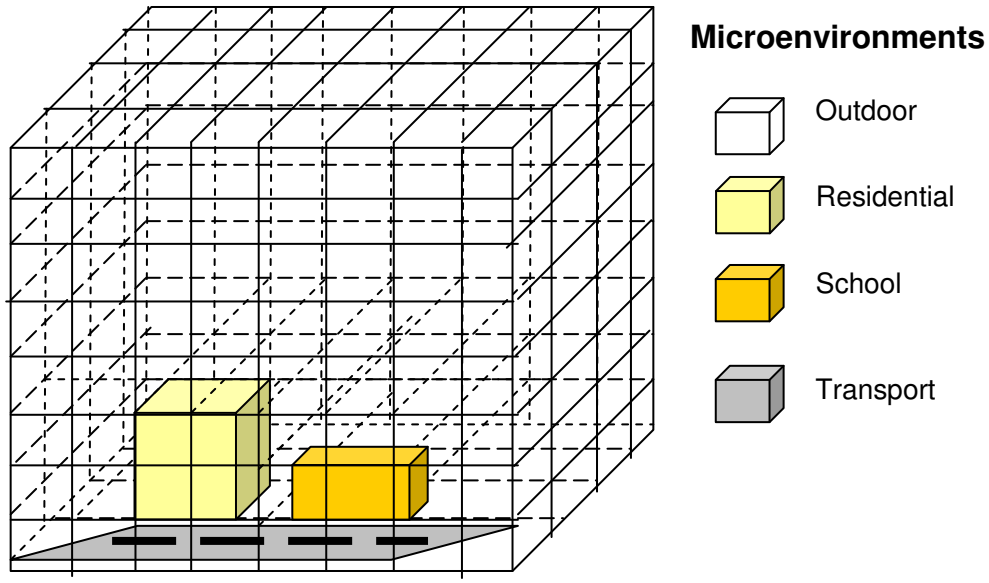

Figure 4.2 - Definition of the 3D microenvironment matrix.

4.1.2. Time-activity pattern

The time-activity pattern combines information on the location of the activity, the period or time when the activity took place (e.g., time of day, phase in life), and the duration of the activity. The activity is here directly associated to the microenvironment where it took place. The movement of an individual within the different microenvironments and the time spent in each one of them are then characterised by its individual time-activity profile.

In MEXPO model, the individual time-activity profiles are traduced by the time spent by each individual in each control volume cell of the microscale model.

4.1.3. Outdoor pollutant concentrations

As already mentioned, VADIS CFD model will be used within MEXPO to estimate the flow and pollutants concentration 3D fields over an urban area. The necessary input to run the CFD model was already discussed in §2.2 and generally includes information on domain size and resolution, building and streets location within the domain, building volumetry characterisation, traffic emission rates and the boundary conditions of the domain in terms of meteorological and pollutant concentration variables. The latter can be provided by measured data at the entrance of the domain, reflecting the urban meteorological and dispersion conditions, or through numerical simulation with air quality models with higher domain ranges, such as mesoscale models.

The 3D characterisation of flow and pollutants dispersion in urban areas provided by VADIS CFD model will also allow MEXPO to assess the exposure of individuals living in high-rise apartment buildings.

VADIS model considers pollutants as inert compounds. In this sense, PM_{10} and NO_2 will be treated as passive pollutants.

4.1.4. Indoor pollutant concentrations

The single-compartment, steady state mass balance equation (Eqn. 1.2) will be used in MEXPO to estimate pollutants concentrations in indoor microenvironments using the outdoor concentrations estimated by the CFD model and the existent indoor emission sources [Burke *et al.*, 2001; Koutrakis *et al.*, 1992]. The air ventilation rate enters in this formulation due to its importance in promoting the dilution of concentrations from indoor sources and its influence in the transportation of outdoor pollutants to indoors in natural ventilation conditions. Assuming that a constant concentration is maintained inside each microenvironment under steady-state conditions,

$$C_{in} = \frac{paC_{out}}{a+k} + \frac{Q_{is}}{(a+k)V} \qquad (1.2)$$

where, C_{in} and C_{out} are, respectively, the indoor and the outdoor concentrations ($\mu g.m^{-3}$); p is the penetration coefficient (dimensionless); a the air exchange rate (h^{-1} or ACH-Air

Change per Hour); k the decay rate (h^{-1}); Q_{is} the mass flux generated by indoor sources ($\mu g.h^{-1}$); and V is the room or building interior volume (m^3).

To determine the indoor pollutant concentrations on the different microenvironments from outdoors, MEXPO model uses the concentration value of the outdoor microenvironment cell adjacent to the respective indoor microenvironment cell where buildings openings, such as windows, are located. The defined methodology is demonstrated in Figure 4.3. The pollutant concentrations for the rest of the indoor microenvironment cells without openings are estimated as an average of the adjacent indoor cells. This methodology is applied for all indoor microenvironments.

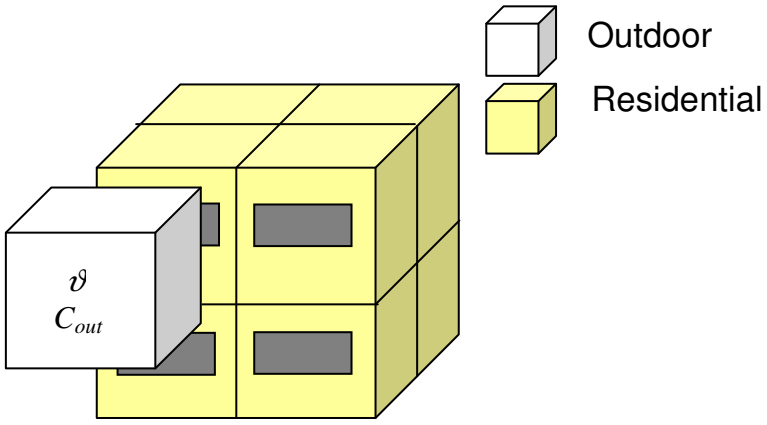

Figure 4.3 - Schematic representation of the methodology for estimation of indoor concentration from outdoors in buildings (ϑ -outdoor wind speed ($m.s^{-1}$); C_{out}-outdoor pollutant concentration ($\mu g.m^{-3}$)).

For vehicles (traffic microenvironment) the indoor concentration will be based on the average concentrations of the adjacent outdoor cells without considering the source emission rate term of Eqn.1.2.

4.1.4.1. Indoor emissions

The indoor pollutant emission rate (source strength) is usually not well known and not constant. Indoor pollutant source strengths are highly variable among buildings, and considered the biggest cause of the variation in pollutant concentrations indoors. Pollutants may be adsorbed by room surfaces during high concentration periods and desorbed again into the air during low concentration periods [EC, 2003].

Indoor emission sources are discussed here specifically for NO_2 and PM_{10} according to the criteria previously presented in §4.1 that determines the assessment of exposure with MEXPO model to pollutants with known acute health effects.

Other important indoor pollutants such as environmental tobacco smoke (ETS) and some volatile organic compounds (VOC) are of interest for their suspected chronic effects related to long term exposure, and in that sense, were not included in the model.

The major indoor sources of NO_2 are tobacco smoke, woodstoves and fireplaces, gas appliances and kerosene heaters [EC, 1993]. Tobacco smoking is considered to have negligible emissions compared to gas cooking [Eatough *et al.*, 1989] and consequently it is not considered here as a source of NO_2. Emissions from gas heating were also neglected since the vast majority of these appliances are exhausted outdoors.

The majority of NO_x from gas combustion is emitted as NO and it is estimated that 20-30% of the undiluted products of combustion is NO_2. Dimitroulopoulou *et al.* (2001) determined an average emission rate of NO_2 from gas stoves of 3.6 $mg.min^{-1}$. This emission rate is included in MEXPO model to characterize the indoor sources of NO_2 in a residence microenvironment, where cooking activities take place.

In large urban areas, the most important source of indoor air particles, in the absence of smoking, is usually outdoor air. Nevertheless, other indoor sources such as resuspension of soil dust, cooking, wood burning, gas heaters can also contribute to the raise of particle matter concentrations indoors [EC, 2006a]. Few data is currently available to characterise PM_{10} indoor emission rates. A probability function proposed by Dimitroulopoulou *et al.* (2006) defines an average emission rate for PM_{10} from indoor cooking activities of 2.5 $mg.min^{-1}$. Wallace (1996) suggested a PM emission rate of 0.018 $mg.min^{-1}$ from other indoor sources than cooking and smoking (e.g. vaccuming, washing, sweep). Thus, the previous emission rates were included in MEXPO model for the characterisation of residence microenvironments. The emission rate associated with PM ressuspension was not considered in the model due to lack of available data.

4.1.4.2. Penetration coefficient and decay rate

As air travels through intentional and unintentional openings in the building envelope gaseous and particle pollutants have an opportunity to interact with surfaces encountered along the way. For air that enters the building the scrubbing effect can remove an amount of some pollutants, so that, in some specific situations in the absence of indoor sources, indoor levels can be lower than those outdoors. This process is incorporated into the model by the building penetration coefficient, a dimensionless factor representing the amount of pollutant of outdoor origin that survives the journey through the building envelope [CA.GOV, 1998]. Thus, the penetration coefficient p is a measure of the ability of a pollutant to penetrate the building envelope; $0 < p < 1$. Based on limited measurements, it is widely believed that, in naturally ventilated buildings, the building envelope presents no barrier to nonreactive pollutants [Thatcher and Layton, 1995]. In EPA (1997) it was concluded that particles less than 10 μm in aerodynamic diameter penetrate building envelopes with an efficiency approaching that of nonreactive gases.

In MEXPO model it is assumed that the penetration coefficient, p, is 1 for NO_2 and PM_{10} pollutants.

The decay rate k of pollutants represents the first-order rate of reduction in the indoor air concentration of a pollutant, due to physical/chemical reactions in air or indoor surfaces, expressed in units of inverse time (e.g. h^{-1}). It depends on many factors, such as scale of turbulence produced by indoor air flow and type of pollutant. For particles, factors such as size, shape, electrostatic charge, and density greatly influence its deposition rate.

Yamanaka (1984) described a decay rate for NO_2 of 0.99 h^{-1}. According to Wu *et al.* (2005) it was assumed a decay rate for PM_{10} of 0.65 h^{-1}.

4.1.4.3. Air exchange rate

The air exchange rate, a, is defined as the volume of indoor air replaced by outside air per unit time and can also be regarded as the efficiency of the air mass exchange [Milner *et al.*, 2005]. It is usually expressed in air changes per hour (ACH or h^{-1}), or as the volume flow rate, Q_v, of the replacement air coming into a room or building per unit volume (usually $m^3.s^{-1}.m^{-3}$ or $l.s^{-1}.m^{-3}$) [EC, 2006a]. Both measurement units are related through the following expression:

$$a = \frac{Q_v}{V} \qquad (4.2)$$

where V is the room or building interior volume (m^3).

MEXPO model allows the estimation of the air exchange rates for the defined indoor microenvironments using an empirical *formulae* for single-sided wind-induced natural ventilation (Eqn. 4.3) [ASHRAE, 1997; Liao *et al.*, 2004]. These conditions are discussed in more detail in §4.2.

$$Q_v = 0.025 E A \vartheta \qquad (4.3)$$

The microscale exposure model combines the 3D flow field estimated by the CFD model with information on windows size and location on buildings, as well as, the interior volume of the indoor microenvironment to estimate the air exchange rate. The wind speed, ϑ, estimated for the outdoor cell adjacent to the indoor microenvironment cell where the window is located is combined with information on the window opening surface, A, to estimate the volume flow rate, Q_v, through the same scheme presented in Figure 4.3.

MEXPO model distinguishes the variation on windows opening, during night and day and for summer and winter conditions, using an opening effectiveness coefficient E (dimensionless). An area of 10 % of the total opening area is considered in case of closed windows, corresponding to the air exchange through unintentional openings [Straw, 2000]. Unintentional or adventitious openings are the cracks, gaps and unknown openings in windows, doors, walls and roof, which are in opposite to the purpose-provided ventilation openings. Ventilation arising from the flow through unintentional openings is known as infiltration (or exfiltration) [Wilson, 1961].

The air exchange rate, a, is then computed using the microenvironment interior volume, that coincides with the respective cell volume, according to Eqn.4.2.

The previous model formulation is used in MEXPO model to determine the ventilation rate in indoor spaces, as residence and school microenvironments. For traffic microenvironment the average air exchange rate of 38.0 h^{-1} proposed by Ott *et al.* (2007) was included in the exposure model, considering an average vehicle speed of 32 $km.h^{-1}$, the driver's window open at a medium position and the rest of the windows closed, and with the car recirculation and fan systems closed.

Table 4.1 summarizes the parameters used in MEXPO model for the determination of the indoor PM_{10} and NO_2 concentrations.

Table 4.1 - Summary of parameters used in MEXPO model.

	Indoor emission rate (Q_{is}) [mg.min^{-1}]		Penetration coefficient (p) [-]	Decay rate (k) [h^{-1}]	Air Exchange rate (a) [h^{-1}]	
	Cooking activity	Cleaning activities			buildings	transport
PM_{10}	2.5	0.018	1	0.65	Equations 4.2/4.3 (a)	38.0
NO_2	3.6	-	1	0.99		

(a) The opening effectiveness coefficient, E, is 0.10 for closed windows.

The ventilation of buildings, with special emphasis on the natural ventilation mechanisms and its relation to indoor air quality, is discussed in the following subchapter.

4.2. Ventilation of buildings

The air exchange rate is a measure of the building ventilation capacity. Ventilation of buildings in general may be done for several reasons, the most important is to remove or dilute the indoor generated pollutants and supply fresh air for human beings. Ventilation can be achieved by natural, mechanical or hybrid processes with the purpose of indoor air quality control, air flow distribution patterns for thermal comfort and passive heating and cooling.

Natural ventilation systems rely on natural forces, such as wind and the temperature difference between a building and its environment, to supply fresh air to buildings interiors [BSI, 1991]. Mechanical ventilation makes use of electrically powered fans or more complex ducting and control systems to supply and/or extract air to and from the building. Air conditioning systems are based on mechanical ventilation systems with various levels of service to provide a fully controlled indoor environment within specified criteria, i.e. temperature, humidity, etc [CIBSEAM10, 1997]. Hybrid ventilation systems can be described as systems providing a comfortable internal environment using both natural and mechanical ventilation systems. It operates according to the variation of the ambient conditions within individual days or the season, to use different features of the two systems optimally in response to the external environment. To achieve energy efficiency demands the hybrid ventilation system is smartly controlled in natural ventilation system or mechanical ventilation system, which is using forces as long as possible and electric fans only if necessary [Heiselberg, 1999].

4.2.1. Natural ventilation

Apart from Northern Europe the dominating European ventilation system is natural ventilation [Niachou and Santamouris, 2005]. Naturally ventilated buildings have several benefits over mechanically ventilated ones, including reduced energy consumption, lower maintenance and capital costs, less space requirements, increased occupant satisfaction when given local control over indoor conditions, high productivity and fewer sick building syndrome complaints [Yang, 2004]. Due to its energy saving capabilities, natural ventilation is seen today as a strategy for sustainable development with a lead role in the climate change abatement scenarios in urban areas. In this sense, this work focused only on the natural ventilation processes.

Natural ventilation is subject to the variability of wind speed, wind direction, air temperature and opening configuration [Straw, 2000]. There are three forms of natural ventilation: wind induced only; temperature difference only; wind and temperature difference. The following descriptions of the different processes refer to a simple cubic structure with ventilation openings located on opposing faces as shown in Figure 4.4.

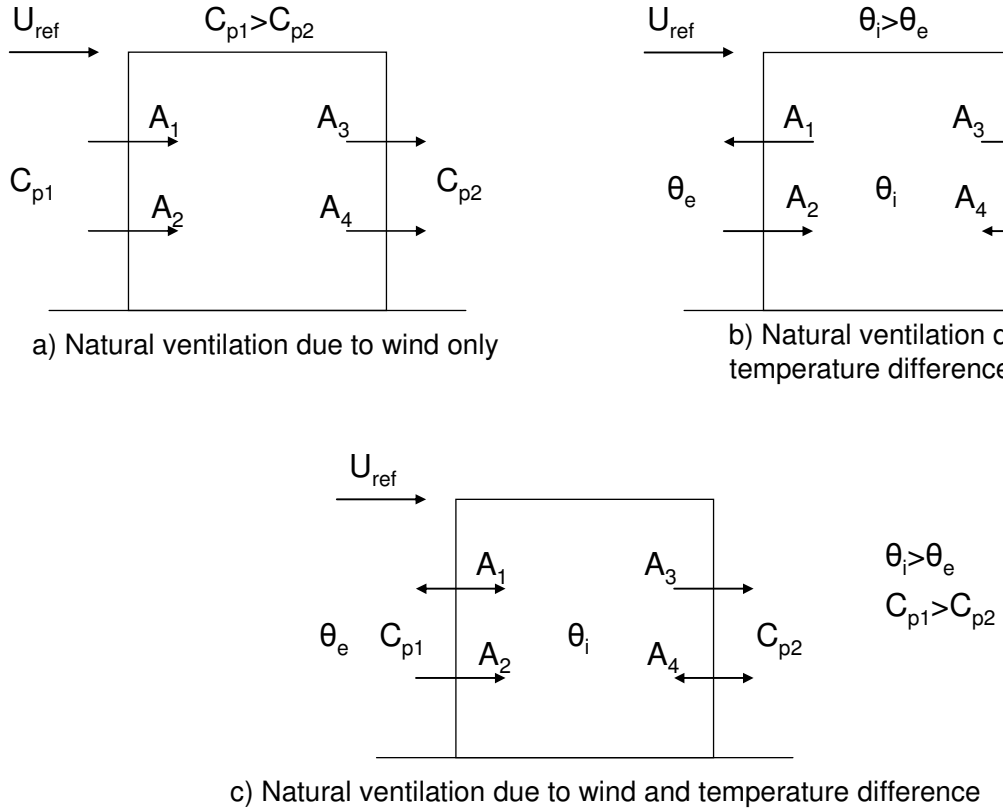

Figure 4.4 - Natural ventilation of a building by the three dominant mechanisms [Straw, 2000].

Ventilation can be induced solely by the action of the wind on the surface of the building, around the location of any openings in the building envelope (Figure 4.4a). The nature of the pressure distribution and the momentum of the incoming wind around the structure drive this form of ventilation, creating local areas of positive pressure (on the windward side) and negative pressure (on the leeward side) on buildings (Figure 4.5). Assuming no fluctuations in the incoming wind, flow is induced as a result of the difference in mean pressures between the building faces containing openings.

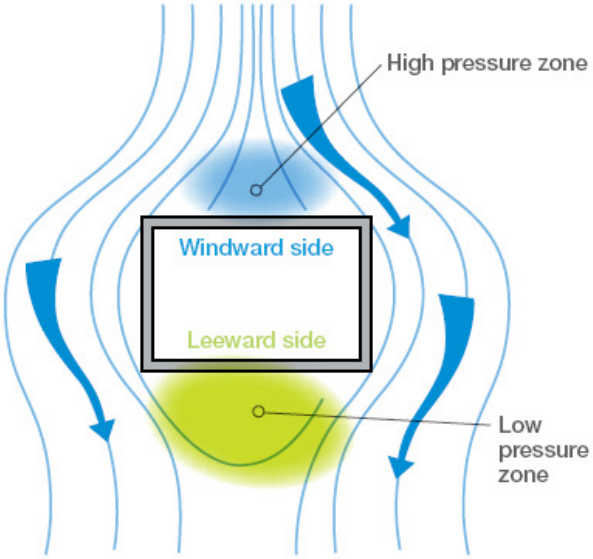

Figure 4.5 - Pressure effect from wind.

If the internal region of a building is at a higher temperature than the external environment the pressure difference leads to a flow of air through openings in the building envelope. In the case of Figure 4.4b, warm air rises vertically and exits through the upper openings (A1 and A3) with this air being replaced by air entering through the lower openings (A2 and A4). Ventilation rate is proportional to both temperature difference and height between openings.

When both wind and thermal effects are present, different ventilation flow patterns are produced depending upon the relative contributions of each. At low temperature differences, flow patterns are similar to those of wind acting alone. If however, temperatures are increased and wind speed is maintained at a constant (low) level a combined effect enhances the air flow through the lower windward and upper leeward

openings and inhibits flow through the upper windward and lower leeward openings (Figure 4.4c).

Papadakis *et al.* (1996) state that for free wind speeds exceeding approximately 1.8 $m.s^{-1}$, thermal buoyancy can be neglected. Hence the assumption that temperature effects are negligible is valid in many cases. This assumption was used in this work.

Natural ventilation can be defined as the movement of outdoor air through intentional openings (doors, windows) and through unintentional openings in the building envelope [Asimakopoulos *et al.*, 2000]. Ventilation rate tends to refer to air exchange that is designed to occur whereas infiltration rate is the air exchange due to cracks and failures in a building envelope.

Natural ventilation is therefore one of the possible strategies for controlling the indoor air quality. Nevertheless, the assumption that ventilation will result in a better indoor air quality may not be valid in urban areas where outdoor pollution levels are high. Thus, it is important to question if the quality of the outdoor air is good enough to be used as ventilation air.

Buildings in an urban environment may be located near important pollutant sources (streets with high traffic density, car parks, exhaust stacks, cooling towers, etc.). Building design must take these local sources into account in order not to introduce high concentration of pollutants from the outside. Hence, siting air intake openings away from these specific pollutant sources is an important measure to control outdoor air pollutants from entering indoors, and consequently influence the indoor air quality conditions [Niachou and Santamouris, 2005]. Also, guaranteeing that a building is effectively sealed from the outdoor environment (building airtightness) can prevent contamination by outdoor infiltration.

4.2.2. Ventilation standards

One of the most important ways to achieve and maintain acceptable indoor air quality is by means of appropriate ventilation. The existing guidelines and standards specify ventilation rates or air change rates which are linked to the minimum acceptable pollutant concentrations. In that sense, and for many years, guidelines were based on metabolic CO_2 concentration on the assumption that the basic pollution source was the occupants' bioeffluents. However, the relevant standards for decades failed to provide sufficient guidelines in order to ensure satisfactory indoor air quality. The major mistake lay

precisely in the expressed or presumed assumption that the buildings' occupants were the main source of pollution. Based on this rationale the standards established a specific ventilation rate according to the different types of space and requirements of the occupants [Avgelis and Papadopoulos, 2004].

Ventilation standards were not yet been established within an European legal basis, therefore, the national standards and regulations are mostly based on national practice and differ very much from countries to countries.

Figure 4.6 depicts the required airflow rates per person for dwellings and offices in accordance to the standards of eight European countries. The higher ventilation rates standards are found for The Netherlands, in case of offices with smoking permission, and the United Kingdom, for dwellings and offices.

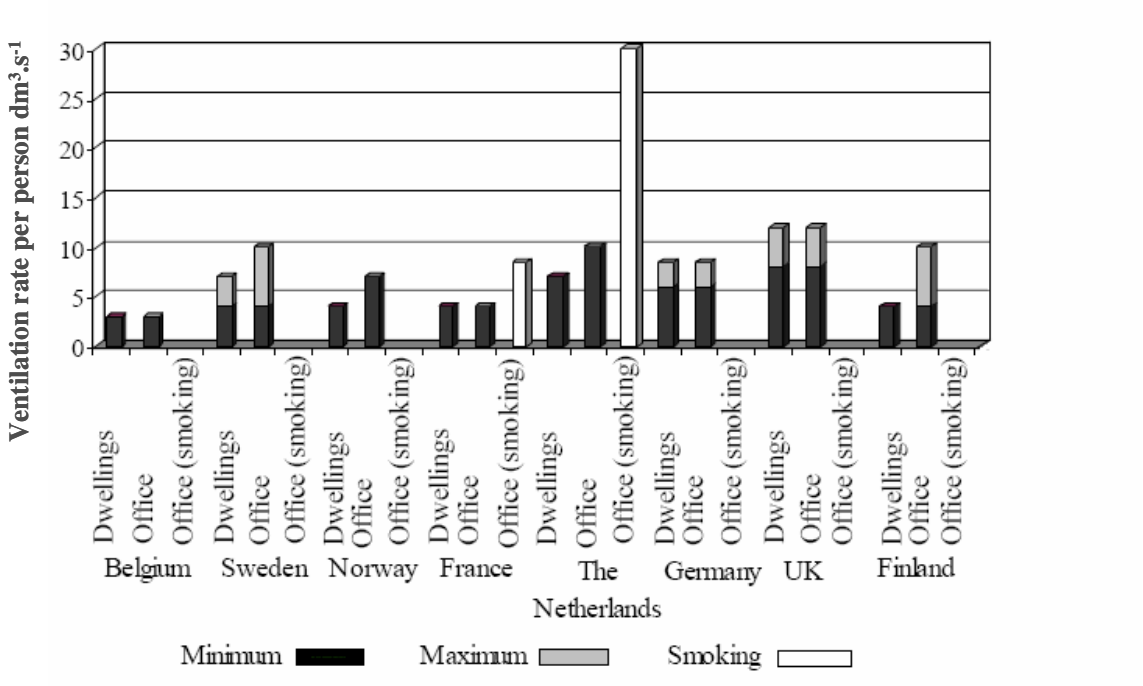

Figure 4.6 - Required ventilation rates per person for dwellings and offices in standards [EC, 2003].

The Portuguese national legislation (Decreto-Lei nº79/2006 de 4 de Abril, Regulamento dos Sistemas Energéticos e de Climatização dos Edifícios (RSECE)) also establishes minimum ventilation rates, per person or per square meters, according to the type of activity, to assure a suitable air quality in indoor spaces (Table 4.2). The indoor air quality is also regulated by the same national legislation through maximum allowed indoor pollutants concentrations, mentioned previously in Chapter 1.

Table 4.2 - Portuguese standards for minimum ventilation rates.

Type of activity		Minimum ventilation rates	
		[m^3.(h.person)$^{-1}$]	[m^3.(h.m^2)$^{-1}$]
Residential	Rooms and living rooms	30	
Comercial	Waiting-rooms	30	
	Commerce stores		5
	Storing areas		5
	Cloak-rooms		10
	Supermarkets	30	5
Meal services	Dining-rooms	35	
	Cafeterias	35	35
	Bar-rooms	35	35
	Kitchens	30	
Hotels	Rooms	30	
	Halls		5
Entertainment	Halls		5
	Lecture halls	30	
	Stage and studios	30	
	Cafeteria/foyer	35	35
	Pools		10
	Gymnasium	35	
Services	Offices	35	5
	Conference-rooms	35	20
	Assembly-rooms	30	20
	Drawing-offices	30	
	Consulting-rooms	35	
	Reception-rooms	30	15
	Computer-rooms	30	
	Lifts		15
Schools	Classrooms	30	
	Laboratories	35	
	Lecture halls	30	
	Librariess	30	
	Bars	35	
Hospitals	Rooms	45	
	Recovery areas	30	
	Terapy areas	30	

The Portuguese standards for schools (classrooms) and residentials (rooms and living rooms) will be used in the following chapter for the evaluation of the estimated ventilation rates as result of the MEXPO model application to a specific urban area.

5. ASSESSMENT OF INDIVIDUAL EXPOSURE TO ATMOSPHERIC POLLUTANTS

This chapter describes the application of MEXPO model to the urban area of Viseu in order to assess the short-term individual exposure to PM_{10} and NO_2 for a group of children, during both summer and winter meteorological conditions. The study area of Viseu was selected in the scope of the SAUDAR project that is briefly introduced in §5.1. Within this project experimental field campaigns were conducted in January and June 2006, providing detailed input data for the MEXPO model application and allowing the evaluation of model performance through comparison between measured and modelled data. MEXPO model application is presented in subchapter §5.2.

5.1. The SAUDAR project

SAUDAR is the Portuguese acronym of the project "The Health and the Air we breath" [URL 5], funded by the Calouste Gulbenkian Foundation. This national project has as main goals to study the relation between air quality (indoor and outdoor) and human health in an urban area presently with no considerable air pollution problems, and to evaluate the foreseen evolution of this relation based on the existent development plans for the region [Borrego *et al.*, 2007a].

Ten Portuguese towns, located in the inland part of the country were previously chosen as possible study area, assuming that currently they do not present air pollution related problems. The town of Viseu was selected among them due to its strategic location in the central Portuguese mainland region, near important road transport networks, and its projected high development in near future. This town has, simultaneously, the highest

population density (190 inhabitants.km^{-2}), the highest birth rate and the lowest mortality rate, in the group of the ten considered towns.

Viseu is a city located in the interior of Portugal with approximately 93000 inhabitants and an area of 507 km^2 [INE, 2001]. Its district is surrounded by the neighbourhood districts of Guarda and Aveiro, on the East and West sides, respectively, and Coimbra in the South (Figure 5.1a). Viseu occupies a strategic position within the international routes that connect the littoral side of Portugal, where the major sea ports are located, to the rest of Europe. In this sense, it is seen as an urban area with an enormous development potential, characterised by a rising economic activity and a young and growing population.

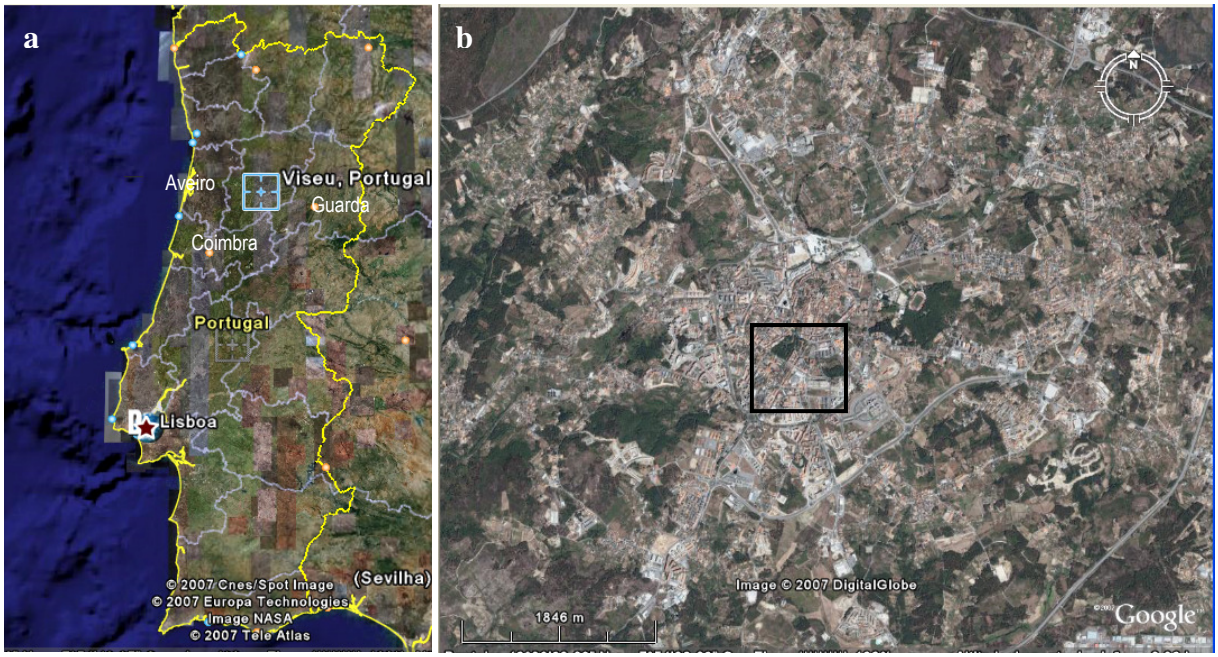

Figure 5.1 - Location of the study area: (a) within Portugal and (b) within the urban area of Viseu.

Presently, there are no indications of critical air quality problems in Viseu. Despite the lack of fixed monitoring sites, past field campaigns conducted in 1990, 1994, 1995 and 2002, using a mobile air quality station located in the centre of the city, show the fulfilment of air quality standards for the measured concentrations of NO_2, SO_2, O_3 and benzene [Borrego *et al.*, 2007b]. Nevertheless, these past monitoring campaigns may not be considered representative of the air quality levels in all urban area of Viseu.

In order to establish a relation between air quality and human health, children were used as air quality biomonitors in this project. Children represent the most vulnerably group of the population, spending more time outdoors and having more immature lungs and higher

ratios of ventilation rate to body weight than adults. Particularly, special attention was given in this study to children with respiratory problems, as asthma, since according to several epidemiological studies [EEA, 2005] there is a clear association between epidemics of asthma attacks in children and local peaks of air pollution.

Asthma is now the most common respiratory disease among western European children, afflicting 7 % of children aged 4 to 10, though there is large variation between countries. The explanation for soaring asthma rates remains uncertain. Asthmatics are particularly sensitive to air quality and several studies have shown a strong link between exposure to air pollution and the aggravation of asthma [Heinrich and Wichmann, 2004; Trasande and Thurston, 2005; Wong and Lai, 2004]. In this sense, a large survey was made in the major elementary schools located in the city centre of Viseu to identify the children with respiratory problems, such as asthma.

In the scope of SAUDAR, experimental field campaigns were conducted within the city centre of Viseu identified in Figure 5.1b, during 20-27 January 2006 and 19-26 June 2006, comprising information on traffic countings for the main roads, indoor and outdoor air quality measurements in houses and schools attended by the group of the selected children with respiratory problems, air exchange rate measurements and children health examinations.

The work conducted within this thesis is focused in the development and application of MEXPO model. In this sense, the information obtained from the distint experimental campaigns were strictly used as input data for the application of MEXPO model to the urban area of Viseu, in order to assess the children exposure to NO_2 and PM_{10} air pollutants, namely, information on the characterisation of the urban area concerning buildings volumetry, traffic countings for the main roads and children time-activity profiles. Measurements of indoor and outdoor air quality and air exchange rate in houses and in a school performed during both campaigns were also used to evaluate model performance through comparison between measured and modelled data.

5.2. MEXPO application

The model was applied to a study area of 1300 m x 1300 m x 90 m, with a resolution of 5 m x 5 m x 3 m, located in the city centre of Viseu. Figure 5.2 presents an aerial fotograph of the study area, providing a detailed image of the urban built-up area. The main roads

within the domain, distinguished by the yellow colour, are identified by the respective names.

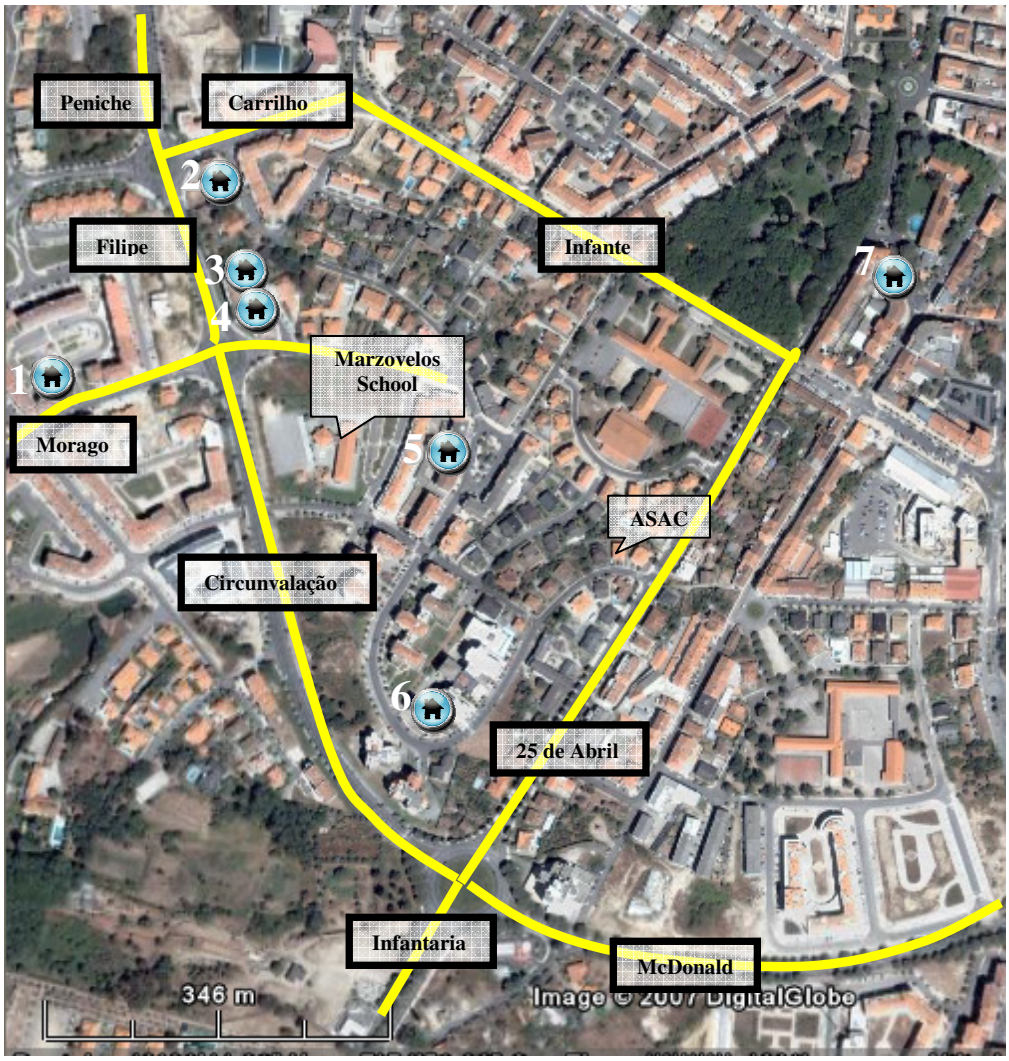

Figure 5.2 - MEXPO study domain located in Viseu city centre.

For this work, a group of seven children with asthma problems attending the elementary school of Marzovelos were selected as study case. These children live, study and have their activities within the study domain, providing the main criteria for their selection. The elementary school EB1,2 of Marzovelos is situated in the city centre of Viseu according to Figure 5.2. All seven children study in the same classroom and also attend the After School Activity Centre (ASAC) that is also located in the same figure. The houses where the selected children live are located in the same figure and are identified by the numbers 1 to 7.

The individual exposure to PM_{10} and NO_2 was estimated for the seven children by MEXPO model for the winter and summer periods of the experimental campaigns conducted under SAUDAR project, respectively, 20-27 January 2006 and 19-26 June 2006. The 21st and 22nd January 2006 and the 24th and 25th June 2006 correspond both to weekends.

Moreover, hourly exposure estimations to the referred pollutants were calculated along with hourly indoor pollutants concentrations and ventilation rates in the children's bedrooms, and Marzovelos and ASAC classrooms. These indoor environments use exclusively natural ventilation conditions through window opening to achieve a satisfactory indoor environment.

The following subchapters described the input data needed to run MEXPO model.

5.2.1. Modelling input data

The input data necessary to run MEXPO was previously described in Chapter 4 (Figure 4.1), comprising information on the characterisation of the built-up area of the study domain, namely: buildings volumetry and respectively location within the domain; traffic emissions; meteorological and pollutant concentrations boundary conditions; microenvironments definition and location within the domain; and time-acitivity profiles of the seven children.

5.2.1.1. Built-up area characterisation

The urban built-up area of the study domain was represented by 142 buildings with different configurations ranging from 9 to 27 m height. Figure 5.3 presents a 3D view of the buildings volumetry introduced in the model.

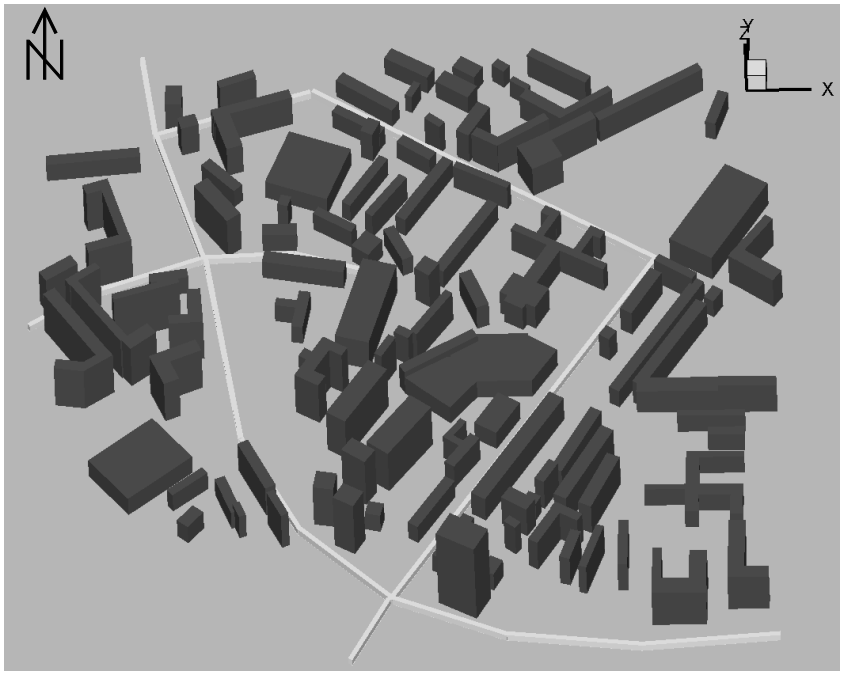

Figure 5.3 - 3D representation of buildings of the study area.

The following figure presents a 2D horizontal perspective of the building's location within the study domain according to a cartesian coordinate system. Buildings are represented in blue colour and the main roads in green.

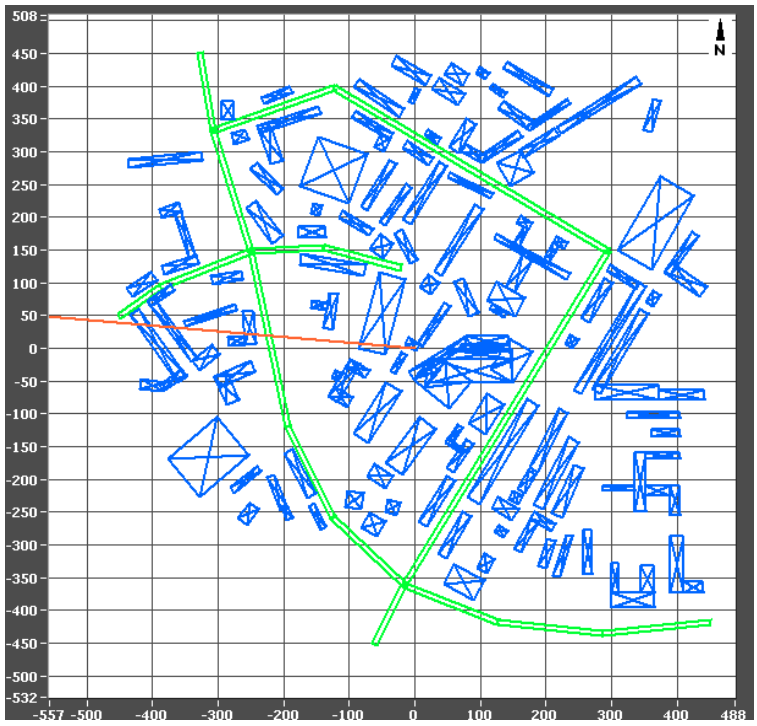

Figure 5.4 - 2D horizontal perspective of building's and road's location within the study domain.

Window areas of 1.17 m^2, 4.80 m^2 and 3.40 m^2 for residential, school and ASAC buildings, respectively, were considered as input data in MEXPO model, according to on-site information. Aditionally, it were also considered effectiveness opening areas of 10% and 20% during night time (9 p.m. to 7 a.m. inclusively) and, 20% and 50 % (8 a.m. to 8 p.m.) during daytime, for the winter and summer periods, respectively.

5.2.1.2. Traffic emissions

Traffic is considered the main pollutant source of the study area. In this sense, the location of the nine main roads of the domain was introduced in the model according to Figure 5.4. The names of the streets are presented in Figure 5.2.

Traffic emissions of PM_{10} and NO_x were estimated with TREM model (Transport Emission Model for Line Sources) for the nine main roads and for both winter and summer periods, using traffic counting data from the SAUDAR experimental campaigns.

TREM was developed at the University of Aveiro [Borrego *et al.*, 2003b; Tchepel, 2003] with the prime objective of supporting the quantification of emissions induced by road traffic. In TREM, roads are considered as line sources and emissions are estimated individually for each road segment considering detailed information on traffic flux (Figure 5.5). Moreover, the average speed approach is used for the emission factors estimation.

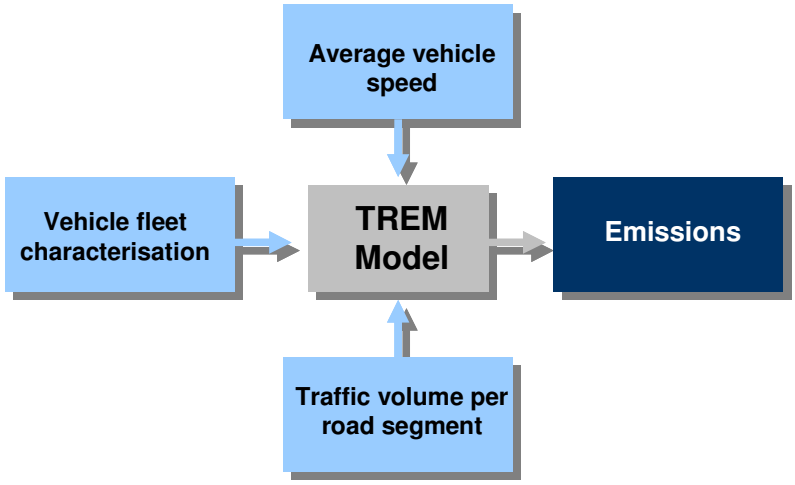

Figure 5.5 - Schematic representation of TREM input data.

Total emission of the pollutant *p* (*Ep*) for each road segment is estimated by the model as following:

$$E_p = \sum_i (e_{ip}(v) N_i) L \qquad (5.1)$$

where $e_{ip}(v)$ is the emission factor for pollutant p and vehicle class i as a function of average speed v; N_i is the number of vehicles of class i and L is the road segment length.

The traffic counting data for different vehicle categories (passenger, commercial, heavy-duty passenger, heavy-duty transport, motorcycles) obtained during both winter and summer experimental campaigns allowed the determination of the hourly PM_{10} and NO_x emissions in four distinct periods: winter season during weekdays, winter season during weekends, summer season during weekdays and summer season during weekends.

Figure 5.6 to Figure 5.9 present the hourly PM_{10} and NO_x emissions of the main roads within the study domain estimated by TREM for the winter and summer periods and for both weekdays and weekends (21st and 22nd January 2006 and the 24th and 25th June 2006).

The analysis of the hourly variation of PM_{10} and NO_x emissions for the winter period in weekedays presented in Figure 5.6 and Figure 5.7 shows maximum emission values at 9 a.m. and 7 p.m. for all roads, coinciding to the transport journeys from home to work at early morning and the return to home at the end of the day, respectively. It is also visible an increase of emissions at lunch time in all roads. The roads Circulação and 25 de Abril are the highest emission sources within the domain following by Infante road.

During the weekend of 21st and 22nd January 2006, PM_{10} and NO_x emissions increase from around 8 a.m. to 9 p.m. in all roads but with highest emission rates for Infante, 25 de Abril and Circunvalação roads. Circunvalação road presents a lower emission rate for the weekend than in weekdays, in opposite to Infante and 25 de Abril.

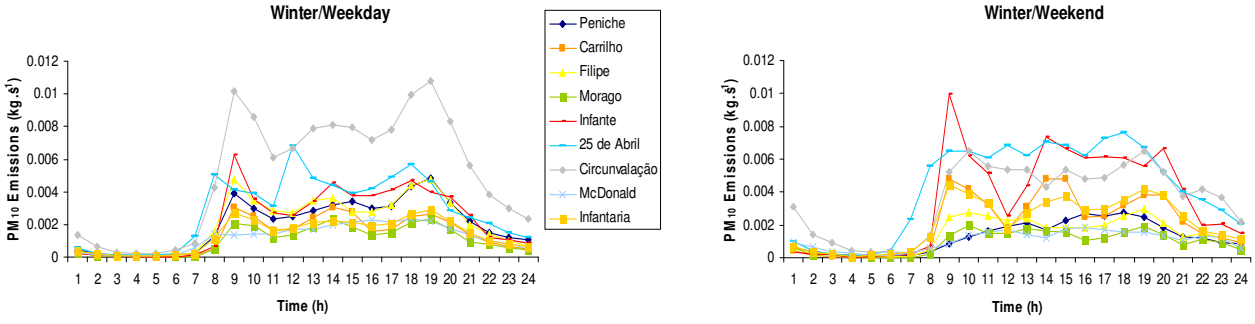

Figure 5.6 - Hourly PM_{10} emissions during weekdays and weekend in the winter period.

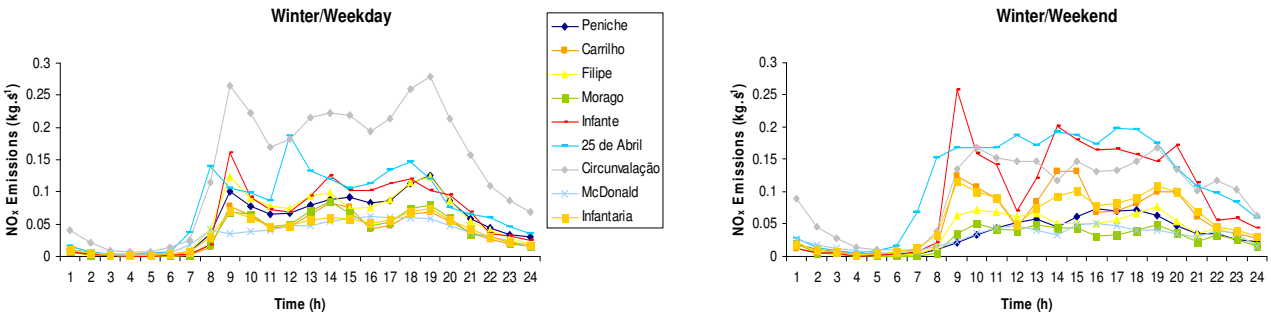

Figure 5.7 - Hourly NO_x emissions during weekdays and weekend in the winter period.

The hourly PM_{10} and NO_x emisions estimated in the summer period at weekdays also shows a similar behaviour from those found during weekdays in the winter period, characterized by an increase of emissions in early morning, lunch time and in late afternoon (Figure 5.8 and Figure 5.9). Nevertheless, for this period 25 de Abril road presents the highest emission rate followed by Infantaria and Circunvalação roads. In the weekend of 24th and 25th June 2006, 25 de Abril and Infantaria presents the highest emission rates during the period of 9 a.m. to 9 p.m.. Emission rates during summer period for all roads are higher from those estimated for the winter period.

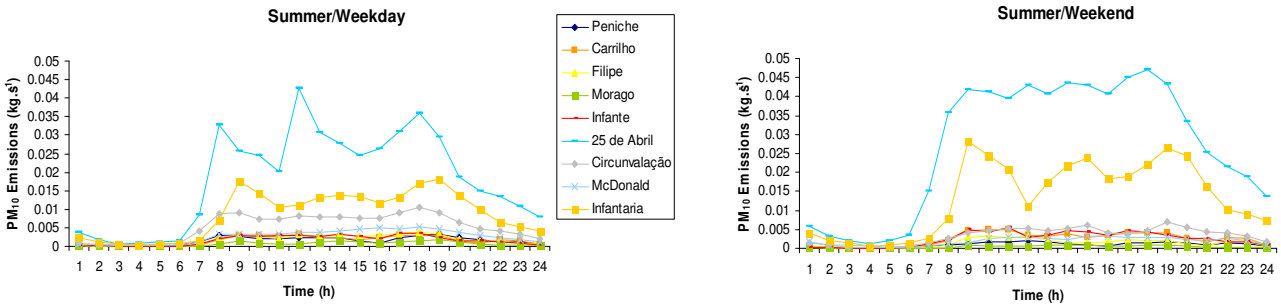

Figure 5.8 - Hourly PM_{10} emissions during weekdays and weekend in the summer period.

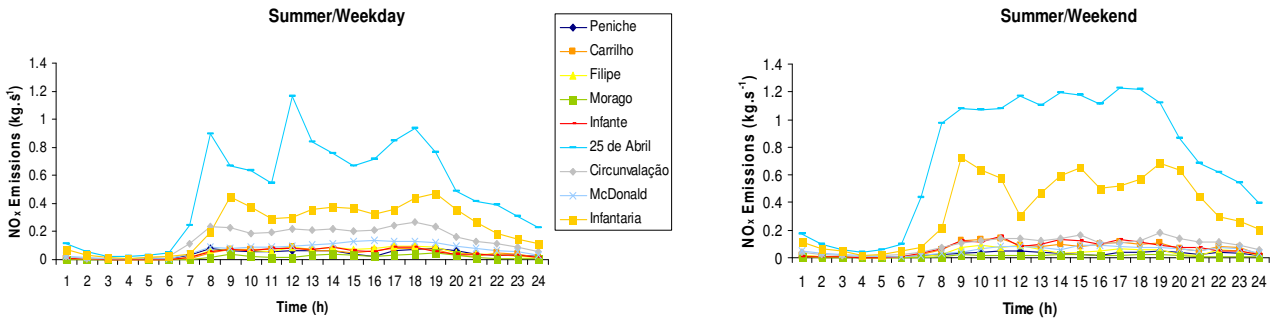

Figure 5.9 - Hourly NO_x emissions during weekdays and weekend in the summer period.

5.2.1.3. Boundary conditions

The mesoscale modelling system MM5/CAMx was applied under the SAUDAR project to determine the meteorological and PM_{10} and NO_2 pollutant concentrations over the Viseu region, to the following simulation periods: 16-27 January 2006 (includes the winter campaign); and 19-26 June 2006 (coincides with the summer campaign) [Borrego *et al.*, 2007b].

The Fifth Generation NCAR/Penn State Mesoscale Model [Dudhia, 1993], commonly named MM5, is a nonhydrostatic meteorological model designed to simulate or predict mesoscale atmospheric circulations, whereas the CAMx (Comprehensive Air Quality Model with Extensions) [ENVIRON, 2004] is an eulerian photochemical dispersion model that allows the assessment of gaseous and particulate air pollution over many scales ranging from urban to continental.

The MM5 model was applied over four different domains, using a nesting technique: Europe (78x92 grid cells with 27 km resolution), Portugal (82x64 grid cells with 9 km resolution), North of Portugal (52x52 grid cells with 3 km resolution) and Viseu district (46x46 grid cells with 1 km resolution). The NCEP/FNL data [URL 6] were used as initial and boundary conditions for the MM5 simulations. The four domains have the same vertical structure with 23 sigma levels, being the first one at 20 m height.

The CAMx model was applied to the two smallest domains (Figure 5.10), using area source emissions of industry and traffic from the national emissions inventory [IA, 2005].

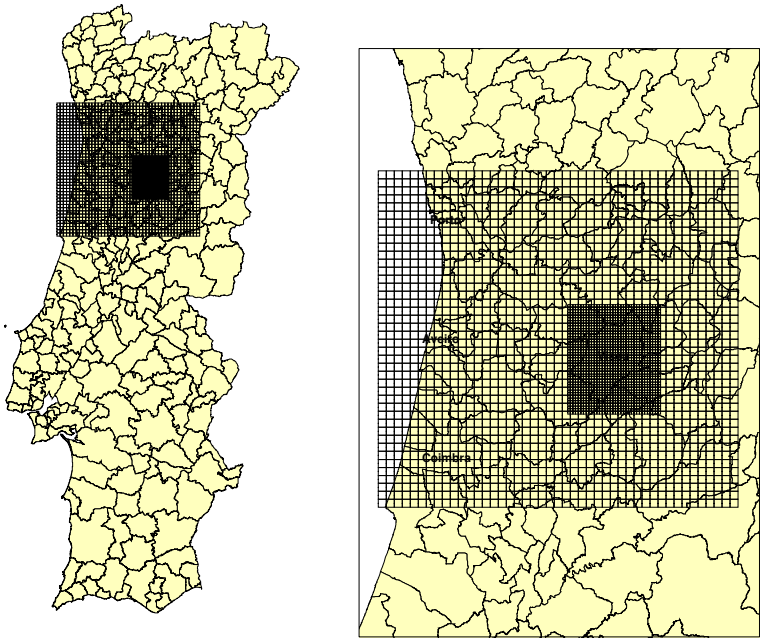

Figure 5.10 - MM5/CAMx simulation domains [Borrego *et al.*, 2007b].

The CAMx results, regarding PM_{10} and NO_2, were validated against experimental data from two mobile air quality laboratories located in the Viseu urban centre (Jugueiros and Marzovelos), during the winter and summer campaigns (Figure 5.11).

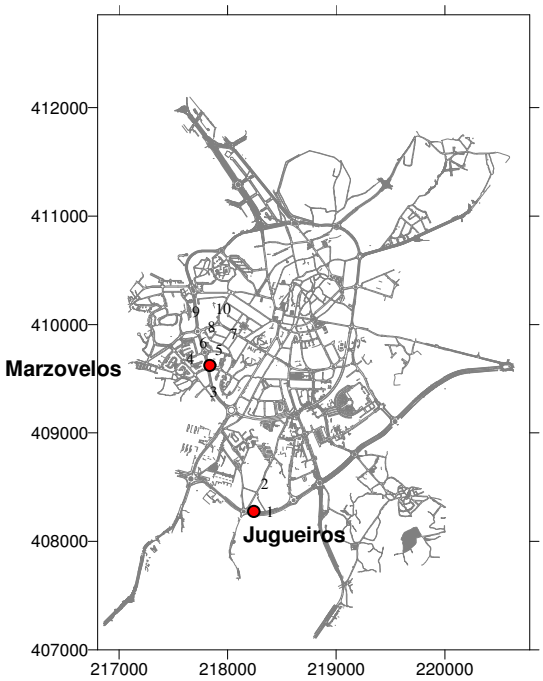

Figure 5.11 - City map of Viseu presenting the location of the mobile air quality laboratories (red dots).

Table 5.1 presents the results of the statistical analysis performed with the BIAS, R and RMSE parameters for the1 km modelling resolution [Borrego *et al.*, 2008].

Table 5.1 - Statistical analysis for 1 km modelling results for the winter and summer campaigns [Borrego *et al.*, 2007b].

			BIAS [µg.m^{-3}]	R	RMSE [µg.m^{-3}]
Winter period	**Jugueiros**	**PM_{10}**	-3.7	0.51	14.0
		NO_2	-72.5	0.62	11.3
	Marzovelos	**PM_{10}**	-3.9	0.71	16.6
		NO_2	33.3	0.67	11.4
Summer period	**Jugueiros**	**PM_{10}**	-3.3	0.41	18.2
		NO_2	21.7	0.11	13.0
	Marzovelos	**PM_{10}**	-3.5	0.16	17.8
		NO_2	-37.4	0.23	15.2

In the winter simulations, a positive BIAS was found for the NO_2 pollutant at the Marzovelos site, indicating a model overestimation, whereas a model underestimation was observed for PM_{10} at both locations and for NO_2, in Jugueiros [Borrego *et al.*, 2007b].

A negative BIAS has also been found for the summer campaign, with the exception of NO_2 pollutant in Jugueiros location. The correlation coefficient ranges from 0.51 to 0.71, and 0.11 to 0.41, for the winter and summer campaigns, respectively. Moreover, the maximum correlations were detected for PM_{10} pollutant in both campaigns. Acceptable results were obtained fro the RMSE parameter.

It is important to stress that the validation of the MM5/CAMx simulations was based on the air quality data acquired at urban locations, which may influence on the obtained results. In fact, previous research studies over Portugal show that mesoscale air quality models perform better for rural background environments than for urban/traffic sites [Monteiro *et al.*, 2007].

The hourly modelling results for 1 km model resolution, at 10 m height, corresponding to the cell located over the Viseu city centre were used as meteorological and concentration boundary conditions for the MEXPO model applications for both winter and summer

simulation periods. The mesoscale modelling results were chosen instead of the experimental data measured during the campaigns, since the latest were taken inside the study domain and do not provide representative flow and pollutants concentrations conditions of the domain entrance.

The hourly values of wind speed and direction at 10 m height estimated by MM5 model for the winter and summer periods are presented in Figure 5.12.

For the winter period, the MM5 model simulated wind speeds ranging from approximately 0.2 $m.s^{-1}$ to 9 $m.s^{-1}$. The highest wind speeds were simulated for the last day of the campaign, 27th January 2006. Wind directions were mainly from North and Northeast on the half campaign period, changing to Northwest in the following days.

Speeds of 0.2 $m.s^{-1}$ to 4 $m.s^{-1}$ with main North and Northwest winds were estimated for the summer campaign by the meteorological mesoscale model.

The typical meteorological conditions for the region during winter, described in the Portuguese climatological atlas [IM, 1974], indicate main winds from East with low wind speeds from 0.5 $m.s^{-1}$ to 1.5 $m.s^{-1}$. Summer typical meteorological conditions also indicate East winds ranging from 1.5 $m.s^{-1}$ to 5.5 $m.s^{-1}$, at morning, and North and Northwest winds of 0.5 $m.s^{-1}$ to 1.5 $m.s^{-1}$ in the afternoon.

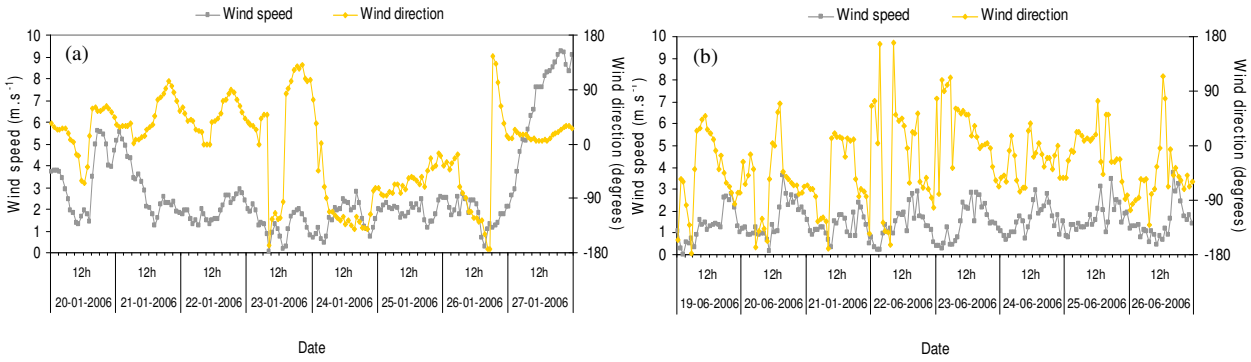

Figure 5.12 - Wind speed and direction results from MM5 model for the winter (a) and summer (b) periods.

Hourly PM_{10} and NO_2 concentrations results from CAMx model for the winter and summer periods are presented in Figure 5.13 and Figure 5.14.

The simulated PM_{10} concentrations are higher in winter than in summer, varying from 15 $\mu g.m^{-3}$ to 40 $\mu g.m^{-3}$ and 8 $\mu g.m^{-3}$ to 30 $\mu g.m^{-3}$ in winter and summer periods, respectively.

The NO_2 concentrations have approximately the same behaviour in both campaigns, with slightly higher values during the summer campaign. Nevertheless, the simulated values of both pollutants concentrations in the ambient air are lower than the current European air quality standards of 50 $\mu g.m^{-3}$ (24 h average) for PM_{10} and 200 $\mu g.m^{-3}$ (1 h average) for NO_2.

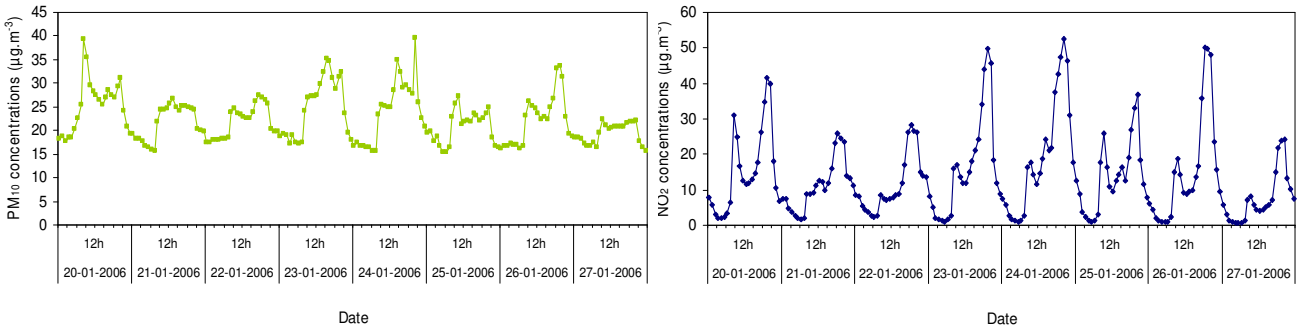

Figure 5.13 - Hourly PM_{10} and NO_2 concentrations results from CAMx model for the winter period.

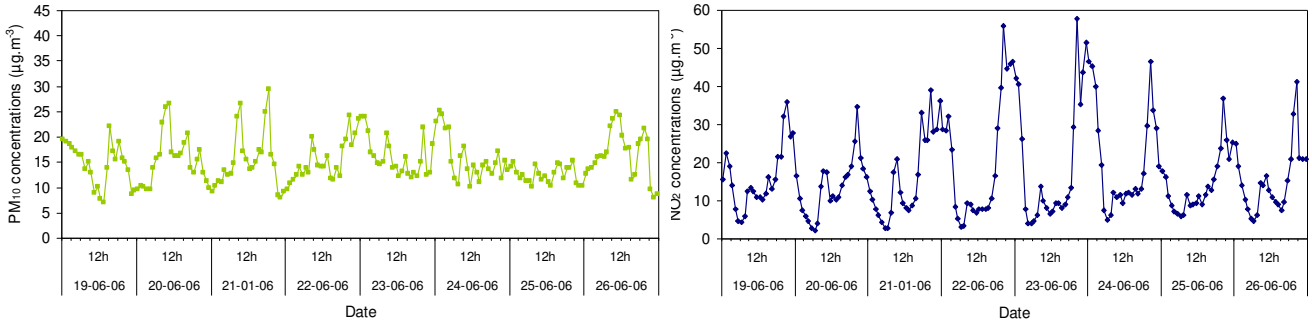

Figure 5.14 - Hourly PM_{10} and NO_2 concentrations results from CAMx for the summer period.

5.2.1.4. 3D microenvironment definition

Five distinct microenvironments were considered in MEXPO model corresponding to the main locations where the selected children spend their time during the winter and summer campaigns: outdoor, residential (bedroom), school, ASAC (After School Activity Center) and transport. A 3D microenvironmet matrix of the study domain was created according to the model resolution of 5 m x 5 m x 3 m. Each cell of the model was then attributed to each one of the defined microenvironments.

This feature of MEXPO model allowed to consider important information concerning the 3D location of microenvironments where children spend their time. The location height of both classrooms on school and ASAC, of transport microenvironment and of residential microenvironments of the seven children are presented in Table 5.2.

The ASAC and school classrooms are located at the ground floor, as well as, the residence of Child 5. The residences of the other children are located at the 3rd (Children 6 and 7) and 4th (Children 1, 2 and 4) floors of high-rise apartment buildings.

Table 5.2- Location height of residential, school, ASAC and transport microenvironments.

Microenvironment	Location height
Residential (Child 1)	10.5 m (4th floor)
Residential (Child 2)	10.5 m (4th floor)
Residential (Child 3)	4.5 m (2nd floor)
Residential (Child 4)	10.5 m (4th floor)
Residential (Child 5)	1.5 m (ground floor)
Residential (Child 6)	7.5 m (3rd floor)
Residential (Child 7)	7.5 m (3rd floor)
School (classroom)	1.5 m (ground floor)
ASAC (classroom)	1.5 m (ground floor)
Transport	1.5 m (ground floor)

5.2.1.5. Time-activity profiles

The previous 3D microenvironment matrix was combined with information on the time-activity profiles of the seven children within the five microenvironments (Figure 5.15). These profiles characterize the movement of the seven children within the study domain during one day with hourly resolution in four distinct periods: winter/weekday, winter/weekend, summer/weekday and summer/weekend. In this sense, hourly 3D matrixes of microenvironment/activity-profiles were created for a typical weekday and weekend of both winter and summer campaigns.

The analysis of Figure 5.15 shows that children 1, 2, 5, 6 and 7 have afternoon classes in the Marzovelos School, while children 3 and 4 attend morning classes in the same school. Also, only children 1, 3, 4, 5 and 6 attend the Afternoon Activity Centre (ASAC). All the selected children have approximately the same time-activity pattern during weekends, both in winter and summer periods.

For all children, the higher fraction of time is spent indoors, more particularly, at home, followed by school and ASAC. Also, it can be observed that little time is spent outdoors or in transport microenvironments.

Figure 5.15 - Time-activity profiles of the selected children.

5.2.2. Modelling results

The application of MEXPO model to the Viseu urban area for both winter and summer periods allowed the estimation of hourly ventilation rates and indoor PM_{10} and NO_2 concentrations in both Marzovelos and ASAC classrooms and in the bedrooms of the seven children. For this purpose, hourly 3D flow and outdoor pollutant concentrations fields were firstly determined according to the model scheme presented in Figure 4.1.

As the final outcome of MEXPO, the hourly individual exposure to PM_{10} and NO_2 pollutants were determined for the seven children during the winter and summer campaigns.

MEXPO results are limited by the time resolution of model inputs. Traffic emission rates, meteorological and pollutant concentration boundary conditions, time-activity profiles are available on an hourly basis. In this sense, model results are provided also in this temporal resolution.

The following subchapter presents the model results concerning the natural ventilation rates, outdoor and indoor pollutants concentrations and, finally, individual exposure estimations.

5.2.2.1. Natural ventilation rate

The simulated hourly ventilation rates in both Marzovelos and ASAC classrooms and in the bedrooms of the seven children (notation Room 1 to Room 7) for the winter simulation period are presented in Figure 5.16 and Figure 5.17.

As previously mentioned in subchapter 4.2.2, the Portuguese legislation defines a minimum ventilation rate for residences and school microenvironments of 30 $m^3.h^{-1}.person^{-1}$. The bedrooms of the seven children have an occupation rate of 1 person corresponding to a minimum ventilation rate of 30 $m^3.h^{-1}$. This limit value is identified in Figure 5.16 by a dotted line. Both Marzovelos and ASAC classroom have an average occupantion rate of 20 children imposing a minimum ventilation rate of 600 $m^3.h^{-1}$ also identified in the figure by a dotted line.

The analysis of Figure 5.16 and Figure 5.17 shows that the highest ventilation rates ocurred during the end of the first and beginning of the second simulated days and in the last day of the campaign, coinciding to the highest wind speeds simulated by the meteorological mesoscale model and used as boundary conditions in these simulations (Figure 5.12). For

these specific days the ventilation rates generally accomplish the Portuguese standard in all children's bedrooms (Figure 5.16). Moreover, the lowest ventilation rate is observed for the bedroom of Child 5, whereas the highest values are estimated for the bedrooms of children 1 and 7.

Figure 5.17 shows that the ventilation standards were never achieved in Marzovelos and ASAC classrooms for the same period.

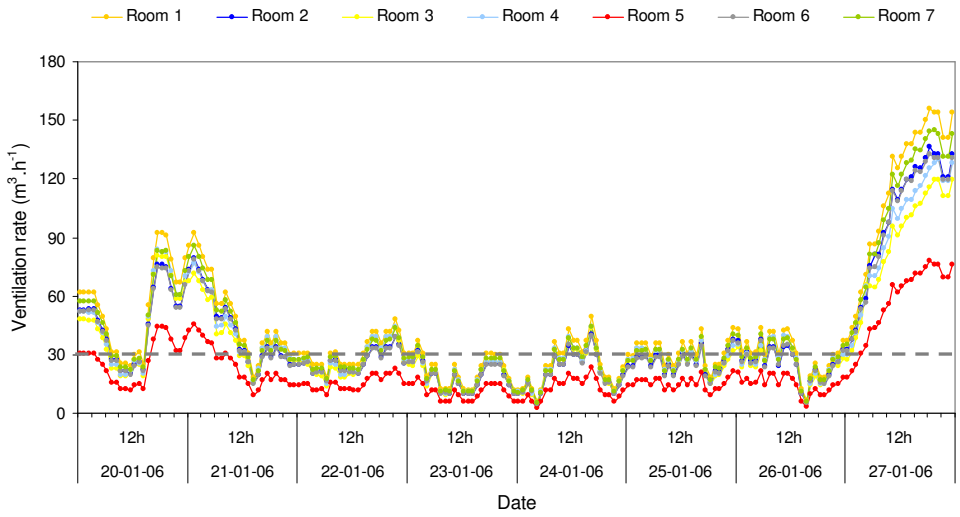

Figure 5.16 - Simulated hourly ventilation rates in children's bedrooms for the winter period.

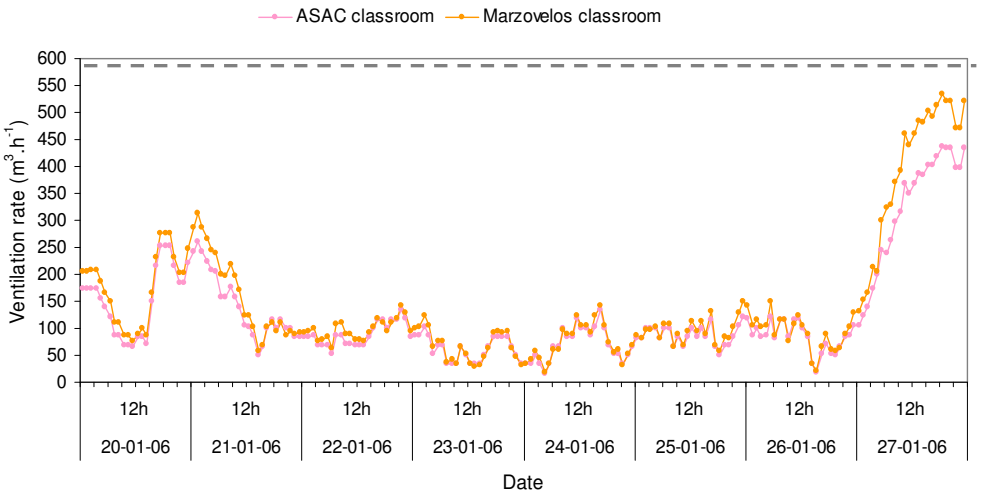

Figure 5.17 - Simulated hourly ventilation rates in Marzovelos and ASAC classrooms for the winter period.

Figure 5.18 and Figure 5.19 present the simulated hourly ventilation rates in the children's bedrooms (notation Room 1 to Room 7) and in Marzovelos and ASAC classrooms for the summer simulation period.

The results show that all children's bedrooms present a ventilation rate above the minimum ventilation standard with the exception of the night periods when there is a decrease of the window opening area. The highest ventilation rates are found during daytime (Figure 5.18). Again, the lowest ventilation rate is observed for the residence of Child 5 and the highest values are estimated for the bedrooms of children 1 and 7

These ventilation rates show an increase of the window opening areas relatively to the winter period.

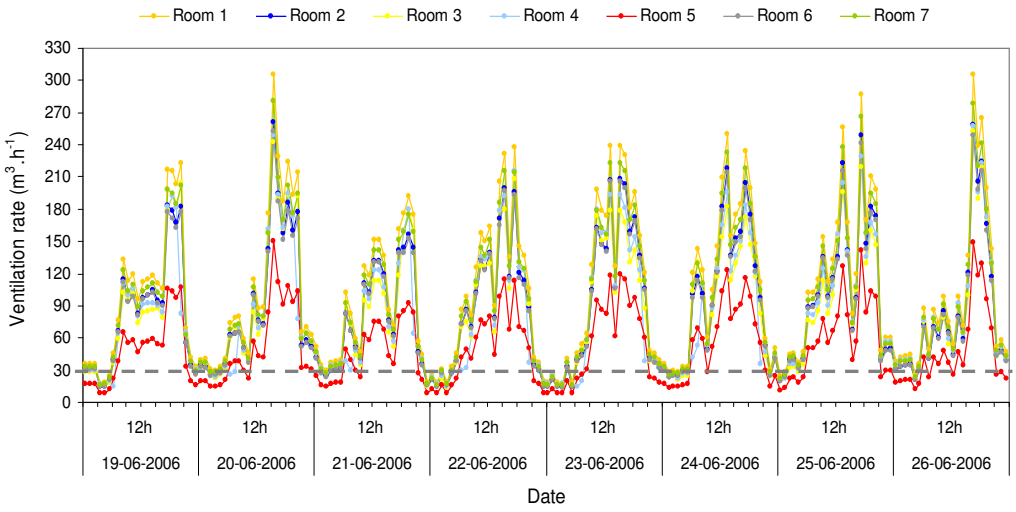

Figure 5.18 - Simulated hourly ventilation rates in children's bedrooms for the summer period.

Results of Marzovelos and ASAC classrooms also indicate an increase of the window opening area during the summer period, contributing to the raise of the ventilation rates. In this sense, the ventilation standards are accomplished during most of the day period with the exception of the 21st of June (Figure 5.19).

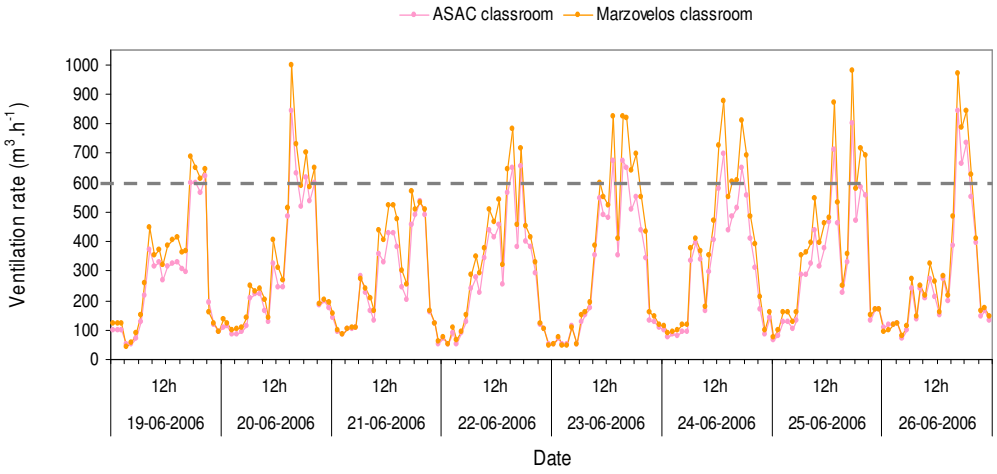

Figure 5.19 - Simulated hourly ventilation rates in Marzovelos and ASAC classrooms for the summer period.

The average ventilation rates found for the different indoor spaces during the winter and summer simulation periods are presented in Figure 5.20. The Portuguese standard for minimum ventilation rates defined for bedrooms and classrooms in Residential and Schools activities are also shown in this figure.

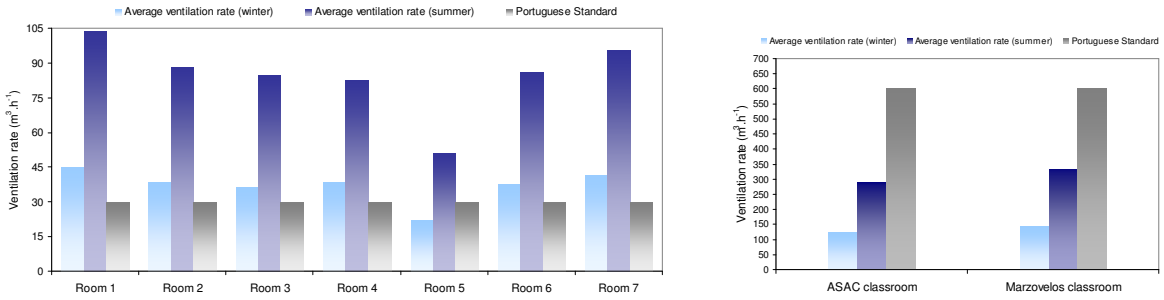

Figure 5.20 - Simulated average ventilation rates for the winter and summer campaigns.

During the winter period, all children's bedrooms accomplish the minimum ventilation requisites imposed by the Portuguese legislation with the exception of the bedroom of Child 5. It is important to mention that the residence of Child 5 is the only located at the ground floor, as mentioned in Table 5.2, where low outdoor wind speed conditions are more frequently observed than in high-rise apartment buildings. The bedrooms of children 1 and 7 present the highest average ventilation rates.

Moreover, the ventilation rates for Marzovelos and ASAC classrooms, during winter, are clearly below the standards, considering a classroom occupation of 20 children.

The small ventilation rates estimated for both classrooms can be explained by the low temperatures found in Viseu region during the winter time that compromise the use of natural ventilation mechanisms to achieve good indoor standards. Low ventilation rates can be responsible to a decrease in the attention and learning capabilities of the children present in the classroom. In this sense, it would be advisable to also include in these classrooms mechanical ventilation mechanisms, such as HVAC (Heating, Ventilating, and Air Conditioning) systems, along with the existent natural ventilation processes in order to achieve the minimum standards imposed by the legislation.

In summer, the average ventilation rates for all children's bedrooms are above the Portuguese standard. Nevertheless, and despite the increase of the window opening area during summer, the ventilation rates in both classrooms are still below the recommended values. Similar to the winter period, this may imply the use of additional ventilation mechanisms to achieve the legal standards. Again, the lowest and the highest ventilation rates are calculated for the bedrooms of Child 5, and children 1 and 7, respectively.

In order to establish confidence in the first MEXPO model results it is important to conduct a validation exercise. For this purpose, experimental values of ventilation rates were measured in the classroom of Marzovelos school, during both winter and summer campaigns, using a tracer gas technique. These experimental values were compared with the modelled data.

Tracer gas techniques are the most popular and important techniques for ventilation measurements in buildings, providing a direct measurement of the total air flow rate of outdoor air to buildings. Tracer gas testing involves the release of a readily detectable tracer into the space under consideration with the subsequent concentration history being recorded. The inflow of free air can be calculated from the concentration history. Tracer gas tests provide a direct measure of the total number of air exchanges that take place within a ventilated space [Straw, 2000].

According to the method of tracer gas injection and the form of mass balance these techniques are classified into three types [Cheong, 2001]: concentration-decay (a short burst of tracer gas is injected into the space in order to establish a uniform concentration within the building and the concentration decay of the tracer is recorded); constant injection (gas is injected at a constant rate and the concentration response is recorded); and

constant concentration (gas is injected into the space under control in order to keep a constant concentration).

The concentration-decay was the method used to measure the ventilation rates during the SAUDAR campaigns. This method involves a one-time injection of tracer gas before the measurement period. The tracer gas CO_2 was released at the interior of the Marzovelos classroom until the indoor concentration had built up to a certain level (approximately 1500 $mg.m^{-3}$). In order to produce a well-mixed and evenly distributed sample in the test space, a portable mixing fan was used. The decay of tracer gas concentration was recorded for the 24th January 2006 and 22nd of June, at 8 p.m., after class activities, maintaing the same ventilation conditions used during classes. The IQ-604 portable probe from Gray Wolf Sensing Solutions was used to record the decay histoty of the CO_2 tracer through infra red technique with sample intervals of 1 minute in both campaigns.

Considering that the ventilation rate is constant during the measurement period, the tracer decay history can be expressed by:

$$C(t) = C(0)e^{-It} \qquad (5.2)$$

C(t), *C(0)* represents the tracer gas concentration at any time and at the beginning of the record time, respectively. The slope of the natural logarithm plot of this tracer concentration, *I*, gives the volume flow rate in air change per hour (ACH).

Figure 5.21 presents the results of tracer gas measurements performed on Marzovelos classroom at 24th January 2006 and 22nd of June, at 8 p.m..

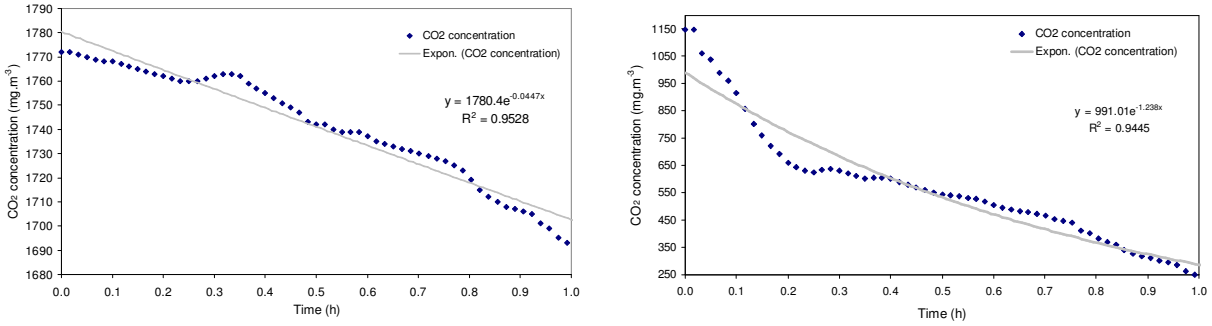

(a) (b)

Figure 5.21 - Measured ventilation rates in Marzovelos classroom during winter (a) and summer (b) campaigns.

The air exchange rate measured in the Marzovelos classroom for the 24th January 2006 at 8 p.m., with a window opening area of 20 %, is 0.0447 h^{-1}, corresponding to a ventilation

rate of 12.17 $m^3.h^{-1}$, for a classroom volume of 272.25 m^3. MEXPO model simulated for the same day and hour and considering equal window opening conditions, a value of 55.24 $m^3.h^{-1}$, indicating a model overestimation, when compared with the measured value.

The value of 1.238 h^{-1} or 337.05 $m^3.h^{-1}$ was measured at Marzovelos classroom in the 22nd of June at 8 p.m. considering a window opening area of 50 %. The simulated value for the same time period and keeping equal ventilation conditions is 414.35 $m^3.h^{-1}$. Again it is noticed a slightly overestimation of model results when compared with measured values.

The available monitoring techniques to measure ventilation rates are expensive and difficult to apply in occupied buildings. These facts limited the existent of more measured ventilation rates in both experimental campaigns, compromising the possibility to perform a more detailed evaluation of the ventilation rate results in all indoor spaces considered in this study.

5.2.2.2. Outdoor air quality

Outdoor 3D fields of PM_{10} and NO_2 concentrations were simulated with MEXPO for both winter and summer periods.

The Derwent-Middleton Correlation was used to estimate NO_2 concentrations from NO_x concentrations derived from the estimated NO_x emissions [Derwent and Middleton, 1996].

$$[NO_2] = 2.166 - [NO_x](1.236 - 3.348A + 1.933A^2 - 0.326A^3) \qquad (5.3)$$

where $A = \log_{10}([NO_x])$. The equation is valid in the range 9 ppb to 1141.5 ppb.

Figure 5.22, Figure 5.23, Figure 5.24 and Figure 5.25 present, as examples, the horizontal view at 4.5 m height of flow and concentration fields of PM_{10} and NO_2 pollutants over the simulation domain for the 20th January 2006 and 20th June 2006, at 4 p.m., respectively.

Outdoor air quality measurements of PM_{10} and NO_2 concentrations were performed at the Marzovelos School playground in both winter and summer campaigns with the automatic equipments Environnement MP101M™ (15 minutes averages) and Environnement AC31M™ (5 minutes averages), respectively. The automatic equipments are integrated in a mobile air quality laboratory, which location in the domain is indicated in Figure 5.22, Figure 5.23, Figure 5.24 and Figure 5.25 with the symbol (✱). The instruments probe is positioned approximately at 4 m height.

The analysis of the PM_{10} and NO_2 concentration patterns for the winter example shows the transport of the main traffic emissions, from Circunvalação and 25 de Abril roads, to southwest, according to the prevailing wind conditions (Figure 5.22 and Figure 5.23). Hot-spots are observed at the downstream buildings, but with concentration values below the daily air quality guidelines of 50 $\mu g.m^{-3}$, for PM_{10}, and the hourly value of 200 $\mu g.m^{-3}$, for NO_2. The measuring location site suffers only a small influence of the the nearby road due to the recirculating effect caused by the downwind buildings. In this sense, the simulated concentrations largely reflect the used boundary conditions.

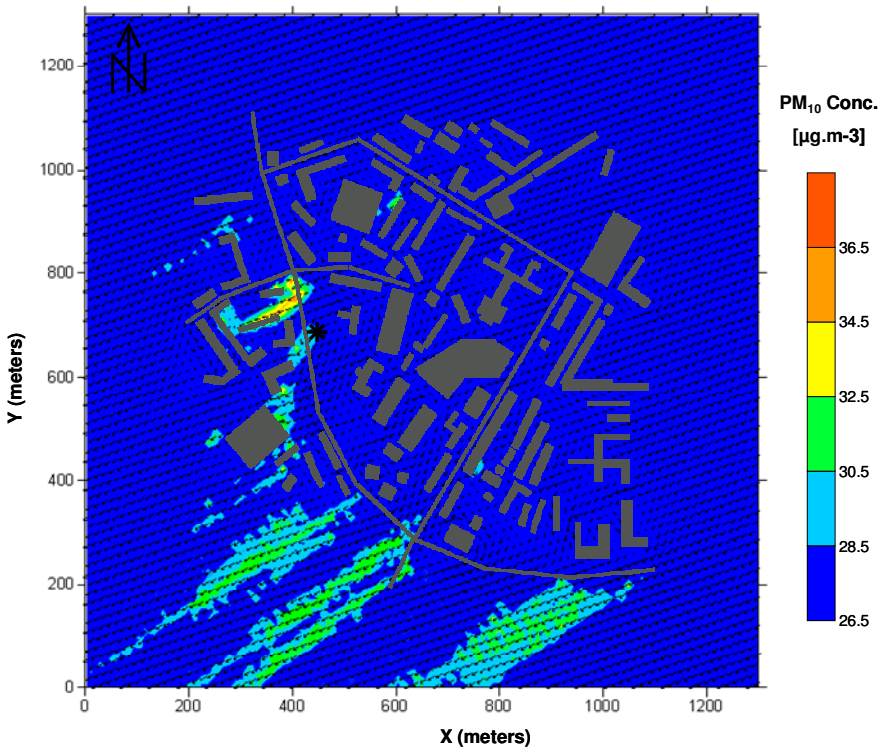

Figure 5.22 - Horizontal view at 4.5 m height of flow and PM_{10} concentration fields for the 20th January 2006 at 4 p.m..

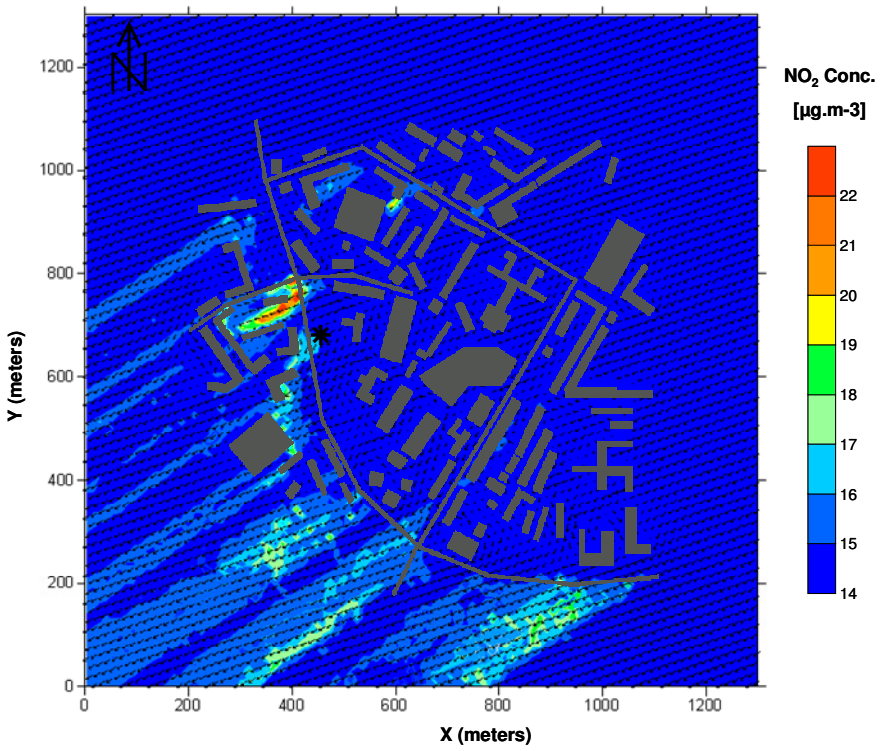

Figure 5.23 - Horizontal view at 4.5 m height of flow and NO_2 concentration fields for the 20th January 2006 at 4 p.m..

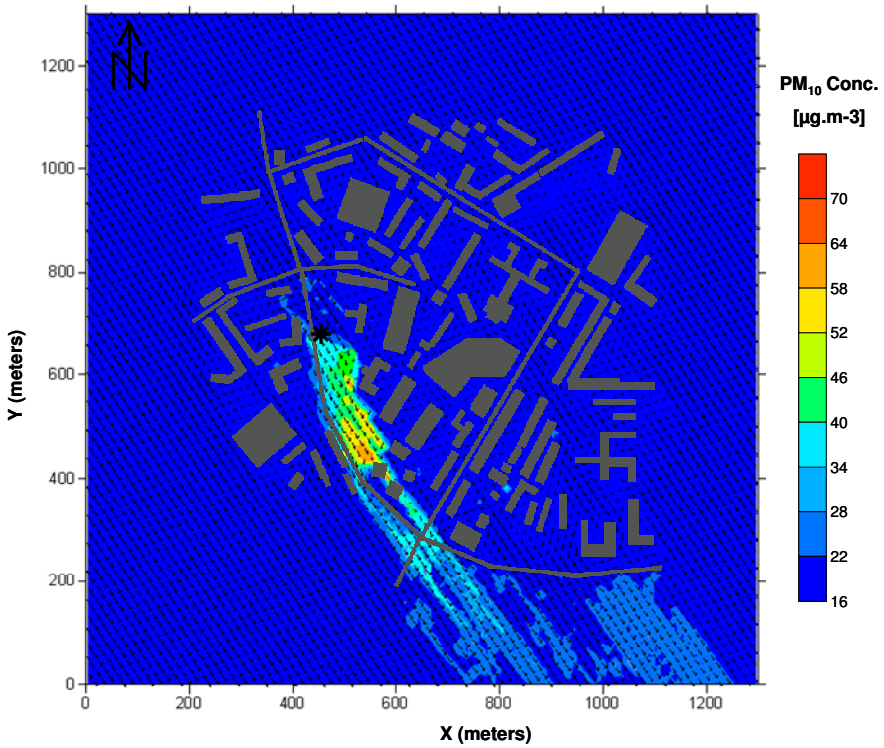

Figure 5.24 - Horizontal view at 4.5 m height of flow and PM_{10} concentration fields for the 20th June 2006 at 4 p.m..

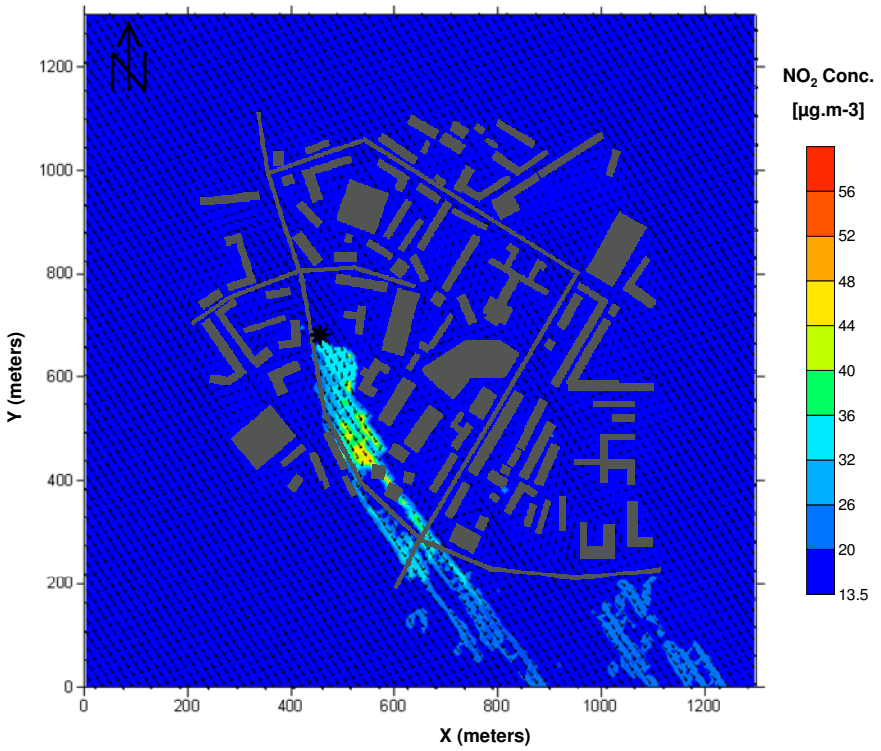

Figure 5.25 - Horizontal view at 4.5 m height of flow and NO_2 concentration fields for the 20th June 2006 at 4 p.m..

According to Figure 5.24 and Figure 5.25, the PM_{10} and NO_2 concentrations are transported to southeast due to the main wind flow. As the previous winter examples, the measuring location is only slightly influenced by the nearest traffic emission sources. The hot-spots formed at the downstream buildings exceed the air quality guideline for PM_{10}, and are below the guideline for the NO_2 pollutant.

Figure 5.26 and Figure 5.27 present the comparison between simulated and measured values of PM_{10} and NO_2 pollutants for the winter period, respectively. An identical analysis is made in Figure 5.28 and Figure 5.29 for the summer period.

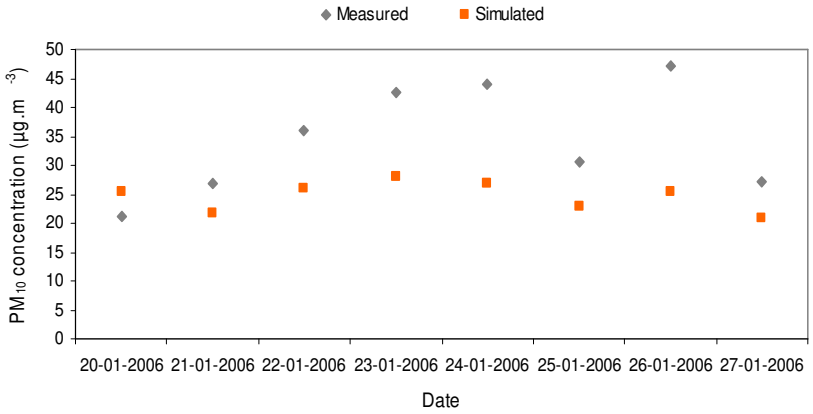

Figure 5.26 - Measured and simulated daily average PM_{10} concentrations at the Marzovelos mobile laboratory for the winter period.

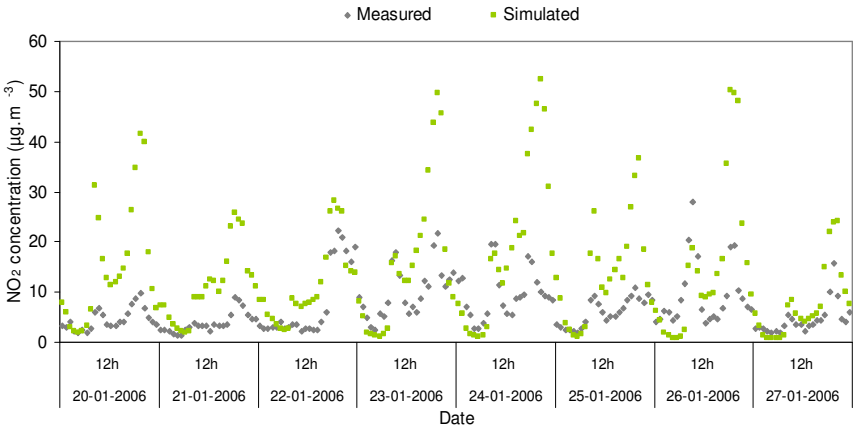

Figure 5.27 - Measured and simulated hourly average NO_2 concentrations at the Marzovelos mobile laboratory for the winter period.

Figure 5.26 indicates an underestimation of the simulated daily average PM_{10} concentrations for the entire winter campaign, with the exception of the 20th of January. Moreover, the model results are able to predict the evolution trend of the measured values, excluding the first simulated day.

The analysis of Figure 5.27 shows a generally overestimation of the NO_2 modelled concentrations during the day and an underestimation in the night periods. It is also notice a similar tendency between model and measured values, especially for the first three days of the campaign.

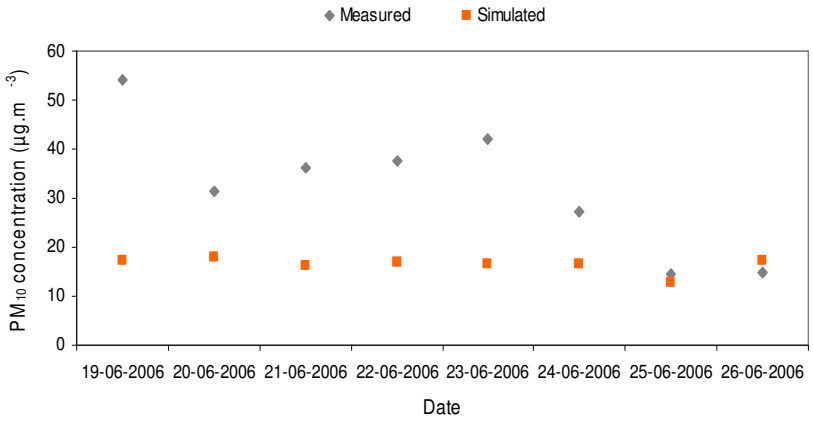

Figure 5.28 - Measured and simulated daily average PM_{10} concentration at the Marzovelos mobile laboratory for the summer period.

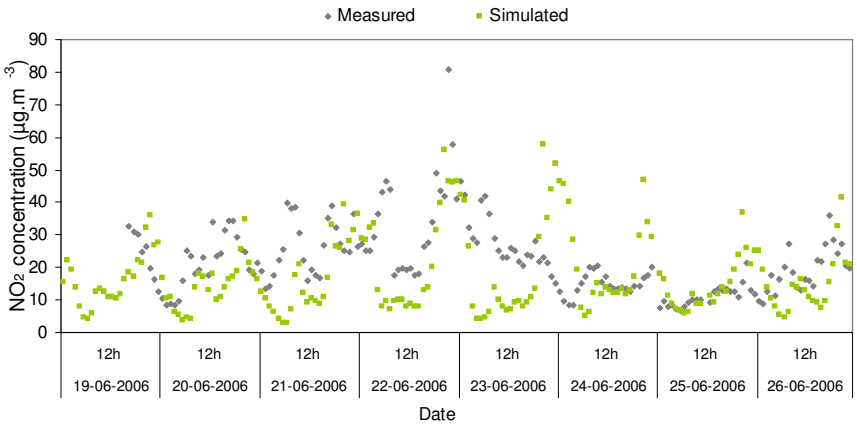

Figure 5.29 - Measured and simulated hourly average NO_2 concentration at the Marzovelos mobile laboratory for the summer period.

The simulated daily average concentrations of PM_{10} during the summer campaign are underestimated during the entire week with the exception of the last day, where is observed a slightly model overestimation (Figure 5.28).

The results of simulated hourly concentrations of NO_2, presented in Figure 5.29, are generally underestimated relatively to the measured values, being also observed a model overestimation for the late evening hours of the 23rd and the 24th of June.

A statistical analysis of the modelling results for PM_{10} and NO_2 concentrations in both campaigns at the Marzovelos mobile laboratory is presented in Table 5.3, using the BIAS, R and RMSE parameters [Borrego *et al.*, 2008].

Table 5.3 - Statistical analysis of modelling results for PM_{10} and NO_2 concentrations in winter and summer campaigns at the mobile laboratory location.

		BIAS [µg.m-3]	R	RMSE [µg.m-3]
Winter campaign	**PM_{10}**	-9.8	0.64	12.3
	NO_2	6.7	0.61	11.8
Summer campaign	**PM_{10}**	-15.8	0.47	19.7
	NO_2	-4.2	0.28	14.7

A negative BIAS is found for PM_{10} pollutant in both winter and summer campaigns, indicating a model underestimation. In addition, a better agreement between modelled and measured values was achieved for the winter simulation than for the summer period. The lowest RMSE is observed for the winter simulation.

The underestimation of PM_{10} model results found for both campaigns may be related to an underestimation of the local emission sources, namely, of nearby traffic sources that are not within the simulation domain. Moreover, fireplaces emissions, which were not accounted in these simulations, may have an important contribution to the local air quality during winter time. The ressuspension dust of the Marzovelos School playground may also be considered an additional source of PM_{10} pollutant that was not included in the simulations. The importance of this possible source increases during dry seasons, such as the one found for the summer campaign.

A model overestimation is observed for the NO_2 concentrations during the winter campaign, whereas a negative BIAS is found for the summer period, indicating a slightly model underestimation. A good agreement between modelled and measured values was found for the winter campaign. A low correlation coefficient was achieved for the summer campaign.

It is important to stress that MEXPO model treats pollutants as non-reactive species. In this sense, the observed NO_2 overestimation for the winter period may be related to the absence of consuming reactions. On the other side, the used boundary conditions have an important contribution on the modelled results at the measuring site. In this sense, it is important to retain the model overestimation observed in the winter mesoscale application.

5.2.2.3. Indoor air quality

Hourly values of indoor PM_{10} and NO_2 concentrations were estimated by MEXPO for both Marzovelos School and ASAC classrooms and for the bedrooms of the seven children, during the winter and summer periods. Moreover, indoor concentrations were diferenciated by their origin for the PM_{10} pollutant: from outdoors (notation C_{io}) and from indoors (notation C_{ii}).

In this MEXPO model application exercise it was considered that in Marzovelos and ASAC classrooms and in children's bedrooms there were no significant indoor sources of NO_2 pollutant, since the main indoor sources of this pollutant are associated to cooking activities. In this sense, the estimated indoor NO_2 concentrations were originated solely from outside air that penetrates indoor.

The PM_{10} emission rate defined for other indoor sources than cooking and smoking, and presented in §4.1.4.1, was used for this application in all considered microenvironments.

The hourly variation of simulated PM_{10} indoor concentrations for the winter period, differentiated by their outdoor (C_{io}) and indoor (C_{ii}) origin, in Marzovelos and ASAC classrooms and in children's bedrooms is presented in Figure 5.30. The total indoor values are also presented in the figures by a blue line.

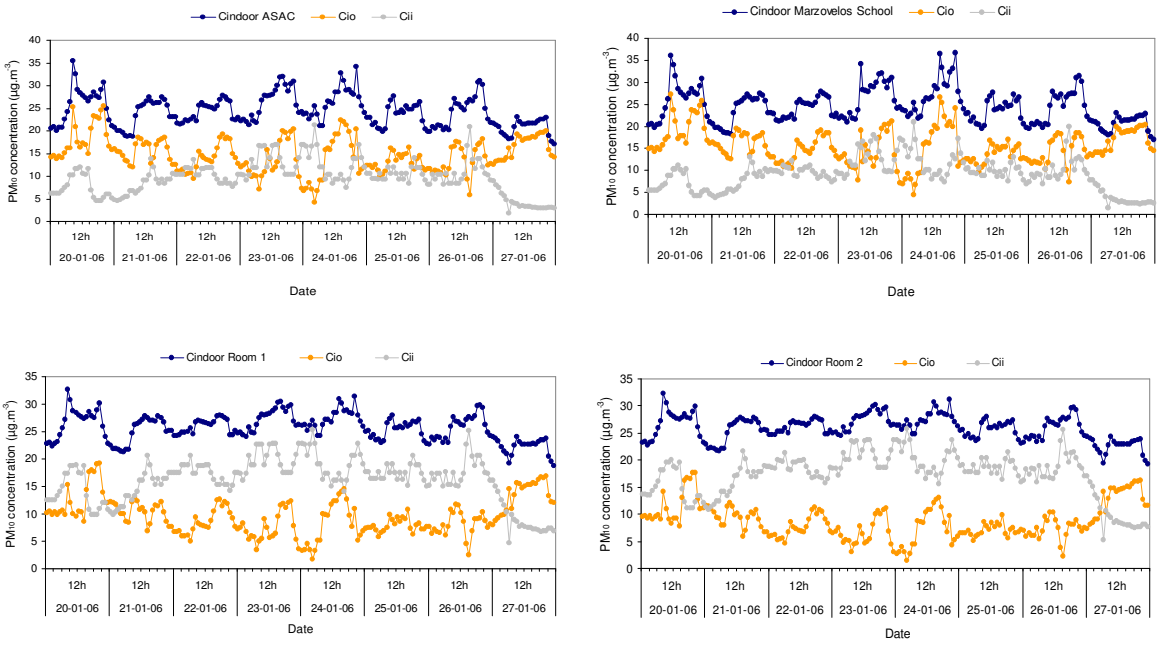

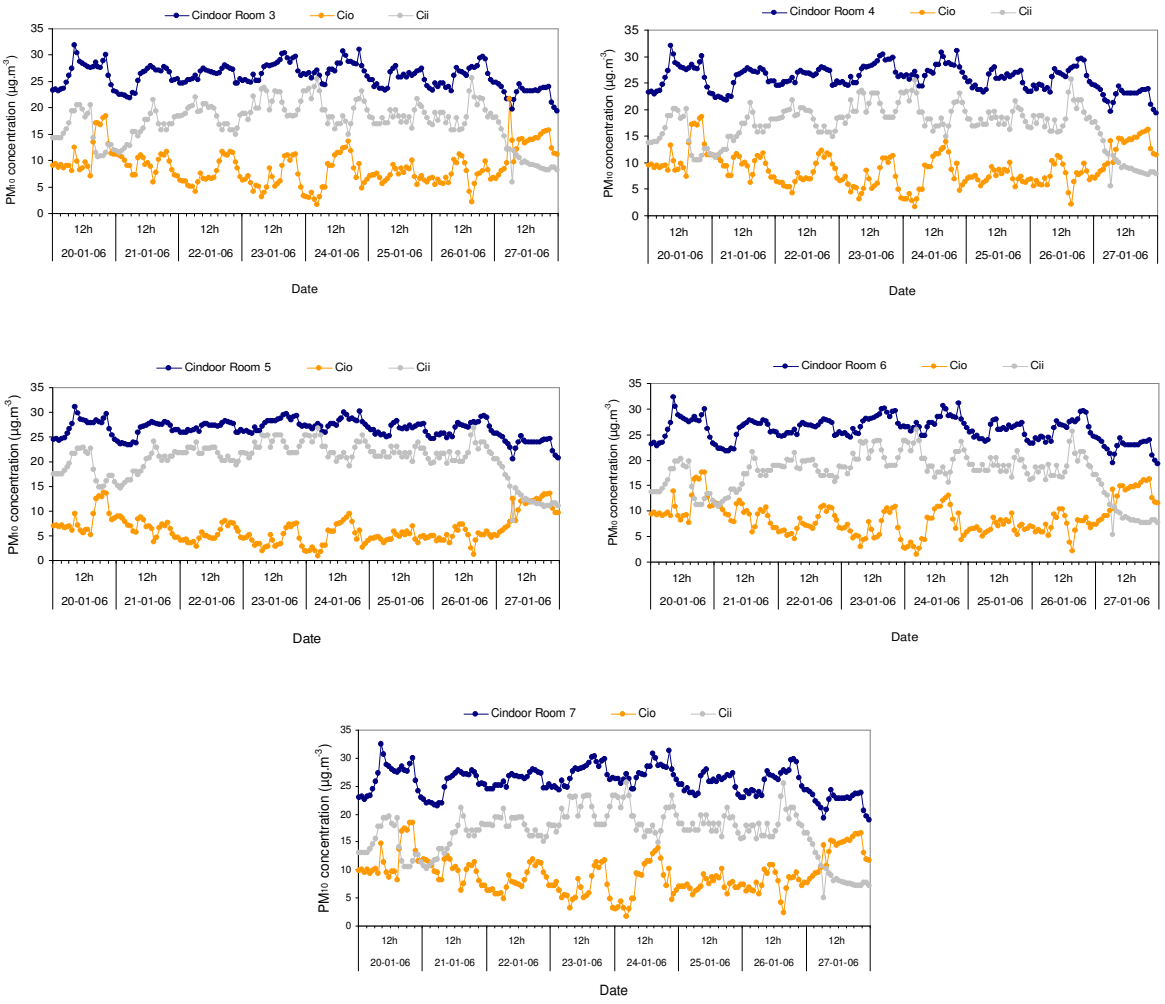

Figure 5.30 - Hourly PM_{10} indoor concentrations simulated for the winter period.

The highest PM_{10} concentrations are found in ASAC and Marzovelos classrooms reaching the value of 37 $\mu g.m^{-3}$. The PM_{10} concentrations in children's bedrooms are below the value of 34 $\mu g.m^{3}$. It is also possible to notice the variation of both outdoor and indoor contributions to the total indoor PM_{10} concentrations, which is directly influenced by the ventilation rates simulated for these indoor spaces. Hence, a high ventilation rate promotes the entrance of outdoor pollutants and the dilution of indoor emissions, while a low ventilation rate increases the effect of the indoor sources on the overall indoor concentration.

In the ASAC and Marzovelos classrooms the PM_{10} concentrations from outdoor origin are the major contributors to the total indoor concentrations due to the high simulated ventilation rates. On the other side, PM_{10} concentrations from indoor origin are the main responsible for the indoor concentrations obtained in children's bedrooms.

The weekly average indoor PM_{10} concentrations in all considered microenvironments for the winter period is shown in Figure 5.31.

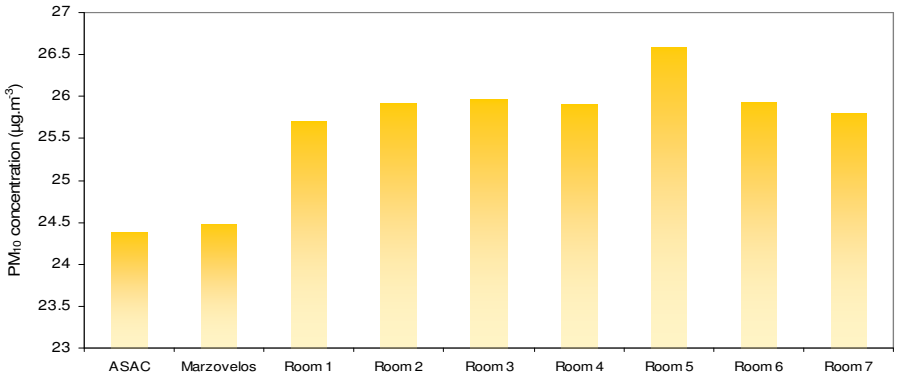

Figure 5.31 - Weekly average indoor PM_{10} concentrations for the winter period.

According to Figure 5.31, Child 5 presents the highest average concentrations during the winter campaign, while the lowest values are found in the residences of Child 1 and 7. MEXPO model simulates a lower average PM_{10} concentration for the ASAC microenvironment than for the Marzovelos school.

The hourly and average indoor/outdoor (I/O) ratio of PM_{10} concentrations were estimated for the winter period considering information on the pollutant concentration on the outdoor cell adjacent to the building window and the indoor concentrations for each of the indoor environments (Figure 5.32).

The analysis of Figure 5.32(a) shows that indoor sources are the dominant contributors to the indoor concentrations of PM_{10} during night time due to the low simulated ventilation rates. The highest and the lowest I/O values are found for the bedroom of Child 5 and both ASAC and Marzovelos classrooms, respectively. During day time, and with the increase of the ventilation rate, the transport of outdoor air to indoors compete with the indoor sources, decreasing the I/O ratio. The average values of I/O ratio confirm the importance of PM_{10} concentrations of indoor origin in the final indoor concentrations (Figure 5.32(b)).

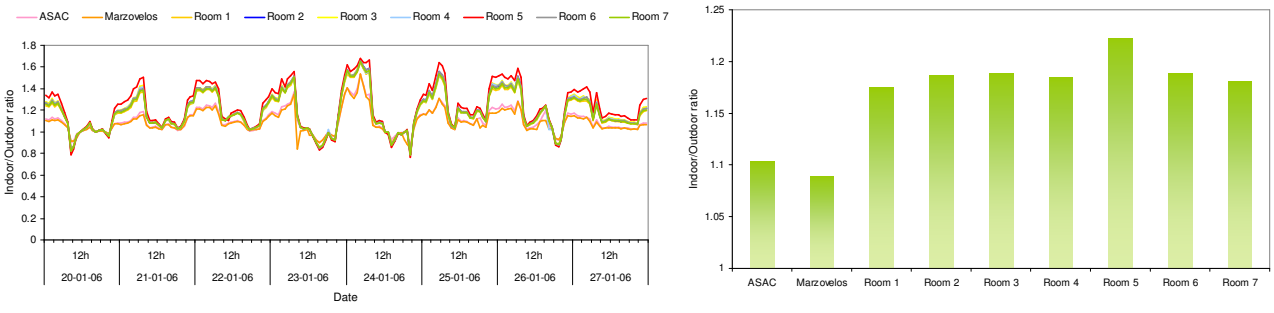

Figure 5.32 - (a) Hourly and (b) average indoor/outdoor ratio of PM_{10} concentrations simulated for the winter period.

During the winter campaign the daily average PM_{10} indoor concentrations were measured in Marzovelos classroom using a gravimetric method. Observations and the correspondent model results are plotted in Figure 5.33.

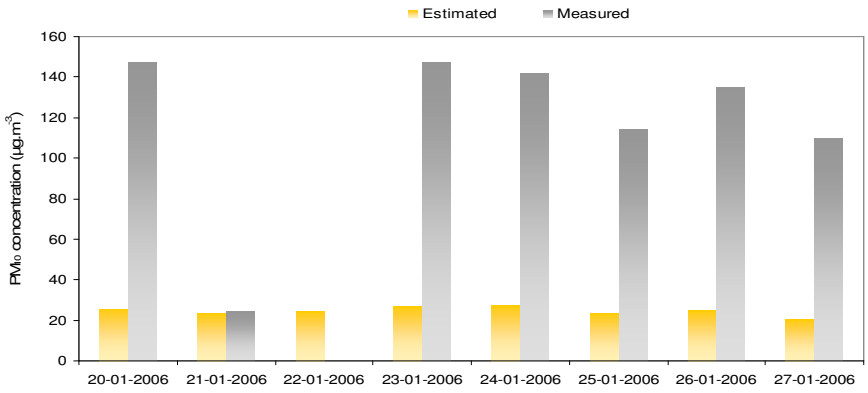

Figure 5.33 - Measured and simulated daily average PM_{10} indoor concentrations in Marzovelos classroom for the winter period.

The analysis of results shows a clear underestimation of model results during weekdays and a good agreement for the weekend (21st of January). There are no measurements available for Sunday, the 22nd January 2006.

The underestimation of indoor concentrations during weekdays may be explained by an undervalue of the PM_{10} indoor emissions. In fact, during the week, particle ressuspension due to student's activity inside the classroom should be considered an important indoor emission source that may have greatly contributed to the high indoor values measured during the campaign. Presently, there is no known quantification on these emissions to be included in the modelling approach.

The hourly indoor NO_2 concentrations estimated by MEXPO for both Marzovelos and ASAC classrooms and children's bedrooms are equally presented in Figure 5.34. The estimated indoor concentrations are only due to the transport of outdoor air to indoors due to natural ventilation mechanisms.

All the simulated values are below the limit value of 200 $\mu g.m^{-3}$, for 1 hour average, of the European Air Quality Directive. The 20th January 2006 presents the highest concentration values of all week simulated. The NO_2 indoor concentrations in the Marzovelos and ASAC classrooms are higher then those simulated for the children's rooms mainly due to the high predicted ventilation rates and the consequent transport of outdoor air to indoors. The bedroom of Child 5 presents the lower indoor NO_2 concentrations due to the lowest simulated ventilation rate.

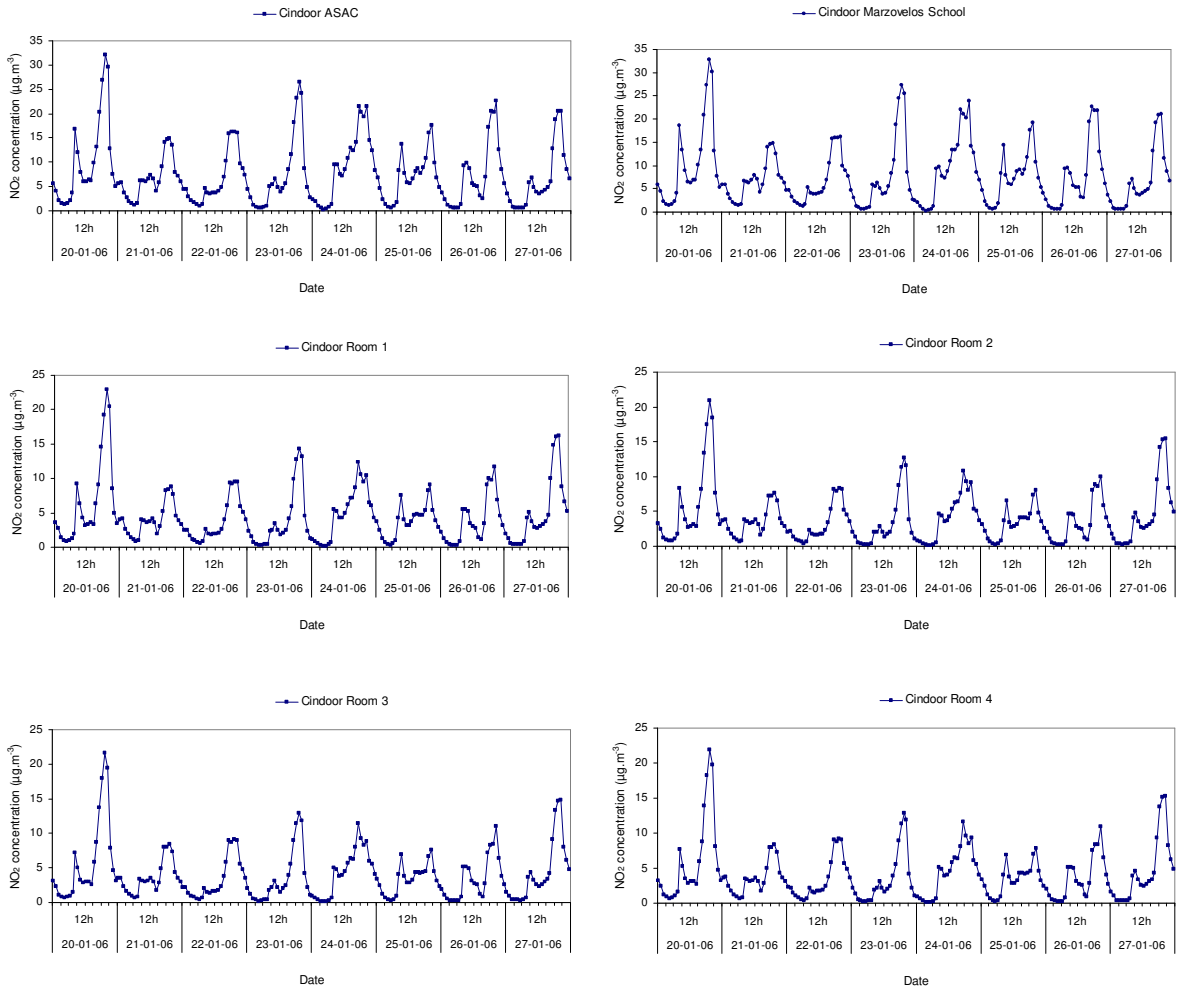

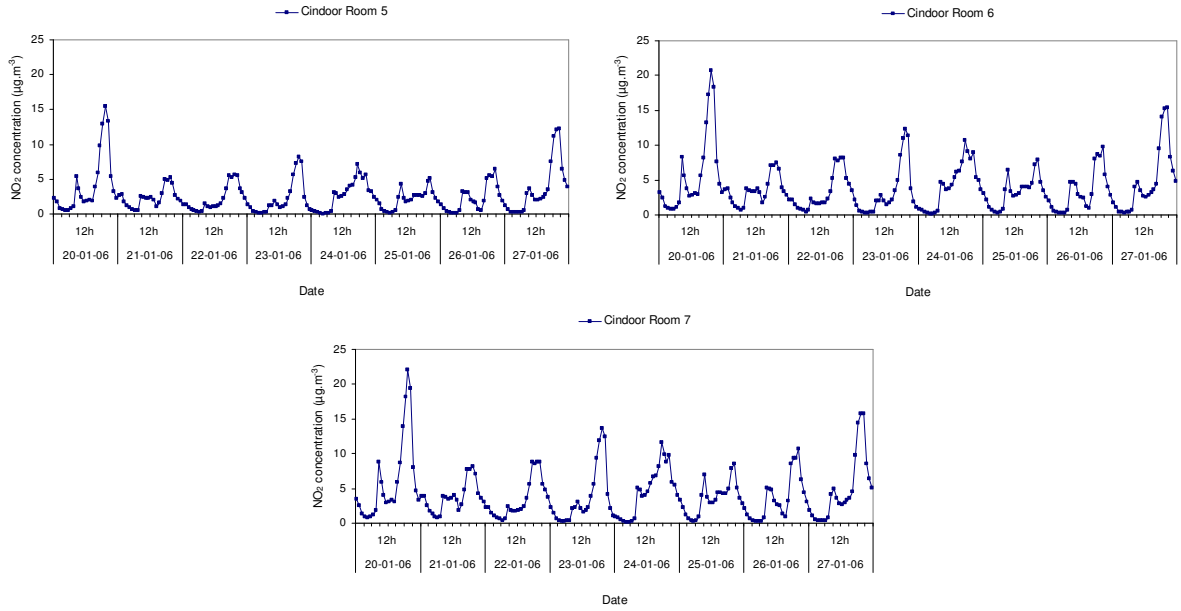

Figure 5.34 - Hourly NO_2 indoor concentrations simulated for the winter period.

The hourly and average indoor/outdoor ratios of NO_2 concentration are presented in Figure 5.35. The results below the unity value show that the hourly outdoor concentrations are higher than the indoor concentrations for all winter campaign with a growing I/O ratio for the 27th January. The average I/O ratios for each of the considered indoor spaces establish a higher and a lower ratio for the Marzovelos classroom and the bedroom of Child 5, respectively. The low ventilation rate found previously for this bedroom associated with the lack of indoor emission sources determine the opposite results of the ones encountered for the PM_{10} pollutant.

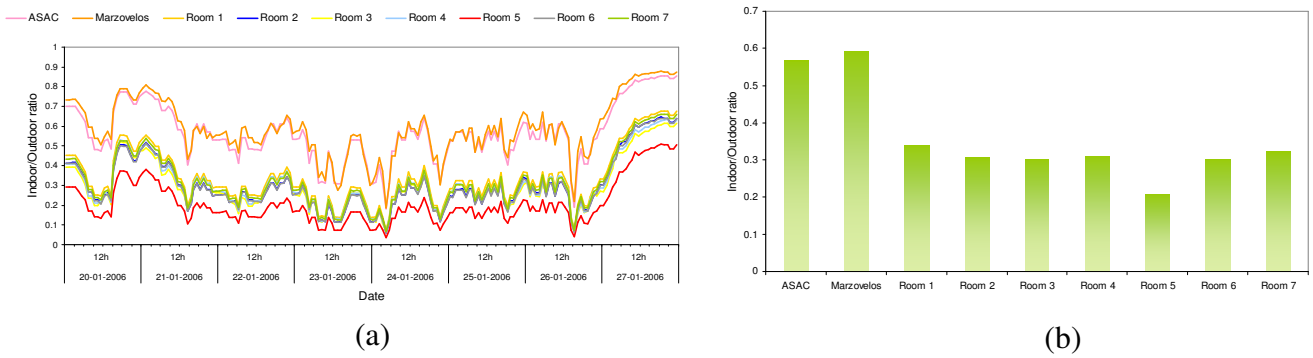

Figure 5.35 - (a) Hourly and (b) average indoor/outdoor ratio of NO_2 concentrations simulated the winter period.

During the winter campaign passive samplers were used to measure the NO_2 concentrations inside the Marzovelos classroom and in the children's bedrooms. The average NO_2 concentrations measured and simulated for the winter campaign are shown in

Figure 5.36. It is important to stress that comparisons performed between measured outdoor NO_2 concentrations from passive samplers and continuous measurements reveal a slightly overestimation of concentrations resulting from the passive sampler technique. This fact may lead to a correspondent overestimation of the measured indoor NO_2 concentrations.

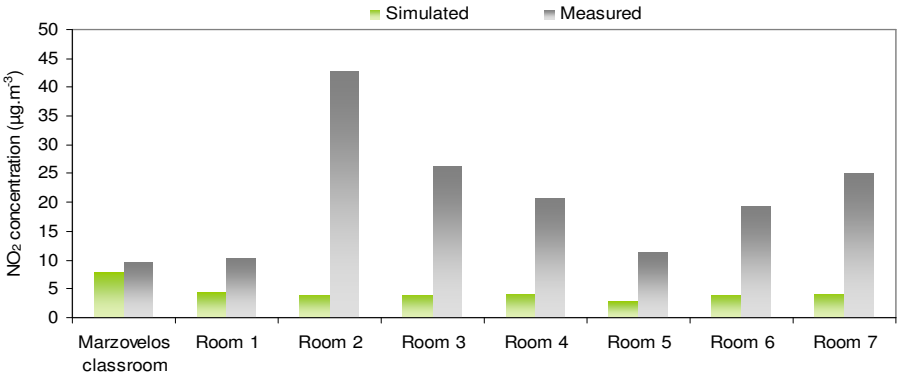

Figure 5.36 - Measured and simulated average indoor NO_2 concentrations in Marzovelos classroom and in children's bedrooms for the winter period.

A good agreement was found for the Marzovelos classroom. On the other side, there is a model underestimation for the children's bedrooms possibly caused by existent indoor sources such as nearby cooking activities and/or most possibly by the fireplaces present in the children's residences that were not accounted in the simulation.

The hourly indoor PM_{10} concentrations simulated for the summer campaign for the ASAC and Marzovelos classroom and for all children's bedrooms are presented in Figure 5.37. These concentrations are also differentiated by their outdoor (C_{io}) and indoor (C_{ii}) origin.

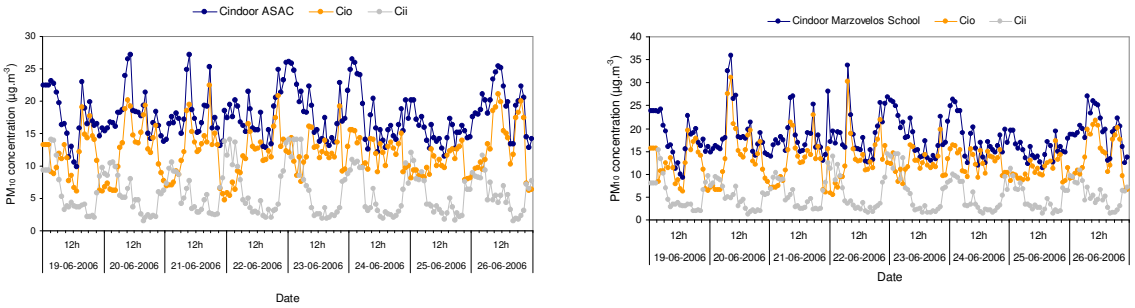

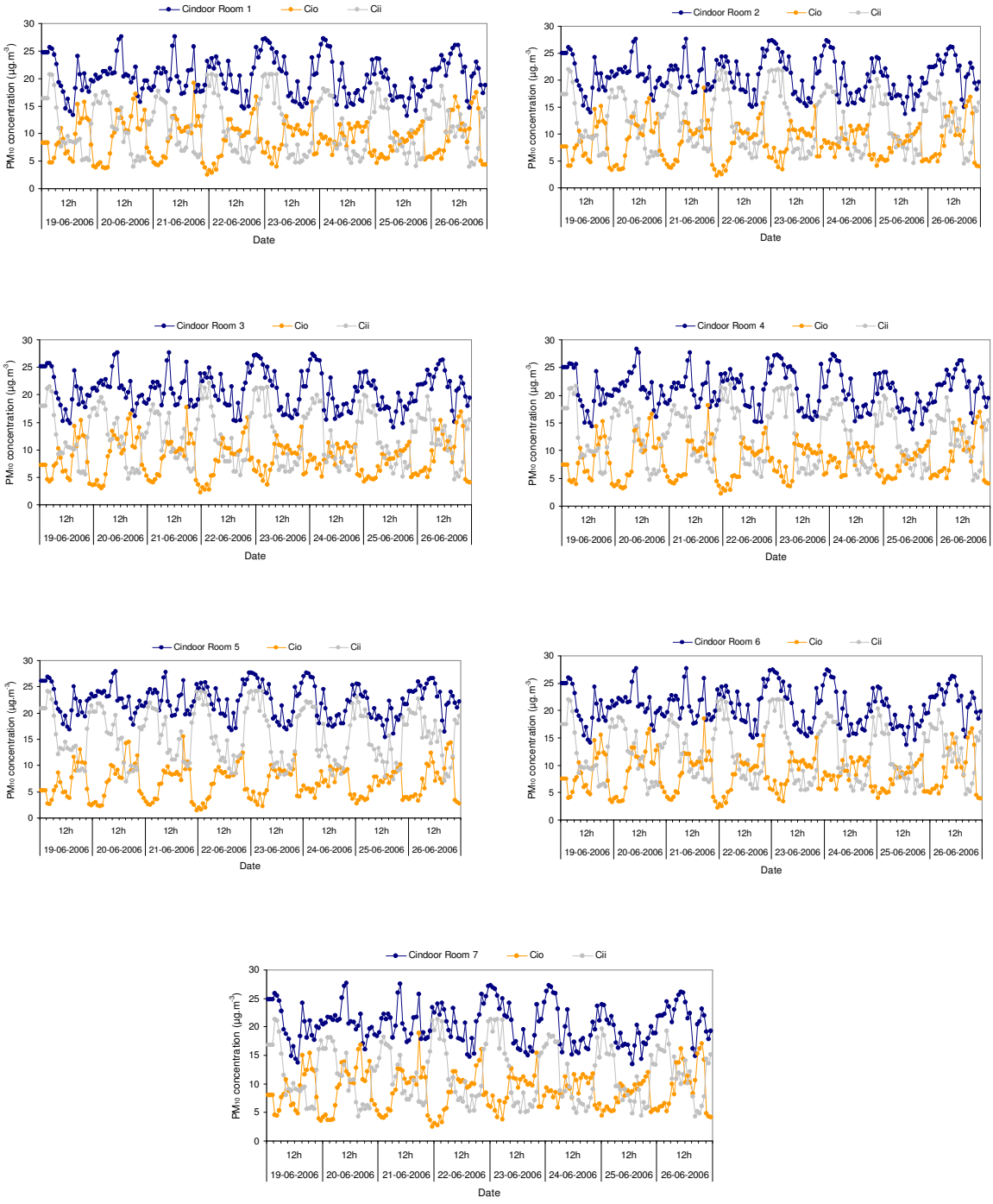

Figure 5.37 - Hourly PM_{10} indoor concentrations simulated for the summer period.

The highest PM_{10} concentrations are found in the Marzovelos classroom reaching the value of 36 $\mu g.m^{-3}$ for the 20th of June. The PM_{10} concentrations in the ASAC classroom and in the children's bedrooms are below the value of 30 $\mu g.m^{3}$. Generally, the simulated values are lower than the ones simulated for the winter campaign.

In the ASAC and Marzovelos classrooms the PM_{10} concentrations from outdoor origin are the major contributors to the total indoor concentrations. On the other side, PM_{10} concentrations from indoor origin are the main responsible for the indoor concentrations obtained in the children's bedrooms.

The weekly average indoor PM_{10} concentrations in all considered microenvironments for the summer period is shown in Figure 5.38.

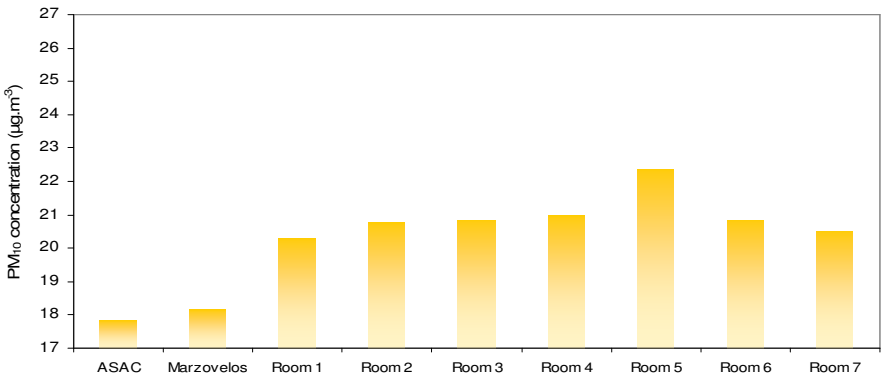

Figure 5.38 - Weekly average indoor PM_{10} concentrations for the summer period.

According to Figure 5.38, the highest average indoor concentrations of PM_{10} are observed in the room of Child 5, while the lowest values are found in the residences of Child 1 and 7. The Marzovelos classroom presents higher concentration values than the ASAC microenvironment.

Figure **5.39** presents the hourly and average I/O ratio of PM_{10} concentrations estimated for the summer period. The hourly I/O values show that the indoor simulated concentrations are higher than the outdoor ones, especially for the children's bedrooms, reaching the 2 orders of magnitude for the first days of the campaign. The average I/O ratios confirm the higher values for the children's bedrooms and the highest one for the bedroom of Child 5. Again this result is mainly due to the low ventilation rates found that do not promote a proper mixing of the indoor concentrations from indoor origin.

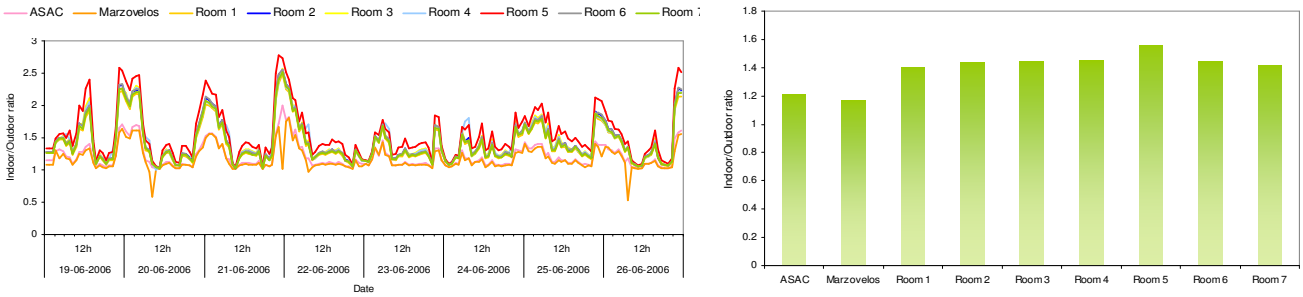

(a) (b)

Figure 5.39 - (a) Hourly and (b) average indoor/outdoor ratio of PM_{10} concentrations simulated for the summer period.

The daily average PM_{10} concentrations were also measured in the Marzovelos classroom for the summer campaign using a gravimetric method. Technical problems occurred in the last three days of the campaign not allowing a quantification of the indoor PM_{10} concentrations. Observed and modelled results for the daily average PM_{10} concentrations in the Marzovelos classroom are presented in Figure 5.40.

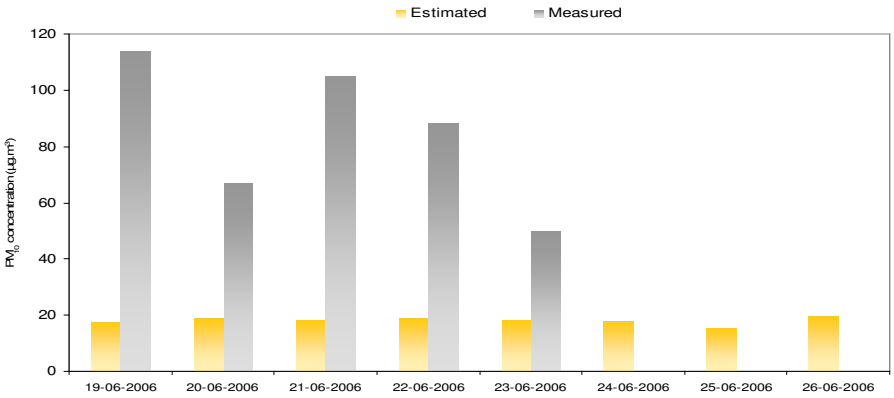

Figure 5.40 - Measured and simulated daily average PM_{10} indoor concentrations in Marzovelos classroom for the summer period.

As already occured for the winter campaign there is an underestimation of model results for weekdays. Again, this may be explained by the existence of important indoor sources, such as ressuspension due to the student's activity, that is currently not quantified and consequently was not accounted in MEXPO model. The lack of experimental data for the weekend (24th and the 25th June) compromises the confirmation of the previous hypothesis.

The hourly indoor NO_2 concentrations for the Marzovelos and ASAC classrooms and the children's bedrooms simulated for the summer campaign period are presented in Figure

5.41. These values represent solely the transport of outdoor air to indoors throught natural ventilation mechanisms.

The values obtained for this time of the year are higher than the ones simulated for the winter period, reaching for the Marzovelos and ASAC classrooms peak values of 50 $\mu g.m^{-3}$ for the 22nd and the 23rd of June. Nevertheless, all the simulated indoor NO_2 concentrations are below the unique reference value of 200 $\mu g.m^{-3}$ for hourly averages of the air quality European guidelines. The lowest NO_2 concentrations are found in the bedroom of Child 5 corresponding to the lowest ventilation rate simulated for the summer period and consequently to a less transport of pollutant from outdoors to indoors.

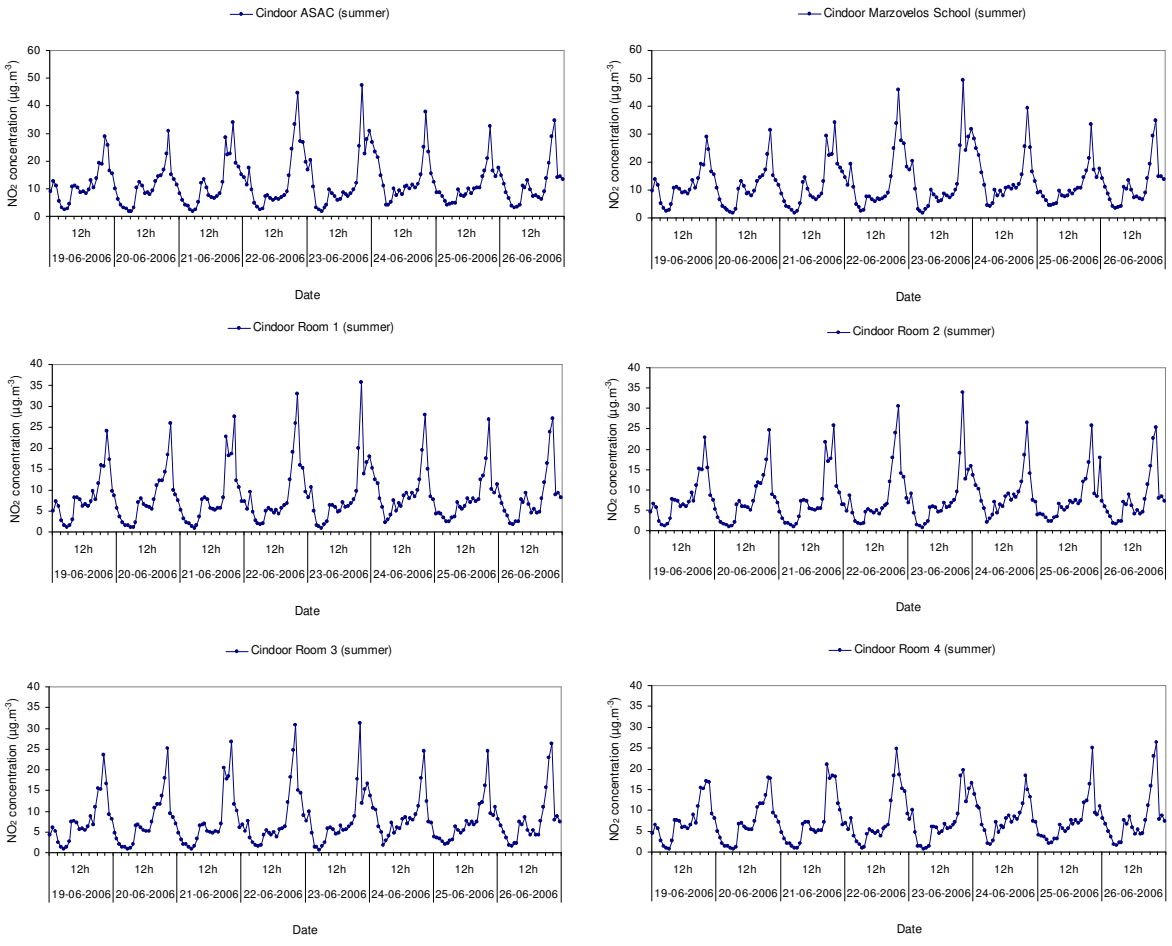

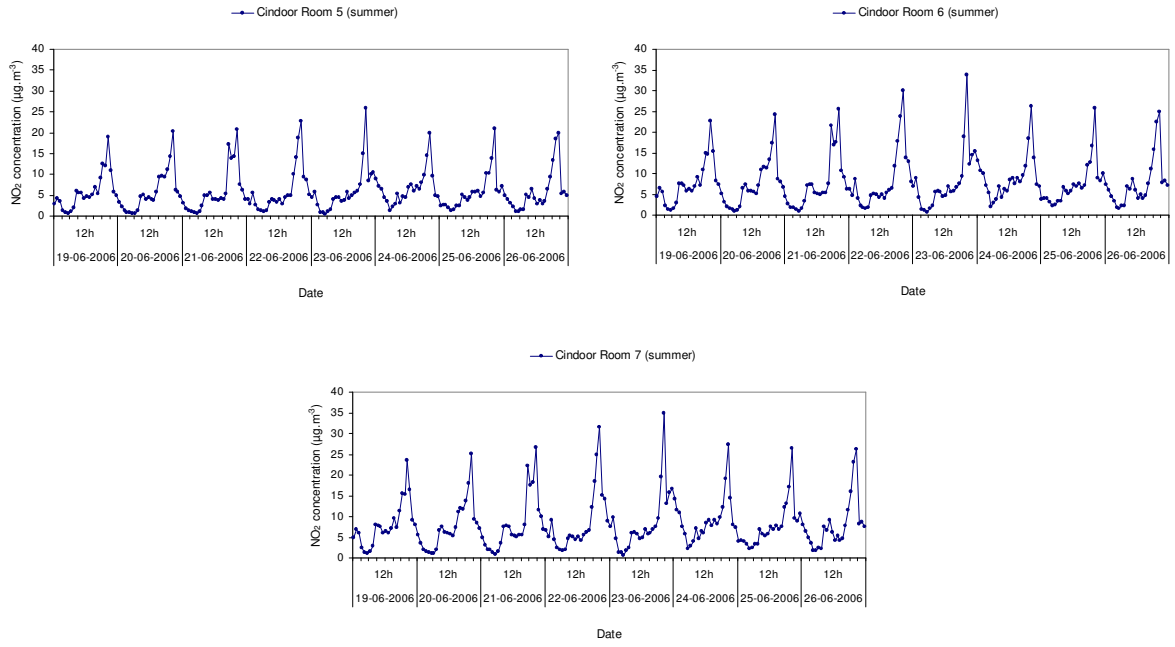

Figure 5.41 - Hourly NO_2 indoor concentrations simulated for the summer period.

The hourly and average I/O ratios of NO_2 concentrations for all considered indoor spaces are presented in Figure 5.42.

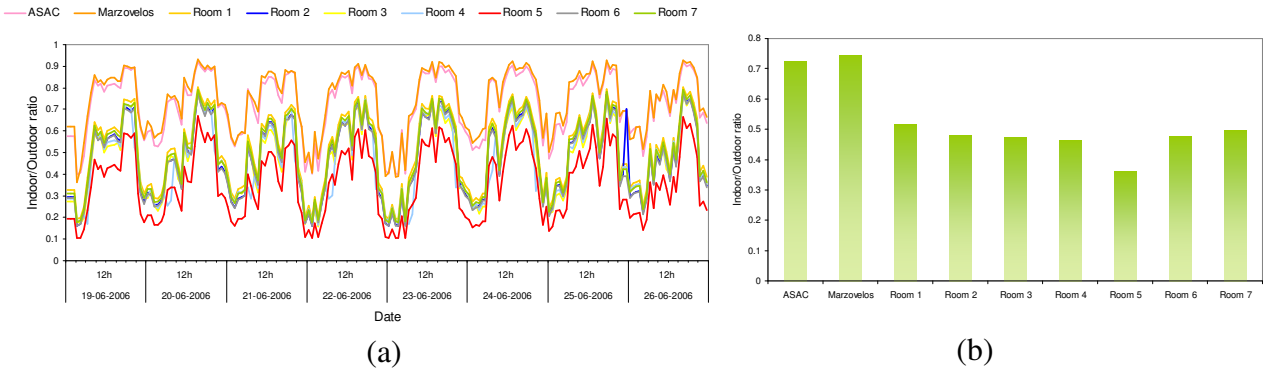

Figure 5.42 - (a) Hourly and (b) average indoor/outdoor ratio of NO_2 concentrations simulated for the summer period.

The highest hourly and average I/O values are found for the Marzovelos and ASAC classrooms and the lowest for the bedroom of Child 5. The variation of the hourly ratios reflects the use of natural ventilation mechanisms during daytime and consequently the increase of the I/O ratios and a decrease during night time.

As already performed during the winter campaign, passive samplers were used to measure the accumulated concentration of NO_2 concentrations inside the Marzovelos and the children's bedrooms. Due to technical problems with the passive sampler used in the

bedroom of Child 2 it was not possible to have a quantification of the respective NO_2 indoor concentration. Figure 5.43 shows the average measured and simulated indoor NO_2 concentrations for the summer period.

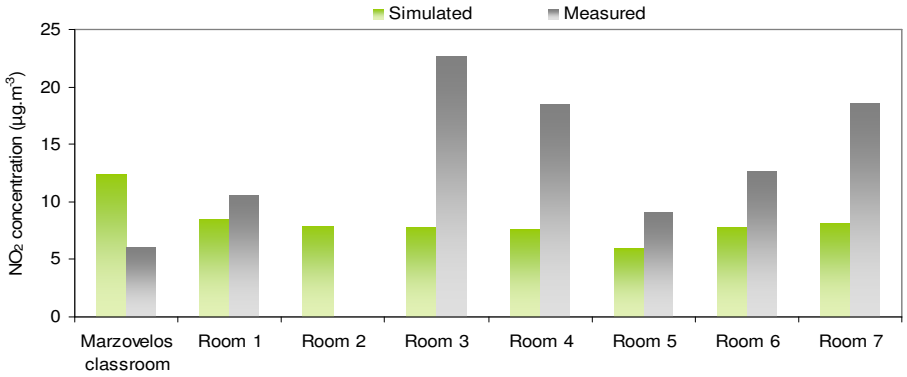

Figure 5.43 - Measured and simulated average indoor NO_2 concentrations in Marzovelos classroom and in children's bedrooms for the summer period.

It is possible to notice an overestimation of model results for the Marzovelos classroom. A slight underestimation of model results is observed in the bedrooms of children 1, 5 and 6. The difference found between measured and estimated NO_2 concentrations in the bedrooms of children 3, 4 and 7, that was already observed during the winter campaign, may confirm that there are missing indoor sources of NO_2 pollutant, such as cooking activities, nearby these indoor spaces.

5.2.2.4. Individual exposure

As the final outcome of MEXPO model, the estimated individual exposures to PM_{10} and NO_2 pollutants for the seven children selected for this study are presented. The hourly and the daily average individual exposure to PM_{10} during the winter period for the seven children is shown in Figure 5.44.

The analysis of Figure 5.44 shows that the highest exposure values occur in the 20th, 23rd and 24th of January, whereas the lowest value is observed for the 27th January. Child 5 presents the highest daily average exposures to PM_{10} pollutant during the winter campaign.

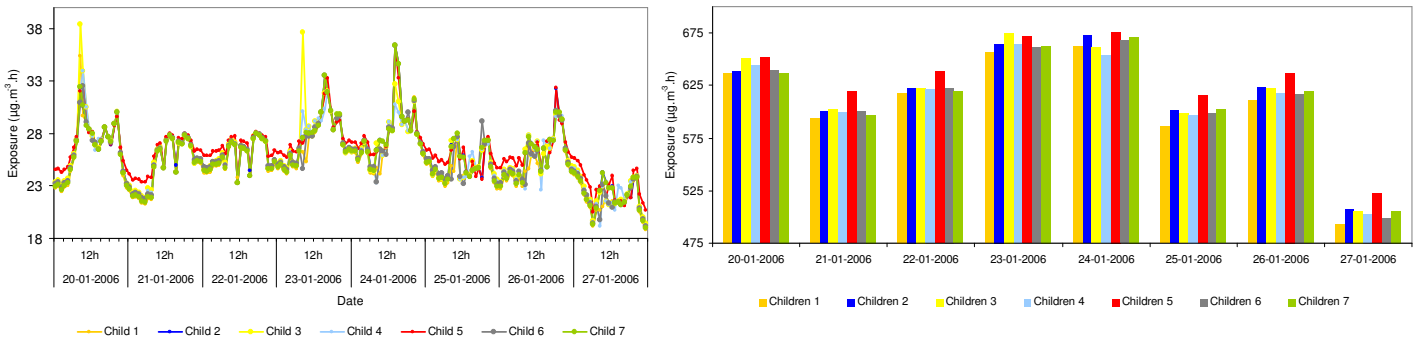

(a) (b)

Figure 5.44 -(a) Hourly individual exposure and (b) daily average individual exposure to PM_{10} for the winter period.

The weekly average individual exposure to PM_{10} during the winter period is presented in Figure 5.45. The analysis of the results confirms that Child 5 is the most exposed to PM_{10} during the winter campaign followed by Child 3 and 2. The less exposed is Child 1.

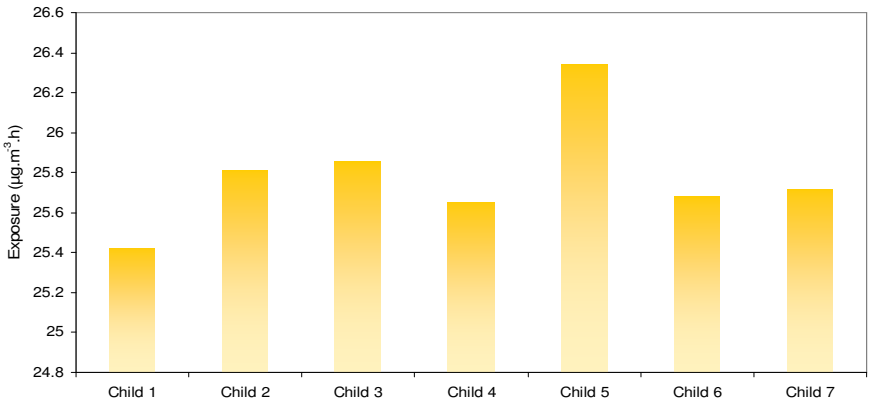

Figure 5.45 - Weekly average individual exposure to PM_{10} for the winter period.

Figure 5.46 presents the hourly and the daily average individual exposure estimates to NO_2 pollutant during the winter campaign. The higher exposure values were found for the 20th and the 27th January. The lowest exposure values were estimated for Child 5 and the highest for Child 1.

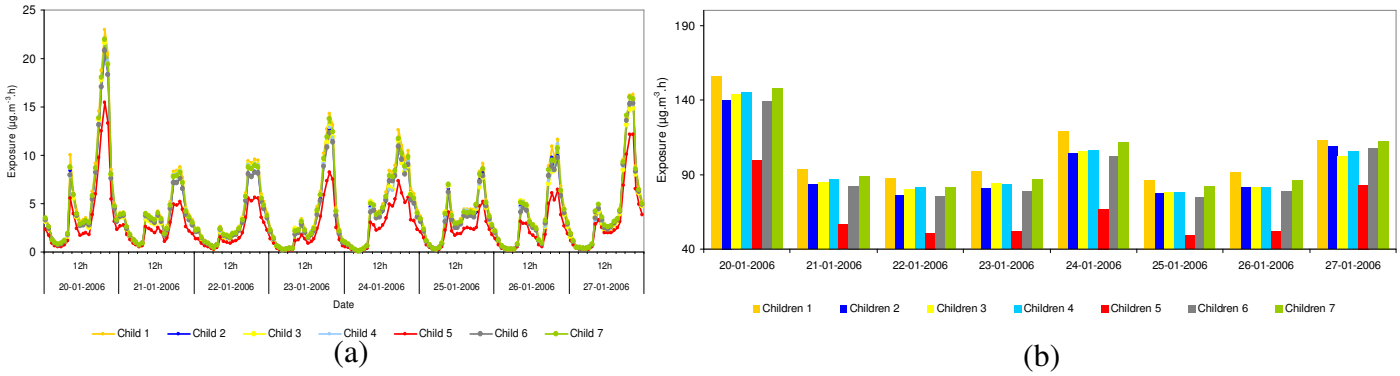

Figure 5.46 - (a) Hourly individual exposure and (b) daily average individual exposure to NO_2 for the winter period.

The weekly average individual exposure to NO_2 during the winter campaign confirms the lowest value for Child 5 and the higher exposure value for Children 1 and 7.

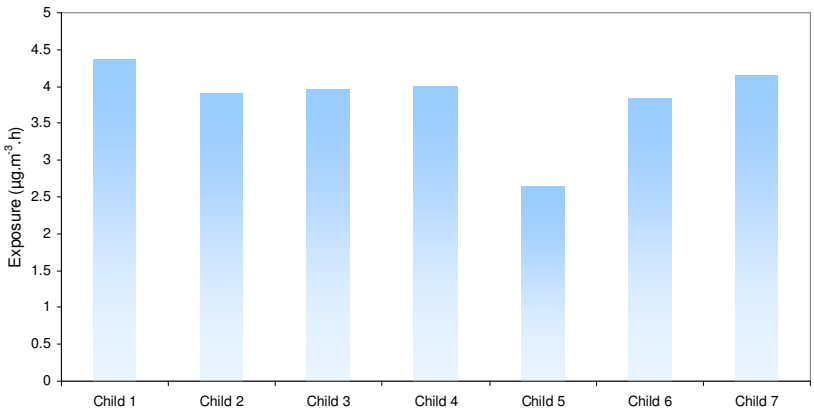

Figure 5.47 - Weekly average individual exposure to NO_2 for the winter period.

The hourly and daily exposures to PM_{10} during the summer campaign are presented in Figure 5.48. The hourly exposure shows an approximately equivalent behaviour for the simulated days with an increase of the exposure levels during daytime and a decrease during the nighttime. The daily average exposure reveals the 25th June as the day with the lowest exposure levels for all children, and the 26th June with the highest exposure values.

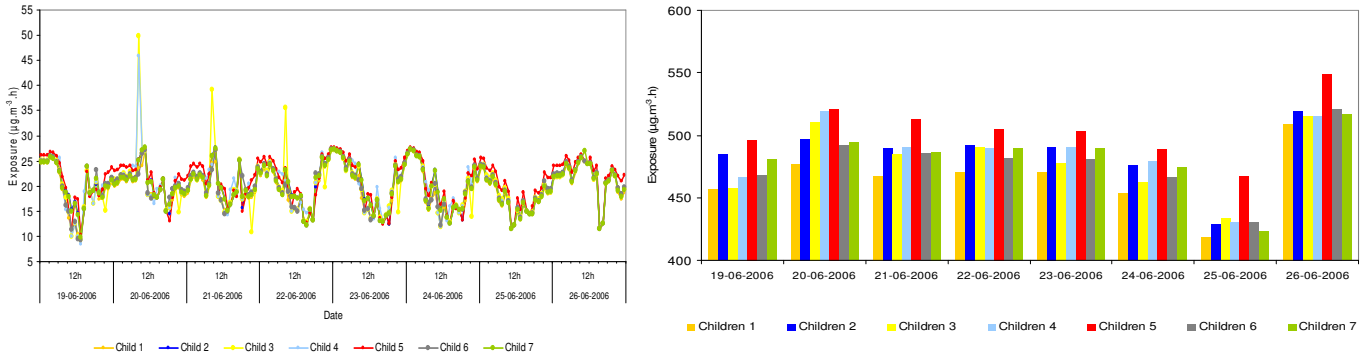

(a) (b)

Figure 5.48 - (a) Hourly individual exposure and (b) daily average individual exposure to PM_{10} for the summer period.

Figure 5.49 presents the weekly average individual exposure to PM_{10} during the summer campaign. The analysis of the figure shows that the highest and the lowest exposure levels correspond to Child 5 and Child 1, respectively.

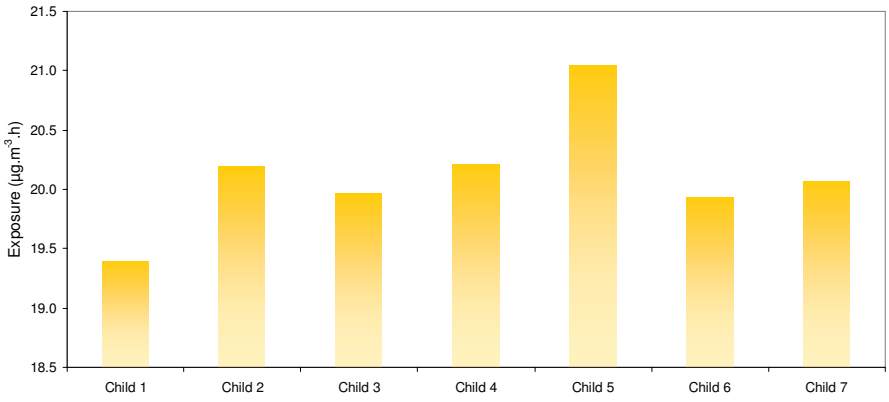

Figure 5.49 - Weekly average individual exposure to PM_{10} for the summer period.

The hourly and the daily average exposure to NO_2 during the summer campaign is presented in Figure 5.50. The highest hourly exposure values are simulated at the end of the 23rd of June. The daily average exposure shows the highest exposure days as the 22nd and the 24th of June.

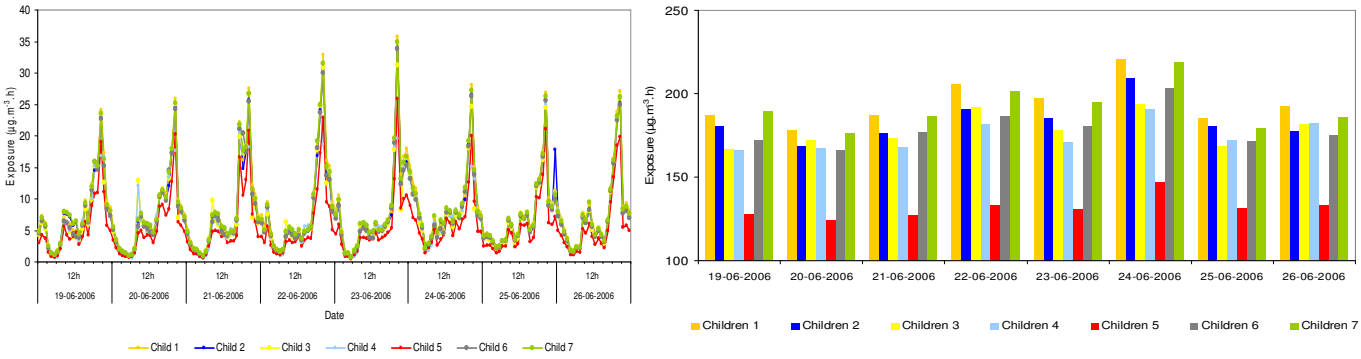

(a) (b)

Figure 5.50 - (a) Hourly individual exposure and (b) daily average individual exposure to NO_2 for the summer period.

The weekly average individual exposure presented in Figure 5.51 shows children 1 and 7 as the most exposed to NO_2 pollutant during the summer campaign. On the opposite, the lowest average exposure was simulated for Child 5.

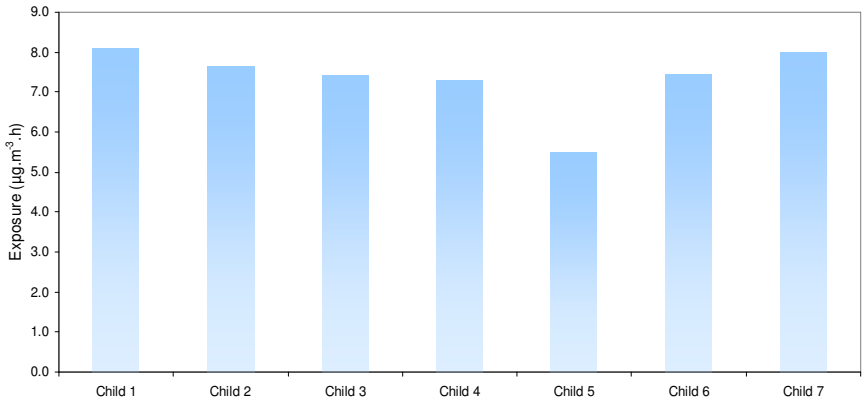

Figure 5.51 - Weekly average individual exposure to NO_2 for the summer period.

5.2.2.5. Discussion of results

Table 5.4 summarizes the main results obtained with the application of MEXPO model to Viseu urban area for the winter and summer periods, allowing a more detailed analysis of the exposure results. The symbols (↑) and (↓) represent the highest and the lowest values achieved for the natural ventilation rate, PM_{10} and NO_2 indoor concentrations and PM_{10} and NO_2 individual exposure.

Table 5.4 - Summary of MEXPO model results for the winter and summer periods.

		winter	summer
Natural ventilation rate		↑ Room 1 and 7 ↓ Room 5	↑ Room 1 and 7 ↓ Room 5
Indoor concentration	**PM_{10}**	↓ Room 1 and 7 ↑ Room 5	↓ Room 1 and 7 ↑ Room 5
	NO_2	↑ Room 1 and 7 ↓ Child 5	↑ Room 1 and 7 ↓ Child 5
Individual exposure	**PM_{10}**	↓ Child 1 and 7 ↑ Child 5	↓ Child 1 and 7 ↑ Child 5
	NO_2	↑ Child 1 and 7 ↓ Child 5	↑ Child 1 and 7 ↓ Child 5

According to Table 5.4, the highest ventilation rates occurred in the bedrooms of children 1 and 7 and the lowest on the residence of Child 5, for both winter and summer periods. These results are directly related to the flow within the urban area and the position of the children's residences in the study domain, considering that similar window opening conditions exists for all residences. The residence's location height also influenced the estimated ventilation rates, since higher outdoor wind speeds are observed for high-rise apartment buildings than for ground floor residences. In fact, the residence of Child 5 is located on the ground floor, whereas children 1 and 7 live on the 4th and 3rd floor, respectively.

The ventilation rates estimation allowed to determine the amount of pollutants entering the different indoor microenvironments and the rate of dilution of the considered indoor emissions. The highest indoor concentrations of PM_{10} pollutant were derived for the bedroom of Child 5, and the lowest for the residences of children 1 and 7, in both winter and summer campaigns. The low ventilation rates estimated for the residence of Child 5 were responsible for a small amount of outdoor air pollution entering indoors and for an increase of the indoor sources influence. The opposite situation is verified for the residences of children 1 and 7, where is observed a greater influence of the outdoor PM_{10} concentrations to the indoor air quality. The good outdoor air quality found for the urban

area of Viseu enabled these results. In this sense, the improvement of the indoor quality by natural ventilation mechanisms is only valid for urban areas with no air pollution problems.

For the NO_2 pollutant, and considering that no indoor sources were used in the simulations, the highest indoor concentrations were found for the residences of children 1 and 7, while the lowest values were estimated for the bedroom of Child 5, in both winter and summer campaigns. With the absence of indoor sources, the indoor concentrations only depend on the amount of outdoor air that enters indoors that is derived by the ventilation rate. Thus, the high ventilation rates found for the bedrooms of children 1 and 7 determined the NO_2 indoor concentrations results.

The individual exposure estimation was based on the amount of time that each children spent in the different microenvironments and on the pollutants concentration in these indoor spaces. The analysis of the children time activity patterns showed that the higher amount of time is spent indoors, more concretely at the residential microenvironment. In this sense, the individual exposure estimation directly depends on the indoor concentrations estimated for this microenvironment. Accordingly, the highest individual exposure to PM_{10} was calculated for Child 5 for both winter and summer simulations, whereas the lowest exposure values were determined for children 1 and 7. As expected, the highest and the lowest individual exposure values to NO_2 were determined for Children 1 and 7, and Child 5, respectively.

The modelling results on individual exposure allow to conclude that children 1, 5 and 7 may have a higher probability to develop related health problems, such as respiratory deseases. Nevertheless, it is also important to refer that the estimated indoor concentrations at the residential environment, where children spent the majority of their time, are still below the only available air quality guidelines from the AQ-FWD.

The validation of the MEXPO model results show that are still improvements to make on the developed methodology, namely: to include the contribution of ressuspension as an important source of PM indoors; and to consider the transport of pollutants between indoor compartments with relevant indoor sources, such as cooking activities. The latter becomes relevant for simulations with the NO_2 pollutant.

The inclusion of the temperature difference on the natural ventilation estimation can also be seen as a pertinent improvement on MEXPO model.

6. CONCLUSIONS

Air pollution is a major environmental health problem affecting particularly the urban populations. Concern focuses not only on ambient air quality in cities but also on the air quality of indoor environments, where people spend most of their time. In fact, it is now well established that indoor air pollution contributes significantly to the global burden of disease of the population. Therefore, the knowledge of this contribution is essential in view of risk assessment and management. It is also known that in the absence of internal sources, indoor air pollutant concentrations depend mainly on the outdoor dispersion processes, the ventilation and airtightness of the building, and the physical and chemical properties of the pollutant.

This important framework determined the main goal of this work through the development of a microscale exposure model capable of estimating the individual exposure to atmospheric pollutants in urban areas. To perfom this goal the exposure model is able to estimate the outdoor flow and pollutant concentrations, considering the influence of the urban built-up area, but also to assess the air exchange rates as result of natural ventilation mechanisms and the indoor pollutant concentrations on the defined microenvironments.

For the purpose of estimating the outdoor pollutant dispersion the developed microscale exposure model MEXPO includes a CFD model (VADIS) that has the advantage to fully characterize the flow and the transport of the urban air pollution on a 3D basis.

The rapidly expanding use of microscale CFD models dictates the need for the proper evaluation of these models through a single procedure accepted within the scientific and wider communities. Chapter 3 deals with this pertinent problem, proposing a basic methodology for the evaluation this type of models. Therefore, VADIS CFD model was evaluated according to the established procedure, using specific model acceptance criteria

that were defined in agreement with the intended model purpose, the study of meteorology and pollutant dispersion in urban areas.

The main innovative features of this work are then related to the inclusion of a CFD model in the exposure model MEXPO combined with the capability of estimating the wind-induced natural ventilation rates in urban buildings and, consequently, to model the indoor pollutant concentrations from outdoor and indoor origins.

Moreover, the model allows characterizing the variation of the natural ventilation rates, indoor concentrations, and indoor/outdoor rates on an hourly basis, if model inputs are provided in the same temporal resolution. This special model aspect plays an advantage relatively to direct measurements techniques that are relative more expensive and time consuming, and that are not feasible for the total indoor microenvironments present in an urban area.

The application of the MEXPO exposure model to Viseu urban area determined that the higher and the lower exposure levels to PM_{10} pollutant in both winter and summer periods occur for Child 5 ,and children 1 and 7, respectively. The opposite is found for the NO_2 pollutant, where Child 5 presents the lowest exposure levels and children 1 and 7 the highest. These results are most determined by the time spent at the residential microenvironment and for the highest and lowest indoor concentrations of PM_{10} and NO_2 pollutants found, respectively, in that microenvironment. Children 1, 5 and 7 are therefore more sensitive to develop respiratory problems such as asthma then the rest of the studied children.

The estimated ventilation rates due to wind-induced natural processes for the analysed indoor environments may provide valuable information concerning the ventilation needs to achieve the minimum indoor standards. This is particular important in classrooms where the learning and attention skills can be greatly influenced by the levels of ventilation and consequently by the indoor CO_2 concentration. The results obtained for the Marzovelos classroom that were slightly overestimated when compared with the few available measurements indicate that additional ventilation measures, such as HVAC systems, should be implemented.

The overestimation of the modelled ventilation rates in Marzovelos classroom can be related to the assumptions made in the window opening areas for the summer and winter periods or even by the methodology used to model the ventilation rates, since the thermal-induced ventilation phenomena were not considered. Future work on this area that is

currently still minor explored can include the testing of more sophisticated natural ventilation modelling techniques.

Despite the large campaigns conducted under the SAUDAR project the available data are still limited to perform a proper evaluation of the model results, in particular in the estimation of ventilation rates. This was mainly due to the fact that available monitoring techniques to measure ventilation rates are expensive and difficult to apply in occupied buildings, compromising the possibility to perform a more detailed evaluation of the ventilation rate results in all indoor spaces considered in this study. On the other side, the latest makes the ventilation rate modelling a major advantage comparing with the existent measuring techniques. Also, concerning the available measured data, it would be important to compare the indoor modelling concentrations with higher temporal resolution measurements in order to assess the variability of model results.

The indoor emission estimates played as one of the most uncertain factors in the MEXPO model results, as expected. This is particular critical in case of PM indoor emissions, where PM ressuspension due to human activity can greatly contribute to the increase of indoor concentrations. NO_2 emissions are associated to combustion processes, such as cooking or heating appliances, and therefore it is important to fully characterize the indoor spaces in order to account for all emission sources.

For the Viseu modelling exercise no indoor sources of NO_2 pollutant were considered to be present in the the children's bedroom. This fact may have contributed to the underestimation of modelling indoor NO_2 concentrations. Therefore, it is important to notice that emission sources, such as cooking activities or fireplaces, taking place in a nearby compartment of the bedroom can be responsible for the increase of the indoor concentration levels of this pollutant.

Despite the inherent difficulties to fully evaluate the model performance the developed methodology may be seen as a valid approach to assess the individual human exposure to atmospheric pollutants in urban areas, replacing direct measurement techniques that are considered invasive and expensive. Moreover, the estimation of the natural ventilation rates and the indoor pollutant concentrations in buildings may be used to provide a first assessment on these variables and to substitute the use of direct measurements that are difficult to obtain on a large spatial and temporal scale.

The methodology developed in MEXPO for the estimation of individual exposure to atmospheric pollution can also be applied for the estimation of the population exposure to

atmospheric pollutants living in an urban area. In this case, it is important to fully characterize the time-activity pattern of the entire population living in the study domain.

The developed exposure model has also an important role in the application to future climate change scenarios with direct consequences in the urban climate, allowing to determine the future human exposure to atmospheric pollutants and, consequently, also the future outdoor and indoor atmospheric pollutants concentrations in an urban area.

Furthermore, the study of the potential impact on human exposure to different emission reduction strategies of atmospheric pollutants can also be carried out with MEXPO model.

REFERENCES

Ackermann-Liebrich, U.; Viegi, G. and Nolan, C. (Eds.), 1995. Time–activity pattern in exposure assessment. EUR 15892 EN. European Commission.

Addison, P.S.; Qu, B.; Nisbet, A. and Pender, G., 1997. A non-Fickian particle-tracking diffusion model based on fractional Brownian motion. International Journal for Numerical Methods in Fluids, 25, 1373-1384.

Allwine, K.J., 2004. Overview of JOINT URBAN 2003 - an atmospheric dispersion study in Oklahoma City. AMS Symposium on Planning, Nowcasting, and Forecasting in the Urban Zone, Seattle, Washington, USA.

Andrade, J.A.F., 1988. Métodos de análise da distribuição de ar em recintos climatizados. Tese de Doutoramento, Faculdade de Engenharia da Universidade do Porto.

Arnold, S.J.; ApSimon, H.; Barlow, J.; Belcher, S.; Bell, M.; Boddy, J.W.; Britter, R.; Cheng, H.; Clark, R.; Colvile, R.N.; Dimitroulopoulou, S.; Dobre, A.; Greally, B.; Kaur, S.; Knights, A.*, et al.*, 2004. Introduction to the DAPPLE Air Pollution Project. Science of the Total Environment, 332, 139-153.

ASHRAE, 1997. Handbook of fundamentals. American Society of Heating, Refrigerating and Air Conditining Engineers. Atlanta, GA.

Asimakopoulos, D.N.; Assimakopoulos, V.D.; Chrisomallidou, N.; Klitsikas, N.; Mangold, D.; Michel, P.; Santamouris, M. and Tsangrassoulis, A., 2000. Energy and climate in the urban built environment. James and James, ISBN 1873936907, 412 pp.

Avgelis, A. and Papadopoulos, A.M., 2004. Indoor Air Quality Guidelines and Standards - A State of the Art Review. International Journal of Ventilation, 3(3), 267-278.

Baek, S.; Kim, Y. and Perry, R., 1997. Indoor air quality in homes, offices and restaurants in Korean urban area-indoor/outdoor relationships. Atmospheric Environment, 31 (4), 529-544.

Bartzis, J.G.; Vlachogiannis, D. and Sfetsos, A., 2004. Thematic area 5: Best practice advice for environmental flows. The QNET-CFD Network Newsletter, Vol. 2, No. 4, pp. 34-39.

Biltoft, C.A., 2001. Customer Report for Mock Urban Setting Test. DPG Document No. WDTC-FR-01-121. West Desert Test Center, U.S. Army Dugway Proving Ground, Dugway, Utah, 58 pp.

Bitan, A., 1992. The high climatic quality city of the future. Atmospheric Environment, 26B, 313-329.

Borrego, C., 1989. Air quality modelling: atmospheric pollutants dispersion with the application of a Lagrangian model. Habilitation, University of Aveiro, Portugal.

Borrego, C.; Miranda, A.I.; Costa, A.M. and Amorim, J.H., 2002. VADIS Street Canyon Model: Operational Prototype. Deliverable D04.4 of SUTRA Project (EVK4-CT-1999-00013). Departamento de Ambiente e Ordenamento, Universidade de Aveiro, AMB-QA-10/02.

Borrego, C.; Schatzmann, M. and Galmarini, S., 2003a. Quality Assurance of Air Pollution Models. In: Air Quality in Cities. Moussiopoulos, N. (Ed.). Springer-Verlag, ISBN 3-540-00842-x

Borrego, C.; Tchepel, O.; Costa, A.M.; Amorim, J.H. and Miranda, A.I., 2003b. Emission and dispersion modelling of Lisbon air quality at local scale. Atmospheric Environment, 37, 5197-5205.

Borrego, C.; Monteiro, A.; Ferreira, J.; Miranda, A.I.; Costa, A.M. and Sousa, M., 2005. Modelling uncertainty estimation procedures for air quality assessment. 3rd International Symposium on Air Quality Management at Urban, Regional and Global Scales, Istanbul, Turkey, 210-219.

Borrego, C.; Tchepel, O.; Costa, A.M.; Martins, H.; Ferreira, J. and Miranda, A.I., 2006. Traffic-related particulate air pollution exposure in urban areas. Atmospheric Environment, 40, 7205-7214.

Borrego, C.; Lopes, M.; Valente, J.; Santos, J.; Nunes, T.; Martins, H.; Miranda, A.I. and Neuparth, N., 2007a. Air Pollution and child respiratory diseases: the Viseu case-study, Portugal. Air Pollution 2007, 23 - 25 April, Algarve, Portugal. Eds. C. Borrego, C.A. Brebbia, WIT Press, Southampton, UK.

Borrego, C.; Miranda, A.I.; Lopes, M.; Nunes, T.; Valente, J.; Ferreira, J.; Santos, P.; Santos, J.; Amorim, J.H.; Martins, H.; Carvalho, A.C.; Costa, A.M.; Tavares, R.; Martins, V.; Monteiro, A.*, et al.*, 2007b. SaudAr - A Saúde e o Ar que respiramos.

Relatório do 3º de actividades. Universidade de Aveiro. AMB-QA-3/2007, Aveiro, Portugal, 84 pp.

Borrego, C.; Monteiro, A.; Ferreira, J.; Miranda, A.I.; Costa, A.M.; Carvalho, A.C. and Lopes, M., 2008. Procedures for estimation of modelling uncertainty in air quality assessment. Environment International. doi:10.1016/j.envint.2007.12.005.

Bostrom, C.-E., 1993. Health risk evaluation of nitrogen oxides. Nitrogen oxides in ambient air - properties, sources and concentrations. Scandinavian Journal of Work, Environment & Health, 19, 9-13.

Bottema, M., 1993. Wind Climate and Urban Geometry. Eindhoven University of Technology. Netherlands, 212 pp.

Britter, R., 2003. Urban air pollution phenomenology. In: Air Quality in Cities. SATURN EUROTRAC-2 Subproject Final Report. Moussiopoulos, N. (Ed.). Springer-Verlag, ISBN 3-540-00842-x, 21-30.

Britter, R. and Schatzmann, M. (Eds.), 2007a. Background and justification document to support the model evaluation guidance and protocol. COST Action 732: Quality assurance and improvement of microscale meteorological models. COST Office Brussels, ISBN 3-00-018312-4, 85 pp.

Britter, R. and Schatzmann, M. (Eds.), 2007b. Model Evaluation Guidance and Protocol Document. COST Action 732: Quality assurance and improvement of microscale meteorological models. COST Office Brussels, ISBN 3-00-018312-4, 27 pp.

BSI, 1991. Code of practice for ventilation principles and designing for natural ventilation. British Standard BS5925.

Builtjes, P., 2003. The problem - Air pollution. In: Air Quality Modeling. Theories, Methodologies, Computational Techniques, and Available Databases and Software. Zannetti, P. (Ed.). EnviroComp Institute and Air & Waste Management Association, 1-12.

Burke, J.; Zufall, M. and Ozkaynak, H., 2001. A population exposure model for particulate matter: case study results for PM2.5 in Philadelphia, PA. Journal of Experimental Analysis and Environmental Epidemiology, 11, 470-489.

CA.GOV, 1998. Development of a Model for Assessing Indoor Exposure to Air Pollutants. Final Report. Contract No. A933-157. California Environmental Protection Agency. Air Resources Board, Research Division, 96 pp.

Carissimo, B.; Jagger, S.F.; Daish, N.C.; Halford, A.; Selmer-Olsen, S.; Riikonen, K.; Perroux, J.M.; Wuertz, J.; Bartzis, J.G.; Duijm, N.J.; Ham, K.; Schatzmann, M. and

Hall, R., 2001. The SMEDIS Database and Validation Exercise. Int. Journal of Environment and Pollution, 16, 614-629.

Casey, M. and Wintergerste, T., 2000. ERCOFTAC SIG "Quality and Trust in Industrial CFD": Best Practice Guidelines. ERCOFTAC.

Chang, J.C. and Hanna, S.R., 2004. Air quality model performance evaluation. Meteo. Atmos. Phys., 87, 167-196.

Chau, C.K.; Tu, E.Y.; Chan, D.W.T. and Burnett, J., 2002. Estimating the total exposure to air pollutants for different population age groups in Hong Kong. Environment International, 27, 617-630.

Cheong, K.W., 2001. Airflow measurement for balancing of air distribution system-Tracer-gas techique as an alternative? Building and Environment, 36, 955-964.

CIBSEAM10, 1997. Natural ventilation in non-domestic buildings. Applications Manual. Chartered Institute of Building Services Engineers.

Colvile, R.N.; Hutchinson, E.J.; Mindell, J.S. and Warren, R.F., 2001. The transport sector as a source of air pollution. Atmospheric Environment, 35, 1537-1565.

Curtis, L.; Rea, W.; Smith-Willis, P.; Fenyves, E. and Pan, Y., 2006. Adverse health effects of outdoor air pollutants. Environment International, 32, 815-830.

Daish, N.C.; Britter, R.E.; Linden, P.F.; Jagger, S.F. and Carissimo, B., 2000. SMEDIS: Scientific model evaluation of dense gas dispersion models. International Journal of Environment and Pollution, 14, 39-51.

Derwent, R.G. and Middleton, D.R., 1996. An empirical function for the ratio NO2:NOx. Clean Air, 26, No. 3/4, 57-60.

Dimitroulopoulou, C.; Ashmore, M.R.; Byrne, M.A. and Kinnersley, R.P., 2001. Modelling of indoor exposure to nitrogen dioxide in the UK. Atmospheric Environment, 35, 269-279.

Dimitroulopoulou, C.; Ashmore, M.R.; Hill, M.T.R.; Byrne, M.A. and Kinnersley, R., 2006. INDAIR: A probabilistic model of indoor air pollution in UK homes. Atmospheric Environment, 40, 6362–6379.

Dudhia, J., 1993. A nonhydrostatic version of the Penn State - NCAR Mesoscale Model: Validation tests and simulation of an Atlantic cyclone and cold front. Monthly Weather Review, 121, 1493-1513.

Eatough, D.J.; Hansen, L.D. and Lewis, E.A., 1989. The chemical characterisation of environmental tobacco smoke. International Symposium on Environmental Tobacco Smoke, McGill University 1989. Lexington Bodis, Lexington, Mass.

EC, 1991. Effects of Indoor Air Pollution on Human Health. Report No. 10. European Collaborative Action Urban Air, Indoor Environment and Human Exposure. Environment and Quality of Life. European Commission. Directorate Joint Research Centre - Institute for Health & Consumer.EUR 14086 EN, 44 pp.

EC, 1993. Indoor Pollution by NO2 in European Countries. Report no. 3. European Collaborative Action Urban Air, Indoor Environment and Human Exposure. Environment and Quality of Life. European Commission. Directorate Joint Research Centre - Institute for Health & Consumer.EUR 12219 EN, 24 pp.

EC, 1994. Model Evaluation Group - Guideline for model developers and Model Evaluation Protocol. European Community DG XII, Major Technological Hazards Programme, Brussels, Belgium.

EC, 2000. The Auto-Oil II Programme. Final Report. European Commission. Directorates General for Economic and Financial Affairs, Enterprise, Transport and Energy, Environment, Research, and Taxation and Customs Union, 134 pp.

EC, 2003. Ventilation, Good Indoor Air Quality and Rational Use of Energy. Report No. 23. European Collaborative Action Urban Air, Indoor Environment and Human Exposure. Environment and Quality of Life. European Commission. Directorate Joint Research Centre - Institute for Health & Consumer.EUR 22503 EN, 106 pp.

EC, 2005. The INDEX project. Critical Appraisal of the Setting and Implementation of Indoor Exposure Limits in the EU. Final Report Directorate Joint Research Centre. EUR 21590 EN, 331 pp.

EC, 2006a. Strategies to determine and control the contributions of indoor air pollution to total inhalation exposure (STRATEX). Report No. 25 European Collaborative Action Urban Air, Indoor Environment and Human Exposure. Environment and Quality of Life. European Commission. Directorate Joint Research Centre - Institute for Health & Consumer.EUR 22503 EN, 79 pp.

EC, 2006b. Development of a methodology to assess population exposed to high levels of noise and air pollution close to major transport infrastructure. Final Report. European Commission. Entec UK Limited, 131 pp.

EC, 2007. Workshop on Indoor Air Health Priorities. VITO and European Commission, Directorate-General Environment. Brussels, 14 pp.

Edwards, R.D.; Jurvelin, J.; Koistinen, K.; Saarela, K. and Jantunen, M., 2001. VOC source identification from personal and residential indoor, outdoor and workplace microenvironment samples in EXPOLIS-Helsinki, Finland. Atmospheric Environment, 35, 4829-4841.

EEA, 1999. Environment in the European Union at the turn of the century. European Environment Agency, Copenhagen, 443 pp.

EEA, 2001. TERM 2001 - Indicators tracking transport and environment integration in the European Union. European Environmental Agency, Copenhagen. ISBN 92-9167-307-2, 60 pp.

EEA, 2005. The European Environment - State and Outlook 2005. European Environment Agency, Copenhagen. ISBN 92-9167-776-0, 584 pp.

EEA, 2007. Air pollution in Europe 1990-2004. EEA Report nº2/2007. European Environment Agency, Copenhagen. ISSN 1725 - 9177 84 pp.

ENVIRON, 2004. Comprehensive Air Quality Model with Extensions - CAMx. Version 4.0, User's guide. ENVIRON International Corporation.

EPA, 1997. Air Quality Criteria for Particulate Matter, Vol. 1, 1076 pp.

Fenger, J., 1999. Urban air quality. Atmospheric Environment, 33, 4877-4900.

Fenger, J.; Hertel, O. and Palmgren, F. (Eds.), 1998. Urban Air Pollution - European Aspects. Kluwer Academic Publishers, 492 pp.

Flemming, J. and Stern, R., 2007. Testing model accuracy measures according to the EU directives—examples using the chemical transport model REM-CALGRID. Atmospheric Environment, 41, 9206-9216.

Franke, J.; Hirsch, C.; Jensen, A.G.; Krüs, H.W.; Schatzmann, M.; Westbury, P.S.; Miles, S.D.; Wisse, J.A. and Wright, N.G., 2004. Recommendations on the Use of CFD in Wind Engineering Proceedings of the International Conference on Urban Wind Engineering and Building Aerodynamics: COST Action C14 - Impact of Wind and Storm on City Life and Built Environment, Rhode-Saint-Genèse, Belgium, C.1.1 - C.1.11.

Franke, J.; Hellsten, A.; Schlünzen, H. and Carissimo, B. (Eds.), 2007. Best practice guideline for the CFD simulation of flows in the urban environment. COST Action 732: Quality assurance and improvement of microscale meteorological models. COST Office Brussels, ISBN 3-00-018312-4, 51 pp.

Georgii, H.-W., 1969. The effects of air pollution on urban climates. Bulletin of the World Health Organization, 40, 624-635.

Gosman, A.D., 1999. Developments in CFD for industrial and environmental applications in wind engineering. Journal of Wind Engineering and Industrial Aerodynamics, 81, 21-39.

Götschi, T.; Oglesby, L.; Mathys, P.; Monn, C.; Koistinen, K.; Hänninen, O.; Georgoulis, L.; Polanska, L.; Jantunen, M. and Künzli, N., 2002. Comparison of Black Smoke and PM2.5 levels in indoor and outdoor environments of four European cities. Environmental Science & Technology, 36 (6), 1191-1197.

Goyala, P.; Chanb, A.T. and Jaiswal, N., 2006. Statistical models for the prediction of respirable suspended particulate matter in urban cities. Atmospheric Environment, 40, 2068-2077.

Gulliver, J. and Briggs, D.J., 2004. Personal exposure to particulate air pollution in transport microenvironments. Atmospheric Environment, 38, 1-8.

Gurjar, B.R. and Lelieveld, J., 2005. New Directions: Megacities and global change. Atmospheric Environment, 39, 391-393.

Hanna, S.R.; Chang, J.C. and Strimaitis, D.G., 1993. Hazardous gas model evaluation with field observations. Atmospheric Environment, 27A, 2265–2281.

Hassan, A.A. and Crowther, J.M., 1998. Modelling of fluid flow and pollutant dispersion in a street canyon. Environmental Monitoring and Assessment, 52 (1-2), 281-297.

Heinrich, J. and Wichmann, H.E., 2004. Traffic related pollutants in Europe and their effect on allergic disease. Current Opinion in Allergy and Clinical Immunology, 4(5), 341-348.

Heiselberg, P., 1999. The hybrid ventilation process - theoretical and experimental work. Air Infiltration Review, 21 (1).

Hertel, O.; Wilhardt, P.; Berkowicz, R. and Skov, H., 1996. Exposure of bus drivers and postmen to air pollution from traffic in their working environment. Proceedings of NOSA/NORSAC Symposium. Risø-R-934 (EN), 20-22 pp.

Hertel, O.; Leeuw, F.D.; Raaschou-Nielsen, O.; Jensen, S.S.; Gee, D.; Herbarth, O.; Pryor, S.; Palmgren, F. and Olsen, E., 2001. Human Exposure to Outdoor Air Pollution (IUPAC Technical Report). Pure Appl. Chem., 73 (6), 933-958.

Hodgson, A.T.; Garbesi, K.; Sextro, R.G. and Daisey, J.M., 1992. Soil-gas contamination and entry of volatile organic compounds into a house near a landfill. J. Air Waste Management Association, 42(3), 277-283.

Hoek, G.; Brunekreef, B.; Verhoeff, A.; van Wijnen, J. and Fischer, P., 2000. Daily mortality and air pollution in the Netherlanda. Journal of the Air and Waste Management Association, 50, 1380-1389.

Hosker, R.P., 1985. Flow around isolated structures and building clusters: a review. ASHRAE trans 91, 1671-1692 pp.

IA, 2005. Instituto do Ambiente. Portuguese National Inventory. Report on Greenhouse Gases, 1990-2003. Web page: www.iambiente.pt.

IM, 1974. Atlas Climatológico de Portugal Continental - Edição Preliminar. Serviço Meteorológico Nacional, Lisboa.

INE, 2001. Instituto Nacional de Estatística. Census 2001.

Jensen, S.S., 1999. A geographic approach to modelling human exposure to traffic air pollution using GIS. Ph. D. Thesis. National Environmental Research Institute, Denmark.

Jicha, M.; Katolicky, J. and Pospisil, J., 2000. Dispersion of pollutants in street canyon under traffic induced flow and turbulence. Environmental Monitoring and Assessment, 65 (1-2), 343-351.

Jo, W.-K. and Lee, J.-Y., 2006. Indoor and outdoor levels of respirable particulates (PM10) and Carbon Monoxide (CO) in high-rise apartment buildings. Atmospheric Environment, 40, 6067–6076.

Johansson, C.; Hadenius, A.; Johansson, P.A. and Jonson, T., 1999. Shape. The Stockholm study on health effects of air pollution and their economic consequences Part I: NO2 and particulate matter in Stockholm-concentrations and population exposure. Swedish National Road Administration, No. 1999:41.

Kastner-Klein, P.; Leitl, B.; Pascheke, F. and Schatzmann, M., 2004. Wind tunnel simulation of the Joint Urban 2003 Tracer Experiment. 84th AMS Annual Meeting, Seattle, USA.

Kousaa, A.; Kukkonenc, J.; Karppinen, A.; Aarnioa, P.a. and Koskentalo, T., 2002 A model for evaluating the population exposure to ambient air pollution in an urban area. Atmospheric Environment, 36, 2109-2119.

Koutrakis, P.; Briggs, S.L.K. and Leaderer, B.P., 1992. Source apportionment of indoor aerosols in Suffolk and Onondaga Counties, New York. Environmental Science and Technology, 26, 521-527.

Kruize, H.; Hanninen, O.; Breugelmans, O.; Lebret, E. and Jantunen, M., 2003. Description and demonstration of the EXPOLIS simulation model: Two examples of modelling population exposure to particulate matter. Journal of Exposure Analysis and Environmental Epidemiology, 13, 87-99.

Lai, M.K.K. and Chan, A.T.Y., 2007. Large-Eddy Simulations on Indoor/Outdoor Air Quality Relationship in an Isolated Urban Building. Journal of Engineering Mechanics, 133 (8), 887-898

Launder, B.E. and Spalding, D.B., 1974. The numerical computation of turbulent flows. Computer Methods in Applied Mechanics and Engineering, 3, 269-289.

Lee, R. and Naesslund, E., 1998. Lagrangian stochastic particle model simulations of turbulent dispersion around buildings. Atmospheric Environment, 32 (4), 665-672.

Leuzzi, G. and Mont, P., 1998. Particle trajectory simulation of dispersion around a building. Atmospheric Environment, 32 (2), 203-214.

Li, X.-X.; Liub, C.-H.; Leung, D.Y.C. and Lam, K.M., 2006. Recent progress in CFD modelling of wind field and pollutant transport in street canyons. Atmospheric Environment, 40, 5640-5658.

Liao, C.-M.; Huanga, S.-J. and Yu, H., 2004. Size-dependent particulate matter indoor/outdoor relationships for a wind-induced naturally ventilated airspace Building and Environment, 39 (4), 411-420.

Lohmeyer, A.; Eichhorn, J.; Flassak, T. and Kunz, W., 2002. WinMISKAM 4.2 microscale flow and dispersion model for built up areas, recent developments. Proceedings of the 11th International Symposium Transport and Air Pollution, Graz, Austria.

Martins, J.M., 1998. Atmospheric pollutants dispersion in low wind conditions. PhD Thesis, Department of Environment and Planning, University of Aveiro.

McNabola, A.; Broderick, B.M. and Gill, L.W., 2008. Reduced exposure to air pollution on the boardwalk in Dublin, Ireland. Measurement and prediction. Environment International, 34(1), 86-93.

Milner, J.T.; Dimitroulopoulou, C. and ApSimon, H.M., 2005. Indoor concentrations in buildings from sources outdoors. Annual Report 2004-2005. UK Atmospheric Dispersion Modelling Liaison Committee. ISBN 0-85951-571-0, 80 pp.

Monn, C., 2001. Exposure assessment of air pollutants: a review on spatial heterogeneity and indoor/outdoor/personal exposure to suspended particulate matter, nitrogen dioxide and ozone. Atmospheric Environment, 35, 1-32.

Monteiro, A.; Miranda, A.I.; Borrego, C.; Vautard, R.; Ferreira, J. and Perez, A.T., 2007. Long-term assessment of particulate matter using CHIMERE model. Atmospheric Environment, 41, 7726 - 7738.

Moussiopoulos, N. (Ed.), 2003. Air Quality in Cities. SATURN EUROTRAC-2 Subproject Final Report. Springer-Verlag, ISBN 3-540-00842-x, 298 pp.

Neofytou, P.; Venetsanos, A.G.; Rafailidis, S. and Bartzis, J.G., 2006. Numerical investigation of the pollution dispersion in an urban street canyon. Environmental Modelling & Software, 21, 525-531.

Niachou, A. and Santamouris, M., 2005. Final Report WP10 - Urban impact in the EU. RESHYVENT European Project - Cluster Project on Demand Controlled Hybrid Ventilation in Residential Buildings with specific emphasis of the Integration of Renewables (ENK6-CT2001-00533). European Commission DG RTD.

Nicholson, S.E., 1975. A pollution model for street-level air. Atmospheric Environment, 9, 19-31.

Oberkampf, W.L.; Trucano, T.G. and Hirsch, C., 2004. Verification, validation, and predictive capability in computational engineering and physics. Appl. Mech. Rev., 57(5), 345-384.

Oke, T.R., 1988. Street design and urban canopy layer climate. Energy and Buildings, 11, 103-113.

Olesen, H.R., 1995. Data sets and protocol for model validation. Workshop on Operational Short-range Atmospheric Dispersion Models for Environmental Impact Assessment in Europe. Int. J. Environment and Pollution, 5, 4-6, 693-701.

Olesen, H.R., 2005. User's Guide to the Model Validation Kit Denmark, 72 pp.

Ott, W.; Klepeis, N. and Switzer, P., 2007. Air change rates of motor vehicles and in-vehicle pollutant concentrations from secondhand smoke. Journal of Exposure Science and Environmental Epidemiology, 1-14.

Papadakis, G.; Mermier, M.; Meneses, J. and Boulard, T., 1996. Measurement and analysis of air exchange rates in a greenhouse with continuous roof and side openings. J. agricultural engineering and resources, 63, 219-228.

Park, S.-K.; Kim, S.-D. and Lee, H., 2004. Dispersion characteristics of vehicle emission in an urban street canyon. Science of the Total Envioronment, 323, 263-271.

Pavageau, M.; Rafailidis, S. and Schatzmann, M., 2001. A comprehensive experimental databank for the verification of urban car emission dispersion models. International Journal of Environment and Pollution, 15, 417-425.

Poupard, O.; Blondeau, P.; Iordache, V. and Allard, F., 2005. Statistical analysis of parameters influencing the relationship between outdoor and indoor air quality in schools. Atmospheric Environment, 39, 2071-2080.

Richardson, L.F., 1910. The approximate arithmetical solution by finite differences of physical problems involving differential equations with an application to the stresses in a masonry dam. Trans. Royal Society London, 210 A, 307-357.

Richardson, L.F., 1927. The deferred approach to the limit. Trans. Royal Society London, 226 A, 229-361.

Riley, W.J.; Mckone, T.E.; Lai, A.C.K. and Nazaroff, W.W., 2002. Indoor particulate matter of outdoor origin: importance of size-dependent removal mechanisms. Environmental Science and Technology, 36, 200-207.

Roache, P.J., 1997. Quantification of uncertainty in Computational Fluid Dynamics. Ann. Rev. Fluid. Mech, 29, 123-160.

Rotach, M.; Vogt, R.; Bernhofer, C.; Batchvarova, E.; Christen, A.; Clappier, A.; Feddersen, B.; Gryning, S.E.; Martucci, G.; Mayer, H.; Mitev, V.; Oke, T.R.; Parlow, E.; Richner, H.; Roth, M.; Roulet, Y.A.; Ruffieux, D.; Salmond, J.A.; Schatzmann, M. and Voogt, J.A., 2005. BUBBLE- An urban boundary layer meteorology project. Theoretical and Applied Climatology, 81, 231-261.

Roy, C.J., 2005. Review of code and solution verification procedures for computational simulation. Journal of Computational Physics, 205, 131-156.

Sabatino, S.; Buccolieri, R.; Pulvirenti, B. and Britter, R., 2007. Flow and pollutant dispersion in street canyons using FLUENT and ADMS-Urban Environmental Modeling and Assessment. ISSN: 1573-2967 (Online); DOI: 10.1007/s10666-007-9106-6.

Schatzmann, M., 2000. Report on COST 615 Action "Database, monitoring and modelling of urban air pollution". International Journal of Environment and Pollution, 14, 18-27.

Schatzmann, M.; Bächlin, W.; Emeis, S.; Kühlwein, J.; Leitl, B.; Müller, W.J.; Schäfer, K. and Schlünzen, H., 2006. Development and Validation of Tools for the

Implementation of European Air Quality Policy in Germany (Project VALIUM). Atmospheric Chemistry and Physics, 6, 3077-3083.

Schatzmann, M. and Britter, R., 2007. Quality Assurance and improvement of microscale meteorological models. 11th International Conference on Harmonisation within Atmospheric Dispersion Modelling for Regulatory Purposes, Cambridge, U.K., 159-163.

Schlesinger, S., 1979. Terminology for Model Credibility. Simulation, 32(3), 103-104

Stern, F.; Wilson, R.V.; Coleman, H.W. and Paterson, E.G., 2001. Comprehensive Approach to Verification and Validation of CFD Simulations - Part 1: Methodology and Procedures. ASME Journal of Fluids Engineering, 123, 793-802.

Stohl, A.; Forster, C.; Frank, A.; Seibert, P. and Wotawa, G., 2005. Technical note: The Lagrangian particle dispersion model FLEXPART version 6.2. Atmos. Chem. Phys., 5, 2461-2474.

Straw, M.P., 2000. Computation and measurement of wind induced ventilation. PhD Thesis, School of Civil Engineering, University of Nottingham, 250 pp.

Stull, R.B., 1988. An introduction to boundary layer meteorology. Kluwer, London.

Tchepel, O., 2003. Emission modelling as a decision support tool for air quality management. PhD Thesis, Department of Environment and Planning, University of Aveiro.

Thatcher, T.L. and Layton, D.W., 1995. Deposition, resuspension and penetration of particles within a residence. Atmospheric Environment, 29 (13), 1487-1497.

Trasande, L. and Thurston, G., 2005. The role of air pollution in asthma and other pediatric morbidities. Journal of Allergy and Clinical Immunology, 115(4), 689-699.

van Wijnen, J.H. and van der Zee, S.C., 1998. Traffic-related air pollutants: exposure of road users and populations living near busy roads. Review of Environmental Health, 13, 1-25.

Vardoulakis, S.; Fisher, B.; Pericleous, K. and Gonzales-Flesca, N., 2003. Modelling air quality in street canyons: a review. Atmospheric Environment, 37, 155-182.

Vardoulakis, S.; Dimitrova, R.; Richards, K.; Hamlyn, D.; Camilleri, G.; Weeks, M.; Sini, J.-F.; Britter, R.; Borrego, C.; Schatzmann, M. and Moussiopoulos, N., 2005. Numerical model inter-comparison for a single block building within ATREUS. 10th International Conference on Harmonisation within Atmospheric Dispersion, Crete, Greece.

VDI, 2005. VDI Guideline on Environmental meteorology - Prognostic micro-scale windfield models - Evaluation for flow around buildings and obstacles.

Versteeg, H.K. and Malalasekera, W., 1995. An introduction to computational fluid dynamics-the finite volume method. Longman Scientific and Technical, New York, 255 pp.

Wallace, L., 1996. Indoor particles: a review. Journal of the Air and Waste Management Association, 46, 98-126.

WHO, 2000. Air quality guidelines for Europe. World Health Organization - Regional Office for Europe, European Series, No. 91, Copenhagen, 288 pp.

WHO, 2001. WHO Strategy on air quality and health. World Health Organization, Occupational and Environmental Health, Protection of the Human Environment, 12 pp.

WHO, 2006. Air quality guidelines for particulate matter, ozone, nitrogen, dioxide and sulfur dioxide. Summary of risk assessment. World Health Organisation, Copenhagen, Denmark. WHO/SDE/PHE/OEH/06.02, 22 pp.

WHO, 2007. Development of WHO Guidelines for Indoor Air Quality. Report on a Working Group Meeting. World Health Organization Regional Office for Europe, 27 pp.

Wilson, A.G., 1961. CBD-23. Air Leakage in Buildings. Institute for Research in Construction (IRC), Canadian Building Digest.

Wong, G.W. and Lai, C.K., 2004. Outdoor air pollution and asthma. Current Opinion in Pulmonary Medicine, 10(1), 62-66.

Wu, J.; Lurmann, F.; Winer, A.; Luc, R.; Turco, R. and Funk, T., 2005. Development of an individual exposure model for application to the Southern California children's health study. Atmospheric Environment, 39, 259-273.

Xiaomin, X.; Zhen, H. and Jiasong, W., 2006. The impact of urban street layout on local atmospheric environment. Building and Environment, 41, 1352-1363.

Yamanaka, S., 1984. Decay rates of nitrogen oxides in a typical Japanese living room. Environmental Science and Technology, 18 (7), 566-570.

Yang, T., 2004. CFD and field testing of a naturally ventilated full-scale building. PhD Thesis, School of Civil Engineering, University of Nottingham, 227 pp.

Yee, E. and Biltoft, C.A., 2004. Concentration Fluctuation Measurements in a Plume Dispersing Through a Regular Array of Obstacles. Boundary-Layer Meteorology 111, 363-415.

Zannetti, P., 1990. Air pollution modelling. Van Nostrand Reinhold, New York.

Websites

URL 1: COST 732 - Quality Assurance and Improvement of Micro-Scale Meteorological Models: http://www.mi.uni-hamburg.de/Home.484.0.html

URL 2: COST 715 - Meteorology Applied to Urban Air Pollution Problems: http://www2.dmu.dk/atmosphericenvironment/cost715.htm

URL 3: COST 728 - Enhancing Mesoscale Meteorological Modelling Capabilities for Air Pollution and Dispersion Applications: http://www.cost728.org/home.htm

URL 4: MDS - Model Documentation System (EioNet – EEA): http://air-climate.eionet.europa.eu/databases/MDS/index_html

URL 5: SAUDAR project - The health and the air we breathe: http://www2.dao.ua.pt/gemac/saudar/default.asp?ing=1

URL 6: NCEP Global Tropospheric Analyses:

http://dss.ucar.edu/datasets/ds083.2/

APPENDIX

A. Scientific Evaluation and Model Verification.

APPENDIX A - Scientific Evaluation and Model Verification.

Table A.1 - Basic information for the Scientific Evaluation questionnaire.

	Questionnaire	
1	Specification of the model purpose(s) e.g. prediction of the flow and/or dispersion of pollutants within an urban area. The required spatial and temporal resolution and accuracy should be stated.	
2	Brief model description.	
3	Equations solved (including the fundamental equation system and any simplifications or approximations introduced).	
4	Spatial (micro, meso, macro) and temporal (minutes, hours, days, years) scale	
5	Turbulence model (CFD models only)	
6	Computational domain.	
7	Grid design and resolution (CFD models only).	
8	Numerical solution approach	
9	Near surface treatment (e.g. wall functions).	
10	Boundary conditions.	
11	Initial conditions.	
12	Input and output data.	
13	Implicit or explicit averaging time for output.	
14	Specification of the source.	
15	Applicability or not to specific scenarios:	time varying input; non-neutral atmosphere; complex terrain; buildings; calm or light wind conditions; heat and mass transfer with underlying surface and other surfaces; chemistry; positively or negatively buoyant pollutants; aerosols and particulate matter; concentration fluctuations (including probability density functions); phase changes; wet and dry deposition; radioactivity; solar radiation; treatment of trees and parks; treatment of surface roughness (general and on building surfaces); traffic induced turbulence.

Table A.2 - Steps to perform Model Verification.

Code verification (performed by code developers)	Provision of information about the general software quality assurance of the code
	Provision of information about the strategies for code verification
	Ideally a demonstration that those modules of the code which are activated for the prediction of the flow and pollutant dispersion are consistent with the conceptual model
Solution verification (when performing validation simulations)	Reduction of the error from incomplete iterative convergence to a negligible magnitude by monitoring the target variables as function of the iteration number
	Repeating the simulation on at least two more grids with systematic coarsening or refinement.
	Estimating the error band of the computed target variables with methods based on generalised Richardson extrapolation.

Table A.3 - VADIS model description under COST 732 Model Inventory [URL 1].

A. General Information

short name	
VADIS	
full name	
Pollutant dispersion in the atmosphere under variable wind conditions	
date of last changes	
11-22-2006 (mm-dd-yyyy)	
Model Version (date and/or revision)	
date	v. 2005
revision	September 2006
responsible for this information	
name	Carlos Borrego
institute	University of Aveiro
address	Dept. Environment and Planning, University of Aveiro, 3810-197 Aveiro, PORTUGAL
zip, city	3810-193 - Aveiro
country	Portugal
phone	+351 234370200
fax	+351 234429290
e-mail	borrego@ua.pt
contact person for model code	
☐ same as person above	
other:	
name	Ana Margarida Costa
institute	University of Aveiro
divisions	Dept. Environment and Planning, University of Aveiro, 3810-197 Aveiro, PORTUGAL
street	3810-193 - Aveiro
zip	3810-193 Aveiro
city	Aveiro
country	Portugal
phone	+351234370200
fax	+351234429290

email anamarg@dao.ua.pt

developeruser

model code available?

yes no

more details VADIS model interface for a friendly user access is available only for research activities.

Level of Knowledge needed to operate model

Basic Intermediate Advanced

remarks

Model use at your institution

Operational for research

other use

further general information on the model

VADIS is a Computational Fluid Dynamic (CFD) model Reynolds-averaged Navier-Stokes (RANS) type.

VADIS functioning is based on two modules, FLOW and DISPER. In the first module a k-e turbulence model calculates the 3D wind field, the turbulent viscosity, the pressure, the TKE (Turbulent Kinetic Energy) and the temperature fields affected by a set of obstacles defined in a Cartesian grid. The solution of the Navier-Stokes equations is made through the SIMPLE solver. The DISPER module uses the data provided by the previous module, namely the wind field, and estimates the 3D concentration field, based on the Lagrangian approach. This methodology assumes that the pollutant spatial and temporal dispersion is conveniently represented by a large number of numerical particles released in the flow.

B. Model Properties

model type and scale

meteorology transport or chemistry & transport

macroscale mesoscale microscale

2D 3D

short term (days) long term (months)

approximations

Boussinesq

anelastic

hydrostatic

☐ flat earth

remarks

meteorological variables

	prognostic	diagnostic
u (horizontal wind)	☑ u	☐ u
v (horizontal wind)	☑ v	☐ v
w (vertical wind)	☑ w	☐ w
ζ (vorticity)	☐ ζ	☐ ζ
pv (potential vorticity)	☐ pv	☐ pv
T (real temperature)	☑ T	☐ T
θ (potential temperature)	☐ θ	☐ θ
θl (liquid water potential temperature)	☐ θl	☐ θl
p (pressure)	☑ p	☐ p
Gph (geopotential height)	☐ Gph	☐ Gph
ρ (density)	☐ ρ	☐ ρ
qv (humidity)	☐ qv	☐ qv
qt (total liquid water)	☐ qt	☐ qt
qlc (liquid water in clouds)	☐ qlc	☐ qlc
qf (total frozen water)	☐ qf	☐ qf
qsc (ice in clouds)	☐ qsc	☐ qsc
qlr (rain)	☐ qlr	☐ qlr
qsh (hail)	☐ qsh	☐ qsh
qsg (graupel)	☐ qsg	☐ qsg
qss (snow)	☐ qss	☐ qss
N (cloud fraction)	☐ N	☐ N
E (turbulent kinetic energy)	☑ E	☐ E
ε (dissipation)	☑ ε	☐ ε
K (exchange koefficient)	☐ K	☐ K
zi (mixing height)	☐ zi	☐ zi

prognostic other

chemical substances

	prognostic	diagnostic
gases		
SO2 (sulphur dioxide)	☐ SO2	☐ SO2
NO (nitric oxide)	☐ NO	☐ NO

	prognostic	diagnostic
NO2 (nitrogen dioxide)	☐ NO2	☐ NO2
NOx (nitrogen oxides)	☐ NOx	☐ NOx
NH3 (ammonia)	☐ NH3	☐ NH3
HNO3 (nitric acid)	☐ HNO3	☐ HNO3
O3 (ozone)	☐ O3	☐ O3
VOC (volatile organic compounds)	☐ VOC	☐ VOC
C6H6 (benzene)	☐ C6H6	☐ C6H6
HCHO (formaldehyde	☐ HCHO	☐ HCHO
CO (carbon monoxide)	☐ CO	☐ CO
CO2 (carbon dioxide)	☐ CO2	☐ CO2
POP (persistent organic pollutants)	☐ POP	☐ POP

other prognostic: passive gases ☑

particles	prognostic	diagnostic
PM 10 (particles < 10µm)	☑ PM 10	☐ PM 10
PM 2.5 (particles < 2.5µm)	☑ PM 2.5	☐ PM 2.5
PM 1.0 (particles < 1.0µm)	☑ PM 1.0	☐ PM 1.0
PM 0.1 (particles < 0.1µm)	☑ PM 0.1	☐ PM 0.1
PPM 10 (primary PM 10)	☐ PPM 10	☐ PPM 10
NH4 (ammonium)	☐ NH4	☐ NH4
SO4 (sulfate)	☐ SO4	☐ SO4
NO3 (nitrate)	☐ NO3	☐ NO3
OSN (organic secondary nitrate)	☐ OSN	☐ OSN

other prognostic:

radioactivity	prognostic	diagnostic
	☐	☐
	☐	☐
	☐	☐

remarks:

parametrizations

turbulence scheme	k-e turbulence scheme. This scheme corresponds to a one-and-a-half order closure that retains the prognostic equations for the zero-order statistics such as mean wind, temperature and the variances of the referred variables. The TKE equation is used in place of the velocity variance equations. A highly-parameterized prognostic equation for

	the dissipation rate is included in addition to the equation for TKE.
deep convection	
surface exchange	Wall functions.
surface temperature	User defined.
surface humidity	
treatment of obstacles	Considered by imposing conditions on interior grid nodes.
radiation	
radiation between obstacles	
radiation in vegetation	
unresolved orographic drag	
clouds / rain	
photolysis rate	
dry deposition	An absorption layer may be defined: a fraction of the particles falling in this layer are considered deposited.
wet deposition	
remarks	

chemistry

chemical transformations ○ calculated ◉ neglected ○ other

gas phase chemistry (give details)

wet phase chemistry (give details)

aerosol chemistry

- ☐ passive aerosol
- ☐ dry aerosol
- ☐ wet aerosol
- ☐ sectional approach
- ☐ modal approach

other
give details

more information on chemistry

nesting

	meteorology	chemistry & transport
one way		
two way		
other		
variables nested		
nesting online / offline	/	/
data exchange by file/array	/	/
time step for data exchange		
explain method		

boundary conditions

	meteorology	chemistry & transport
surface	Roughness parameter, temperature (wall functions used)	
top	Symmetry	
lateral inflow	Wind and temperature profiles, direct input or developed over unobstructed field till convergence	
lateral outflow	Free, except for mass balance kept correct	

data assimilation

	meteorology	chemistry & transport
nudging technique		
adjoint model		
3D-VAR		
4D-VAR		
OI		
explain method		

initialization

meteorology	chemistry & transport

describe procedure	The wind field may be (optionally) developed over the unobstructed domain till convergence	

coordinate system and projection

vertical
- ☑ z coordinate
- ☐ surface fitted grid
- ☐ pressure coordinate
- ☐ sigma coordinate

horizontal
- ☑ cartesian
- ☐ Lambert conformal
- ☐ latitude / longitude
- ☐ rotated lat. / long.

remarks

numeric

	meteorology	chemistry & transport
Euler	☑	☐
Lagrange		☑
other		
uniform / nonuniform grid	☐ / ☐	☐ / ☐
grid Arakawa	☐A ☐B ☐C ☐D ☐E	☐A ☐B ☐C ☐D ☐E
time integration		
explicit	☐	☐
split-explicit	☐	☐
semi-implicit	☐	☐
time step same as meteorology		☐
other		
momentum equations		
scalar quantities		
additional information		

chemistry solver (give details)

input data (name sources for data, e.g. website)

orography

land use	
obstacles	buildings, through node redefinition
vegetation	
meteorology	wind and temperature profiles, ground temperature
concentrations	
emissions	
remarks	

C. Model Validation and Application

validation & evaluation

- ☐ analytic solutions [1]
- ☑ evaluated reference dataset [2]
- ☑ model intercomparison [3]
- ☐ additional validation and evaluation efforts [4]

meteorology	[2]	[3]
u (horizontal wind)	☑ u	☑ u
v (horizontal wind)	☑ v	☑ v
w (vertical wind)	☑ w	☑ w
T (temperature)	☑ T	☑ T
qv (humidity)	☐ qv	☐ qv
qlc (liquid water in clouds)	☐ qlc	☐ qlc
qsc (ice in clouds)	☐ qsc	☐ qsc
qlr (rain)	☐ qlr	☐ qlr
zi (mixing height)	☐ zi	☐ zi
other		
testcase description		
testcase references		
used data set		
reference for evaluation		
remarks		

chemistry & transport	[2]	[3]
SO2 (sulphur dioxide)	☐ SO2	☐ SO2
NO (nitric oxide)	☐ NO	☐ NO
NO2 (nitrogen dioxide)	☐ NO2	☐ NO2
NOx (nitrogen oxides)	☐ NOx	☐ NOx
NH3 (ammonia)	☐ NH3	☐ NH3

HNO3 (nitric acid)	☐HNO3	☐HNO3
O3 (ozone)	☐O3	☐O3
VOC (volotile organic compounds)	☐VOC	☐VOC
C6H6 (benzene)	☐C6H6	☐C6H6
HCHO (Formaldehyde)	☐HCHO	☐HCHO
CO (carbon monoxide)	☐CO	☑CO
CO2 (carbon dioxide)	☐CO2	☐CO2
POP (persistent organic pollutants)	☐POP	☐POP
other		
testcase description		
testcase references		
used data set		
reference for evaluation		
remarks		

application examples

2. Wind flow simulations were performed by VADIS and compared with CHENSI model under ATREUS network.

a) Project title

Advanced Tools for Rational Energy Use towards Sustainability with emphasis on microclimatic issues in urban applications (ATREUS) network (http://aix.meng.auth.gr/atreus/).

b) Relevant references

S. Vardoulakis et al. Intercomparison of CFD models within ATREUS: Single building configuration, presented to the ERCOFTAC Meeting on Urban Scale CFD, Nottingham (UK), 9-10 September 2004.

K. Richards et al. A wind tunnel investigation of thermal effects within the vicinity of a single block building with leeward wall heating, accepted to the ERCOFTAC Meeting on Urban Scale CFD, Nottingham (UK), 9-10 September 2004.

S. Vardoulakis, R. Dimitrova, K. Richards, D. Hamlyn, G. Camilleri, M. Weeks, J-F. Sini, R. Britter, C. Borrego, M. Schatzmann, N. Moussiopoulos, Numerical model inter-comparison for a single block building within ATREUS, accepted for oral presentation at the 10th International Conference on Harmonisation within Atmospheric Dispersion, 17-20 October, 2005, Crete, Greece.

c) Project's short description

The project research objectives include:

• The study of the urban energy budget taking into account the local and microclimatic conditions,

• Use of the knowledge gathered by latest studies on wind flow modifications by urban structures, their geometry and dimensions,

• Development of city maps to allow the determination of optimum arrangements of groups of buildings to optimise the exchange processes for an area of the city or for the city as a whole,

• Study of the flow and turbulence characteristics within a street canyon with special

emphasis in the boundary layers of building walls and roofs,
• Investigation of the thermal effects on flow modification within street canyons with special regard to low wind speed conditions around buildings,
• Evaluation of the wind field around buildings,
• Determination of the exploitable RES potential on the urban areas, and
• Determination of heating and cooling loads of the buildings, and their impact on the urban microclimate.
d) more details on Model performance
Both the micro-scale numerical models used (VADIS and CHENSI) were extensively validated against the experimental data for both the isothermal (cold cube) and thermal cases. Both codes made representative predictions of the mean velocity field for the cold cube case but tended to over predict mean turbulent kinetic energy in regions of impingement, a common problem when using RANS codes with variants of the standard k-e turbulence model. In both cases improvements in overall predictions were observed when non-uniform inflow boundary conditions, the same as that recorded in the wind tunnel were applied. With respect to the thermal cases CHENSI generally performed better at predicting the mean temperature field and resulting modifications in the velocity distribution within fair agreement with the experimental data at the model centre-plane. Predictions were further improved through applying a new thermal wall condition, obtained from the experimental data, based on the heat flux at the heated face of the cube. In general VADIS over-predicted the buoyancy force and mean temperature field in the wake of the model. Difficulties with VADIS in applying the thermal conditions to more complex domain meant only CHENSI was further used to make predictions of wind and temperature fields within the more complex 'Lisbon' geometry. The VADIS code encountered difficulties with these simulations primarily due to the recent addition of wall functions into the code. VADIS is an in-house code developed at GEMAC/UA and is always under development. This compounded with limited time meant that this problem with VADIS could not be fully resolved within ATREUS. However work will continue in this area.

2.Comparisons were made against FLUENT model
a) Project title
SUTRA Project
b) Relevant references
BORREGO, C.; TCHEPEL, O.; COSTA, A.M.; AMORIM, J.H. and MIRANDA, A.I. – Emission and dispersion modelling of Lisbon air quality at local scale. Atmospheric Environment: Elsevier, Vol. 37 (2003), p. 5197-5205.
c) Project's short description
The primary objective of SUTRA was to develop a consistent and comprehensive approach and planning methodology for the analysis of urban transportation problems, that helps to design strategies for sustainable cities. This included an integration of socio-economic, environmental and technological concepts including the development, integration, and demonstration of tools and methodologies to improve forecasting, assessment and policy level decision support. VADIS model was one of the numerical tools used in the above mentioned project. The model was applied to the Lisbon city centre in order to evaluate the air pollution associated to road traffic. The study domain covers an area of 450 m x 450 m and is characterised by strictly perpendicular streets including several one-way roads and a pedestrian zone. During the simulation period,

wind direction was mainly from Northwest, with velocities varying between 1 m s-1 and 6 m s-1. Background concentrations entering the model domain were based on CO average concentrations measured at an urban monitoring station that is not directly influenced by the emission sources. Hourly simulation were conducted with VADIS to obtain CO concentration levels for a typical summer day, which was chosen using a statistical meteorological approach. Several traffic management scenarios were developed and evaluated using the TREM (Transport Emission model for Line Sources) and VADIS results.

d) more details on Model performance

Hourly CO concentrations obtained with VADIS for the Lisbon city centre were compared with concentration values measured by an air quality station located in the study domain and with FLUENT results. There is a good agreement between predicted and measured values between 0 a.m. and 3 p.m. for the simulated day. Moreover, during the time period when model estimations and measurements show some discrepancy, the results obtained with FLUENT and VADIS are very similar, indicating that the trend of both models to underestimate the CO concentrations could be justified by a possible inaccuracy associated with initialisation data. Due to the low CO background concentration (77 µg m-3), the modelling results are not affected by the background values. A quantitative analysis to determine modelling uncertainties has been applied to the estimated CO concentration values. The analysis is based on the definition of maximum deviation of the measured and calculated levels during the considered period. To be compared with modelling quality objectives established by the Directive (200/69/EC), 8-hour average CO values were evaluated. Based on this approach, the average uncertainty of the model prediction for this study corresponds to 15 %, achieving 52 % as a maximum for the 8-hour average period from 1 to 8 p.m.. This value slightly exceeds the 50 % acceptability limit defined by the Directive.

domain size

		met min	met max	c&t min	c&t max
horizontal	[km]	0.01	2	0.01	2
vertical	[m]	1	200	1	200

model resolution

		met min	met max	c&t min	c&t max
horizontal	[km]				
vertical	[m]				

minimum computer resources required

type	PC: Windows 9x, 2000 and NT (typically 256 Mb RAM required); Workstation: Unix.
time needed for run	Extremely dependent on number of computational cells and grid resolution. Typical CPU run time of ~6h for a 200000 cells simulation on a Pentium III 700 MHz.
storage	Typically around 25 Mb per simulation.

D. Additional Information on the Model

documentation

PhD thesis written in Portuguese with VADIS description:
Martins, JM, 1998, Dispersão de poluentes na atmosfera em condições de vento fraco, PhD thesis, Dep. Ambiente e Ordenamento, Universidade de Aveiro.
Master dissertation written in Portuguese with model application:
COSTA, A.M. – Avaliação da Qualidade do Ar ao Nível Local: contributo para o desenvolvimento urbano sustentável. Dissertação apresentada à Universidade de Aveiro para obtenção do grau de Mestre em Poluição Atmosférica, Departamento de Ambiente e Ordenamento, Universidade de Aveiro, Aveiro, Portugal. Fevereiro 2003.

SUTRA European Project (EVK4-CT-1999-00013) Deliverables:
D04.3 – VADIS Street Canyon Model: Methodology Description
D04.4 – VADIS Operational Street Canyon Model (operational prototype).

references

BORREGO, C.; TCHEPEL, O.; COSTA, A.M.; AMORIM, J.H. and MIRANDA, A.I. – Emission and dispersion modelling of Lisbon air quality at local scale. Atmospheric Environment: Elsevier, Vol. 37 (2003) pp. 5197-5205.

BORREGO, C.; TCHEPEL, O.; COSTA, A.M.; MARTINS, H.; FEREEIRA, J. and MIRANDA, A.I. - Traffic-related particulate air pollution exposure in urban areas. Atmospheric Environment: Elsevier, Vol. (2006), pp. (in press).

BORREGO, C.; TCHEPEL, O.; SALMIM, L; AMORIM, J.H.; COSTA, A.M. and JANKO, J. – Integrated modelling of road traffic emissions: application to Lisbon air quality management. Cybernetics and Systems: An International journal. Taylor & Francis, Vol. 35, Numbers 5-6 (2004), p. 535-548.

web page

www.dao.ua.pt/gemac